



ΕΘΝΙΚΟ ΜΕΤΣΟΒΙΟ ΠΟΛΥΤΕΧΝΕΙΟ  
ΣΧΟΛΗ ΗΛΕΚΤΡΟΛΟΓΩΝ ΜΗΧΑΝΙΚΩΝ  
ΚΑΙ ΜΗΧΑΝΙΚΩΝ ΥΠΟΛΟΓΙΣΤΩΝ  
ΤΟΜΕΑΣ ΕΠΙΚΟΙΝΩΝΙΩΝ ΗΛΕΚΤΡΟΝΙΚΗΣ ΚΑΙ ΣΥΣΤΗΜΑΤΩΝ  
ΠΛΗΡΟΦΟΡΙΚΗΣ

**Μέτρηση κατανεμημένων τάσεων σε χάλυβες με την χρήση των  
μαγνητοσυστολικών γραμμών καθυστέρησης (MDL)**

**ΔΙΔΑΚΤΟΡΙΚΗ ΔΙΑΤΡΙΒΗ**

Ελένη Ε. Μαγγιώρου

Αθήνα, Σεπτέμβριος, 2024





ΕΘΝΙΚΟ ΜΕΤΣΟΒΙΟ ΠΟΛΥΤΕΧΝΕΙΟ  
ΣΧΟΛΗ ΗΛΕΚΤΡΟΛΟΓΩΝ ΜΗΧΑΝΙΚΩΝ  
ΚΑΙ ΜΗΧΑΝΙΚΩΝ ΥΠΟΛΟΓΙΣΤΩΝ  
ΤΟΜΕΑΣ ΕΠΙΚΟΙΝΩΝΙΩΝ ΗΛΕΚΤΡΟΝΙΚΗΣ ΚΑΙ ΣΥΣΤΗΜΑΤΩΝ  
ΠΛΗΡΟΦΟΡΙΚΗΣ

**Μέτρηση κατανεμημένων τάσεων σε χάλυβες με την χρήση των  
μαγνητοσυστολικών γραμμών καθυστέρησης (MDL)**

**ΔΙΔΑΚΤΟΡΙΚΗ ΔΙΑΤΡΙΒΗ**

Ελένη Ε. Μαγγιώρου

**Συμβουλευτική επιτροπή:** Ευάγγελος Χριστοφόρου

Πάυλος-Πέτρος Σωτηριάδης

Ιωάννης Π. Ξανθάκης

Εγκρίθηκε από την επταμελή εξεταστική επιτροπή την 26<sup>η</sup> Σεπτεμβρίου 2024.

Ευάγγελος Χριστοφόρου  
Καθηγητής Ε.Μ.Π

Ιωάννης Π. Ξανθάκης  
Καθηγητής Ε.Μ.Π

Πάυλος-Πέτρος Σωτηριάδης  
Καθηγητής Ε.Μ.Π

Αφροδίτη Κτενά  
Καθηγήτρια Ε.Κ.Π.Α

Πέτρος Τσακίριδης  
Αναπληρωτής Καθηγητής Ε.Μ.Π

Γεώργιος Παναγόπουλος  
Επίκουρος Καθηγητής Ε.Μ.Π

Εμμανουήλ Χουρδάκης  
Επίκουρος Καθηγητής Ε.Μ.Π

Αθήνα, Σεπτέμβριος, 2024

---

Ελένη Ε. Μαγγιώρου

Διδάκτωρ Ηλεκτρολόγος Μηχανικός και Μηχανικός Υπολογιστών Ε.Μ.Π.

Copyright © Ελένη Μαγγιώρου, 2024

Με επιφύλαξη παντός δικαιώματος. All rights reserved.

Απαγορεύεται η αντιγραφή, αποθήκευση και διανομή της παρούσας εργασίας, εξ' ολοκλήρου ή τμήματος αυτής, για εμπορικό σκοπό. Επιτρέπεται η ανατύπωση, αποθήκευση και διανομή για σκοπό μη κερδοσκοπικό, εκπαιδευτικής ή ερευνητικής φύσης, υπό την προϋπόθεση να αναφέρεται η πηγή προέλευσης και να διατηρείται το παρόν μήνυμα. Ερωτήματα που αφορούν τη χρήση της εργασίας για κερδοσκοπικό σκοπό πρέπει να απευθύνονται προς τον συγγραφέα.

Οι απόψεις και τα συμπεράσματα που περιέχονται σε αυτό το έγγραφο εκφράζουν τον συγγραφέα και δεν πρέπει να ερμηνευθεί ότι αντιπροσωπεύουν τις επίσημες θέσεις του Εθνικού Μετσόβιου Πολυτεχνείου.

# Περίληψη

---

Η παρούσα εργασία επικεντρώνεται στη μελέτη των μαγνητοσουσταλτικών γραμμών καθυστέρησης (MDL) και των μηχανικών τους εφαρμογών. Αρχικά, εξετάζεται η δημιουργία, η διάδοση και η ανίχνευση ενός ελαστικού παλμού σε διατάξεις MDL. Αυτή η μελέτη κατέστησε δυνατή την κατανόηση των μηχανισμών και των παραμέτρων που επηρεάζουν τη δημιουργία και ανίχνευση του ελαστικού παλμού, όπως είναι τα πεδία διέγερσης και λήψης, καθώς και η μηχανική επίδραση στη γραμμή καθυστέρησης. Η κατανόηση αυτών των παραμέτρων οδήγησε στην ανάπτυξη διαφόρων διατάξεων MDL ως αισθητήρες. Οι βασικές ιδιότητες των MDL, όπως η ευαισθησία, η γραμμικότητα και η υστέρηση, προσδιορίστηκαν λεπτομερώς, όπως και οι μέθοδοι προσαρμογής τους στις απαιτήσεις διαφορετικών εφαρμογών. Επιπλέον, αναλύθηκε η εξάρτηση των ιδιοτήτων αυτών από διάφορους παράγοντες, όπως το πεδίο, η συχνότητα, η τάση, η θερμοκρασία και ο χρόνος.

Η εργασία εισάγει επίσης τη μαγνητοελαστική ομοιομορφία, την ταχύτητα του ήχου και την ανάλυση των MDL, τρεις ιδιότητες που καθορίζουν την απόδοση των συστημάτων αυτών. Διερευνήθηκαν διάφορα μαγνητοελαστικά υλικά, καταλήγοντας στο συμπέρασμα ότι οι άμορφες ταινίες και τα σύρματα είναι ιδιαίτερα κατάλληλα για αισθητήρες, χωρίς να αποκλείονται τα λεπτά φιλμ. Οι ιδιότητες αυτών των υλικών μπορούν να χρησιμεύσουν ως βάση δεδομένων για μηχανικές εφαρμογές, ιδιαίτερα στην ανάπτυξη αισθητήρων.

Η εργασία εστιάζει στην παρουσίαση των κυριότερων αισθητήρων MDL. Για λόγους κατανόησης, οι αισθητήρες αυτοί κατηγοριοποιήθηκαν σε τρεις βασικές κατηγορίες: αισθητήρες θέσης, αισθητήρες τάσης και αισθητήρες πεδίου. Αναπτύχθηκαν διάφοροι αισθητήρες θέσης βασισμένοι σε τροποποίηση πλάτους ή χρόνου καθυστέρησης, οι οποίοι είναι ικανοί να μετρήσουν είτε στατική είτε δυναμική μετατόπιση. Αναπτύχθηκαν επίσης διάφοροι αισθητήρες τάσης, όπως αισθητήρες τάσης εφελκυσμού, αισθητήρες πίεσης και αισθητήρες δύναμης, οι οποίοι προσφέρουν σημαντικά πλεονεκτήματα σε σύγκριση με τις υπάρχουσες τεχνολογίες. Επιπλέον, παρουσιάστηκαν αισθητήρες πεδίου βασισμένοι στην τεχνική MDL, οι οποίοι προσφέρουν δυνατότητα μέτρησης κατανομής με ακρίβεια. Επιπλέον, αναπτύχθηκαν τεχνολογίες κατασκευής που επιτρέπουν τη χαμηλού κόστους και με αποδεκτή ακρίβεια παραγωγή αισθητήρων.

Εκτός από τις τεχνολογικές εφαρμογές, η εργασία εξετάζει κρίσιμες εφαρμογές των MDL σε τομείς όπως οι μη καταστροφικές δοκιμές, οι μελέτες πήξης αίματος και χημικών σύνθετων υλικών καθώς και στις εφαρμογές στη δομική και μεταλλευτική μηχανική. Ως μια επιπλέον εφαρμογή της τεχνικής MDL, παρουσιάστηκε μια μέθοδος για τη μέτρηση των καμπυλών  $M(H)$  και  $\lambda(H)$ , η οποία επιτρέπει τον προσδιορισμό του βρόχου και της ομοιομορφίας του μαγνητισμού και της μαγνητοσυστολής κατά μήκος ενός μαγνητοσυστατικού υλικού.

Τέλος, η διατριβή εξετάζει τις προκλήσεις που προκύπτουν από την εφαρμογή αυτών των τεχνικών σε πραγματικές συνθήκες, όπως οι περιβαλλοντικές επιδράσεις και η ανάγκη για υψηλή ευαισθησία και ακρίβεια. Επίσης, αναλύεται η δυνατότητα βελτίωσης της απόδοσης των μετρήσεων μέσω της περαιτέρω εξέλιξης των υλικών και των μεθόδων ανάλυσης δεδομένων, επιτρέποντας έτσι την ευρύτερη εφαρμογή των MDL σε πιο απαιτητικές βιομηχανικές χρήσεις.

**Λέξεις-κλειδιά:** μαγνητοσυστατικές γραμμές καθυστέρησης, αισθητήρες θέσης, αισθητήρες τάσης, αισθητήρες πεδίου, τεχνολογία MDL, μαγνητοελαστικά υλικά.

# Abstract

---

This work focuses on the study of magnetostrictive delay lines (MDLs) and their engineering applications. Initially, the generation, propagation, and detection of an elastic pulse in MDL arrangements are examined. This study enabled a deep understanding of the mechanisms and parameters affecting the generation and detection of the elastic pulse, such as the excitation and biasing fields, as well as the mechanical impact on the delay line. Understanding these parameters led to the development of various MDL configurations used as sensors. The fundamental properties of MDLs, including sensitivity, linearity, and hysteresis, were determined in detail, along with methods for tailoring these properties to meet the requirements of different applications. Additionally, the dependence of these properties on various factors such as field, frequency, stress, temperature, and time was analyzed.

The work also introduces magnetoelastic uniformity, sound velocity, and MDL resolution—three properties that define the performance of these systems. Various magnetoelastic materials were investigated, concluding that amorphous ribbons and wires are particularly suitable for sensing applications, without excluding thin films. The properties of these materials can serve as a database for engineering applications, particularly in sensor development.

The work focuses on presenting the main MDL sensors. For clarity, these sensors are categorized into three main types: position sensors, stress sensors, and field sensors. Several position sensors based on amplitude or time delay modulation were developed, capable of measuring either static or dynamic displacement. Various stress sensors, such as tensile stress sensors, pressure sensors, and force digitizers, were also developed, offering significant advantages over existing technologies. Additionally, MDL-based field sensors were presented, which offer distribution measurement capabilities with acceptable measurement uncertainty. Manufacturing technologies that allow for low-cost production with acceptable accuracy were also developed.

In addition to technological applications, the work explores critical MDL applications in fields such as non-destructive testing, blood coagulation studies, and chemical composite materials, as well as in structural and mining engineering. As an additional application of the MDL technique, a method for measuring  $M(H)$

and  $\lambda(H)$  curves was presented, which allows for the determination of the magnetization and magnetostriction uniformity along the length of a magnetostrictive material.

Finally, the thesis examines the challenges arising from the application of these techniques in real-world conditions, such as environmental effects and the need for high sensitivity and accuracy. The potential for improving measurement performance through further development of materials and data analysis methods is also discussed, thus enabling the broader application of MDLs in more demanding industrial uses.

**Keywords:** magnetostrictive delay lines, position sensors, stress sensors, field sensors, MDL technology, magnetoelastic materials.

# Acknowledgments

---

This doctoral dissertation represents the culmination of a long-term and intensive personal effort, which has been supported by the continuous help of many individuals. Their contributions and support have been crucial for the completion of this work, and I would like to express my sincere gratitude to everyone who contributed in any way to this endeavor.

First and foremost, I wish to extend my heartfelt thanks to my supervisor, Professor Evangelos Christoforou, from the Department of Communications, Electronics, and Computer Systems at the School of Electrical and Computer Engineering, National Technical University of Athens (NTUA). Professor Christoforou has been a constant source of support and inspiration throughout this process. His dedication to guiding my research, his invaluable scientific advice, and his continuous presence were pivotal factors for the successful completion of my dissertation. Our discussions and his feedback not only improved the quality of my research but also helped me develop a deeper understanding of the fundamental principles of my field. It was not only his academic support that helped me progress but also the personal encouragement he provided during moments of doubt and difficulty, equipping me with the necessary tools to continue.

Additionally, I would like to express my gratitude to Professor Ioannis Xanthakis, Emeritus Professor at the School of Electrical and Computer Engineering, NTUA, in the Department of Electromagnetic Applications, Optoelectronics, and Electronic Materials. His trust in my research abilities and his guidance with great wisdom and patience were critical to the development and completion of my dissertation. His contribution to my scientific journey and his continuous encouragement laid the foundation for my progress.

Moreover, I wish to express my warmest thanks to Professor Pavlos-Petros Sotiropoulos, from the Department of Communications, Electronics, and Computer Systems. His contribution to my research journey was both crucial and valuable. From the beginning of my dissertation, Professor Sotiropoulos guided me with scientific precision, providing support where needed during critical phases of the research.

Special thanks are also due to Professor Aphrodite Ktena, from the Department of Electrical Installations at the National and Kapodistrian University of Athens (NKUA). Her contribution to my scientific development was invaluable, as her extensive knowledge in her field and her logical thinking provided the foundation upon which my research journey was built. Professor Ktena not only offered me the necessary scientific knowledge but also continuously encouraged me to evolve and face challenges. Her guidance was exceptionally valuable, serving as a cornerstone for the realization and successful completion of this dissertation. Furthermore, her teaching approach, which is based on methodical and analytical problem-solving, helped me develop skills that extend beyond this specific research. Her influence on my thinking and scientific development is something for which I will always be grateful, as she prepared me for future endeavors.

Also, I would like to express my sincere gratitude to Associate Professor Petros Tsakiridis, whose guidance and continuous support played a crucial role in the completion of my PhD thesis. As an Associate Professor in the Laboratory of Physical Metallurgy, in the Department of Metallurgy and Materials Technology, of the School of Mining and Metallurgical Engineering at the National Technical University of Athens, Professor Tsakiridis introduced me to fundamental and advanced methods of material characterization, such as Scanning Electron Microscopy (SEM). His expertise in a wide range of modern analytical techniques has been invaluable for my learning and understanding of these methods, which became essential tools for my research. Working with him has been both invaluable and pivotal for my development as a researcher.

I would also like to express my heartfelt thanks to the other members of my examination committee for their invaluable contribution during my doctoral dissertation. My appreciation for them is deep and sincere, as their contribution was decisive for the completion of my research efforts. Specifically, I would like to mention:

- Assistant Professor George Panagopoulos from the School of Electrical and Computer Engineering at NTUA, Department of Communications, Electronics, and Computer Systems, for his valuable contribution and guiding observations.
- Assistant Professor Emmanouil Chourdakis from the School of Electrical and Computer Engineering at NTUA, Department of Communications, Electronics, and Computer Systems, for his support and valuable advice.

The contribution of all committee members was crucial for the completion of my research efforts, and my appreciation for them is deep and sincere.

Additionally, I would like to express my special gratitude to my colleagues and friends from the Laboratory of Electronic Sensors at the School of Electrical and Computer Engineering, NTUA. Their contribution to my research journey was critical on many levels. From the beginning of my dissertation, their constructive criticism and valuable observations helped me identify and address the gaps and challenges of my research with clarity and effectiveness. Our collaboration was a source of inspiration and encouragement, as the different perspectives and suggestions that emerged from our discussions shaped the final form of this dissertation. Even more importantly, this interaction contributed to my development as a researcher, enhancing my critical thinking and broadening my scientific approach. My gratitude to them is deep and sincere, as their contribution will accompany me throughout my academic journey.

Finally, I would like to express my heartfelt gratitude to all those who, in any way, contributed to the successful completion of this doctoral dissertation. Their support, whether moral, psychological, or spiritual, was invaluable and crucial to my journey. Their presence, encouragement, and belief in my abilities helped me remain focused on my goals, even in the most challenging moments. Their contribution was not limited to daily support but constituted a foundation upon which the entire journey of this dissertation was built. Without them, this work would not have been completed with the same success, and for that, I thank them from the bottom of my heart. Their contribution will always accompany me, serving as a bright example of the value of solidarity and collaboration in life and science.



# Table of Contents

Περίληψη .....	1
Abstract .....	3
List of Tables.....	13
List of Figures.....	27
<b>FIGURE 5.35. THE RESPONSE OF THE ABSOLUTE AND INCREMENTAL ANGULAR POSITION SENSOR.....</b>	<b>35</b>
<b>1 MAGNETIC EFFECTS IN SENSING .....</b>	<b>41</b>
1.1 DOMAIN WALL DYNAMICS. ....	42
1.2 DOMAIN ROTATION DYNAMICS.....	44
1.2.1 <i>Dependent mechanisms.</i> .....	46
1.3 SENSORS BASED ON MAGNETIC EFFECTS AND MATERIALS .....	48
1.3.1 <i>Position sensors</i> .....	48
1.3.2 <i>Mass sensors</i> .....	49
1.3.3 <i>Field sensors</i> .....	50
1.3.4 <i>Security sensors</i> .....	51
1.3.5 <i>Multipurpose sensors</i> .....	51
1.4 APPLICATIONS OF SENSORS BASED ON MAGNETIC EFFECTS AND MATERIALS .....	52
1.4.1 <i>Industrial applications</i> .....	52
1.4.2 <i>Biomedical applications</i> .....	53
1.4.3 <i>Military applications</i> .....	54
1.4.4 <i>Environmental applications</i> .....	54
1.4.5 <i>Automotive applications</i> .....	55
1.4.6 <i>Laboratory sensors</i> .....	56
1.4.7 <i>Domestic applications</i> .....	56
<b>2 MAGNETOSTRICTIVE DELAY LINE ARRANGEMENTS .....</b>	<b>57</b>
2.1 THE COIL-COIL ARRANGEMENT .....	57
2.1.1 <i>Magnetostriction modeling</i> .....	61
2.1.2 <i>An alternative way of modeling the coil-coil MDL arrangement</i> .....	64
2.2 ARRAY CONDUCTORS PERPENDICULAR TO ARRAYS OF MDLS .....	66
2.2.1 <i>Single conductor perpendicular to a single MDL</i> .....	67
2.2.2 <i>Array of conductors perpendicular to an array of MDLs</i> .....	71
2.2.3 <i>Array of balanced conductors perpendicular to an array of MDLs</i> .....	73
2.2.4 <i>Array conductors parallel to MDL arrays</i> .....	74
2.2.5 <i>Non magnetic MDL waveguides</i> .....	78
2.2.6 <i>Coil-less MDL set-up</i> .....	80
2.2.7 <i>Coily MDL set-up</i> .....	83
2.2.8 <i>Circumferential MDL set-ups</i> .....	87
2.2.9 <i>Remarks and conclusions on the various MDL arrangements</i> .....	91
<b>3 MDL PROPERTIES .....</b>	<b>93</b>
3.1 THE BASIC MDL PROPERTIES.....	93
3.2 SENSITIVITY .....	93
3.2.1 <i>Linearity</i> .....	94

3.1.3	Hysteresis .....	95
3.1.4	Tailoring the basic properties .....	96
3.3	PARAMETRIC DEPENDENCE OF THE MDL RESPONSE.....	98
3.2.1	DC Field dependence .....	98
3.2.2	Pulsed field dependence .....	101
3.2.3	Frequency dependence.....	102
3.2.4	Stress dependence .....	102
3.2.5	Temperature dependence .....	103
3.2.6	Temporal dependence .....	104
3.2.7	Response delay .....	104
3.2.8	Reflections, after-effects and signal dispersion .....	105
3.2.9	Experimental procedure of the determination of the MDL parametric response .....	106
3.4	MAGNETOELASTIC RESPONSE AND MAGNETOELASTIC UNIFORMITY .....	107
3.3.1	Magnetoelastic uniformity .....	108
3.3.2	Fast magnetoelastic uniformity determination.....	113
3.3.3	Normalization method and algorithm.....	117
3.5	SOUND VELOCITY AND ITS UNIFORMITY .....	118
3.6	MDL RESOLUTION .....	124
3.5.1	MDL impulse response.....	129
<b>4</b>	<b>MATERIALS FOR MDLS .....</b>	<b>131</b>
4.1	THE CLASSIC POLY-CRYSTALLINE MAGNETOSTRICTIVE WIRES AND RIBBONS.....	131
4.2	THE RAPIDLY QUENCHED MAGNETOCTRICTIVE ALLOYS .....	134
4.2.1	Amorphous ribbons .....	137
4.2.2	Amorphous wires.....	145
4.2.3	Amorphous glass covered wires .....	149
4.3	THIN FILMS.....	156
4.4	NEGATIVE MAGNETOSTRICTIVE MATERIALS .....	164
4.5	COMPOSITES .....	167
<b>5</b>	<b>POSITION SENSORS BASED ON MDLS.....</b>	<b>169</b>
5.1	MOVING PERMANENT MAGNET MEASUREMENT .....	170
5.1.1	Sensors based on MDL pulsed voltage output measurement.....	170
5.1.2	Sensors based on MDL delay time response measurement .....	178
5.1.3	Long coil position sensor .....	180
5.1.4	Circumferential MDL and corresponding position sensor.....	185
5.1.5	A new type of inexpensive and accurate position sensor .....	187
5.1.6	Accelerometers based on dynamic moving magnet displacement .....	203
5.2	MOVING SOFT MAGNET MEASUREMENT.....	209
	<b>FIGURE 5.35. THE RESPONSE OF THE ABSOLUTE AND INCREMENTAL ANGULAR POSITION SENSOR.....</b>	<b>216</b>
5.3	MOVING NON MAGNETIC CONDUCTING DISK MEASUREMENT .....	217
<b>6</b>	<b>STRESS SENSORS BASED ON MDLS.....</b>	<b>221</b>
6.1	TENSILE STRESS SENSORS.....	222
6.1.1	A low compliance beam structure force sensor based on this the sensor topology .....	227
6.1.2	Improvement of the sensor: a 2-dimensional stress sensing element.....	229
6.1.3	Manufacturing the tensile stress sensors .....	231

6.2	PRESSURE GAUGES.....	233
6.2.1	<i>Distribution pressure sensors based on this principle idea.....</i>	235
6.3	FORCE DIGITIZERS .....	239
6.4	LOAD CELLS AND TORQUE METERS.....	245
6.4.1	<i>The load cell.....</i>	246
6.4.2	<i>The torque meter.....</i>	247
6.4.3	<i>Experiments.....</i>	249
6.5	THIN FILM THICKNESS SENSORS.....	254
<b>7</b>	<b>FIELD SENSORS BASED ON MDLS .....</b>	<b>259</b>
7.1	ANOTHER FIELD SENSOR ARRAY .....	264
<b>8</b>	<b>APPLICATIONS OF MDLS .....</b>	<b>267</b>
8.1	NON DESTRUCTIVE TESTING USING MDLS .....	267
8.1.1	<i>The state of the art.....</i>	267
8.1.2	<i>Magnetostrictive Delay Lines in Magnetic Anomaly Based Defect Detection.....</i>	268
8.1.3	<i>Magnetostrictive Delay Lines in Eddy Current Based Defect Detection .....</i>	272
8.1.4	<i>Magnetostrictive Delay Lines in Permeability Measurements .....</i>	275
8.1.5	<i>On the use of MDLs for Non-destructive Testing.....</i>	276
8.2	MDLS FOR CHEMICAL AND BIOMEDICAL ENGINEERING APPLICATIONS.....	277
8.2.1	<i>The state of the art in blood coagulation and curing point measurements .....</i>	278
8.2.2	<i>The proposed sensing element.....</i>	279
8.2.2	<i>Experiments.....</i>	283
8.2.3	<i>Discussion .....</i>	288
8.3	MDLS FOR CIVIL AND MINING ENGINEERING APPLICATIONS.....	291
8.4	MDLS FOR SPORTS FIELD APPLICATIONS .....	294
8.4.1	<i>The sensor.....</i>	295
8.4.2	<i>Experiment and discussion .....</i>	297
8.5	MDLS IN THE DETERMINATION OF THE PROPERTIES OF MAGNETOSTRICTIVE MATERIALS .....	300
8.5.1	<i>M-H loop.....</i>	301
8.5.2	<i><math>\lambda</math>-H loop.....</i>	302
8.5.3	<i>On the <math>M(H)</math> and <math>\lambda(H)</math> results .....</i>	303
8.6	MDLS FOR RESIDUAL STRESS MONITORING IN MAGNETOSTRICTIVE CYLINDERS AND TUBES.....	304
8.6.1	<i>The under test cylinder and tube .....</i>	305
8.6.2	<i>Magnetoelastic uniformity set-up.....</i>	305
8.6.3	<i>Longitudinal sound velocity monitoring set-up.....</i>	306
8.6.4	<i>Fast magnetoelastic uniformity set-up.....</i>	307
8.6.5	<i>Experiment results and Discussion.....</i>	308
	<b>CONCLUSIONS AND FUTURE WORK .....</b>	<b>315</b>
	<b>REFERENCES.....</b>	<b>317</b>
	<b>PUBLICATIONS .....</b>	<b>333</b>



# Εκτενής περίληψη

---

Η διατριβή εξετάζει σε βάθος τις Μαγνητοσυσταλτικές Γραμμές Καθυστέρησης (MDLs) και τις εφαρμογές τους ως αισθητήρες σε διάφορους τομείς, επικεντρώνοντας την έρευνα στην ανάπτυξη και βελτιστοποίηση αυτής της τεχνολογίας για μετρήσεις υψηλής ακρίβειας και ευαισθησίας. Οι MDLs αποτελούν μια προηγμένη τεχνολογία ανίχνευσης που αξιοποιεί μαγνητικά φαινόμενα για τη μέτρηση φυσικών παραμέτρων, όπως τάση, μαγνητικό πεδίο και μετατόπιση.

Αρχικά, η διατριβή εξετάζει τα μαγνητικά φαινόμενα που αποτελούν τη βάση λειτουργίας των MDLs, όπως η μαγνητοαντίσταση, η μαγνητο-εμπέδηση, η μαγνητοσυστολή, η ηλεκτρομαγνητική επαγωγή και το φαινόμενο Hall. Η θεωρητική ανάλυση εστιάζει στις δυναμικές των τοιχωμάτων των μαγνητικών τομέων (domain wall dynamics) και στις δυναμικές περιστροφής των τομέων (domain rotation dynamics), οι οποίες καθορίζουν την απόκριση των μαγνητικών υλικών. Αυτοί οι μηχανισμοί παίζουν κεντρικό ρόλο στη λειτουργία των μαγνητικών αισθητήρων, επιτρέποντας τη μετάδοση και ανίχνευση ελαστικών παλμών που προκύπτουν από τη μαγνητοσυστολή των υλικών.

Έτσι, παρουσιάζεται μια εις βάθος ανάλυση των βασικών μαγνητικών φαινομένων που χρησιμοποιούνται για την κατασκευή αισθητήρων και των εφαρμογών τους σε διάφορους τομείς. Οι μαγνητικοί αισθητήρες κατέχουν εξέχουσα θέση στη σύγχρονη τεχνολογία λόγω της εφαρμογής τους σε αυτοκινητιστικά συστήματα, ιατρικές συσκευές, βιομηχανικές διαδικασίες και στρατιωτικά συστήματα.

Το πρώτο κεφάλαιο της διατριβής παρουσιάζει μια εις βάθος ανάλυση των βασικών μαγνητικών φαινομένων που χρησιμοποιούνται για την κατασκευή αισθητήρων και των εφαρμογών τους σε διάφορους τομείς. Οι μαγνητικοί αισθητήρες κατέχουν εξέχουσα θέση στη σύγχρονη τεχνολογία λόγω της εφαρμογής τους σε αυτοκινητιστικά συστήματα, ιατρικές συσκευές, βιομηχανικές διαδικασίες και στρατιωτικά συστήματα. Στο κεφάλαιο γίνεται μια εκτενής κατηγοριοποίηση των αισθητήρων με βάση τρία βασικά κριτήρια:

- Το αντικείμενο μέτρησης: φυσικά ή χημικά μεγέθη.

- Το φαινόμενο και το υλικό στο οποίο βασίζεται η λειτουργία του αισθητήρα: αισθητήρες βασισμένοι σε αγώγιμα, ημιαγώγιμα, διηλεκτρικά, μαγνητικά και υπεραγώγιμα υλικά.
- Οι εφαρμογές τους: βιομηχανικές, μεταφορικές, ιατρικές, στρατιωτικές, οικιακές και περιβαλλοντικές.

Το κεφάλαιο επικεντρώνεται στα μαγνητικά φαινόμενα που χρησιμοποιούνται συνήθως στην ανάπτυξη αισθητήρων, όπως η μαγνητοαντίσταση, η μαγνητο-εμπέδηση, η μαγνητοσυστολή, η ηλεκτρομαγνητική επαγωγή και το φαινόμενο Hall. Η βασική θεωρία για τα μαγνητικά υλικά που χρησιμοποιούνται στους αισθητήρες βασίζεται στη δυναμική των τοιχωμάτων των μαγνητικών τομέων (domain wall dynamics) και στην περιστροφή των μαγνητικών τομέων (domain rotation dynamics). Αυτοί οι μηχανισμοί είναι καθοριστικοί για την κατανόηση των μαγνητικών επιδράσεων που εμπλέκονται στην κατασκευή αισθητήρων και οδηγούν στη δημιουργία ενός μεγάλου εύρους ανιχνευτικών συστημάτων.

Στις εφαρμογές ανίχνευσης μικρών μαγνητικών πεδίων και μηχανικών αισθητήρων, είναι κρίσιμο να επιλέγονται υλικά με ελάχιστες ατέλειες για να μειωθεί η μαγνητοελαστική απόκριση. Ενδεικτικά, υλικά όπως τα σύρματα FeCoSiB με μαγνητοσυστολή στο επίπεδο του 0.1 ppm είναι κατάλληλα για εφαρμογές που απαιτούν υψηλή ακρίβεια. Για την επίτευξη αυτής της ιδιότητας, το υλικό περνάει από διαδικασίες θερμικής ανόπτησης, υπό ελεγχόμενες συνθήκες θερμοκρασίας και πεδίου, με σκοπό τη μείωση των εσωτερικών τάσεων που δημιουργούνται από ελαττώματα.

Οι δυναμικές περιστροφές των μαγνητικών τομέων περιγράφονται με βάση δύο κύριες φάσεις: την μη αναστρέψιμη περιστροφή και την αναστρέψιμη περιστροφή. Η μη αναστρέψιμη περιστροφή συμβαίνει όταν οι μαγνητικοί τομείς προσανατολίζονται από έναν εύκολο άξονα (easy axis) σε έναν άλλο που βρίσκεται πιο κοντά στον άξονα του εξωτερικού μαγνητικού πεδίου. Η αναστρέψιμη περιστροφή ακολουθεί την μη αναστρέψιμη διαδικασία και σχετίζεται με μικρότερες μετατοπίσεις των τομέων προς την κατεύθυνση του εξωτερικού πεδίου. Οι μαγνητικοί τομείς δεν επιστρέφουν πάντα στον αρχικό άξονα μετά την απομάκρυνση του εξωτερικού πεδίου.

Η μη αναστρέψιμη περιστροφή σχετίζεται με την εμφάνιση του φαινομένου Barkhausen, το οποίο προκαλεί θόρυβο και επηρεάζει την ακρίβεια του αισθητήρα. Αντίθετα, η αναστρέψιμη περιστροφή μειώνει τον θόρυβο, γεγονός που την καθιστά προτιμητέα για εφαρμογές που απαιτούν υψηλή ακρίβεια και ευαισθησία, όπως οι μηχανικοί αισθητήρες και οι αισθητήρες πεδίου.

Ένα σημαντικό μέρος της ανάλυσης αφορά τη χρήση της τεχνικής των μαγνητοσυστολικών γραμμών καθυστέρησης (Magnetostrictive Delay Lines - MDL) για την ανάπτυξη αισθητήρων μέτρησης μετατόπισης, τάσης και πεδίου. Αυτή η τεχνική βασίζεται στο φαινόμενο της μαγνητοσυστολής, όπου μια αλλαγή στο μαγνητικό πεδίο προκαλεί μικρές μηχανικές παραμορφώσεις στο υλικό, οι οποίες μπορούν να ανιχνευτούν και να χρησιμοποιηθούν για την ακριβή μέτρηση φυσικών μεγεθών. Οι MDL αισθητήρες έχουν βρει ευρεία χρήση σε βιομηχανικές, αυτοκινητιστικές και στρατιωτικές εφαρμογές λόγω της υψηλής ευαισθησίας, της ακρίβειας και του χαμηλού κόστους παραγωγής.

Στην συνέχεια, παρουσιάζονται οι βασικές ιδιότητες των αισθητήρων MDL, όπως η γραμμικότητα, η ευαισθησία και η υστέρηση, καθώς και οι τρόποι προσαρμογής αυτών των ιδιοτήτων για διαφορετικές εφαρμογές. Η παραμετρική εξάρτηση της απόκρισης των MDL αισθητήρων από παράγοντες όπως το πεδίο, η συχνότητα, η τάση, η θερμοκρασία και ο χρόνος, αναλύεται διεξοδικά, προσδιορίζοντας έτσι τη βέλτιστη χρήση των υλικών αυτών.

Οι αισθητήρες που βασίζονται στα μαγνητικά φαινόμενα παρουσιάζουν ιδιαίτερο ενδιαφέρον σε τομείς όπως οι βιομηχανικές εφαρμογές, οι ιατρικές συσκευές, οι μη καταστροφικοί έλεγχοι και οι εφαρμογές ασφαλείας. Ειδικότερα, αναλύονται εφαρμογές των MDL αισθητήρων σε περιβάλλοντα όπου απαιτείται υψηλή ευαισθησία, όπως οι ανιχνευτές μετατοπίσεων και τάσης, αλλά και σε πιο σύνθετες εφαρμογές, όπως η ανίχνευση πεδίων και οι αισθητήρες ασφάλειας.

Συνοψίζοντας, καταλήγουμε ότι οι μαγνητικοί αισθητήρες, και ειδικά αυτοί που βασίζονται στις μαγνητοσυστολικές γραμμές καθυστέρησης, προσφέρουν ευρείες δυνατότητες για μελλοντικές τεχνολογικές και βιομηχανικές εφαρμογές. Ωστόσο, η επιτυχής εφαρμογή τους εξαρτάται από τη σωστή επιλογή και προσαρμογή των υλικών, καθώς και από την ανάπτυξη μεθόδων που επιτρέπουν τη βελτίωση της ακρίβειας και της απόδοσης.

Ένα σημαντικό εμπόδιο που αναφέρεται είναι οι περιβαλλοντικοί παράγοντες που μπορούν να επηρεάσουν την απόδοση των αισθητήρων, όπως οι αλλαγές στη θερμοκρασία και η παρουσία εξωτερικών μαγνητικών πεδίων. Η υστέρηση και ο μαγνητικός θόρυβος είναι άλλοι παράγοντες που επισημαίνονται ως προκλήσεις, ειδικά στις εφαρμογές που απαιτούν υψηλή ευαισθησία και χαμηλή αβεβαιότητα στις μετρήσεις. Αυτές οι προκλήσεις μπορούν να αντιμετωπιστούν με την περαιτέρω εξέλιξη των μαγνητικών υλικών και τη βελτιστοποίηση των τεχνικών ανίχνευσης, βελτιώνοντας τη σταθερότητα των συστημάτων και μειώνοντας τις επιδράσεις των εξωτερικών παραγόντων.

Στο πρώτο κεφάλαιο γίνεται σαφές ότι η τεχνολογία των μαγνητοσυστολικών αισθητήρων έχει μεγάλες δυνατότητες για εξέλιξη, ιδιαίτερα μέσω της βελτίωσης των υλικών και της ανάπτυξης νέων τεχνικών επεξεργασίας δεδομένων που θα επιτρέψουν την ευρύτερη εφαρμογή τους σε βιομηχανικές και επιστημονικές εφαρμογές. Τέλος, η χρήση αυτών των αισθητήρων σε πιο απαιτητικές περιβαλλοντικές συνθήκες αναμένεται να επεκταθεί, με την ανάπτυξη υλικών που είναι ανθεκτικά σε ακραίες συνθήκες και με την ενσωμάτωση πιο ευαίσθητων και ακριβών μεθόδων ανίχνευσης.

Το δεύτερο κεφάλαιο της διατριβής παρουσιάζει τις διάφορες αρχιτεκτονικές διατάξεις που χρησιμοποιούνται για τη δημιουργία, διάδοση και ανίχνευση ελαστικών παλμών σε μαγνητοσυσταλτικά υλικά. Η ανάλυση επικεντρώνεται σε διαφορετικές διατάξεις MDL, με στόχο την αξιοποίηση της τεχνολογίας αυτής για τη βελτιστοποίηση της απόδοσης των αισθητήρων σε βιομηχανικές, στρατιωτικές και άλλες εφαρμογές.

Η πρώτη διάταξη που εξετάζεται είναι η κλασική διάταξη πηνίου-πηνίου (coil-coil), στην οποία δύο πηνία, το ένα για διέγερση και το άλλο για ανίχνευση, τοποθετούνται στα άκρα της γραμμής καθυστέρησης. Η διάταξη αυτή είναι βασική για τη λειτουργία των MDL, καθώς επιτρέπει τη δημιουργία ελαστικών παλμών μέσω της εφαρμογής παλμικού ρεύματος στο πηνίο διέγερσης και την ανίχνευσή τους από το πηνίο ανίχνευσης. Η προσθήκη κολλητικής ουσίας χρησιμοποιείται για την αποτροπή ανακλάσεων που θα μπορούσαν να επηρεάσουν την ακρίβεια της μέτρησης.

Μια άλλη διάταξη είναι αυτή που χρησιμοποιεί ευθυγραμμισμένους αγωγούς με τις MDL, είτε ορθογώνια είτε παράλληλα τοποθετημένους σε σχέση με την MDL. Αυτή η προσέγγιση επιτρέπει τη μετάδοση παλμών ρεύματος με μεγαλύτερη ακρίβεια, ενώ μειώνει τις πιθανές παρεμβολές που θα μπορούσαν να προκύψουν από τον συνδυασμό πολλών παλμών. Αυτές οι διατάξεις είναι σημαντικές για εφαρμογές όπου απαιτείται υψηλή ανάλυση και ακρίβεια στη μετάδοση σημάτων.

Μία άλλη ενδιαφέρουσα προσέγγιση που παρουσιάζεται είναι η χρήση μη μαγνητικών και μη μαγνητοσυστολικών υλικών ως ακουστικών κυματοδηγών. Σε αυτήν την περίπτωση, τα υλικά αυτά χρησιμοποιούνται για τη διάδοση των ελαστικών παλμών που δημιουργούνται από τις MDL, επιτρέποντας τη χρήση των αισθητήρων σε περιβάλλοντα όπου οι μαγνητικές ιδιότητες πρέπει να ελαχιστοποιηθούν. Αυτή η διάταξη επεκτείνει τις δυνατότητες των MDL για εφαρμογές όπου οι μαγνητικές αλληλεπιδράσεις μπορεί να είναι προβληματικές.

Η επόμενη διάταξη που αναλύεται είναι η διάταξη χωρίς πηνίο (coil-less). Σε αυτήν τη διάταξη, η μετάδοση των ελαστικών παλμών επιτυγχάνεται χωρίς τη χρήση πηνίων διέγερσης και ανίχνευσης, κάτι που απλοποιεί σημαντικά τη δομή της διάταξης και προσφέρει ευκολία κατασκευής, καθώς και μείωση κόστους. Αυτή η διάταξη είναι ιδιαίτερα ενδιαφέρουσα για εφαρμογές χαμηλού κόστους όπου η απλότητα είναι βασικό κριτήριο.

Η ανάλυση συνεχίζεται με τη διάταξη όπου η MDL τυλίγεται γύρω από έναν αγωγό παλμικού ρεύματος, επιτρέποντας τη διάδοση εγκάρσιων ελαστικών κυμάτων. Αυτή η διάταξη παρέχει τη δυνατότητα ανίχνευσης με μεγαλύτερη ακρίβεια, καθώς η περιφερειακή τοποθέτηση των στοιχείων βελτιώνει την απόδοση του συστήματος ανίχνευσης.

Τέλος, η διάταξη περιφερειακής τοποθέτησης (circumferential) περιλαμβάνει έναν αγωγό παλμικού ρεύματος με την MDL τοποθετημένη περιφερειακά γύρω από αυτόν. Η συμμετρία της διάταξης επιτρέπει τη διάδοση εγκάρσιων ελαστικών κυμάτων και τη βελτίωση της ανίχνευσης σε εφαρμογές όπου η ακριβής καταγραφή των παλμών είναι κρίσιμη.

Το κεφάλαιο καταλήγει στο ότι οι διάφορες διατάξεις MDL προσφέρουν σημαντικές δυνατότητες για την κατασκευή ακριβών και ευαίσθητων αισθητήρων για τη μέτρηση μετατόπισης, τάσης και πεδίου. Η κάθε διάταξη παρουσιάζει μοναδικά χαρακτηριστικά που την καθιστούν κατάλληλη για συγκεκριμένες εφαρμογές, προσφέροντας έτσι τη δυνατότητα προσαρμογής ανάλογα με τις απαιτήσεις του εκάστοτε συστήματος. Συγκεκριμένα, η χρήση μαγνητοσυστολικών υλικών και η προσαρμογή των παραμέτρων τους επιτρέπει την αύξηση της ακρίβειας των μετρήσεων και την ευρύτερη εφαρμογή τους σε βιομηχανικά περιβάλλοντα, στρατιωτικά συστήματα και άλλα πεδία όπου απαιτείται υψηλή ακρίβεια και αξιοπιστία.

Το τρίτο κεφάλαιο της διατριβής, παρουσιάζει τις βασικές ιδιότητες που χαρακτηρίζουν τη λειτουργία των MDL και την απόδοσή τους. Αναλύονται οι κύριες ιδιότητες, όπως η ευαισθησία, η γραμμικότητα και η υστέρηση, καθώς και η εξάρτησή τους από διάφορους παραμέτρους, όπως το μαγνητικό πεδίο, η συχνότητα και η τάση. Το κεφάλαιο χωρίζεται σε διάφορα τμήματα που εξετάζουν τις επιδράσεις αυτών των παραμέτρων και τους τρόπους με τους οποίους μπορούν να προσαρμοστούν για βέλτιστη λειτουργία.

Βασικές Ιδιότητες MDL

Οι βασικές ιδιότητες των MDL, όπως η ευαισθησία, η γραμμικότητα και η υστέρηση, ορίζουν εν μέρει την ποιότητα της διάταξης. Αυτές οι ιδιότητες συνδέονται άμεσα με τις συναρτήσεις  $\lambda(H)$  και  $M(H)$ , που καθορίζουν τη μαγνητοσυσταλτική συμπεριφορά. Η ευαισθησία ενός MDL ορίζεται ως η παρατηρήσιμη αλλαγή στην τάση εξόδου για την μικρότερη δυνατή αλλαγή σε ένα παράμετρο που επηρεάζει την απόκρισή του. Για παράδειγμα, το μέγιστο πλάτος εξόδου της παλμικής τάσης για ένα κλασικό πολυκρυσταλλικό υλικό είναι της τάξης των λίγων mV, ενώ σε ειδικά προετοιμασμένα υλικά μπορεί να φτάσει τα εκατοντάδες mV.

Η γραμμικότητα αναφέρεται στην μονοτονική σχέση της απόκρισης του MDL με τις παραμέτρους που την επηρεάζουν. Τα περισσότερα MDL χαρακτηρίζονται από μη γραμμική συμπεριφορά λόγω των ιδιοτήτων της μαγνήτισης και της μαγνητοσυστολής, καθώς και των ακουστικών ιδιοτήτων του υλικού. Στη γραμμική περιοχή, η εξάρτηση της τάσης εξόδου από τα φυσικά μεγέθη είναι μονοτονική, αλλά η αβεβαιότητα της μέτρησης εξαρτάται από το πεδίο διέγερσης και τις μηχανικές επιδράσεις.

Η υστέρηση είναι ίσως η πιο σημαντική ιδιότητα των MDL, καθώς ορίζεται ως η διαφορά στην απόκριση όταν αυξάνεται ή μειώνεται μια παράμετρος, όπως το μαγνητικό πεδίο ή η τάση. Αν και η υστέρηση είναι αναμενόμενη σε πολλά μαγνητοσυσταλτικά υλικά, σε ορισμένα MDL δεν παρατηρείται λόγω της λειτουργίας τους στην περιοχή μη υστερητικής συμπεριφοράς.

#### Εξάρτηση από Παραμέτρους

Η απόκριση ενός MDL εξαρτάται από διάφορες παραμέτρους, όπως:

- Εξάρτηση από το DC πεδίο: Το DC μαγνητικό πεδίο έχει άμεση επίδραση στην ένταση της μαγνητοσυσταλτικής απόκρισης.
- Εξάρτηση από την παλμική τάση: Η μεταβολή της τάσης διέγερσης επηρεάζει το πλάτος της τάσης εξόδου.
- Εξάρτηση από τη συχνότητα: Η συχνότητα των εφαρμοζόμενων σημάτων επηρεάζει την απόκριση της συσκευής, καθώς η μαγνητοσυσταλτική συμπεριφορά είναι συχνά εξαρτώμενη από τη συχνότητα.
- Εξάρτηση από τη μηχανική καταπόνηση: Η εφαρμογή τάσης ή στρέψης μπορεί να τροποποιήσει τη μαγνητοσυσταλτική συμπεριφορά, γεγονός που αξιοποιείται σε αισθητήρες τάσης και μετατόπισης.

- Εξάρτηση από τη θερμοκρασία: Οι αλλαγές θερμοκρασίας μπορούν να τροποποιήσουν την ελαστική απόκριση και τη μαγνητοσυσταλτική σύζευξη, επηρεάζοντας την ευαισθησία του MDL.

Η μαγνητοελαστική ομοιομορφία (MEU) ορίζεται ως η μεταβολή του πλάτους της παλμικής τάσης εξόδου του MDL σε σχέση με τη θέση της διέγερσης ή της ανίχνευσης. Αυτή η ιδιότητα επηρεάζεται από τα μαγνητικά πεδία και τη μηχανική καταπόνηση. Η βελτίωση της ομοιομορφίας επιτυγχάνεται μέσω διαδικασιών όπως η θερμική ανόπτηση, που μειώνει τις εσωτερικές τάσεις του υλικού και αυξάνει την ακρίβεια της διάταξης.

Η χρονική εξάρτηση της απόκρισης των MDL είναι σημαντική για τη βελτίωση της ακρίβειας και της ανάλυσης των αισθητήρων. Η ανάλυση των αποτελεσμάτων δείχνει ότι η ακριβής ρύθμιση των παραμέτρων, όπως η γεωμετρία της διάταξης και οι συνθήκες ανόπτησης, μπορεί να βελτιώσει την ανάλυση έως και 1 mm.

Το κεφάλαιο καταλήγει στο ότι οι βασικές ιδιότητες των MDL μπορούν να προσαρμοστούν μέσω διαφόρων τεχνικών, βελτιώνοντας την απόδοσή τους σε ένα ευρύ φάσμα εφαρμογών. Οι αισθητήρες που βασίζονται σε MDL είναι ιδιαίτερα κατάλληλοι για εφαρμογές που απαιτούν υψηλή ευαισθησία και ακρίβεια, ενώ οι τεχνικές βελτιστοποίησης των ιδιοτήτων τους, όπως η ανόπτηση και η γεωμετρία των διατάξεων, διασφαλίζουν την αποτελεσματική λειτουργία τους.

Το τέταρτο κεφάλαιο της διατριβής, αναλύει τα διάφορα υλικά που χρησιμοποιούνται στην ανάπτυξη των MDL και τονίζει τη σημασία της σωστής επιλογής υλικών για την επίτευξη της βέλτιστης απόδοσης. Κάθε κατηγορία υλικών διαθέτει διαφορετικές ιδιότητες που τα καθιστούν κατάλληλα για συγκεκριμένες εφαρμογές, ανάλογα με τις απαιτήσεις του εκάστοτε αισθητήρα ή διάταξης.

Αρχικά, εξετάζονται τα πολυκρυσταλλικά σύρματα και ταινίες από μέταλλα όπως ο σίδηρος (Fe) και το νικέλιο (Ni), καθώς και τα κράματά τους. Αυτά τα υλικά είναι ευρέως χρησιμοποιούμενα λόγω της σταθερότητάς τους, ωστόσο παρουσιάζουν περιορισμούς ως προς την ευαισθησία και την μαγνητοσυσταλτική τους απόκριση, ιδιαίτερα όταν υπάρχουν μικρορωγμές και ατέλειες στην επιφάνειά τους. Οι ατέλειες αυτές περιορίζουν τη διάδοση των ελαστικών κυμάτων και μειώνουν την ακρίβεια των αισθητήρων, καθιστώντας τα πολυκρυσταλλικά υλικά κατάλληλα μόνο για εφαρμογές που δεν απαιτούν υψηλή ευαισθησία.

Μια πιο προηγμένη κατηγορία υλικών είναι τα ταχέως ψυχόμενα μαγνητοσυσταλτικά κράματα, με χαρακτηριστικά παραδείγματα τα άμορφα κράματα όπως το Fe-Si-B. Τα υλικά αυτά παρουσιάζουν

σημαντικά βελτιωμένες μαγνητικές και μηχανικές ιδιότητες σε σύγκριση με τα πολυκρυσταλλικά κράματα, λόγω της άμορφης δομής τους, που προσφέρει καλύτερη διάδοση των ελαστικών κυμάτων και υψηλότερη ευαισθησία. Ιδιαίτερα, το κράμα Fe<sub>78</sub>Si<sub>7</sub>B<sub>15</sub> έχει αποδειχθεί ότι είναι ιδιαίτερα αποτελεσματικό σε πολλές εφαρμογές MDL, εξαιτίας της σταθερότητας και της μηχανικής αντοχής του.

Επίσης, το κεφάλαιο εστιάζει στα λεπτά φιλμ από μαγνητοσυσταλτικά υλικά, όπως το Fe-Si-B. Αυτά τα υλικά είναι ιδανικά για μικροσκοπικές διατάξεις MDL, χάρη στις σύγχρονες τεχνικές παρασκευής τους, όπως η εναπόθεση μέσω ψεκασμού RF και η χρήση ηλεκτρονικών δεσμών. Η δυνατότητα κατασκευής μικροδιατάξεων πάνω σε υποστρώματα από πυρίτιο επιτρέπει τη δημιουργία εξαιρετικά ευαίσθητων αισθητήρων, με μεγάλη ακρίβεια στις μετρήσεις.

Μια άλλη κατηγορία υλικών που εξετάζεται είναι τα αρνητικά μαγνητοσυσταλτικά υλικά, όπως το FeCoSiB. Αυτά τα υλικά παρουσιάζουν ιδιαίτερο ενδιαφέρον λόγω της συμπεριφοράς τους σε εφαρμογές τάσης και ροπής, όπου η έξοδος τάσης αυξάνεται ή μειώνεται ανάλογα με την εφαρμοζόμενη πίεση. Αυτή η ιδιότητα τα καθιστά κατάλληλα για ειδικές εφαρμογές αισθητήρων που απαιτούν ακριβή μέτρηση μηχανικών δυνάμεων.

Τέλος, το κεφάλαιο αναφέρεται στα συνθετικά υλικά, τα οποία αποτελούν μια αναδυόμενη κατηγορία με μεγάλο δυναμικό για μελλοντικές εφαρμογές. Τα συνθετικά υλικά αποτελούνται από μαγνητικά ή μαγνητοσυσταλτικά συστατικά που ενσωματώνονται σε μήτρα μη μαγνητικών υλικών. Αν και δεν είναι ακόμα πλήρως ανεπτυγμένα για MDL, υπόσχονται να προσφέρουν νέες δυνατότητες στη μαγνητοελαστική σύζευξη και να βελτιώσουν τη σχεδίαση ευαίσθητων διατάξεων MDL στο μέλλον. Συνολικά, το κεφάλαιο καταλήγει στο ότι η επιλογή του κατάλληλου υλικού για την κατασκευή MDL είναι κρίσιμη για την απόδοση των αισθητήρων. Τα άμορφα κράματα και τα λεπτά φιλμ αποτελούν τις πλέον υποσχόμενες λύσεις για τις περισσότερες εφαρμογές, ενώ τα πολυκρυσταλλικά και τα αρνητικά μαγνητοσυσταλτικά υλικά προσφέρουν λύσεις για συγκεκριμένες εξειδικευμένες χρήσεις.

Το πέμπτο κεφάλαιο της διατριβής, επικεντρώνεται στις εφαρμογές των MDL για την ανίχνευση θέσης. Αυτοί οι αισθητήρες χρησιμοποιούνται σε γραμμές παραγωγής, εργαστήρια δοκιμών και ιατρικές συσκευές. Παρουσιάζεται μια ανάλυση των τεχνικών μέτρησης και των βασικών αρχών λειτουργίας των αισθητήρων θέσης, με έμφαση στις εφαρμογές που απαιτούν υψηλή ακρίβεια, καθώς και σε συστήματα χαμηλού κόστους.

Οι αισθητήρες θέσης μπορούν να κατηγοριοποιηθούν σε διάφορες τεχνικές μέτρησης, όπως τα συστήματα μετατόπισης κινούμενων μόνιμων μαγνητών, που βασίζονται στην ανίχνευση τάσης από τα MDL. Αυτές οι συσκευές χρησιμοποιούν μόνιμους μαγνήτες και μπορούν να ανιχνεύσουν μετατοπίσεις έως και 20 mm με βάση τη μεταβολή της τάσης εξόδου που προκαλείται από την αλλαγή του πεδίου μαγνητικής πόλωσης. Η ακρίβεια αυτών των αισθητήρων εξαρτάται από τη γεωμετρία και την απόσταση μεταξύ του μαγνήτη και της γραμμής καθυστέρησης, προσφέροντας μικρές αποκλίσεις.

Επιπλέον, παρουσιάζονται αισθητήρες που βασίζονται στη μέτρηση του χρόνου καθυστέρησης του σήματος, όπου οι γραμμές καθυστέρησης επιτρέπουν την ανίχνευση θέσης με υψηλή ακρίβεια, έως και 10 μm. Αυτοί οι αισθητήρες είναι ανθεκτικοί στις περιβαλλοντικές επιδράσεις και κατάλληλοι για βιομηχανικές εφαρμογές, όπου η κίνηση της κεφαλής ανίχνευσης ή του μαγνήτη μπορεί να υπολογιστεί μέσω του χρόνου καθυστέρησης.

Τέλος, το κεφάλαιο συζητά τη χρήση περιφερειακών MDL σε συστήματα ανίχνευσης θέσης, όπου η παραγωγή αισθητήρων γίνεται με τεχνικές λεπτών υμενίων, προσφέροντας ευελιξία και οικονομία στην παραγωγή. Αυτοί οι αισθητήρες παρέχουν δυνατότητα μαζικής παραγωγής και εξαιρετική επαναληψιμότητα ιδιοτήτων, καθιστώντας τους κατάλληλους για ευρείες βιομηχανικές εφαρμογές.

Το κεφάλαιο συνοψίζει τις δυνατότητες των MDL να λειτουργούν ως αισθητήρες θέσης σε διάφορες εφαρμογές, από συστήματα χαμηλού κόστους έως συστήματα υψηλής ακρίβειας.

Το έκτο κεφάλαιο της διατριβής αφορά τους αισθητήρες τάσης που βασίζονται στις μαγνητοσυσταλτικές γραμμές καθυστέρησης (MDL), και εξετάζει διάφορες διατάξεις και τεχνολογίες για τη μέτρηση τάσης, εστιασμένες σε εφαρμογές όπως οι αισθητήρες εφελκυσμού, τα πιεσόμετρα και τα δυναμόμετρα. Η χρήση των MDL σε αυτές τις εφαρμογές προσφέρει σημαντικά πλεονεκτήματα, λόγω της υψηλής ευαισθησίας και της ακρίβειάς τους.

Στους αισθητήρες εφελκυσμού, οι οποίοι χρησιμοποιούνται για την ανίχνευση δυνάμεων τάσης σε υλικά, η αρχή λειτουργίας βασίζεται στην αλλαγή της τάσης εξόδου του MDL όταν το υλικό υφίσταται μηχανική καταπόνηση. Αυτές οι διατάξεις παρουσιάζουν ιδιαίτερη σημασία για εφαρμογές όπου απαιτείται υψηλή ακρίβεια στις μετρήσεις της τάσης, με λύσεις που ενισχύουν την ευαισθησία, όπως η χρήση χαμηλής συμμόρφωσης στη δομή της δέσμης.

Στους αισθητήρες πίεσης που βασίζονται σε MDL καταγράφουν πιέσεις σε διάφορα σημεία της διάταξης, καθιστώντας τα κατάλληλα για εφαρμογές στη βιομηχανική και δομική μηχανική, όπου η υψηλή ακρίβεια

στις μετρήσεις της πίεσης είναι κρίσιμη. Αυτή η τεχνολογία εξασφαλίζει την καταγραφή με ακρίβεια σε απαιτητικά περιβάλλοντα, συμβάλλοντας στην επίλυση μηχανικών προκλήσεων.

Παράλληλα, τα δυναμόμετρα και οι μετρητές ροπής που χρησιμοποιούν MDL για την καταγραφή δυνάμεων και ροπών αποτελούν αναπόσπαστο μέρος δοκιμών υλικών και μηχανικών εφαρμογών, όπου η ακρίβεια στη μέτρηση των δυνάμεων είναι απαραίτητη. Αυτά τα δυναμόμετρα επιτρέπουν την ακριβή αξιολόγηση των μηχανικών χαρακτηριστικών των υλικών σε βιομηχανικές και επιστημονικές εφαρμογές.

Συμπερασματικά, οι αισθητήρες που βασίζονται στις MDL προσφέρουν σημαντικά πλεονεκτήματα, όπως χαμηλό κόστος, υψηλή ευαισθησία και ακρίβεια, καθιστώντας τους ιδανικούς για πολλές εφαρμογές τόσο στη βιομηχανία όσο και στην έρευνα. Η ευελιξία αυτών των τεχνολογιών τις καθιστά κατάλληλες για πλήθος απαιτητικών εφαρμογών σε διαφορετικούς τομείς.

Το έβδομο κεφάλαιο της διατριβής ασχολείται με τους αισθητήρες πεδίου που βασίζονται στις μαγνητοσυσταλτικές γραμμές καθυστέρησης (MDL). Αυτοί οι αισθητήρες βασίζονται στην αρχή λειτουργίας των MDL, όπου η απόκριση της MDL μεταβάλλεται λόγω της παρουσίας μαγνητικού πεδίου. Οι αισθητήρες μπορούν να αναπτυχθούν σε διατάξεις μονοδιάστατων ή πολυδιάστατων συστοιχιών, επιτρέποντας τη μέτρηση της κατανομής ενός μαγνητικού πεδίου κατά μήκος ή σε περισσότερες διαστάσεις. Η τεχνική αυτή προσφέρει την δυνατότητα χαμηλής υστέρησης και ακριβούς ανίχνευσης, με ευαισθησία της τάξης του νανοτέσλα (nT).

Η βασική αρχή λειτουργίας ενός αισθητήρα μαγνητικού πεδίου περιλαμβάνει τη μετάδοση παλμικού ρεύματος μέσω ενός αγωγού τοποθετημένου κάθετα στην MDL. Το παλμικό ρεύμα παράγει μαγνητικό πεδίο που μετατρέπεται σε ελαστικό παλμό λόγω του φαινομένου μαγνητοσυστολής, και ανιχνεύεται από την MDL. Το πλάτος της ανιχνευόμενης τάσης εξόδου εξαρτάται από το μαγνητικό πεδίο, επιτρέποντας τη δημιουργία ενός αισθητήρα μαγνητικού πεδίου.

Οι αισθητήρες MDL μπορούν να διαμορφωθούν σε μονοδιάστατες ή πολυδιάστατες διατάξεις, χρησιμοποιώντας σειρά παλμικών αγωγών κάθετων στις MDL, δημιουργώντας έτσι μία σειρά ελαστικών παλμών που ανιχνεύονται από την MDL. Αυτή η τεχνολογία επιτρέπει τη μέτρηση μαγνητικών πεδίων σε πραγματικό χρόνο, προσφέροντας ευελιξία και ακρίβεια στις εφαρμογές όπου είναι απαραίτητη η ακριβής καταγραφή του πεδίου.

Συνολικά, το κεφάλαιο καταλήγει ότι οι αισθητήρες πεδίου MDL παρέχουν μοναδικές δυνατότητες στην ανίχνευση και καταγραφή μαγνητικών πεδίων, με δυνατότητες ανάπτυξης πολυδιάστατων συστοιχιών για πιο σύνθετες εφαρμογές.

Το όγδοο κεφάλαιο της διατριβής εστιάζει στις εφαρμογές των Μαγνητοσυσταλτικών Γραμμών Καθυστέρησης (MDLs) σε διάφορους τομείς, όπως η βιομηχανία, η βιοϊατρική μηχανική και η πολιτική μηχανική. Οι MDLs προσφέρουν καινοτόμες λύσεις σε θέματα ανίχνευσης, παρέχοντας υψηλή ευαισθησία και ακρίβεια σε κρίσιμες μετρήσεις.

Ένας από τους βασικούς τομείς εφαρμογής των MDLs είναι οι μη καταστρεπτικές δοκιμές (NDT), οι οποίες χρησιμοποιούνται για την ανίχνευση ελαττωμάτων σε υλικά. Μέσω ανάλυσης μαγνητικών ανωμαλιών και ρευμάτων δινορρευμάτων, οι MDLs μπορούν να ανιχνεύσουν ρωγμές και φθορές σε κατασκευές, όπως γέφυρες και τούνελ, επιτρέποντας τη συνεχή παρακολούθησή τους και την έγκαιρη συντήρηση. Στη βιοϊατρική και χημική μηχανική, οι MDLs βρίσκουν εφαρμογές στην ανίχνευση της πήξης του αίματος, καθώς και στον προσδιορισμό του χρόνου στερεοποίησης υγρών σε χημικές διαδικασίες. Οι MDL αισθητήρες παρέχουν ακριβείς μετρήσεις, επιτρέποντας την ανάπτυξη ιατρικών συσκευών και τη βελτίωση των χημικών διεργασιών. Στον τομέα της μηχανικής, οι MDLs χρησιμοποιούνται για την παρακολούθηση τάσεων και πιέσεων σε κατασκευές, όπως φράγματα και γέφυρες, προσφέροντας αξιόπιστες μετρήσεις σε πραγματικό χρόνο. Αυτές οι τεχνολογίες συμβάλλουν στην αποφυγή αστοχιών και στην έγκαιρη συντήρηση των κατασκευών.

Συνολικά, οι MDLs προσφέρουν πληθώρα εφαρμογών σε διάφορους τομείς, καθιστώντας τις μια ευέλικτη και αποδοτική τεχνολογία αισθητήρων για μη καταστρεπτικές δοκιμές, βιομηχανικές, βιοϊατρικές και αθλητικές εφαρμογές.



# List of Tables

---

<b>Table 5.1.</b> Range of acceleration due to displacement and time duration.	197
<b>Table 8.1.</b> Values of the coefficient $a$ of Figure 8.14.	278
<b>Table 8.2.</b> Comparison between MDL, B-H Loop and Eddy Current setups.	305



# List of Figures

---

<b>Figure 1.1.</b> Modes of propagation of domain walls. (a) Low energy walls (b) high energy walls	35
<b>Figure 1.2.</b> Irreversible and reversible rotation in magnetic domains. (a) Irreversible orientation along easy axis A or B, (b) Reversible small magnetization angle rotation (SMA).	37
<b>Figure 2.1.</b> The basic MDL arrangement. (1) Excitation coil, (2) Magnetostrictive delay line, (3) Search coil.	49
<b>Figure 2.2.</b> A typical $\sigma(H)$ function.	50
<b>Figure 2.3.</b> Microstrain with respect to space.	51
<b>Figure 2.4.</b> Propagating elastic pulse along the length of the MDL.	51
<b>Figure 2.5.</b> Voltage output with respect to time.	52
<b>Figure 2.6.</b> The detected MDL pulsed voltage output. The first impulse response is due to the pulsed excitation field. The main pulsed voltage output follows, with a characteristic amplitude $V_0$ . The small waveforms following the main pulsed output are reflections of the propagating elastic pulse at the ends of the magnetostrictive medium (Time units in seconds and voltage amplitude in Volts).	53
<b>Figure 2.7.</b> Comparison of experimental and theoretical data for biasing field using equation 1.1 to 1.5	56
<b>Figure 2.8.</b> Pulsed current conductor orthogonal to the MDL. (1) MDL, (2) Pulsed current conductor, (3) Search coil.	59
<b>Figure 2.9.</b> Short duration of the excitation field results in a single voltage output pulse.	61
<b>Figure 2.10.</b> Long duration of the excitation field results in two discrete voltage output pulses.	62
<b>Figure 2.11.</b> A pulsed current conductor array set orthogonal to an array of MDLs.	63
<b>Figure 2.12.</b> Two discrete pulses detected due to two, simultaneously excited pulsed current conductors.	64
<b>Figure 2.13.</b> Balanced current conductor MDL arrangement, (1), Pulsed current conductor, (2) MDL, (3) Search coil.	65
<b>Figure 2.14.</b> Array of balanced conductors on top and below and perpendicular to an array of MDLs.	66

<b>Figure 2.15.</b> Pair of pulsed current conductors, parallel to the MDL. (1) Pulsed current conductors, (2) MDL, (3) Conducting disk, (4) Search coil.	67
<b>Figure 2.16.</b> A two-dimensional digitiser based on the set-up shown in Figure 2.15. (1) MDL, (2) Pulsed current conductor, (3) Search coil, (4) Conducting disk	68
<b>Figure 2.17.</b> Pulsed current conductor – MDL – soft element set-up. (1) Pulsed current conductor, (2) MDL, (3) Soft magnetic element, (4) Magnetic anomaly or moving permanent magnet, (5) Search coil.	68
<b>Figure 2.18.</b> MDL with non-magnetic acoustic waveguide. (1) Magnetostrictive element used for generation of micro-strains, (2) Magnetostrictive element used for the detection of micro-strains, (3) Glass acoustic waveguide, (4) Pulsed current excitation coil, (5) Search coil, (6) Biasing coil at the region of excitation, (7) Biasing coil at the search region, (8) Arrangement support.	70
<b>Figure 2.19.</b> Typical output waveforms concerning the set-up of Figure 2.18, using magnetostrictive elements of different length L.	71
<b>Figure 2.20.</b> The basic idea for the coil-less MDL is to use the magnetostrictive material as part of the current conducting path.	73
<b>Figure 2.21.</b> The coil-less MDL set-up. (1) Magnetostrictive element for microstrain generation. (2) Acoustic waveguide (for example glass), (3) Magnetostrictive element for microstrain detection, (4) Pulsed current conductor, (5) Detecting conductor.	75
<b>Figure 2.22.</b> The coily MDL set-up. (1) Pulsed current conductor, (2) Solenoid-like MDL, (3) Search coils, (4) Peak and hold electronics.	76
<b>Figure 2.23.</b> The schematic and the magnetization process of the circumferential MDL arrangement.	80
<b>Figure 2.24.</b> The magnetoelastic operation of the circumferential MDL arrangement.	82
<b>Figure 3.1.</b> Typical MDL dependence on pulsed field.	87
<b>Figure 3.2.</b> Typical hysteretic MDL response of polycrystalline Fe, Ni and FeNi wires, after heat treatment.	87
<b>Figure 3.3.</b> A typical improvement of the MDL response of FeSiB amorphous ribbon after thermal and field annealing.	89

<b>Figure 3.4.</b> Typical MDL waveform outputs under various biasing fields. Left waveform corresponds to co directional bias and pulsed fields. Right picture illustrates opposing bias and pulsed fields. Horizontal axis corresponds to time.	90
<b>Figure 3.5.</b> Typical MDL dependence on dc biasing field for heat treated amorphous Fe-rich wire.	91
<b>Figure 3.6.</b> Analysis of the biasing field effect.	92
<b>Figure 3.7.</b> Typical MDL dependence on the pulsed excitation field for a Ni wire after field annealing in 300°C for 1 hr under 1 kA/m and Ar atmosphere.	93
<b>Figure 3.8.</b> Typical frequency MDL response concerning as-cast Fe, Ni and Fe-Ni wires.	94
<b>Figure 3.9.</b> Typical response of the MDL dependence on applied load under various amplitudes of simultaneously applied biasing field.	95
<b>Figure 3.10.</b> Typical temperature response of MDLs, for Fe, Ni and FeNi polycrystalline wires.	95
<b>Figure 3.11.</b> The computerized set-up for the characterization of magnetostrictive fibres. (1) Magnetoelastic sample, (2) search coil, (3) biasing coil for the search coil, (4) excitation coil, (5) biasing coil for the excitation coil, (6) mechanical terminations of the sample, (7) step motor for torsion on the sample, (8) step-motor and micro-positioner for tensile stress on the sample, (9) step-motor and linear translator for coil displacement, (10) arbitrary waveform generator, (11) RF amplifier, (12) digital oscilloscope, (13) computer, (14) triple power supply.	98
<b>Figure 3.12.</b> The MDL characterization system.	99
<b>Figure 3.13.</b> Experimental set-up for the measurement of the magnetoelastic uniformity. (1) MDL support, (2) fixed support, (3) exciting coil, (4) optic bench, (5) movable support, (6) detector coil, and (7) pair of coils for applying dc bias field.	100
<b>Figure 3.14.</b> Typical $V_o(x)$ response concerning an as-cast tested amorphous $Fe_{78}Si_7B_{15}$ ribbon.	101
<b>Figure 3.15.</b> $V_o(x)$ response of amorphous $Fe_{78}Si_7B_{15}$ ribbon after 1 hr heating in 350°C under Ar atmosphere.	102
<b>Figure 3.16.</b> $V_o(x)$ response of amorphous $Fe_{78}Si_7B_{15}$ ribbon after 1 hr field annealing in 350°C and 800 A/m under Ar atmosphere.	102
<b>Figure 3.17.</b> Uniformity of an as cast amorphous wire delay line.	104
<b>Figure 3.18.</b> Uniformity of the line after stress relief process.	104
<b>Figure 3.19.</b> Uniformity of a stress-current annealed amorphous wire delay line.	105

<b>Figure 3.20.</b> Arrangement of the device. (1) Magnetostrictive delay line (MDL), (2) Exciting coil, (3) Receiving coil, (4) Long, short-circuited coil, (5) Applied weight on the MDL, (6) Current amplifier.	106
<b>Figure 3.21.</b> Fast MEU response of amorphous wire (horizontal axis in time).	107
<b>Figure 3.22.</b> Fast MEU response of amorphous ribbon (horizontal axis in time).	108
<b>Figure 3.23.</b> Fast MEU response in a twisted amorphous wire (horizontal axis in time).	108
<b>Figure 3.24.</b> Electronic experimental set-up for the sound velocity measurements. (1) MDL, (2) Excitation coil, (3) Search coil, (4) Biasing coil, (5) Electrical conducts for current passing through the MDL, (6) Applied load on the MDL, (7) Optic bench, (8-18) Electronics for excitation and delay time measurement.	111
<b>Figure 3.25.</b> The dependence of the longitudinal sound velocity on the biasing field in $Fe_{77.5}Si_{7.5}B_{15}$ amorphous wire tested in the as-cast state (bold circles) and after stress-relief process at 330°C (white triangles) and 370°C (black triangles) for 45 min and 15 min respectively.	113
<b>Figure 3.26.</b> The longitudinal sound velocity dependence on the bias magnetic field, for $Fe_{77.5}Si_{7.5}B_{15}$ amorphous wire tested after stress-relief process at 370°C for 15 minutes tested under 0 (black circles), 1.6 (white points), 5.7 (Black triangles) and 12 MPa (white triangles) applied tensile stress.	114
<b>Figure 3.27.</b> The dependence of the longitudinal sound velocity on the applied tensile stress for $Fe_{77.5}Si_{7.5}B_{15}$ amorphous wire tested after stress-relief process at 370°C for 15 minutes, under 0 A/m (black circle) and 90 A/m (white triangle) bias magnetic field.	115
<b>Figure 3.28.</b> The MDL resolution is defined as the minimum distance between two consequent excitation points in order to detect two distinct voltage pulses. (1) MDL, (2) Search coil, (3) and (4) Pulsed current conductors. In most crystalline MDLs such a distance is 80 mm.	117
<b>Figure 3.29.</b> The effect of stress current annealing on the MDL pulsed voltage output dependence on the applied excitation current.	118
<b>Figure 3.30.</b> The dependence of the voltage output $V_o$ on the pulsed current width $T$ .	119
<b>Figure 3.31.</b> The dependence of the MDL resolution on the number of turns of the receiving coil.	120

<b>Figures 3.32.</b> The dependence of the amplitude of the voltage output $V_o$ on the number of turns of the receiving coil.	121
<b>Figures 3.33.</b> Optimized MDL output with respect to the excitation pulse (y-axis in mVolts and x-axis in $\mu\text{s}$ ).	121
<b>Figure 3.34.</b> The MDL impulse response, for different pulse widths and amplitudes (y-axis in mVolts, x-axis in $\mu\text{s}$ ). (a) $H=0.8$ A/m, (b) $H=1.6$ kA/m, (c) 2.4 kA/m.	122
<b>Figure 4.1.</b> Microcracks on the surface of a magnetostrictive material prohibit the propagation of elastic waves.	123
<b>Figure 4.2.</b> Scattering centers cause reflections and magnetoelastic non-uniformity.	124
<b>Figure 4.3.</b> Absence of defects results in a significant improvement of non-uniformity.	124
<b>Figure 4.4.</b> Shape induced anisotropy may occasionally help the improvement of the magnetoelastic properties.	125
<b>Figure 4.5.</b> TEM diffraction pattern (left) suggests amorphous phases in Fe-rich ribbons, accompanied by repeatable and unhysteretic MDL response. Even partial nano-crystalline ribbon (right) resulted in small and hysteretic MDL response.	128
<b>Figure 4.6.</b> Nano-crystalline Fe-rich alloys cannot operate as MDLs due to the very small $\partial(H)$ function mainly due to the co-existence of positive and negative magnetostrictive phases.	128
<b>Figure 4.7.</b> A typical dependence of the MDL response $V_o$ on the applied pulsed field $H_e$ .	131
<b>Figure 4.8.</b> Longitudinal sound velocity dependence as-cast (a) and heat treated (300°C for 1 hr in Ar atmosphere) amorphous ribbons.	133
<b>Figure 4.9.</b> Typical absolute amplitude MDL voltage output dependence on the applied biasing field at the excitation (a) and search (b) regions, concerning as-cast amorphous Fe-rich ribbon. Measurements have been realized by exciting with pulsed excitation field $H_e$ 200 A/m (white triangles), 400 A/m (circles) and 600 A/m (black triangles).	135
<b>Figure 4.10.</b> Pulse width dependence of the MDL for as-cast amorphous ribbons under different excitation currents.	136
<b>Figure 4.11.</b> MDL voltage output dependence on biasing field, concerning as-cast Fe-rich amorphous wires. The presence of the large Barkhausen jump can be observed.	137
<b>Figure 4.12.</b> Stress dependence of amorphous wires used as MDLs.	138
<b>Figure 4.13.</b> Torsion dependence of amorphous wires used as MDLs.	139

<b>Figure 4.14.</b> Sound velocity dependence of $\text{Fe}_{78}\text{Si}_7\text{B}_{15}$ of as-cast (a) and stress-relieved (b) wires.	139
<b>Figure 4.15.</b> Pulsed current width normalized MDL response in amorphous as-cast wires.	140
<b>Figure 4.16.</b> Magnetoelastic uniformity response for a glass removed CGA wire by chemical etching.	143
<b>Figure 4.17.</b> MDL voltage output dependence on the pulsed exciting current field for the GCA wire.	144
<b>Figure 4.18.</b> The MDL dependence of $V_o$ on the bias field at the region of excitation.	144
<b>Figure 4.19.</b> Magnetoelastic uniformity response for a complete glass removal GCA wire.	145
<b>Figure 4.20.</b> Pulsed width response of GCA wires.	147
<b>Figure 4.21.</b> Magnetoelastic uniformity in as-cast ribbons, wires and high frequency annealed glass covered wires.	147
<b>Figure 4.22.</b> The configuration of the thin film MDL.	149
<b>Figure 4.23.</b> The 6 miniature MDLs silicon wafer schematic.	150
<b>Figure 4.24.</b> The process sequence in the miniature MDL fabrication.	151
<b>Figure 4.25.</b> The linear longitudinal and transverse magnetostriction of Ni and $\text{Fe}_{70}\text{Si}_6\text{B}_{20}\text{C}_4$ alloy films.	152
<b>Figure 4.26.</b> Thin film MDL output dependence on pulsed excitation current.	153
<b>Figure 4.27.</b> Thin film MDL output dependence on the displacement of a $\text{Nd}_1\text{Fe}_{12}\text{B}_1$ permanent	153
<b>Figure 4.28.</b> MDL thin film using MR element as search means. (a) Top view, (b) Side view. (1) Substrate or wafer, (2) Insulating layer, (3) $\text{Fe}_{70}\text{B}_{15}\text{Si}_{15}$ thin film, (4) Cu thin film acting as pulsed current conductor, (5) insulating layer, (6) Three-layered MR structure, (7) $\text{Fe}_{70}\text{B}_{15}\text{Si}_{15}$ thin film operating as MDL medium.	154
<b>Figure. 4.29.</b> A thin film arrangement using an electrostrictive delay line, coupled with magnetostrictive material.	154
<b>Figure 4.30.</b> Operation of the SAW based thin film. (a) Operation of the electrostrictive delay line coupled with a magnetostrictive material, (b) effect of biasing field in the arrangement, (c) effect of applied load on the arrangement.	155
<b>Figure 4.31.</b> Stress dependence of Fe, Ni and Fe-Ni polycrystalline wires after flash annealing. Ni wire illustrated the expected increasing response, as negative magnetostrictive material.	157

<b>Figure 4.32.</b> Applying pressure on a negative magnetostrictive MDL under various pulsed excitation currents $I_e$ results in a decrease of the MDL output: the MDL acts as acoustic waveguide.	158
<b>Figure 4.33.</b> Applying tensile stress on a negative magnetostrictive MDL results in an increase of the MDL output.	158
<b>Figure 5.1.</b> Moving magnet displacement sensor causes change of the elastic pulse at the excitation region. (1) MDL, (2) Excitation coil, (3) Search coil, (4) Moving magnet.	163
<b>Figure 5.2.</b> Distribution displacement sensor based on the sensing element of Figure 5.1. (1) MDL, (2) Array of pulsed current conductors, (3) Search coil, (4) Array of moving magnets.	164
<b>Figure 5.3.</b> Moving magnet on top of the search coil changes permeability and flux at the measurement region. (1) MDL, (2) Excitation coil, (3) Search coil, (4) Moving magnet.	165
<b>Figure 5.4.</b> Distribution displacement sensor based on the sensing element of Figure 5.2. (1) MDL, (2) Array of pulsed current conductors, (3) Search coil, (4) Array of moving magnets.	165
<b>Figure 5.5.</b> Response of the sensor of Figure 4.1 using as-cast amorphous $Fe_{78}Si_7B_{15}$ ribbons.	167
<b>Figure 5.6.</b> Response of the sensor of Figure 4.3 using as-cast amorphous $Fe_{78}Si_7B_{15}$ ribbons.	167
<b>Figure 5.7.</b> Response of the sensor of Figure 4.1 using FeCoCrSiB wire as MDL.	169
<b>Figure 5.8.</b> Response of the sensor of Figure 4.3 using FeCoCrSiB wire as MDL.	169
<b>Figure 5.9.</b> A 3-dimensional digitizer based on the sensor of Figure 4.1.	170
<b>Figure 5.10.</b> Moving either the excitation or the search coil results in a change of the MDL voltage output delay time. (1) MDL, (2) Excitation coil, (3) Search coil.	171
<b>Figure 5.11.</b> Moving magnet position sensor based on the delay time of the MDL output due to the displacement of the magnet along the long search coil. (a) the schematic operation, (b) a rather industrial schematic, representing the sensor structure. (1) MDL, (2) Excitation coil, (3) Search coil, (4) Moving permanent magnet.	173
<b>Figure 5.12.</b> The position sensor. (1) Magnetostrictive delay line, (2) Excitation coil, (3) Array of search coils, (4) Moving magnet, (5) Application specific circuit, (6) Excitation circuit, (7) Analogue amplifier, (8) Oscillator/counter, (9), Analogue to digital converter.	175
<b>Figure 5.13.</b> A typical response of the sensor illustrated in Figure 4.12.	176
<b>Figure 5.14.</b> Circumferential MDL and corresponding delay-time based moving magnet position sensor.	178

<b>Figure 5.15.</b> The schematic of the new position sensor. (1) Magnetostrictive delay line (MDL), (2) Pulsed current conductors, (3) Conducting connector for the pulsed current conductors, (4) Search coil, (5) Soft magnetic material, (7) Movable permanent magnet, (9) Conducting connection for the pulsed current conductor connection on the electronic board, (10a) Electronic pulsed current generation circuit, (10b) Electronic received signal conditioning circuitry, (11) ASIC integrating circuit for (10a) and (10b), (12) DC power supply pins, (13) Pins for the transmission of the conditioned signal out of the sensor, (14) Pins for the delivery of the searched signal from the search coil, (15) Pins for the pulsed current transmission to the pulsed current conductors. (A) Electromechanical part of the position sensor, named sensing element, including the MDL, pulsed current conductors, soft magnetic ribbon and insulating (preferably plastic) film separators, (B), Sensor electronic board including pulsed current conductor connection, search coil, pulsed current generation circuit and received signal conditioning circuitry and (C) Termination of the position sensor, hosting the conducting connector for the pulsed current conductors covering the end of the MDL.	180
<b>Figure 5.16.</b> Cross section of the sensing element including the permanent magnet acting as sensing core. (1) Magnetostrictive delay line (MDL), (2) Pulsed current conductor, (5) Soft magnetic material, (6) Foam holding the MDL in position without attenuating the propagating elastic pulse, (7) Movable permanent magnet, (8), Insulating (plastic) film separator.	181
<b>Figure 5.17.</b> The set-up used for the determination of most of the developed position sensors.	183
<b>Figure 5.18.</b> Field dependence of the sensor using amorphous FeSiB and Fe crystalline wires.	185
<b>Figure 5.19.</b> Sensor voltage output dependence on temperature concerning amorphous $Fe_{78}Si_7B_{15}$ MDL and $Ni_3Fe$ polycrystalline ribbon.	186
<b>Figure 5.20.</b> Sensor voltage output dependence on temperature concerning polycrystalline Fe MDL and $Ni_3Fe$ polycrystalline ribbon.	186
<b>Figure 5.21.</b> Uncertainty measurement of the position sensor using as-cast amorphous $Fe_{78}Si_7B_{15}$ wire and magnetically annealed $Ni_3Fe$ polycrystalline ribbon.	187
<b>Figure 5.22.</b> Application of the sensor in measuring position, velocity and acceleration of a moving pneumatic piston, with respect to a steady position sensor. (1) Moving permanent magnet at the end of the moving piston, (2) Moving piston, (3) Groove able to hold the sensor and the electronic board.	187

<b>Figure 5.23.</b> Application of the sensor in measuring the absolute ground velocity of a moving magnetic body, with respect to a steady position sensor. (1) Moving magnetic body parallel to the position sensor with velocity $v$ , which is measured by the position sensor. (A) Position sensing element, (B) Sensor electronic board.	188
<b>Figure 5.24.</b> Application of the sensor in measuring the absolute ground velocity of a moving object with respect to a not moving permanent magnet. (1) Permanent magnet fixed in position, (2) Moving object parallel to the permanent magnet fixed in position with velocity $v$ , carrying the position sensing element (A) and its electronics (B).	189
<b>Figure 5.25.</b> Application of the sensor in measuring liquid level. (1) Permanent magnet on top of liquid, (2) Tank with liquid, (3) Surface of liquid of the tank, (4) Floater on top of liquid. (A) Position sensing element.	190
<b>Figure 5.26.</b> Accelerometer schematic arrangement. (1) Magnetostrictive delay line, (2) Glass substrate, (3) Detecting coil, (4) Permanent magnet, (5) Pulsed voltage integrator, (6) Field screening soft magnetic material.	196
ie response of the sensor.	198
<b>Figure 5.28.</b> Temperature dependence of the accelerometer.	199
<b>Figure 5.29.</b> Accelerometer output dependence with (a) and without (b) magnetic shielding.	199
<b>Figure 5.30.</b> Accelerometer output response dependence on the maximum displacement of the moving magnet.	200
<b>Figure 5.31.</b> Measuring the displacement of soft magnetic materials. (1) Soft magnetic core, (2) MDL, (3) Pulsed current conductor, (4) Search coil.	202
<b>Figure 5.32.</b> Response of the sensing elements illustrated in Figure 4.31.	204
<b>Figure 5.33.</b> Response of the sensing element shown in Figure 4.31d under various distances of the sensing cores.	205
<b>Figure 5.34.</b> Basic diagram of the absolute and incremental angular position sensor working according to the MDL principle. (1) MDL, (2) Search or Receiving coil, (3) Balanced pulsed current conductors, (5) Soft magnetic tape.	207
<b>Figure 5.35.</b> The response of the absolute and incremental angular position sensor.	208
<b>Figure 5.36.</b> A 2-dimensional tactile array based on the sensing principles demonstrated in Figure 5.31.	208

<b>Figure 5.37.</b> Arrangement of the moving conducting disk position sensor. (1) MDL, (2) Pulsed current conductor, (3) Receiving coil, (4) Moving conducting disk.	210
<b>Figure 5.38.</b> The response of the sensor moving conducting disk position sensor.	211
<b>Figure 5.39.</b> A two - dimensional digitiser based on the MDL technique and the displacement of a conducting disk. (1) MDL, (2) Pulsed current conductor, (3) Receiving coil, (4) Moving disk.	211
<b>Figure 6.1.</b> The schematics of various tensile stress sensing arrangements. (1) Sensing core, (2) MDL, (3) Pulsed current conductor, (4) Search coil.	214
<b>Figure 6.2.</b> Typical response of the tensile stress sensing arrangements illustrated in Figure 6.1.	217
<b>Figure 6.3.</b> A low compliance beam structure force sensor. (1) MDL, (2) and (3) Ribbon sensing cores to be stressed and compressed respectively, (4) 1.5 mm thick non magnetic support of the sensing cores, (5) Three-layer support for the MDL, (6) Beam support.	219
<b>Figure 6.4.</b> The response of the sensor of Figure 5.3, using Vitrovac 7605 magnetoelastic ribbon.	221
<b>Figure 6.5.</b> Basic diagram of a two-dimensional discrete force sensor. (1) MDL (2) Pulsed current conductor. (3) Point of applied force F (4) Active core.	221
<b>Figure 6.6.</b> Sensor arrangement. (a) Discrete tensile stress sensor; (b) one-dimensional sensing array. (1) MDL, (2) Pulsed current conductors, (3) MDL 3. Delay line support, (4) Search or receiving coil, (5) Epoxy glass ribbons, used as supports of the active core, (6) Copper for soldering the active core, (7) Active core.	223
<b>Figure 6.7.</b> Basic procedure for manufacturing the beam force sensor. (1) 1.5 mm thick fiber glass bar orthogonal to the delay line, (2) 0.1 mm thick fiber glass planes, (3) 0.1 mm thick fiber glass bars for making the MDL channels, (4) Fiber glass bars parallel to the MDL, (5) MDL, (6) Compressible ribbon, (7) Stressable ribbon.	223
<b>Figure 6.8.</b> The basic principle of the MDL pressure gauge.	225
<b>Figure 6.9.</b> Response of the MDL pressure gauge.	226
<b>Figure 6.10.</b> A pressure distribution sensor based on the MDL pressure gauge. (1) MDL, (2) Search coil, (3) Pulsed current conductor.	228
<b>Figure 6.11.</b> Schematic of the force digitizing sensing element.	231

<b>Figure 6.12.</b> The reflection response on force of the force digitizing sensing element of Figure 6.11.	233
<b>Figure 6.13.</b> Force digitizing array sensor. (1) MDL, (2) Pulsed current conductor.	234
<b>Figure 6.14.</b> Detail of the sensing element of the digitizer: ( 1) MDL, (2) MDL substrate, and (3) substrate used to apply transform pressure to the line.	235
<b>Figure 6.15.</b> Schematic of the load cell and torque meter sensing element.	238
<b>Figure 6.16.</b> Operation of the load cell (a) and torque meter (b).	240
<b>Figure 6.17.</b> Load response of amorphous Fe-rich wires after different treatment.	242
<b>Figure 6.18.</b> Dependence of the MDL pulsed voltage output $V_o$ on the applied stress using amorphous ribbon, wire and glass covered wire.	243
<b>Figure 6.19.</b> A typical MDL response on the applied torsion using amorphous wire.	243
<b>Figure 6.20.</b> Dependence of the MDL voltage output $V_o$ on the applied torsion using amorphous wire and glass covered wire.	244
<b>Figure 6.21.</b> Schematic of the thin film thickness sensor based on the MDL technique. (1) Magnetostrictive element, (2) Glass substrate, (3) Current conductors at the excitation region, (4) Silver paint, (5) Current conductors at the sensing region, (6) Pulse generator, (7) Oscilloscope, (8) PC.	247
<b>Figure 6.22.</b> The response of the sensor of Figure 6.21.	249
<b>Figure 7.1.</b> MDL output waveform change with applied bias field at the receiving coil, using amorphous wire. Numbers from 1 to 10 indicate the amplitude of the applied bias field opposing the pulsed excitation field multiplied by 100 A/m.	253
<b>Figure 7.2.</b> MDL voltage output dependence on dc bias field applied at the excitation (a) and search region (b).	254
<b>Figure 7.3.</b> MDL field sensor response using amorphous ribbon in the as-cast form and after annealing.	255
<b>Figure 7.4.</b> MDL field sensor response using amorphous ribbon after stress-current annealing and various excitation currents.	255
<b>Figure 7.5.</b> A long coil MDL array field sensor.	256
<b>Figure 8.1.</b> A single point field sensor for magnetic anomaly non-destructive testing.	261
<b>Figure 8.2.</b> A magnetic anomaly distribution sensor.	262
<b>Figure 8.3.</b> Magnetic anomaly NDT sensor based on the arrangement of Figure 2.20.	263

<b>Figure 8.4.</b> A typical response of the sensor of Figure 7.3 in measuring width and depth of cracks as well as diameter of holes in metallic surfaces.	264
<b>Figure 8.5.</b> Detecting cracks on a metallic surface using a combination of MDLs and eddy currents.	265
<b>Figure 8.6.</b> Operation of the sensor of Figure 8.5	266
<b>Figure 8.7.</b> Response of the sensor based on Figure 8.4, concerning aluminum artificial defects. Different voltage outputs at the same delay time or artificial defects, correspond to different excitation current $I_e$ .	267
<b>Figure 8.8.</b> Arrangement based on the sensor of Figure 5.1c, used for permeability measurement. (1) MDL, (2) Pulsed current conductors, (3) Search coil, (4) Reference soft ferromagnetic material, (5) Under test ferromagnetic surface.	268
<b>Figure 8.9.</b> Typical MDL voltage dependence on the permeability of ferritic steel.	268
<b>Figure 8.10.</b> The coagulation-sensing element.	272
<b>Figure 8.11.</b> Overcoming the problem of mass quantity.	274
<b>Figure 8.12.</b> The schematic of the experimental set-up for the blood coagulation measurement.	276
<b>Figure 8.13.</b> A typical dependence of the MDL pulsed voltage output on coagulation time.	277
<b>Figure 8.14.</b> MDL pulsed voltage output dependence on coagulation time.	277
<b>Figure 8.15.</b> Typical distortion of the MDL output waveforms with curing time.	279
<b>Figure 8.16.</b> Typical dependence of the MDL pulsed voltage output on the curing of the above mentioned liquids.	280
<b>Figure 8.17.</b> Correlation between exponential coefficient $a$ and the index of diabetes measured in blood.	282
<b>Figure 8.18.</b> Measuring blood coagulation using reflections of the MDL set-up.	283
<b>Figure 8.19.</b> Reflection based blood coagulation time measurement.	283
<b>Figure 8.20.</b> Dependence of the MDL reflection amplitude of time, during blood coagulation.	284
<b>Figure 8.21.</b> Schematic of the tensile stress sensor.	285
<b>Figure 8.22.</b> A cordless arrangement of the tensile stress sensor.	285
<b>Figure 8.23.</b> A typical response of the tensile stress sensor, for different pulsed excitation current amplitudes.	286

<b>Figure 8.24.</b> MDL output dependence on the distance between tensile stress sensing core and MDL set-up.	286
<b>Figure 8.25.</b> Response of the tensile stress sensor concerning various gaps of sensing core and MDL.	287
<b>Figure 8.26.</b> The sensor arrangement. (a) Schematic of the sensor, (b) Details of the pair of conductors: (1) array of parallel conductors sandwich, (2) rechargeable battery, (3) MDL, (4) search coil, (5) ground of current conductors, (6) long jump field, (7) insulating soft plastic springs, and (8) MDL support.	289
<b>Figure 8.27.</b> Acoustic dispersion in as-cast wires (rectangles) and ribbons (rhombs).	291
<b>Figure 8.28.</b> Acoustic attenuation in as-cast wires (rectangles) and ribbons (rhombs).	292
<b>Figure 8.29.</b> Acoustic dispersion in annealed wires (rectangles) and ribbons (rhombs).	292
<b>Figure 8.30.</b> Acoustic attenuation in annealed wires (rectangles) and ribbons (rhombs).	292
<b>Figure 8.31.</b> The uncertainty of our sensing system with respect to classical metric measurement.	293
<b>Figure 8.32.</b> Permeability (a) and magnetization loops (b) concerning $Fe_{78}Si_7B_{15}$ amorphous wire after stress-current annealing.	294
<b>Figure 8.33.</b> Permeability (a) and magnetization loops (b) concerning $Fe_{78}Si_7B_{15}$ amorphous ribbon after thermal annealing.	295
<b>Figure 8.34.</b> Normalized MDL response on biasing field at the excitation point (a) and integration of the MDL voltage output corresponding to the dc $\lambda$ -H loop (b).	296
<b>Figure 8.35.</b> Normalized $V_o/H_e$ MDL response on the pulsed field (a) and integration of $V_o/H_e$ corresponding to the ac $\lambda$ -H loop (b).	296
<b>Figure 8.36.</b> The schematic of the classic MEU instrument. The 5-turn excitation coil (1) was used to generate the elastic pulse, while the 300-turn search coil (2), developed on top of two substrates (3). The search coil was sliding on the under test cylinder (4), while its peak pulsed voltage output was monitored.	299
<b>Figure 8.37.</b> The schematic of the sound velocity instrument. The assembly of the excitation (1) and search (2) coils, fixed at a distance of 70 mm between them, developed on a single substrate, was sliding along the length of the magnetostrictive tube (4), measuring the delay time between the excitation and the voltage output pulse.	299
<b>Figure 8.38.</b> A typical pulsed voltage output of the search coils of Figures 8.36 and 8.37. The time scale (X-axis) is in seconds and the voltage scale is in Volts.	300

<b>Figure 8.39.</b> The schematic of the fast MEU instrument. The 5-turn excitation coil (1) was used to generate the elastic pulse, while the two-layer 900 mm long search coil (2), developed on top of a long substrate was steady in position, to test without moving the under test cylinder (4).	301
<b>Figure 8.40.</b> Response of the classic MEU instrument, illustrating the dependence of the pulsed voltage output of the search coil on the distance from the excitation coil. The effect of the two artificially made stress fields at a 40 cm distance between each other is clearly observable. After overpassing each stress field, the amplitude of the propagating elastic pulse decreases due to reflections at the stress field area.	301
<b>Figure 8.41.</b> Response of the sound velocity instrument, illustrating the dependence of the delay time excitation and detected pulse, corresponding to the change of sound velocity of the material, since the two coils are fixed in position. No damping effect is observable, as expected.	302
<b>Figure 8.42.</b> Response of the fast MEU instrument, illustrating the dependence of the pulsed voltage output of the search coil on the distance from the excitation coil. The response is similar to the response of the classic MEU, without sliding need of the search coil.	303
<b>Figure 8.43.</b> The schematic of the B-H loop and eddy current instrument. The 300-turn secondary coil (1) was developed directly on top of the plastic substrate (2), while the three-times longer excitation coil (3) was on top of the search coil. The assembly was sliding on the under test cylinder or tube (4), while the peak voltage output of the secondary coil was monitored.	304
<b>Figure 8.44.</b> B-H loop response	305
<b>Figure 8.45.</b> Eddy current response	305

# 1 Magnetic effects in sensing

Sensors and transducers have an increasing interest because of their importance in many technological applications [1]. All modern vehicles and transportation means use a vast variety of sensors and transducers, thus allowing a safer and more comfortable way of driving and commuting. The operation of all medical instruments is based on sensors. Industry is also employing more and more transducers for the monitoring and control of production lines.

In the literature, sensors have been categorized in several ways [2]. In the present work, they are categorized according to the following three principles: the first one is the subject of measurement, the most significant divisions being physical and chemical sensors; the second principle concerns the physical phenomenon and material on which the operation of the sensor is based, the main categories being conducting, semiconducting, dielectric, magnetic and superconducting sensors; and the third one concerns their applications, the main categories being industrial, transportation, automotive, medical, military, domestic and environmental sensors.

Magnetic sensors play a significant role in physical measurements used in all kinds of applications [3,4]. The most often used magnetic phenomena in today's magnetic sensor technology are the magneto-resistance [5], the magneto-impedance [6], the magnetostriction [7], the electromagnetic induction [8] and the Hall effect [9]. The dynamics of magnetic domains is the main mechanism responsible for magnetic effects used in sensing applications [10]. Any possible use of the dynamic response of this mechanism can result in a sensing element. There are two distinct cases of domain dynamics, one of which is the domain wall dynamics and the other one the domain rotation dynamics. There also exist dependent effects derived from these dynamics, both macroscopic and microscopic.

Magnetostriction, a particular effect in magnetic materials, has been thoroughly investigated in terms of theory and modeling as well as in terms of experimental details and applications [11-16]. The theory of magnetostriction is mainly based on the principles of micromagnetics [17]. The applications concern

sensors and actuators, requiring materials of engineering magnetostriction constant in the order of 10 ppm and 1000 ppm, respectively.

A technique that utilizes the magnetostriction effect in the design and development of sensors measuring displacement, stress and field is the magnetostrictive delay line (MDL) technique [18], analyzed in this Thesis. In this work, the main topologies, properties and materials based and used in the MDL technique as well as their sensing applications are presented. The promising results of these sensors in industrial, automotive and military applications make them attractive in terms of sensitivity, uncertainty and cost.

The main magnetic effects used in sensing are based on domain wall and domain rotation dynamics as well as the macroscopic and microscopic mechanisms dependent on domain dynamics. These effects are briefly presented bearing in mind that a key parameter in magnetic sensors is the hysteresis in their response. Hysteresis should be negligible in applications like mechanical and field sensors in order to improve the uncertainty level of the sensors, but it should be heavily present in applications like security sensors to improve the stability of the stored information.

---

## **1.1**     *Domain wall dynamics.*

---

The dynamics of domain walls and their corresponding use in sensor applications concern their nucleation and mobility or propagation in the magnetic substance [19]. There are two mechanisms of domain wall propagation, namely the bowing process and the parallel motion of the domain walls. The mode of propagation depends on the energy stored in these walls. Low energy walls propagate through the bowing process as shown in Figure 1.1a while high energy walls propagate more rigidly as shown in Figure 1.1b. The bowing process is more likely to occur in soft magnetic materials, which are low pinning materials, while the more rigid motion occurs in the harder ones. The reversibility of the domain wall propagation determines the presence or not of hysteresis in the phenomenon used in the sensing element and depends mainly on the defects in the magnetic substance and the pinning effect of magnetic dipoles. Domain wall dynamics are used for small field measurements as well as for mechanical sensors based on small field measurements [20].

Therefore, the sensor designer using domain wall dynamics should tailor the magnetic material with respect to the application in request. If the case is a sensor based on domain wall propagation with hysteresis in the minimum possible amplitude, the material should include as less defects as possible and be as soft as possible. This may be controlled through the composition of the material, as well as through annealing of the material in order to minimize the internal stresses generated by the above-mentioned defects, targeting coercive fields of the order of 1 A/m [21].

In this case, the material should have low magnetostriction and correspondingly low magneto-elastic response to avoid cross-talk with possibly uncontrollable stray magneto-elastic waves. One can fulfil both requirements by using FeCoSiB wires of magnetostriction in levels of 0.1 ppm, after thermal annealing and sometimes magnetic field annealing [22], while using a magnetostrictive substance may result in high levels of Barkhausen noise. Typical annealing conditions are of the order of 30-60°C /min for the rising temperature, steady state conditions of 300°C - 750°C for 10 – 60 minutes and finally slow cooling in Ar atmosphere for about 12-24 hours.

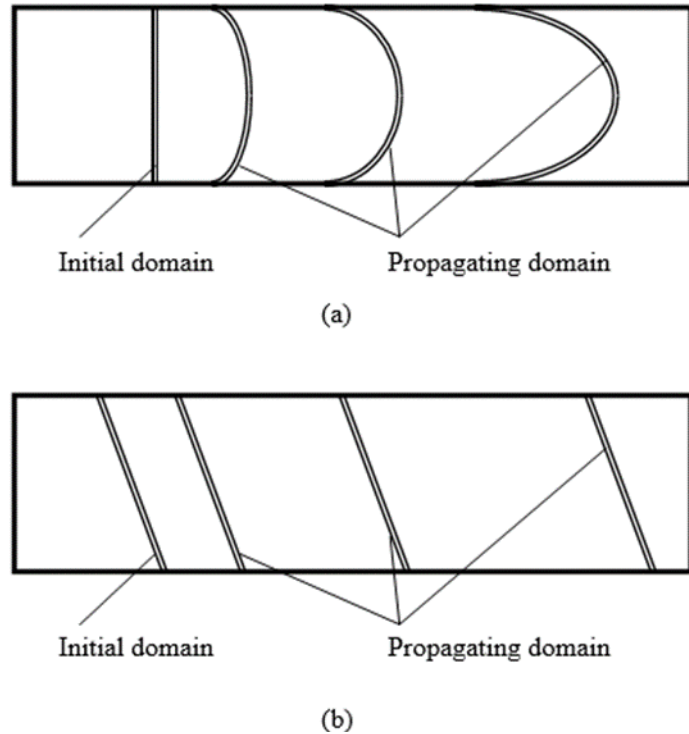


**Figure 1.1.** Modes of propagation of domain walls. (a) Low energy walls (b) high energy walls

Typical field conditions during annealing are 800 – 8000 A/m. Another technique also used in the material tailoring is the stress – current annealing, with typical values of tensile stress and current of 100 – 500 MPa and 100 – 300 mA respectively [23]. On the contrary, in security sensors the pinning defects or the controllable introduction of defects on the surface of the material can result in a significant improvement of the sensor stability.

---

## 1.2 *Domain rotation dynamics.*

---

Domain rotation dynamics have two distinct areas of operation, the irreversible and the reversible area [24]. Irreversible rotation occurs when the magnetic domains, oriented along a given easy axis A, re-orient along another easy axis B, closer to the axis of the external field H, because of the presence of this field, as shown in Figure 1.2a. Reversible domain rotation occurs after the irreversible rotation process has taken place. Since the new easy axis B is, in general, not the same as the axis of the external field H, the magnetic dipoles rotate reversibly towards the axis of the external field H, as shown in Figure 1.2b. After the removal of the external field, the magnetic domains rotate back to the easy axis direction B, along which they had been initially and irreversibly re-orientated. In general, magnetic domains do not return back to their initial easy axis A.

Both reversible and irreversible processes are associated with the presence of magnetostriction. The irreversible process is additionally responsible for the small or large Barkhausen jumps, introducing magnetic noise in the sensing element. Employing the irreversible process results in hysteresis in magnetic rotation, as well as in a relatively higher level of noise with respect to the reversible process. Both hysteresis and noise affect the uncertainty of any possible magnetic device used for sensing. Therefore, if the aim is the development of a sensor, where hysteresis and noise should be minimized, only the reversible area of domain rotation should be used.

On the contrary if the aim is high hysteresis, the irreversible area of the domain rotation should be used. The domain rotation effect has found applications mainly in the field of mechanical sensors [25]. The dynamic behaviour of these processes can result in elastic waves, propagating along the magnetic substance. This is precisely the basis of the MDL technique [26-29]. The MDL technique has been extensively studied in order to understand its operation and optimize its performance [30-33] using a variety of methods [34-39].

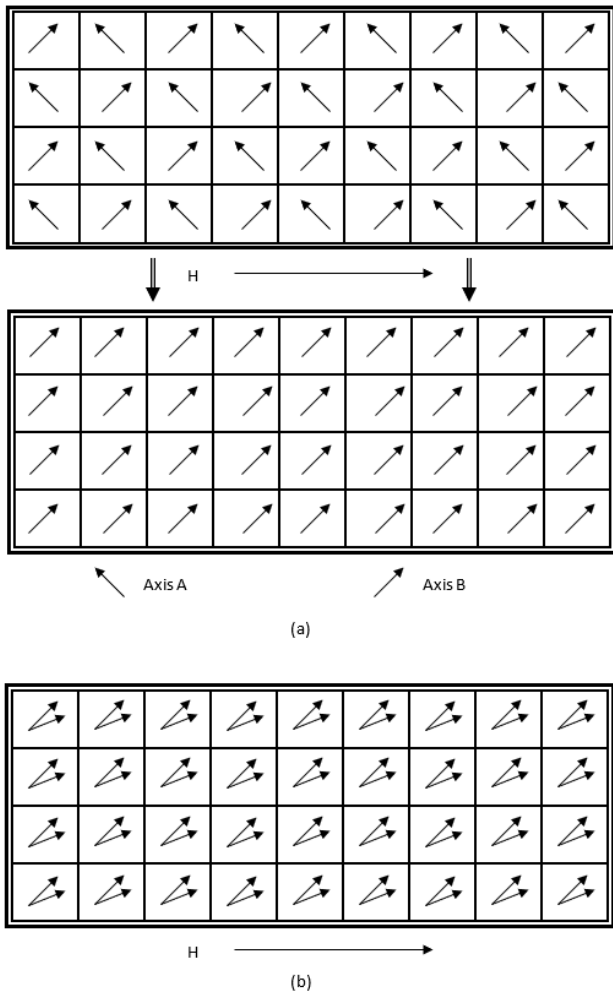


**Figure 1.2.** Irreversible and reversible rotation in magnetic domains. (a) Irreversible orientation along easy axis A or B, (b) Reversible small magnetization angle rotation (SMA).

A vast variety of magnetostrictive materials have been developed up to now. Today, the materials exhibiting the largest possible magnetostriction are the recently developed magnetic shape memory (MSM) alloys [40], exhibiting dimensional changes in the order of 1% to 10%. Their operation is based on the martensitic – austenitic transformation even at room temperature due to the change of the biasing field.

Before the development of MSM alloys, the materials exhibiting the largest magnetostriction were the rare earth – transition metal alloys, with saturation magnetostriction in the order of 800 ppm to 2000 ppm [41-43]. Combination of rare earth elements and magnetic substances, like iron, nickel and cobalt, resulted in the development of Terfenol and other similar alloys, which have been extensively used in engineering applications.

Soft magnetostrictive alloys based on iron, nickel and cobalt exhibit a relatively low

magnetostriction in the order of 30-100 ppm and are generally used as MDLs. The needs in modern sensor development would not allow the use of the classical polycrystalline materials and led to the development of the amorphous magnetostrictive alloys, like ribbons, wires and glass-covered wires, prepared by rapid quenching techniques [44-49].

The amorphicity of the used magnetostrictive material helps in the minimization of the irreversible rotation process, because of the minimization of the coercive field and the field range responsible for the irreversible domain rotation. The need for miniaturization has led research groups to develop MDL

arrangements in thin film structure, thus enhancing the possibility of developing integrated systems [50-52]. Furthermore, the need for better sensor characteristics has led to the development of nano-crystalline magnetostrictive ribbons and wires [53-55] with even lower hysteresis, which can be used as MDLs, provided that they can exhibit magnetostriction. Recently, an interesting composite material including magnetostrictive substance in a non-magnetic matrix has been proposed for magnetoelastic applications [56].

When designing a sensor using the effect of domain rotation, one should tailor the magnetic material in order to minimize the amplitude of the external field responsible for the irreversible rotation process and correspondingly maximize the external field range for reversible rotation. Annealing techniques have been employed, targeting the proper tailoring of the magnetostrictive elements [57-63]. These techniques mainly include heat annealing, field annealing and stress-current annealing, not only eliminating the defects of the material, but also re-orienting the magnetic anisotropy in order to eliminate the irreversible swift process of the domain rotation. The elimination of the irreversible process occurs simply because of the absence of an easy axis direction near the direction of the external field  $H$ . In this case, the magnetic field in the field annealing process should be perpendicular to the easy axis of the material. The magnitudes of temperature and field are similar to those in the case of domain wall dynamics.

The  $\mu(H)$  function is the most important characteristic regarding the MDL operation, since it can model the operation of an MDL set-up and consequently a sensor arrangement based on the MDL technique. Proper tailoring should take into consideration the dynamic response of  $\mu(H)$  with respect to frequency and not only the saturation magnetostriction constant  $\lambda_s$  or the static magnetostriction function. A number of instruments have been developed in order to measure the dynamic characteristics of this function as well as the engineering magnetostriction constant  $\lambda_s$  [64-71]. An excellent review of such measurement techniques is given in [72].

---

### 1.2.1 Dependent mechanisms.

---

Apart from the domain wall and domain rotation dynamics, there are other dependent magnetic effects, which can be measured and used as macroscopic electrical and magnetic properties of the material.

The most well-known and used effect is the magneto-resistance effect [73-78], observed mainly in magnetic thin films. According to this effect, the dc electrical resistance of a magnetic film changes about 2-3%, with respect to the externally applied magnetic field, due to the magnetic domain rotation and in

some cases due to domain wall nucleation. The most significant magneto-resistive effect, the “giant” magneto-resistive effect, appears in magnetic thin film multi-layers where the change in resistance hovers in the range of 50-80% at room temperature. This “giant” effect is due to the perpendicular anisotropy of the magnetic layers causing a large magnetic moment rotation. Recently, the “colossal” magneto-resistive effect has been observed in magnetic oxides, offering even larger changes in resistance, but in cryogenic environments. The magneto-resistive effect is mainly used in field sensors and recording media applications. Another effect, which has also found applications, is the ac magneto-resistance effect or magneto-impedance effect [79-85]. According to this effect, the ac resistance or impedance of a magnetic substance varies with the applied field. This effect also exists in non-ferromagnetic materials due to the skin effect, although its amplitude is much smaller than in ferromagnetic materials. In some zero-magnetostrictive wires, with circumferential magnetic anisotropy, the magneto-impedance changes more than 100% with respect to the applied external field. Although this effect has only recently been studied, it has already been used in industrial and automotive applications due to its great sensitivity in magnetic field.

Another effect attracts the interest of the field sensor market and mainly the recording media market. This is the spin valve effect [86-90], according to which an especially designed magnetic arrangement exhibits non-symmetrical B-H response. This property allows very well localized field measurements with an acceptable accuracy. Apart from that, the spin tunneling effect has also been used in recording media and accurate field measurements [91,92].

Apart from these, the rather classical inductive effects [93] have been implemented in the form of the fluxgate set-up [94] for accurate field detection and linear variable differential transformer (LVDT) for displacement sensing [95]. Other related electromagnetic effects such as the Hall effect, the Quantum Hall effect and the SQUID are also able to detect field. With the exception of magneto-elasticity, which is used for direct detection of mechanical sizes, the main sensing application of magnetic effects and materials is the detection of magnetic field. Once the field or field change has been measured, one can map the measurement to another physical size, like displacement, stress, flow etc.

---

## **1.3 Sensors based on magnetic effects and materials**

---

The magnetic effects and materials described in the previous section have been used as the core of many sensing elements [96-98]. These sensing elements are divided into five distinct families, namely position, mass, field, security and smart sensors. Other sensors also exist, like temperature sensors, but still in a rather research level.

---

### **1.3.1 Position sensors**

---

Position sensors occupy a relatively large percentage in the global sensor market. The position sensor family can be divided into three main subcategories: the terminating switches, the absolute, differential & angular sensors and finally the velocity sensors and accelerometers. The terminating switches are simple field sensors with a threshold checker, operating like on-off switches. Their vast majority concerns magneto-resistive (MR) devices, since the cost of mass production poor quality MR elements is small. Their main competitor is the capacitive switch based on capacitance change. The second subcategory includes absolute, differential & angular sensors. Absolute sensors are able to detect the absolute distance between two points [99-102]. These two points are usually the exciting and detecting means. Examples of absolute position sensors are the MDL sensors [103,104], the linear variable differential transformer (LVDT) and the linear inductive sensor using closed magnetic paths. Their sensitivity and uncertainty could reach 10  $\mu\text{m}/\text{m}$  or 10 ppm and 100  $\mu\text{m}/\text{m}$  or 100 ppm respectively. Their cost is in the order of 0.1 kEuro/sensor. Their competitor is the ultrasonic position sensor, which is less expensive but less accurate too.

Differential position sensors detect the length the sensing head travels and not the absolute position. The most important differential position sensor utilizing magnetic effects is the magnetic tape. A magnetic head reads the flux as it passes on top of a permanent magnet tape, having opposing magnetic finite permanent magnets. This tape is a corded device and is constructed from a series of hard magnets arranged in up and down orientations of magnetization. The sensitivity and uncertainty of these sensors can be in the order of 1  $\mu\text{m}$  and 10  $\mu\text{m}/\text{m}$  respectively. Their cost is in the order of 1 kEuro/meter. Their competitor is the optical tape and has similar properties.

Angular sensors can be either absolute or differential. The most classic sensor is the rotating tooth, which is a differential sensor, used in many important applications like ABS in cars. As the disk holding the magnetic teeth is rotating, a magnetic head counts them by means of a train of pulses. Interesting angular sensors based on inductive and magnetic techniques have also been proposed in the past [105,106].

Velocity sensors and accelerometers are based either on the calculation of the response of absolute or differential position sensors, or on direct detection of velocity or acceleration [107]. Although most of the velocity sensors or accelerometers are based on position sensors, the development of 'pure' accelerometers is of interest. A simple velocity meter or accelerometer can be an inductive sensor using an inertia magnetic mass, moving on top of a coil. The motion of the magnetic mass introduces a change in the magnetic flux of the coil. Accelerometers based on magnetostrictive materials have been proposed in the past, using the dynamic motion of a permanent magnet [108,109].

Dilatometers are a special category of position sensors with very high sensitivity of the order of tens of nm and very low range of measurement of the order of microns. Typical examples of dilatometers based on magnetic materials are special designs of LVDTs, having as main competitor the capacitive dilatometers. All these devices can be found either corded or cordless. Cordless sensors are more preferable for obvious practical reasons in most applications.

---

### 1.3.2 Mass sensors

---

Mass sensors are divided into three main categories: the load cells, the pressure sensors and the torque meters; the flow meters and mass flow meters are a derivative sensing application. All these devices can be based on position or strain sensors detecting indirectly the applied stress. The most classical example is the strain gauge. However, the magnetostrictive materials and their corresponding arrangements can detect directly the applied stress and therefore the load, pressure and torque on them, using the magnetization change caused by the stress-induced anisotropy.

Load cells measuring tensile stress directly are mainly based on inductive arrangements using a material sensitive to tensile stress as ferromagnetic core [110-114]. Such a core is usually a positive magnetostrictive material. The permeability decreases dramatically with stress, so that the output of the coil decreases correspondingly. Accelerometers can also be based on such arrangements. The MDL

technique has also been involved in direct stress measurement. Typical values of sensitivity and uncertainty of these devices are 10-100 ppm and 100-300 ppm respectively, with an average cost of 1 kEuro/sensor. Pressure gauges have also been proposed, based mainly on thin film arrangements, using the piezomagnetic effect [115-118].

A vast variety of torque sensors has been realized so far [119-129]. One principle is the use of pre-annealed magnetic materials under torsion. The magneto-impedance effect and the MDL set-up have been proposed in the past as torque meters, both illustrating very competitive properties. The sensitivity and uncertainty of these devices was comparable and equal to 100 ppm and 1000 ppm respectively, with a cost of 1 kEuro/sensor. Flow sensors based on electromagnetic techniques are well known in industry. Recently, flow meters have also been proposed, using the effect of bending stress on an amorphous wire.

---

### 1.3.3 Field sensors

---

This is probably the largest sector in the magnetic sensor market. The most frequently used field sensors are the ones used for the measurement of small field variations or field gradient or magnetic anomaly detection (MAD) [131]. Optic fibres are widely used as magnetometers [132-136]. The most important techniques and effects used to develop field sensors based on magnetic materials are the magneto-resistance effect, the magneto-impedance effect and inductive techniques like fluxgates. Historically, fluxgates have been the state of the art in low field sensing and gradient field measurement [137,138]. Their principle of operation is based on the differential inductive response of coils connected in series opposition, resulting in levels of sensitivity and uncertainty in the order of 1 pT and 10 pT respectively. Magnetostriction has also been used in field sensing but only in special applications [139-143].

Magneto-resistance field sensors as described in the previous chapter employ the multi-layer structure exhibiting vertical magnetic anisotropy of the ferromagnetic layers. These sensors are manufactured in mass production, facilitating thin film techniques, thus allowing low cost of manufacturing in the order of 10-100 Euro/sensor. Their sensitivity and uncertainty, in the order of 1 nT and 10 nT respectively, are enhanced with respect to the more traditional Hall effect sensors.

The recently developed magneto-impedance (MI) effect in amorphous and nanocrystalline wires allows much better levels of sensitivity and uncertainty, in the order of 1-10 pT and 100 pT respectively. The cost

of such a device used to be in the order of 100 – 300 Euro/sensor, while recent advances in miniature MI elements allowed sensitive performance [144-147] and drop of the price below 10 Euros/sensor. These good specifications allow the use of MI sensors in industrial and automotive applications in comparison to magneto-resistance sensors. Generally, the problem in many magnetic thin film sensors is that the sensor characteristics become less attractive compared to the bulk sensing elements. An interesting combination of the MI and the fluxgate effect on a thin film structure has also shown promising results in two dimensional field measurements, by using amplitude and pulse width modulation techniques, offering sensitivity at the level of 1 pT [148]. Other magnetic principles, like the Wiedemann effect, have been also developed in the past for field measurement [149]. The MDL technique has also been employed in field sensing, as demonstrated later in this work.

All these sensors based on magnetic effects and materials have a major competitor with respect to their performance: the SQUID sensors based on the Josephson effect, allowing single magnetic quantum measurement, is the today's absolute state of the art in field measurements with sensitivity in the order of 1 fT.

---

### **1.3.4 Security sensors**

---

The read & write sensors fall under two main categories: the recording media and the security sensors. The recording media, including both writing surfaces and reading heads are rather out of the scope of this work, despite the fact that the reading heads based on magnetic effects mainly employ giant MR sensors. The security sensors [150] are based on the combination of different magnetic properties, for example different B-H loops of materials, in order to generate a code based on a series of magnetic signatures, which allows the recognition of an object without direct optical observation. This family of sensors can be used in applications where optical bar coding is impossible for practical reasons.

---

### **1.3.5 Multipurpose sensors**

---

These sensors are in fact the so-called smart sensors [151], including three different subcategories, the multi-parameter sensors, the self-learning sensors and the reacting sensors. The multi-parameter sensors

are able to detect more than one physical size. An example is a magneto-elastic arrangement, based on negative magnetostrictive ribbons, which is able to detect field and stress at the same time. This is due to the fact that the pulsed output of the sensor is modulated only by amplitude due to the ambient field, while the pulse width is modulated only by the tensile stress. The self-learning sensors have the ability of self-calibration and auto-scaling of the range of measurement. The reacting sensors are complete electromechanical systems, which are able to sense and consequently react with respect to the measurement. An example is a missile driving sensor, which includes a precise field navigation sensor which measures the direction of motion of the missile and a reacting system, changing the direction of the missile with respect to a pre-loaded order.

---

## **1.4 Applications of sensors based on magnetic effects and materials**

---

The above-described sensing elements are used in a vast variety of applications. The main categories of such applications, namely industrial, biomedical, military, environmental, automotive, laboratory and domestic applications are being briefly overviewed here.

---

### **1.4.1 Industrial applications**

---

The main field in industrial applications is the non-destructive testing and evaluation (NDT&E). When magnetic materials are used as sensing elements, the eddy current technique (ECT) or magnetic anomaly detection (MAD) testing is used [152-155]. Both sensing techniques require the use of small field sensors. The most commonly used sensors for this purpose are the Hall sensors, offering sensitivity in the order of 0.1 mT. The giant magneto-resistive (GMR) elements, offer an improved sensitivity in the order of 1  $\mu$ T. Furthermore, the recently developed MI elements, offer a sensitivity of 10 –100 pT. The value of sensitivity reflects the ability of the sensor to detect small field variations, which corresponds to the size of an existing

crack or defect. MDL sensing elements have also been proposed, able to perform distribution measurements, despite their current disadvantage of poor sensitivity.

The second more frequent field of industrial applications is the position, velocity and acceleration/vibration controllers [156-160]. The vast majority of these sensors are position switches based on the GMR effect, with a repeatability better than  $10^{-12}$  and cost  $\sim 10$  Euro/sensor. For a more precise control in the order of  $1 \mu\text{m}$ , differential position sensors are used based on the magnetic permanent magnet tape arrangement, with a cost  $\sim 1$  kEuro/sensor. MDLs have also been employed in hydraulic piston control. Industrial control also requires the use of mass sensors, like load cells, torque meters and pressure gages.

Up to this moment the vast majority of such industrial sensors is based on conducting or semiconducting materials. Strain gauges are the most commonly used sensors for load measurement. Today's load sensors are based on miniaturized elements fabricated by lithography techniques, thus allowing better performance and a drastic reduction of their cost. The MDL technique has also been used for some interesting applications of load and derivative size measurements, with sensitivity better than strain gauge arrangement, as demonstrated later. Interesting studies on the use of magnetostrictive materials as actuating elements has also been presented in the past [161-163].

---

### 1.4.2 Biomedical applications

---

Other significant applications of sensors based on magnetic materials and effects are the biomedical applications [164-169]. The most traditional sensing system is the encephalograph, an arrangement of field sensor arrays able to detect fields in the range of  $10 \text{ pT}$ . The most widely used sensor array is the SQUID system, with a sensitivity of  $1 - 10 \text{ fT}$  and a cost in the order of  $1 \text{ MEuro}$  per measuring system. Recently MI sensors have started to be used in such applications, having the disadvantage of lower sensitivity in the order of  $10 - 100 \text{ pT}$  but a cost in the order of  $10 \text{ kEuro}$  per measuring system. Apart from that, another family of biomedical sensors based on magnetic effects is a new type of cardiograph, which is simpler in operation and less expensive than the classic electrocardiograph, although it does not perform all the measurements obtained with the latter. It requires a set of two MI sensors one for each wrist and costs  $\sim 1 \text{ kEuro/sensor}$ . A latest development, partially due to the developments in DNA evaluation,

concerns micromachined field array sensors with a spatial resolution in the order of 1 mm and a cost in the order of 100 Euro/sensor. These devices are mainly based on the GMR effect, while MI sensors are currently tested for the same application.

---

### **1.4.3 Military applications**

---

Although not very popular, the military applications of sensors including devices based on magnetic materials cover a large sector of the global sensor market, in terms of budget and importance. One significant application is the anti-mining control system. So far, the low field or field gradient or magnetic anomaly detection systems are the only existing devices able to detect mines. The more sophisticated the mines become the less iron they use and therefore more sensitive and accurate field sensors are required. Many types of sensors have been used for this purpose, from fluxgates to MI and MR sensors. Their sensitivity in today's sensors is in the order 10 – 100 pT. It is said that the budget of anti-mining control process in Balkans in the next decade is to be of the order of 300 million Euros.

Another military application used also for domestic applications is the magnetic signature. According to this, the military and not only vehicles are equipped with coils supplied by a given, usually coded, current waveform. Detecting the field produced by such current results in recognition of the given type of vehicle. Applications of this system mainly refer to boats. Another application is the missile navigation. At this moment, the state of the art of this application is based on gyroscopes based on inertia mass control or global positioning systems (GPS), but research is under way in order to employ field sensors. The principle of operation is based on the field variation measurement and corresponding corrective action due to the earth's field. GMR and GMI sensors have been employed for this purpose.

---

### **1.4.4 Environmental applications**

---

In the last decades, the environmental protection became vital for the whole globe. Therefore, the measurement of many parameters affecting the environmental status is of paramount importance. The monitoring of the electromagnetic radiation is a significant part of this process [170]. The method of detecting such a radiation is the field monitoring. The range of measurement with respect to frequency extends from dc up to 30 GHz fields.

An easily understandable example is the mobile telecommunication electromagnetic pollution, where the measurement of the radiation in the range of 1-2 GHz determines the correct control and use of antennas and cellular phones. The sensitivity of all these measurements ranges from a few nT up to a few mT. Sensors based on magnetic materials, like fluxgates, govern mainly the low frequency market of these sensors. GMI field sensors are currently under test for the same application while they are also beginning to be used in higher frequency measurements.

A distinct environmental application of dc field sensors is the space field monitoring. Every satellite is equipped with field sensors in order to perform meteorological measurements apart from craft navigation. The most traditional kind of sensor used for such an application is the fluxgate, while GMR and GMI field sensors have been employed recently to compete with the performance, cost and operational difficulties arising from the size of fluxgates, offering promising results. Another environmental application is the counting process in domestic areas. Counting of vehicles in traffic arteries with corresponding corrective actions in traffic signalling is an important issue in all large towns.

---

### **1.4.5 Automotive applications**

---

Nowadays, automotive applications of sensing elements are of increasing significance, probably due to marketing reasons apart from their significance in passive or active safety process. Car or road accidents have unfortunately a large percentage of accidents per day. This is a reason why the number of sensors used in modern cars is continuously increasing, being greater than 1,500 today.

Sensors based on magnetic materials govern some of these sensing applications [171]. The most classical and well-known sensor is probably the angular positioning magnetic sensor used to activate the ABS system in the brakes of the cars. A ring with teeth of permanent magnetic material is rotating with the wheel motion and a field sensor is monitoring the rotation of the wheel. Any sudden and unexpected blockage of the wheels during braking energizes the anti-block system (ABS) thus relieving the braking pressure for some fraction of the second.

Another application of magnetic effect sensors in vehicles is the torque sensor used in wheel steering and shaft operation monitoring. It is still at the laboratory development stage, but it is expected to enter the industrial production shortly. Very recently, a GMI field sensor has been used to control the position of a car [172,173], for cruising and parking reasons. Such positioning sensors are also under test to assist the

driving process by means of informing the driver for the status of the car path and even react to an incorrect decision of the driver. Other car engine applications of torque sensing have been proposed in the past [174].

---

### **1.4.6 Laboratory sensors**

---

In the field of laboratory sensors, the science of metrology governs the applications of sensors and systems based on magnetic materials. The most widely used application is the field calibration secondary standards based on accurate field sensors. Fluxgates are the most widely used family of magnetic sensors for this reason. Another application is the atomic force (AFM), magnetic force (MFM) and scanning tunnelling (STM) microscopy, according to which a detailed topography of a flat surface can be determined with atomic resolution.

An interrogating stylus is vibrated on top of the surface generating forces (Van der Waals for the AFM, magnetic forces for the MFM and electric forces for the STM) with respect to the topography of the under test surface. Recently, a new MFM system has been introduced, having magnetic nano-wire as stylus, promising sensitivity in the order of 0.1 nm [175]. Apart from these sensing instruments, in the metrology related to Current & Mass primary standard experiments, a new technique based on magnetic materials is experimentally tested, aiming to occupy the artifact of the kilogram. Using the Lorenz and Ampere's Law, an experimental facility, using a Quantum Hall Effect based implementation of the Volt and Ohm, is used to determine the kilogram and the Ampere [176].

---

### **1.4.7 Domestic applications**

---

Domestic applications of sensors based on magnetic materials mainly include navigation sensors, security sensors, as well as recording media for CD and DVD reproduction. The electronic compass is a small field vector sensor, which is the state of the art in modern navigation aids. The magnetic security sensors are used when optical bar coding systems cannot be used due to harsh environmental operation or disability of optical observation.

# 2 Magnetostrictive delay line arrangements

The MDL topologies are to be presented in this chapter. The first arrangement is the rather classical coil – coil set-up used for elastic pulse generation and detection, while the second and the third concern the use of straight conductors, orthogonal and parallel to the MDL respectively, used for pulsed current transmission and corresponding to elastic pulse generation. The fourth one demonstrates the possibility of using non-magnetic and non-magnetostrictive materials as acoustic waveguides for the elastic pulse propagation. The fifth arrangement shows a coil-less MDL set-up, while the sixth illustrates an arrangement where the MDL is wound around the excitation pulsed current conductor. Finally, the seventh arrangement uses a straight pulsed current conductor, while the MDL is circumferentially deposited around it, thus allowing transverse elastic wave propagation and detection.

---

## 2.1 The coil-coil arrangement

---

The most classical MDL arrangement, the coil-coil MDL set-up, is to be presented in this section, as shown in Figure 2.1. A short excitation coil and a short search (named also detecting or receiving) coil are placed around each one of the two ends of the MDL. The delay line is terminated using latex adhesive to eliminate acoustic reflections. Details of the various versions of such arrangements can be found in [177-181] and are presented hereinafter.

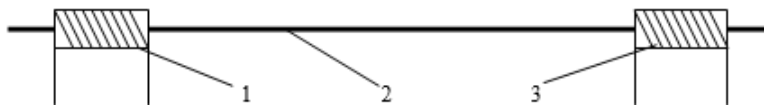


**Figure 2.1.** The basic MDL arrangement. (1) Excitation coil, (2) Magnetostrictive delay line, (3) Search coil.

As described in the previous section, magnetostrictive materials subjected to either low or high frequency fields, tend to undergo either domain wall motion or magnetic domain rotation respectively, always towards the direction of the externally applied field. Thus, applying external bias or pulsed field along the MDL axis results initially in Barkhausen jumps, which contribute to the hysteretic and irreversible part of the  $\lambda(H)$  function and consequently in small angle rotation which is the anhysteretic and reversible part of the said  $\lambda(H)$  function.

Therefore, polarizing the MDL with a dc bias field  $H_{dcx}$ , results in an elongation of the material  $\delta\lambda_o$ , illustrated as a point  $(\delta\lambda_o, H_{dcx})$  on the  $\lambda(H)$  function, shown on Figure 2.2. When a pulsed field  $H_e(t)$  is additionally applied at the region where the bias field has been applied, a similar but dynamic elongation  $\delta\lambda(t)$  occurs, as shown in Figure 2.3, resulting in an elastic wave propagating along the MDL, following the classical wave equation, as shown in Figure 2.4.

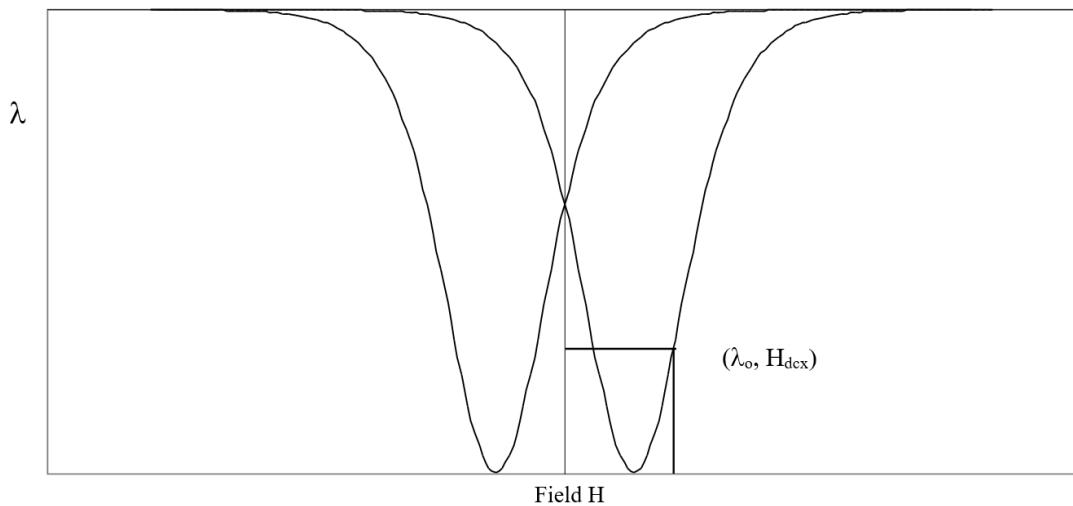


**Figure 2.2.** A typical  $\lambda(H)$  function.

In classical magnetostrictive materials, the optimum pulsed field width is in the order of  $\mu s$ . Thus, the wavelength of the propagating elastic wave is in the order of several mm. Therefore, in the most common MDL elements, where the MDL cross section is a tenth of  $mm^2$ , a Lamb wave is propagating. Using materials with higher frequency response or larger cross section can result in surface acoustic wave propagation. Skin effect plays an important role in modeling and tailoring the behaviour of the microstrain generation and propagation.

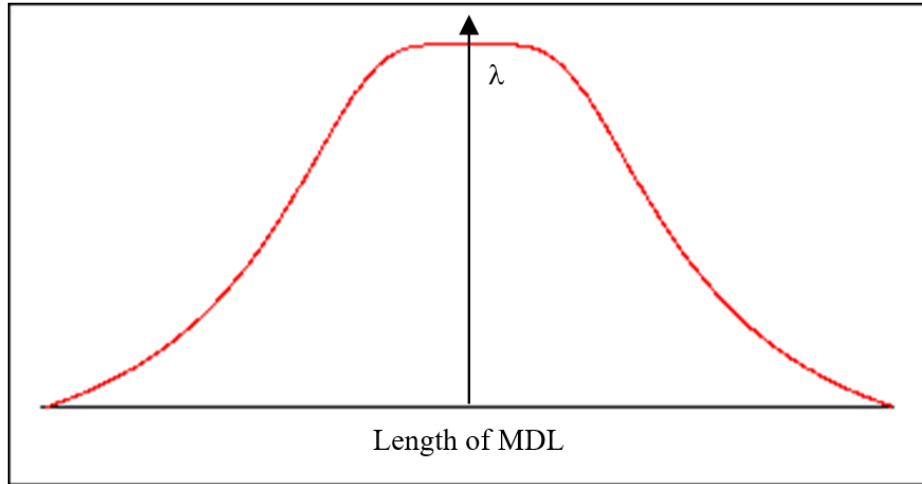


**Figure 2.3.** Microstrain with respect to space.

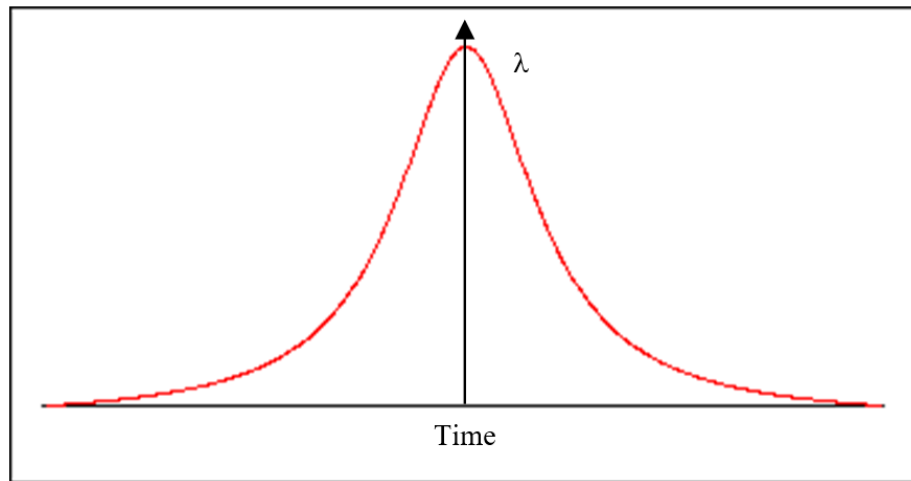


**Figure 2.4.** Propagating elastic pulse along the length of the MDL.

The pulsed field along the MDL, responsible for the elastic wave generation follows a decaying profile extending from the fully magnetized central region to a limit which is practically of the order of the excitation coil diameter, indicating the active region of the magnetostrictive material involved in the microstrain generation.

This elastic wave propagates along the length of the MDL, mainly as a longitudinal elastic wave, because of the shape of the acoustic wave guide: the short cross section with respect to the wavelength and the dimensions of the MDL eliminate any transverse and quasi-transverse waves.

The propagating elastic wave, in its course, changes the local magnetization component along the MDL axis, provided that the MDL is locally magnetized. The total, macroscopic change of the magnetic flux along the axis of the wire is the result of the statistical sum of local infinitesimal changes in the orientation of magnetic dipoles, in the course of the propagating elastic wave. Thus, the magnitude of the biasing field determines the change of the local magnetization component along the MDL axis. This is actually the inverse magnetostriction effect. In some materials, the earth's field can be enough to polarize and consequently cause the presence of such effect.

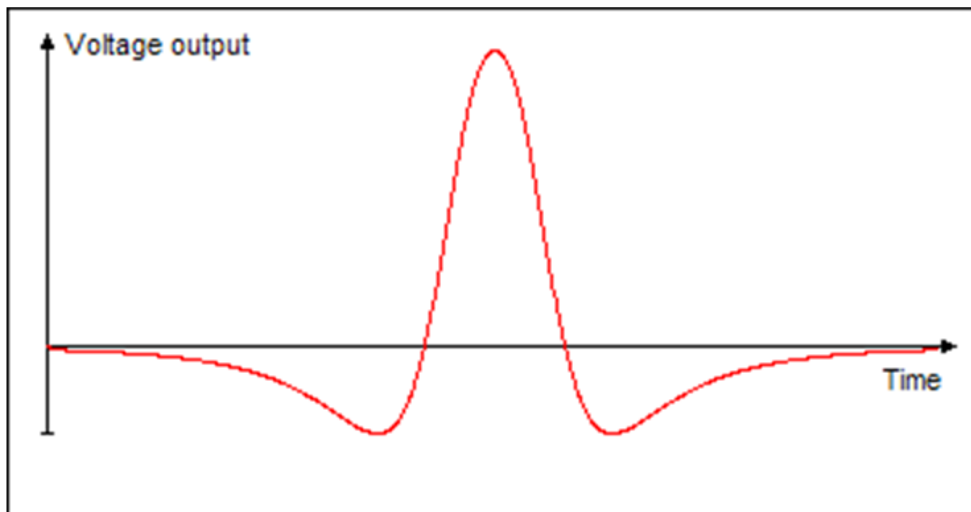


**Figure 2.5.** Voltage output with respect to time.

Thus, if an inductive means, like a search coil, is set around the MDL, a pulsed voltage proportional to the first derivative of the flux is induced across its ends, as shown in Figure 2.5. The search coil should be set at a distance  $x$  from the elastic wave point of origin (PO), which ought to be small enough to cause negligible attenuation and large enough to avoid electromagnetic coupling between excitation and detection means. Such pulsed voltage output is received with a delay time proportional to the distance  $x$  and inversely proportional to the longitudinal sound velocity of the magnetostrictive element. A real pulsed voltage output waveform, with the corresponding delay time from the excitation pulse observed as impulse response, is shown in Figure 2.6. In this case, the relatively small waveforms following the main pulse are due to reflections of the propagating elastic pulse.

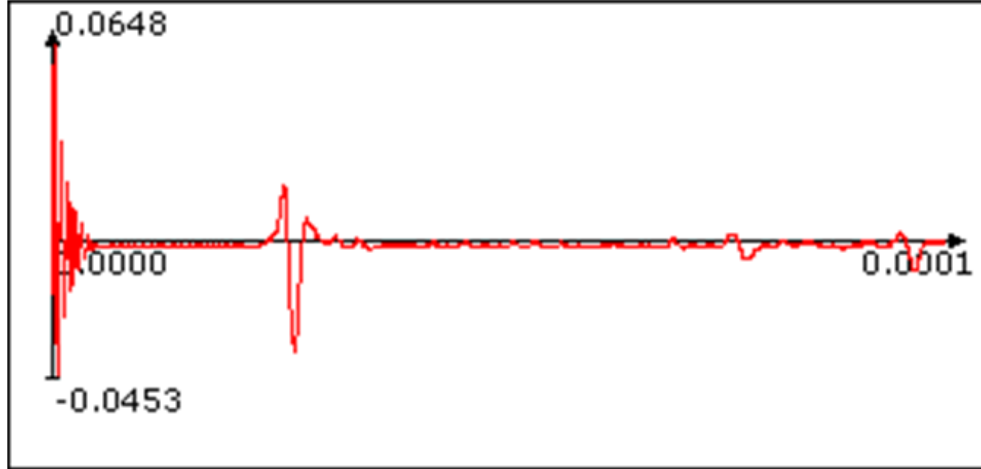


**Figure 2.6.** The detected MDL pulsed voltage output. The first impulse response is due to the pulsed excitation field. The main pulsed voltage output follows, with a characteristic amplitude  $V_0$ . The small waveforms following the main pulsed output are reflections of the propagating elastic pulse at the ends of the magnetostrictive medium (Time units in seconds and voltage amplitude in Volts).

### 2.1.1 Magnetostriction modeling

At the atomic level, magnetostriction is the aggregate result of the deformations of the crystal lattices inside the domains that tend to align with the domain magnetization. The deformation of a crystal lattice is due to the interactions between the atomic moments occupying its sites that result in altering the bond lengths. When the bonds lie at an angle  $\phi$  to the domain magnetization, the magnetoelastic energy tends to align the bonds with the domain magnetization, but is counterbalanced by the elastic bond energy. At the macroscopic level, one can think of the energy added to the system because of an externally applied field,  $\Delta E_m$ , as being counterbalanced by the change in elastic bond energy,  $\Delta E_{el}$  along the MDL axis:

$$\Delta E_m = \Delta E_{el} \Leftrightarrow \Delta M \cdot \Delta H = \frac{1}{2} k \Delta \lambda^2 \Leftrightarrow \frac{\Delta M}{\Delta H} = \frac{1}{2} k \left( \frac{\Delta \lambda}{\Delta H} \right)^2 \quad (2.1)$$

where  $k$  is the macroscopic elastic constant of the material, related to Young's modulus  $E_v$ , and  $\Delta \lambda$  is the elongation caused by the change in magnetization  $\Delta M$ .

$$\text{For } \Delta H \rightarrow 0, \frac{d\lambda}{dH} \propto \sqrt{\frac{dM}{dH}} \quad (2.2)$$

The derivative  $\frac{dM}{dH}$  corresponds to the differential susceptibility  $\chi_{diff}$ , of the magnetic material, which can be described by a function of the form:

$$\chi_{diff} = \frac{dM}{dH} \propto \left(\frac{H}{c} + \chi_0\right) e^{-\frac{H}{c}} \quad (2.3)$$

where  $c$  is a fitting constant with field dimensions related to  $K_1$  and  $M_s$  and  $\chi_0$  the initial susceptibility.

The above mentioned equation is the solution to a second order linear differential equation whose characteristic equation is:  $x^2 + cx + c = 0$ , as in the critical damping case in resonance. Thus

$$\frac{d\lambda}{dH} \propto \lambda_s \sqrt{\left(\frac{|H|}{c} + \chi_0\right)} e^{-\frac{|H|}{c}} = \lambda_s e^{\frac{\chi_0}{2}} \sqrt{\frac{|H|}{c} + \chi_0} e^{-\frac{1}{2}\left(\frac{|H|}{c} + \chi_0\right)} \quad (2.4)$$

where  $\lambda_s$  the saturation magnetostriction constant. Hence:

$$\begin{aligned} \lambda(H) &= \int \frac{d\lambda}{dH} \propto \lambda_s e^{\frac{\chi_0}{2}} \int \sqrt{\frac{|H|}{c} + \chi_0} \cdot e^{-\frac{1}{2}\left(\frac{|H|}{c} + \chi_0\right)} dH = \\ &= \lambda_s e^{\frac{\chi_0}{2}} \left( \frac{\sqrt{u} \cdot \text{erf}\left(\sqrt{\frac{1}{2}\left(\frac{|H|}{c} + \chi_0\right)}\right)}{4\sqrt{2}} - 2e^{-\frac{1}{2}\left(\frac{|H|}{c} + \chi_0\right)} \cdot \sqrt{\left(\frac{|H|}{c} + \chi_0\right)} \right) \end{aligned} \quad (2.5)$$

where  $\text{erf}(x)$  is the error function and:

$$\text{erf}\left(\sqrt{\frac{1}{2}\left(\frac{|H|}{c} + \chi_0\right)}\right) = \frac{2}{\sqrt{\pi}} \int_0^x e^{-\left(\frac{|H|}{c} + \chi_0\right)} dx = \frac{2}{\sqrt{\pi}} \sum_{n=0}^{\infty} \frac{(-1)^n}{n!(2n+1)} x^{2n+1} \quad (2.6)$$

Thus:

$$\lambda(H) \propto \lambda_s e^{\frac{\chi_0}{2}} \left( \frac{\sqrt{u} \cdot \sum_{n=0}^{\infty} \frac{(-1)^n}{n!(2n+1)} x^{2n+1}}{2\sqrt{2\pi}} - 2e^{-\frac{1}{2}\left(\frac{|H|}{c} + \chi_0\right)} \cdot \sqrt{\frac{|H|}{c} + \chi_0} \right), x = \frac{1}{2}\left(\frac{|H|}{c} + \chi_0\right) \quad (2.7)$$

Experimental data, have illustrated that in the case of anhysteretic behaviour, the  $\lambda(H)$  function can be fitted by  $\lambda(H) = \lambda_s(1 - e^{-cH^2})$ ,  $c > 0$ , where the positive number  $c$  is an adaptive parameter. In the case of hysteretic evidence this model could become  $\lambda(H) = \lambda_s(1 - e^{-c(H \pm H_c)^2})$ ,  $c > 0$ .

The Energetic Model (EM) relates the fitting constant  $c$  to microscopic parameters of the material. At weak fields,

$$c = \left(\frac{M_s}{\chi_0}\right)^2 = \left(\frac{q \cdot k}{\mu_0 \cdot M_s}\right)^2 = \left(\frac{c_q \cdot K_1}{\mu_0 \cdot M_s}\right)^2 \quad (2.8)$$

and at strong fields,

$$c = \frac{2g \cdot H_s^2}{g + \sqrt{2 - 4g + g^2}} \approx H_s^2 = \left(\frac{c'_g \cdot K_1}{\mu_0 \cdot M_s}\right)^2 \quad (2.9)$$

where  $g$ ,  $h$ ,  $k$ ,  $q$  are the parameters of the EM:

$$g = \left(c_g \cdot \frac{\mu \cdot M_s^2}{K_1}\right), h = \frac{H_s}{\exp(g \cdot \ln 2)}, k = c_k \cdot E_Y \cdot \lambda_s^2, q = \frac{c_q}{c_k} \cdot \frac{K_1}{E_Y \cdot \lambda_s^2} \quad (2.10)$$

with  $c_g$ ,  $c_h$ ,  $c_k$  and  $c_q$  being the model's dimensionless microscopic constants. With the anisotropy

field  $H_k = \frac{2K_1}{\mu_0 \cdot M_s}$ , the saturation field  $H_s = \frac{c'_g \cdot H_k}{2}$  ( $c'_g$  is a proportionality constant) and  $c_q$  and  $c'_g$  being of

the same order of magnitude, an average value for  $c$  at both weak and strong fields is defined by  $c =$

$$2 \frac{c_q \cdot c'_g}{c_q + c'_g} \cdot \left(\frac{K_1}{\mu_0 \cdot M_s}\right)^2 = \left(\frac{H_s}{c'}\right)^2 \quad (2.11)$$

In order to prove the principle of the described formalism, experimental data were obtained using a Fe<sub>78</sub>Si<sub>7</sub>B<sub>15</sub> amorphous ribbon MDL, exhibiting  $\lambda_s \sim 30-32$  ppm. The sample was previously stress-current annealed under 350 MPa and 100 mA, to remove internal stresses and improve its magnetostrictive behavior and uniformity of magnetic domains. The MDL set-up was operating by incrementing the peak value of the pulsed current  $I_e$  from 1 to 13.6A and back. The bias field at the arrangement was varied from 0 to 130 A/m at each  $I_e$  amplitude. The output voltage is related to the dynamic response of the anhysteretic  $\lambda(H)$  function and is a function of the pulsed current waveform.

The peak voltage is maximum at a bias field of 16 A/m for all  $I_e$ . Considering the induced voltage,

$$V(t) \propto \frac{dB}{dt} \propto H_{dc} \frac{d\lambda}{dt} = H_{dc} \frac{d\lambda}{dH_e} \frac{dH_e}{dt} \Rightarrow V_0 = H_{dc} \max\left\{\frac{dH_e}{dt}\right\} \frac{d\lambda}{dH_e} = A_0 \frac{d\lambda}{dH_e} \quad (2.12)$$

where  $A_0$  is a constant related to  $I_e$  and  $\lambda_s$ .

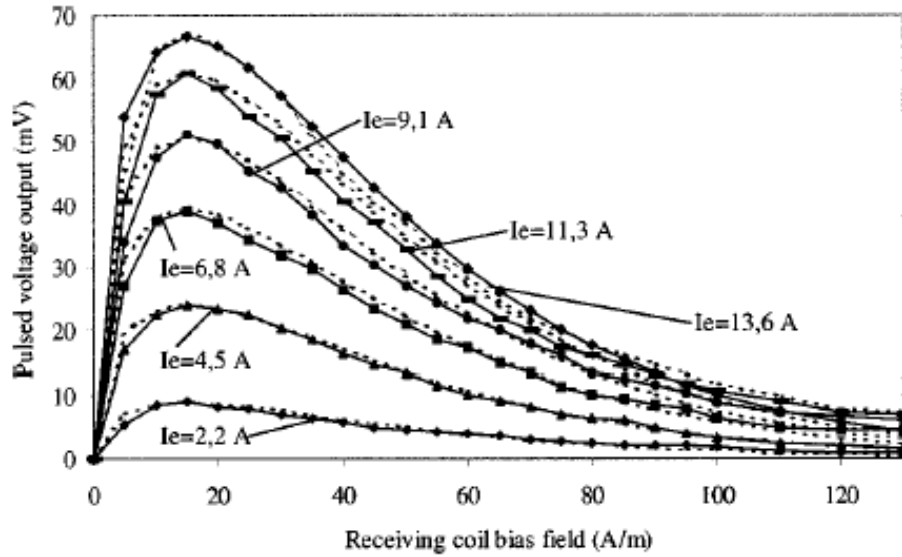


**Figure 2.7.** Comparison of experimental and theoretical data for biasing field using equation 2.1 to 2.5.

Figure 2.7 shows the experimental and theoretical data, concerning the dependence of the MDL peak amplitude  $V_0$  on the DC bias field at the region of the receiving coil, at various values of  $I_e$ , producing the field  $H_e$ , for several amplitudes of  $I_e$ . As expected, the value of  $c$  turns out to be the same for all theoretical curves:  $c=15$  A/m. This suggests that  $c$  is indeed related to material constants.  $A_0$  exhibits a linear dependence on  $I_e$  with signs of saturation for higher currents.

---

### 2.1.2 An alternative way of modeling the coil-coil MDL arrangement

---

Following the basic MDL set-up as illustrated in Figure 2.1, the MDL is activated by transmitting pulsed current  $H_e(t) = H_e \cdot f(t)$ , through the excitation coil or the pulsed current conductor. Pulsed current generates a pulsed magnetic field along the magnetostrictive element. This field generates a pulsed microstrain at the region of excitation of the magnetostrictive element,  $\lambda(H_{oe} + H_e(t))$  due to the magnetostriction effect. Since the magnetostrictive material is in the shape of cylinder or ribbon, it can operate as acoustic waveguide.

Therefore, the pulsed microstrain propagates along the length of the magnetostrictive element as longitudinal acoustic pulse. As soon as it arrives at the region of the search coil, it is detected as pulsed

voltage output, proportional to the first derivative of the propagating pulse, due to the inverse magnetostriction effect.

The generation and detection of the pulsed microstrain is possible and repeatable due to the presence of biasing fields at the acoustic stress point of origin and the search area,  $H_{oe}$  and  $H_{or}$  respectively, which orient the magnetic dipoles in a given direction. The propagating pulsed microstrain induces stresses  $\sigma(\lambda)$  in the MDL. These stresses act as effective field  $H_\sigma = f(\sigma)$  in the MDL, added in the already existing biasing field along its length. Provided that the microstrain propagates without dispersion and after effects, which is applicable for the front acoustic wave, it arrives at the region of the search coil, inducing such an effective field  $H_\sigma$  along the length of the MDL. Thus, the flux within the magnetic region inside the search coil is:

$$\Phi(t) = S \cdot \mu(H_{or}) \cdot (H_{or} + H_\sigma) \quad (2.13)$$

where  $S$  is the cross section of the magnetostrictive element. Thus, the voltage output  $V_o(t)$  at the search coil is:

$$V_o(t) = -\frac{d\Phi}{dt} = -A \cdot \mu(H_{or}) \cdot \frac{dH_\sigma}{dt} \quad (2.14)$$

Where  $A$  includes  $S$  and search coil parameters. Provided that excitation pulsed field is relatively small, the effective field and stress are assumed to be proportionally related:

$$H_\sigma = f(\sigma) = a \cdot \lambda(H_{oe} + H_e(t)) \quad (2.15)$$

Thus  $V_o(t)$  becomes:

$$\begin{aligned} V_o(t) &= -A \cdot a \cdot \mu(H_{or}) \cdot \frac{d\lambda(H_{oe} + H_e(t))}{dt} = -A \cdot a \cdot \mu(H_{or}) \cdot \frac{d\lambda}{dH} \frac{d(H_{oe} + H_e(t))}{dt} \\ &= -A \cdot a \cdot \mu(H_{or}) \cdot \frac{d\lambda}{dH} \cdot H_e \cdot \frac{df(t)}{dt} \end{aligned} \quad (2.16)$$

Thus the peak to peak magnitude of  $V_o(t)$ ,  $V_o$  is given by:

$$V_o = -A \cdot a \cdot c \cdot H_e \cdot \mu(H_{or}) \cdot \frac{d\lambda}{dH} \quad (2.17)$$

where  $c$  is the maximum of  $\frac{df(t)}{dt}$ .

In the case that  $H_e, H_{oe}$  are not changing and  $H_{or}$  changes,  $V_o$  becomes:

$$V_o = -A \cdot a \cdot c \cdot c_1 \cdot H_e \cdot \mu(H_{or}) = C_1 \cdot \mu(H_{or}) \quad (2.18)$$

where constant  $c_1 = (d\lambda/dH)_{max}$ . Coefficient  $C_1$  is a constant, mainly dependent on the material and the fields at the excitation regions. Under these conditions  $\mu(H_{or})$  is proportional to  $V_o$ .

In case that  $H_e, H_{or}$  are constant and  $H_{oe}$  changes,  $V_o$  becomes:

$$V_o = -A \cdot a \cdot c \cdot H_e \cdot \mu(H_{or}) \cdot \frac{d\lambda}{dH} = C_2 \cdot \frac{d\lambda}{dH} \quad (2.19)$$

where  $C_2$  is a constant, mainly dependent on the material and the excitation field and biasing field at the excitation and receiving regions respectively. Under these conditions  $\frac{d\lambda}{dH}$  is proportional to  $V_o$ . When  $H_{oe}, H_{or}$  are constant and  $H_e$  changes,  $V_o$  becomes:

$$V_o = -A \cdot a \cdot c \cdot H_e \cdot \mu(H_{or}) \cdot \frac{d\lambda}{dH} = C_3 \cdot H_e \cdot \frac{d\lambda}{dH} \quad (2.20)$$

Thus  $\frac{V_o}{H_e} = C_3 \cdot \frac{d\lambda}{dH}$ , where  $C_3$  is a constant, mainly dependent on the material and the biasing fields at the excitation and receiving regions.

As shown in Chapter 8, apart from being useful in MDL behaviour description, this approach can also lead towards the use of this MDL arrangement for the experimental determination of the M-H and  $\lambda$ -H loops of magnetostrictive ribbons and wires as well as their corresponding uniformity functions. All the above mentioned equations used for the coil-coil MDL arrangement can also be used for the case of the next presented arrangement concerning conductors perpendicular to MDLs.

---

## 2.2 *Array conductors perpendicular to arrays of MDLs*

---

In the integrated sensor array market, the existing techniques are mainly the fiber optic and microelectronic miniatures, obtaining range of measurement and spatial resolution of the order of 1 km and 1 m for the case of optic fibers and 1 mm and 1 $\mu$ m for the case of microelectronic technologies respectively. Targeting the filling of the gap between optic fibers and microelectronic miniatures, the MDL technology aims to the realization of integrated sensor arrays having range of measurement and spatial resolution of the order of 1 m and 1 mm respectively.

Many arrangements have been realized to meet this purpose, which are analyzed in this work. One of these techniques, being in fact one of the very first methods, is the employment of array conductors perpendicular to arrays of MDLs. These arrangements may also lead to sensing tactile arrays.

### 2.2.1 Single conductor perpendicular to a single MDL

The simplest possible arrangement of excitation, consisting of a single pulsed current conductor orthogonal to the MDL, is shown in Figure 2.8. Concerning this set-up, the pulsed field  $H(x, t)$ , along the length of the MDL, caused by pulsed current  $I(t)$  is given by:

$$H(x, t) = f(x) \cdot I(t) = \frac{1}{2\pi\sqrt{a^2+x^2}} \cdot \cos \alpha \cdot I(t) = \frac{1}{2\pi\sqrt{a^2+x^2}} \cdot \frac{a}{\sqrt{a^2+x^2}} \cdot I(t) = \frac{a}{2\pi(a^2+x^2)} \cdot I(t) \quad (2.21)$$

where  $a$  is the distance between pulsed current conductor and MDL.

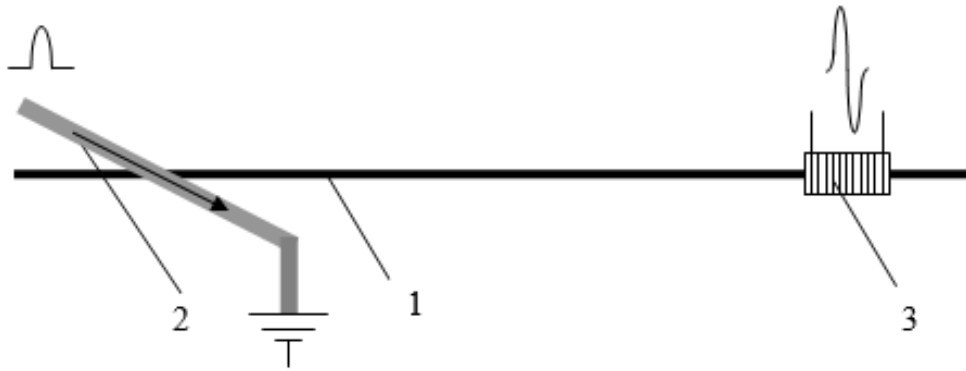


**Figure 2.8.** Pulsed current conductor orthogonal to the MDL. (1) MDL, (2) Pulsed current conductor, (3) Search coil.

In order to further analyze the generation, propagation and detection of elastic pulses, one may study the pulsed excitation field and its detailed contribution to the generation of local pulsed microstrains in space and time, their sum-up to a single elastic pulse in space and time, which propagates along the MDL and finally the detection of the propagating pulse by the search coil.

The pulsed current  $I(t)$  is assumed to consist of a rising ramp from 0 to  $I_o$  for  $0 < t < n_1T$ , a steady state current  $I_o$  for  $n_1T < t < n_2T$  and a falling ramp from  $I_o$  to 0 for  $n_2T < t < n_3T$ , where  $T$  is the time increment and  $n_i$  integer numbers.

In the case of anhysteretic behavior, the microstrains caused by the pulsed field  $H(x, t)$  can be given by the following phenomenological model based on experimental evidence:

$$\lambda(H) = \lambda_s(1 - e^{-aH^2}), a > 0 \quad (2.22)$$

where the positive number  $c$  is an adaptive parameter, which will be discussed later. In the case of hysteretic evidence this model becomes:

$$\lambda(H) = \lambda_s(1 - e^{-a(H \pm H_c)^2}), a > 0 \quad (2.23)$$

For simplification reasons, only the anhysteretic response is being considered. The microstrains  $\lambda(x, t)$  caused by the rising pulsed current are summed up as a group of strains  $G_r(x, t)$  :

$$G_r(x, t) = \sum_{n=1}^{n_1} \lambda_s \left( 1 - e^{-\alpha \frac{\left(\frac{nI_0}{n_1}\right)^2}{a^2 + (x - (n_3 + n_2 + n_1 - n) \cdot T \cdot v)^2}} \right) \quad (2.24)$$

with  $v$  the longitudinal sound velocity of the MDL. The microstrains  $\lambda(x, t)$  caused by the steady state pulsed current are summed up as a group of strains  $G_s(x, t)$ , which follows  $G_r(x, t)$  :

$$G_s(x, t) = \sum_{n=n_1}^{n_2} \lambda_s \left( 1 - e^{-\alpha \frac{(I_0)^2}{a^2 + (x - (n_3 + n_2 - n) \cdot T \cdot v)^2}} \right) \quad (2.25)$$

Finally, the microstrains  $\lambda(x, t)$  caused by the falling pulsed current are summed up as a group of strains  $G_f(x, t)$ , which follows  $G_s(x, t)$  :

$$G_f(x, t) = \sum_{n=n_2}^{n_3} \lambda_s \left( 1 - e^{-\alpha \frac{\left(\frac{(n-n_3)I_0}{n_3}\right)^2}{a^2 + (x - (n_3 - n) \cdot T \cdot v)^2}} \right) \quad (2.26)$$

These groups of microstrains propagate along the magnetostrictive wire as an elastic pulse. This elastic pulse causes a flux change along the volume of the material it propagates, which can be detected by the search coil set around the wire. Provided that the pulsed current is short, the change of the flux in the wire gives a single pulsed voltage output, as illustrated in Figure 2.9.

If the pulsed current has a long steady state, the first derivative of the elastic pulse, which corresponds to the pulsed voltage output breaks into two pulses, opposite in signs which are detected by the search coil, as illustrated in Figure 2.10. The operation of this type of MDL is very similar to the operation of the coil-coil MDL arrangement. As it will be shown in next chapters, these arrangements may be used for various sensing elements and arrays or distribution sensors.

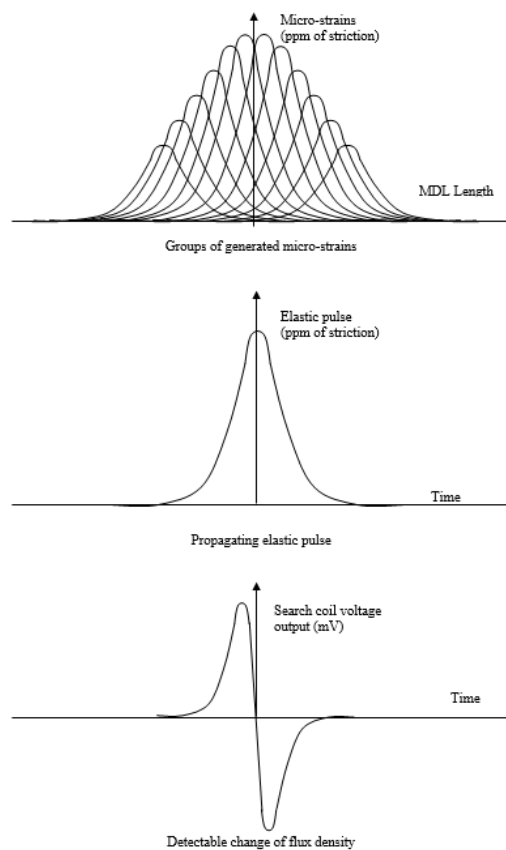


**Figure 2.9.** Short duration of the excitation field results in a single voltage output pulse.

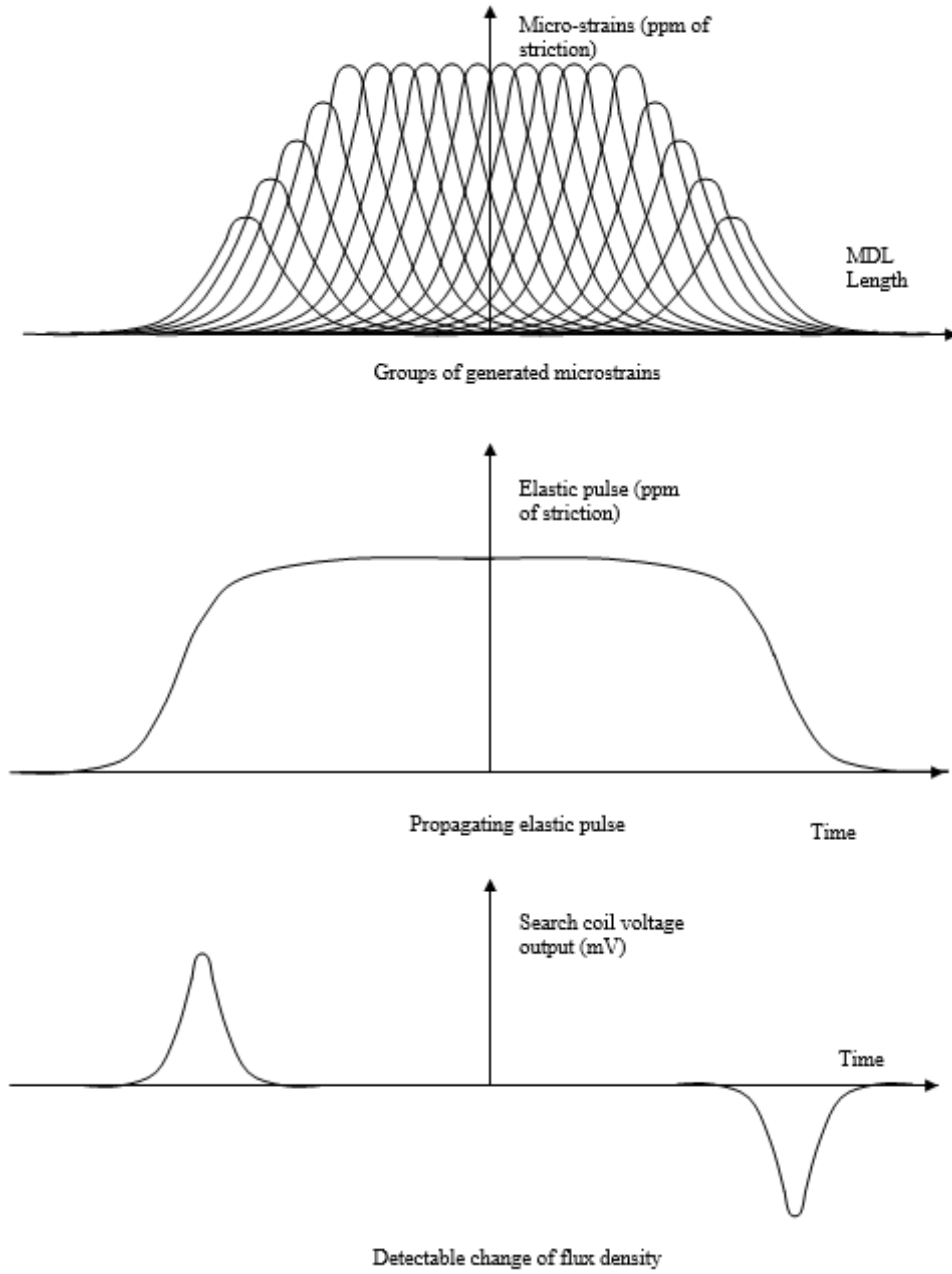


**Figure 2.10.** Long duration of the excitation field results in two discrete voltage output pulses.

---

## 2.2.2 Array of conductors perpendicular to an array of MDLs

---

The basic arrangement is illustrated in Figure 2.11. A pulsed current conductor array used for pulsed current transmission is set orthogonal to an array of MDLs. Small field permanent magnets can be fixed at the MDL receiving coils, in order to maximize the voltage output. Small field permanent magnets can also be arranged at the intersections of conductors and MDLs, in order to maximize or/and stabilize the MDL voltage output.

Transmitting pulsed current through the excitation conductors, the generated acoustic pulses travel with the longitudinal sound velocity along the MDL and therefore, they are detected by the search coil as a train of voltage pulses. As an example, considering two conductors transmitting pulsed current perpendicular to a single MDL, at distances  $x$  and  $y$  respectively, as illustrated in Figure 2.12, the pulsed voltage outputs will be detected with a delay time equal to  $x/v$  and  $y/v$  respectively, where  $v$  is the longitudinal sound velocity of the MDL.

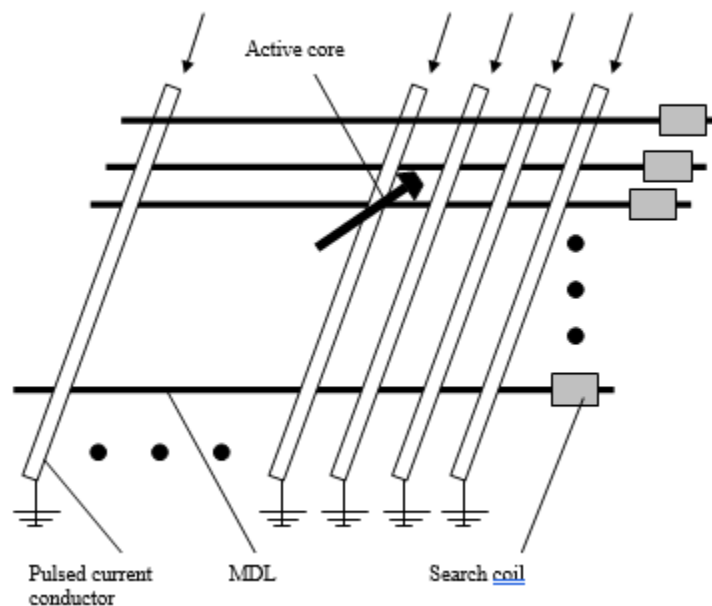


**Figure 2.11.** A pulsed current conductor array set orthogonal to an array of MDLs.

Such an arrangement can be used as the basis of integrated array sensing elements as it will be shown in following chapters, taking into account that each intersection of pulsed current conductor and MDL corresponds to a single sensing point. The type of sensor to be realized depends on the given application.

As an example, an integrated temperature distribution sensor can be realized, using an array of parallel conductors, perpendicular to a single MDL, using a temperature sensitive element, like thermistors or platinum wires connected in series with the current conductors. Such an inexpensive arrangement may offer a spatial range and resolution of temperature measurement of the order of several meters and a few mm respectively, which can't easily be realized by any other sensing technique. Other examples of analog multiplexers may also exist, as it will be analyzed in next chapters.

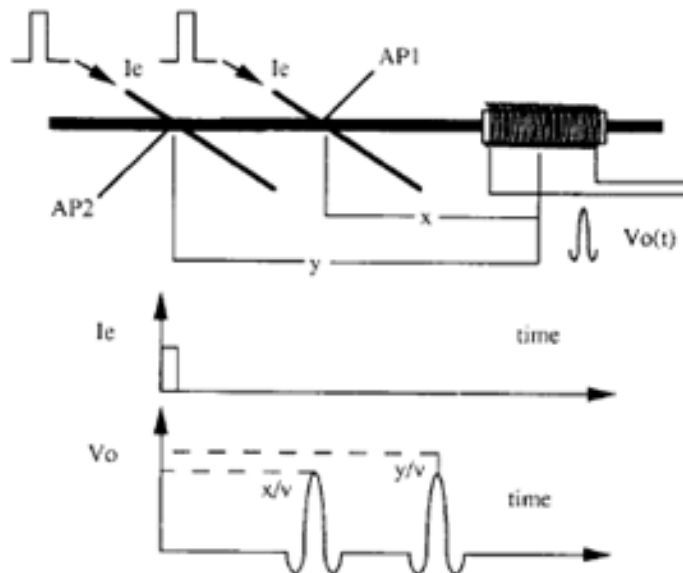


**Figure 2.12.** Two discrete pulses detected due to two, simultaneously excited pulsed current conductors.

The types of sensors which can be the outcome of such an arrangement are mainly based on the modification of the pulsed and biasing fields at the conductor – MDL intersection. Such a modification may be due to many reasons, like ambient field change, temperature affecting the resistance of the pulsed current conductors etc.

---

### 2.2.3 Array of balanced conductors perpendicular to an array of MDLs

---

Using a pair of conductors perpendicular to an MDL, in a way that the conductors above and below the MDL are in equal distances from the MDL, as shown in Figure 2.13 and transmitting pulsed current of the same direction through both conductors, then, the magnetic flux in the MDL is balanced out, resulting in zero microstrain generation and propagation and consequently in zero pulsed voltage output across a sensing or search coil set at the one end of the MDL for elastic pulse detection. Practically, such mechanical and voltage pulses are never zero but always below a threshold, which can be considered as an offset value instead of a sensitivity criterion. We called the arrangement of these two conductors a “balanced” arrangement due to the balancing of magnetic flux in the MDL.

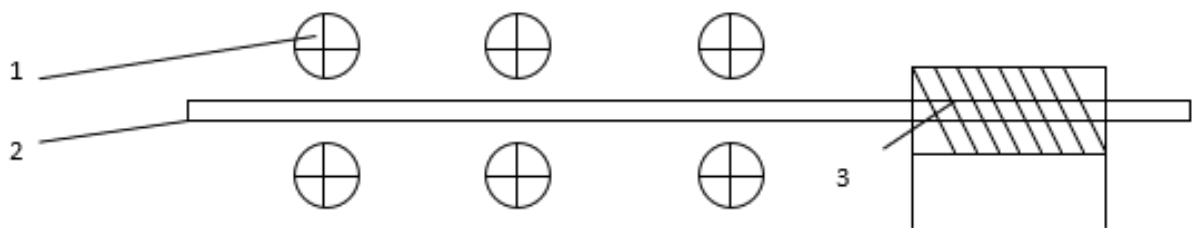


**Figure 2.13.** Balanced current conductor MDL arrangement, (1), Pulsed current conductor, (2) MDL, (3) Search coil.

Such a balance of magnetic flux can be destroyed by the ferromagnetic coupling of a soft magnetic material at the conductors – MDL intersection and the MDL itself, thus allowing the use of such a set-up in sensors. As it will be shown in next chapters, displacement, stress and non-destructive sensors have been developed, based on this idea.

Such an arrangement can be repeated in two dimensions by means of using an array of balanced conductors on top and below and perpendicular to an array of MDLs, as illustrated in Figure 2.14. These MDLs may use search coils at their one end in order to detect and serialize the elastic pulses coming from each sensing element defined by the intersection of each balanced conductor pair and each MDL.

In all these integrated sensor array MDL arrangements the search coils may also be replaced by other means of measuring magnetic flux changes, like MR and GMR films, MI and GMI wires etc, since all these

devices are able to measure flux and flux changes. Search coils can also be replaced by a magnetostrictive waveguide arranged in an angle not equal to  $90^\circ$  with respect to the array of MDLs.

Thus, elastic waves may be coupled, serialized in the above mentioned magnetostrictive waveguide. Then, they can propagate and be detectable by a search coil. However, it is worth mentioning that experimental evidence suggests the use of coils for sensitivity and hysteresis reasons.

The basic problem of such an arrangement is the repeatability and the uniform behavior of the MDL in order to allow predictable, repeatable and uniform response of the integrated sensor arrays. Such a problem exists and will be discussed and treated in the next chapter.

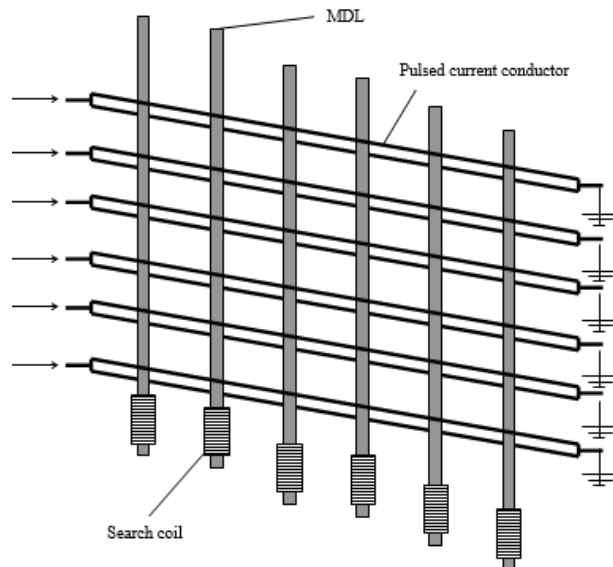


**Figure 2.14.** Array of balanced conductors on top and below and perpendicular to an array of MDLs.

---

## 2.2.4 Array conductors parallel to MDL arrays

---

Targeting an improved spatial resolution and better sensor performance, the arrangement of array conductors parallel to a single MDL or an array of MDLs may be useful in some applications. The two types of such an arrangement will be presented here.

### **2.2.4.1 Parallel conductor – MDL set-up**

The arrangement of pulsed current conductor or a pair of pulsed current conductors, parallel to the MDL is shown in Figure 2.15. A search coil is around the MDL at the one end of it. MDL may be terminated by latex adhesive at the two ends in order to eliminate acoustic reflections. A small field magnet bar is set close to the MDL in order to maximize the output of the search coil. In such an arrangement, the pulsed

field generated by the pulsed current transmission, penetrates orthogonally the MDL, thus not allowing the generation of microstrains due to the magnetostriction effect. In fact, even if an elastic wave is generated along the width of the MDL, it can't propagate along the length of the MDL, which acts as longitudinal acoustic signal waveguide.

Approaching a conducting disk close to the MDL-conductor arrangement, eddy currents are caused on the conducting disk. Keeping unchanged the pulsed current and the biasing field along the MDL, the amplitude of the pulsed eddy currents in the disk increase as the distance between disk and MDL decreases. Such eddy currents cause a pulsed magnetic field along the length of the MDL, which in turn causes a pulsed voltage output, induced in the detecting coil.

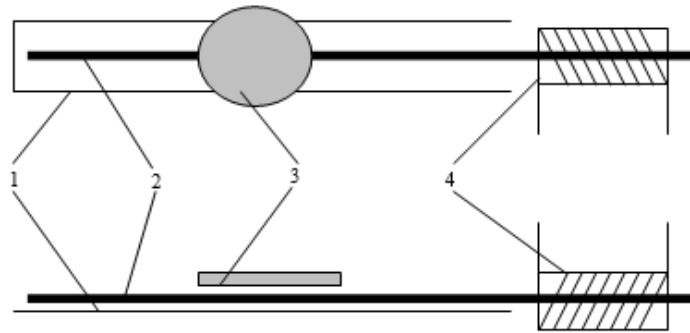


**Figure 2.15.** Pair of pulsed current conductors, parallel to the MDL. (1) Pulsed current conductors, (2) MDL, (3) Conducting disk, (4) Search coil.

The higher the eddy currents, the higher the magnitude of the detected voltage output is. The delay time between voltage output and excitation pulse defines the position of the conducting disk. Displacement of the conducting disk, along the MDL results in a change of the delay time between excitation pulse and detected voltage.

The arrangement of Figure 2.16 could also be used as a two-dimensional digitizer following the set-up shown in Figure 2.15. This set-up allows for the measurement of the three-dimensional motion of the conducting disk with corresponding results in the output of the search coils of the MDLs. More than one conducting disks can be set along the length of an MDL, thus making an integrated displacement distribution sensor.

The resolution of such a sensor is defined as the minimum distance between two active cores, in which discrete voltage outputs can be obtained. Such a distance has been found to be 8 cm. Applications of this

arrangement, as well as of the rest of the MDL set-ups will be shown in the next chapters related to MDL sensor applications.

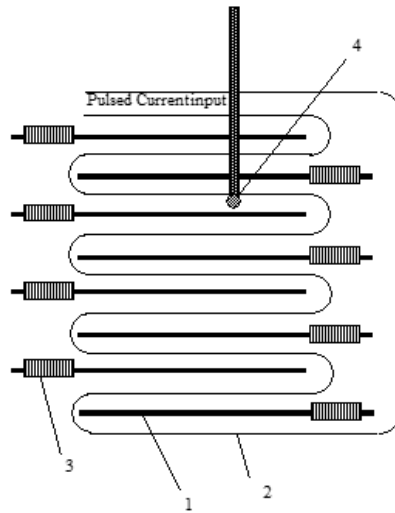
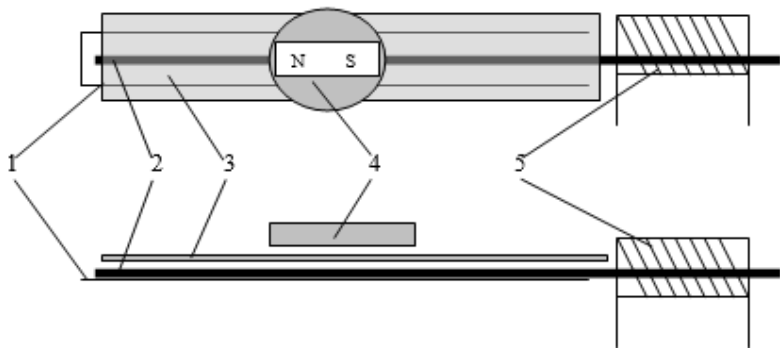


**Figure 2.16.** A two-dimensional digitiser based on the set-up shown in Figure 2.15. (1) MDL, (2) Pulsed current conductor, (3) Search coil, (4) Conducting disk.

### **2.2.4.2 Conductor – MDL – soft magnetic element set-up**

As shown in Figure 2.17, the conductor – MDL – soft magnetic element set-up (A), comprises of a magnetostrictive ribbon or wire (1), in the shape of an acoustic waveguide, to act as a magnetostrictive delay line



(MDL), a pair of parallel pulsed current conductors (2), which is parallel to the magnetostrictive element, to act as the transmission means of pulsed current, a soft magnetic ribbon (5), parallel to the set-up of the magnetostrictive element and parallel conductors, to act as flux concentrator and eddy current generator. The end of the MDL is preferably set inside the search coil (4), to avoid discrete reflections causing secondary pulsed voltage outputs.

**Figure 2.17.** Pulsed current conductor – MDL – soft element set-up. (1) Pulsed current conductor, (2) MDL, (3) Soft magnetic element, (4) Magnetic anomaly or moving permanent magnet, (5) Search coil.

The arrangement operates as follows: Pulsed current is transmitted into the pulsed current conductor. Such pulsed current causes transverse pulsed magnetic field along the magnetostrictive element. Consequently, the transverse pulsed magnetic field cannot generate an elastic pulse into the magnetostrictive element.

But the pulsed current causes eddy currents into the soft magnetic material (5) equally spread into the soft magnetic material, provided that the soft magnetic material is electrically and magnetically uniform. These eddy currents generate microstrains of the same amplitude along the length of the magnetostrictive element, if magnetoelastically uniform. These microstrains cancel each other allowing no propagating elastic pulse, apart from the edge of the magnetostrictive element or the soft magnetic material.

A local magnetic anomaly along the arrangement causes magnetic flux change at a given volume of the soft magnetic material. Such a magnetic flux changes the magnetic permeability at this volume and therefore changes the penetration depth of eddy currents at this given volume. This change of penetration depth results in different amplitude of eddy currents with respect to the rest of the body of the soft magnetic material.

Thus, the eddy currents at the boundary between the magnetized and the non magnetized volume are different. Such difference results in a break of the symmetry of eddy currents. Therefore an elastic pulse is generated propagating along the magnetostrictive element, which is detected by the magnetic flux receiver or search coil (4) by means of a pulsed voltage. Such pulsed voltage is received with a delay time proportional to the distance between permanent magnet and magnetic flux receiver and inversely proportional to the longitudinal sound velocity of the MDL.

Moving the position of the permanent magnet, results in a change of the delay time of the pulsed voltage output. Thus, the change of the delay time of the pulsed voltage output is the output of the sensing element, while the displacement of the permanent magnet is its input. The amplitude of the pulsed voltage output may also inform about the size of the local magnetic anomaly.

---

## 2.2.5 Non magnetic MDL waveguides

---

Using MDLs for sensing applications, it is of decisive importance to take into consideration the fact that their response is a combination of the magnetoelastic properties of the magnetostrictive material at the acoustic stress point of origin and the region of the receiving coil, as well as the mechanical and magnetic properties of the rest of the delay line, which is used as acoustic waveguide. Up to this moment, the magnetostrictive material has been presented as acoustic waveguide as well as magnetoelastic actuator, thus facilitating the ease of its use. But in the meantime it sets a limit in the mechanical properties of the used material as a waveguide and the properties of sensing elements based on this idea. A number of these sensors have a response based on the mechanical properties of the acoustic waveguide, an example being load cells and torque sensors.

The motivation for the realization of this arrangement was the development of a new set-up, where the properties of this waveguide could be tailored in order to improve the basic properties of the given set-up, like linearity, sensitivity, hysteresis and noise level, by tailoring the mechanical properties of the acoustic waveguide. This has been obtained by using the schematic arrangement illustrated in Figure 2.18. In this set-up, magnetostrictive material is connected on the substrate, using glue or soldering on a non-magnetic acoustic waveguide at two distinct areas of it, to be used as the acoustic stress regions of origin and detection respectively.

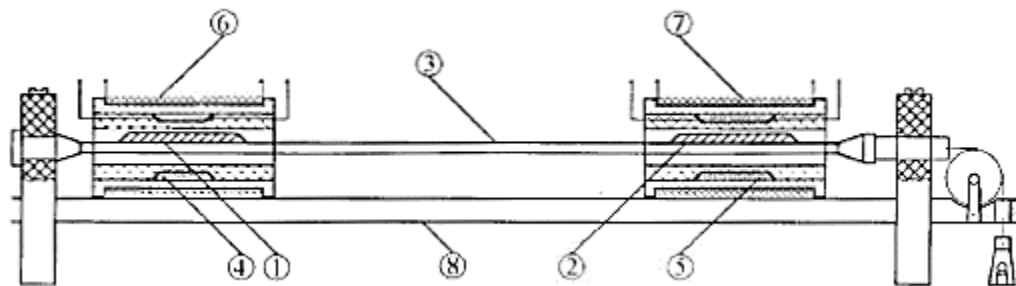


**Figure 2.18.** MDL with non-magnetic acoustic waveguide. (1) Magnetostrictive element used for generation of micro-strains, (2) Magnetostrictive element used for the detection of micro-strains, (3) Glass acoustic waveguide, (4) Pulsed current excitation coil, (5) Search coil, (6) Biasing coil at the region of excitation, (7) Biasing coil at the search region, (8) Arrangement support.

Hence, passing pulsed magnetic field along the acoustic waveguide and consequently along the magnetostrictive material at the acoustic stress point of origin, elastic stress is generated on it. The coupling between the magnetostrictive material and the acoustic waveguide results in transmission of the elastic pulse in the waveguide, which then propagates along its length as an acoustic signal. Such a signal arriving at the region of the second magnetostrictive material is also transmitted in it due to the above mentioned coupling, generating a magnetic flux change due to the inverse magnetostriction effect, which is received by means of a search coil set around the region of the magnetostrictive material.

Stressing or torsioning the whole arrangement mainly results in changing the elastic properties of the acoustic waveguide, thus resulting in a change at the propagating acoustic signal. Furthermore, moving a permanent magnet on top of the arrangement may also result in a modification of the output signal of the search coil. The geometry and material of the acoustic waveguide as well as its coupling with the magnetostrictive materials characterizes the response of this MDL set-up, thus enabling the broader tailoring of the MDL response.

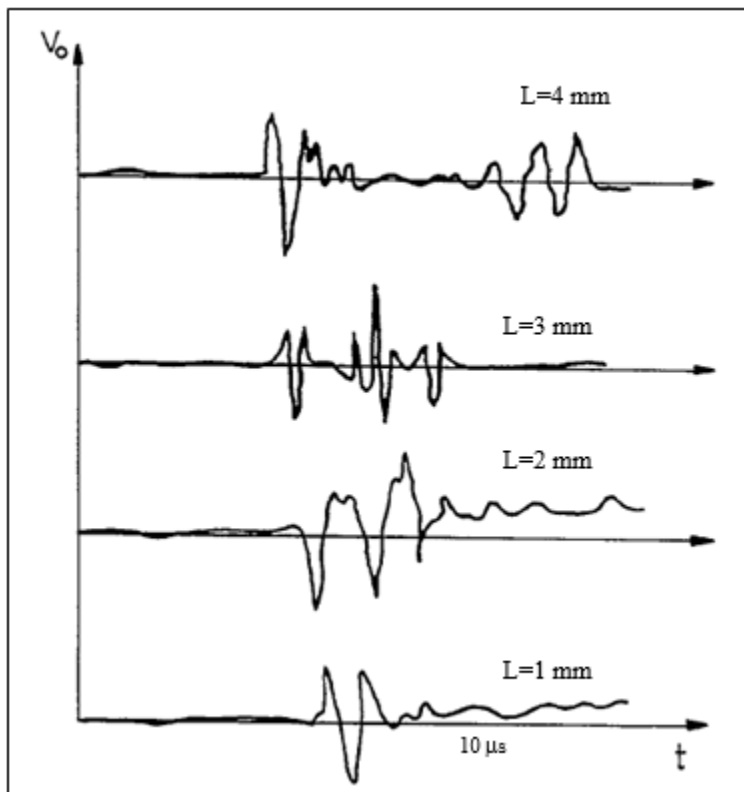


**Figure 2.19.** Typical output waveforms concerning the set-up of Figure 2.18, using magnetostrictive elements of different length  $L$ .

As a matter of example, we used Fe-rich amorphous wire specimen in the as-cast form as a magnetostrictive material and glass tube as an acoustic waveguide. Magnetostrictive material and acoustic waveguide were carefully connected by using acrylic glue. The diameter and length of the Fe-rich amorphous wire specimen were 150 microns and 3 mm respectively, while the diameter and length of the glass tube were 2 mm and 30 cm respectively.

It can be seen that the dimensions of the magnetostrictive material and the cross section of the acoustic waveguide have been selected in order to be of the same order to facilitate their coupling. The arrangement may serve as stress, pressure or load sensor. A typical output waveform is illustrated in Figure 2.19.

Such a response is mainly dependent upon the elastic properties of the acoustic waveguide provided that the magnetostrictive material characteristics as well as its connection with the acoustic waveguide are well standardised. Thus, the desired sensing output defines and tailors the kind of the elastic waveguide, which now can be selected out of a wider range of materials, not necessarily required to be magnetostrictive.

---

## 2.2.6 Coil-less MDL set-up

---

Another MDL arrangement able to be miniaturized down to the micrometer scale, without coils and air gaps, thus allowing a simple and cost effective manufacturing process, in the form of thick and thin films is presented hereinafter.

The main idea is to use the magnetostrictive material as a part of the current conducting path as shown in Figure 2.20. The passing current, transverse to the MDL axis, simulates the excitation coil or conductor behaviour. Let us consider a portion of a magnetostrictive element (m-element for short) preferably in the shape of a ribbon, connected with two conductors. When voltage is supplied to the two conductors, current is transmitted through the m-element, which is in touch with the two conductors. Such current causes a magnetic field  $H(t)$ , the profile of which can be determined by the Ampere's Law as:

$$H(t) = \frac{1}{2(w+d)} \cdot I(t) \cong \frac{1}{2w} \cdot I(t) \tag{2.27}$$

where  $w$  and  $d$  are the width and the thickness of the m-element respectively, provided that  $d \ll w$ . Supplying a pulsed voltage to the two conductors, pulsed current is transmitted through the surface of the m-element within a small depth, due to the skin effect, so that the field given by equation 2.27 approximates the pulsed field applied to the m-element, orthogonal to the direction of the pulsed current. This field is controlled by the thickness of the m-element, under controlled conditions of pulsed current. Considering a pulsed current peak of the order of 0.1 A and a material width of the order of  $10 \mu\text{m}$ , like in ribbons, the resulting pulsed field is of the order of 5 kA/m, which is high enough to saturate most of the soft magnetostrictive materials. With such an excitation, the dispersion of the acoustic wave is controlled only by the pulsed field duration and the conducting length of the m-element. It is noted that the peak current excitation in the conventional MDL technique is of the order of 10 A.

The corresponding MDL arrangement is illustrated in Figure 2.21. The generated elastic wave at the acoustic stress point of origin is coupled with the glass substrate and consequently with the second magnetostrictive element, generating small angle rotation of the magnetization of dipoles, and a corresponding magnetic flux component variation in the form of a pulse,  $dB_x(t)$  to it. For the case of a rectangular magnetostrictive element, such  $dB_x(t)$  change, results also in a  $dB_y(t)$  change. This flux change gives rise to a pulsed voltage output across the magnetostrictive element in both  $x$  and  $y$  directions. The two magnetostrictive elements are set at the two ends of the glass waveguide to avoid reflections and magnetoelastic after effects.

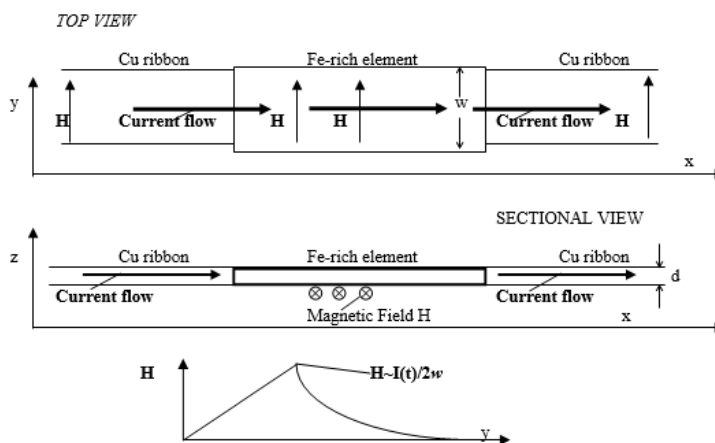


**Figure 2.20.** The basic idea for the coil-less MDL is to use the magnetostrictive material as part of the current conducting path.

The properties of this arrangement remain as good as for the classical MDL set-ups. The realized experiments on stress, field and magnet displacement show a monotonic decrease of the output signal from 100% down to zero.

Accordingly, controlling the acoustic wave generation, propagation and detection by magnetic annealing and geometrical arrangement, one can modify it by the well-known parameters affecting the behaviour of magnetoelastic waves and approach a linear or quasi-linear response, thus helping the output signal conditioning. It is also expected that the new MDL response should keep the same unhysteretic response of the classical MDL set-up.

Such an arrangement is competent against the other magnetic techniques, namely being the magnetoresistance and magnetoimpedence techniques in the domain of miniaturization, where it was not competent before. The ability of miniaturization, the monotonic response and the possibility of unhysteretic behaviour are the key-factors allowing the claim that such technique overcomes the present state of the art in sensing principles based on magnetic materials.

Furthermore, a relative advantage of using such sensing arrangement instead of semiconductor based in micromachining techniques is that less lithography, etching and micromachining process is required for the new MDL set-up, although it is sensitive and not well operating in environments with unknown ambient magnetic fields.

Another possible arrangement could be the use of only one magnetostrictive element for generating and detecting the magnetoelastic wave, by using the reflected wave in the glass acoustic waveguide end. The main problem is the signal conditioning of the reflected and detected acoustic waveguide, since its amplitude is one order of magnitude smaller than the excitation signal. A solution to that could be the use of a highly sensitive sample and hold electronic circuitry for the reflected signal.

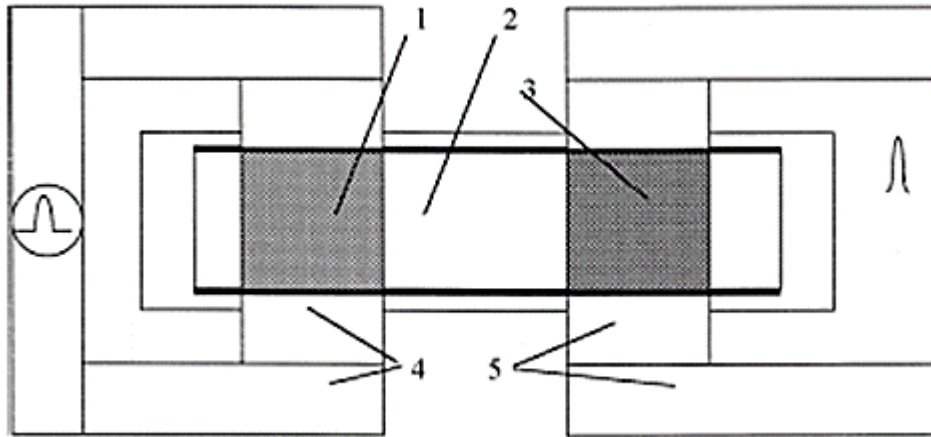


**Figure 2.21.** The coil-less MDL set-up. (1) Magnetostrictive element for microstrain generation. (2) Acoustic waveguide (for example glass), (3) Magnetostrictive element for microstrain detection, (4) Pulsed current conductor, (5) Detecting conductor.

Determining, controlling and tailoring the easy and hard axis of the magnetostrictive material can result in the control and tailoring of the range and accuracy of the magnitudes of field, stress and displacement. Magnetic annealing can also help in relieving the stresses on the magnetic surface attached to the substrate, increasing thus the total sensitivity of the arrangement. Furthermore, packaging the whole device with shielding material could probably help in the sensor uncertainty improvement.

---

### 2.2.7 Coily MDL set-up

---

For some given applications, there was a clear need for the improvement of the MDL spatial resolution and the uncertainty levels of the MDL position sensors. The need for such an improvement led to the development of a new coily MDL arrangement, using a magnetostrictive ribbon or wire wound around a straight conducting cylinder. Passing pulsed current through the straight conductor, the delay line is excited along the whole length of it. In case of uniform conditions of magnetoelastic behavior, microstrains are generated only at the two ends of the MDL. Provided that the uniformity of magnetic and

magnetoelastic conditions along the length of the MDL are broken for any physical reason, the above described symmetry is also broken, resulting in a propagating elastic wave which is detected as pulsed voltage output between the two far-end pulses  $V_{01}$  and  $V_{02}$  respectively. The modification of the pulsed voltage outputs due to this physical reason, breaking the magnetoelastic uniformity of the MDL, allows the use of the set-up as a sensing element of this physical reason.

The new set-up is illustrated in Figure 2.22. According to this set-up, a pulsed current generator is used to transmit current to a metallic tube (1) made of a low resistivity metal used as pulsed current conductor, preferably made of copper. Conductive spikes, housed in the metallic tube ends, are used to transmit pulsed current through the metallic tube connectors, to allow uniform distribution of the pulsed current density on the surface of the conducting tube. A magnetostrictive material (2) in the form of a ribbon or wire is wound around the conducting tube forming a single-layer solenoid, paying attention in obtaining no stress along the length of it, forming a coily magnetostrictive delay line. Two receiving coils (3) are set at the ends of this coily MDL and their output is driven to a voltage holder (4) and then to an analog to digital converter (ADC), as well as to an oscillator and a delay time counter (ODC). Finally, the outputs of the ADC and ODC are driven to a comparator and display unit. The two far-end pulses are propagating as elastic waves, and are detected by the receiving coils as two discrete pulsed voltage outputs,  $V_{01}$  and  $V_{02}$  respectively. These voltages have a delay between them proportional to the wound length of the MDL. The ends of the delay line are terminated on the pulsed current conductor by means of welding.

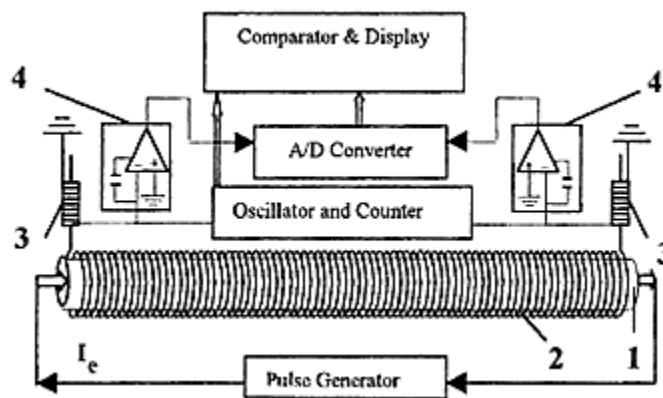


**Figure 2.22.** The coily MDL set-up. (1) Pulsed current conductor, (2) Solenoid-like MDL, (3) Search coils, (4) Peak and hold electronics.

There are two ways to break this magnetoelastic uniformity. One is the modification of the ambient field and the other one is the force or the pressure on the MDL, both applied in a local region of the MDL. Modification of the biasing field results in non-uniform and therefore non-zero local microstrains, while force or pressure on the ribbon or wire MDL results in additional acoustic reflections or damping. Both signals can propagate and be detected as magnetoelastic pulsed voltage outputs. In our application, the modification of biasing field is more often used, since it does not affect the lifetime of the MDL due to the mechanical load on it. The ways of breaking this magnetoelastic uniformity using local ambient field change are biasing field at a given region or permanent magnet displacement, both being close to the MDL.

The magnetic field change can be used for magnetic field distribution measurement purposes and most importantly in non-destructive distribution testing of magnetic surfaces. Magnetizing or saturating the under test magnetic surface, in case of no cracks and defects, the ambient field on top of the under test surface is more or less uniform, thus no breaking the MDL magnetoelastic symmetry occurs. In the presence of cracks and defects, this magnetoelastic symmetry is broken resulting in a local microstrain in the MDL. The size and the delay time of this microstrain can define the size and the position of the crack or defect. Furthermore, the MDL can be used as multiplexing means, serializing a number of these microstrains, allowing non-destructive distribution measurements.

The permanent magnet displacement can be used for position sensors by means of using either a moving magnet along the length of the conducting tube or a moving magnet vertical to it. In both cases, the sensing elements are cordless. In the case of a moving magnet along the length of the conducting tube, the sensor output is the delay time of the pulsed voltage corresponding to the region where the permanent magnet breaks the symmetry of the MDL, while the input is the position of the permanent magnet on top of the conducting tube. Therefore, the sensitivity of the arrangement is improved by a ratio equal to the diameter of the coily MDL cross-section or the diameter of the pulsed current conducting tube over the pitch of the of the coily MDL set-up. Since the above mentioned diameter and pitch are practically of the order of 50 and 0.5 mm respectively, the sensitivity is improved by a factor of 100. Such sensitivity cannot be further improved, due to mechanical and electric noise and jittering. Additionally to that, a magnet or an array of magnets can be set close to the MDL, so that their displacement, vertical to the pulsed current conductor axis in different MDL regions, will cause separated elastic strains and therefore separated voltage outputs.

Furthermore, having broken the magnetoelastic symmetry of the delay line by local change of ambient field, this MDL set-up can be used for measuring stress and torque applied along the length of the pulsed current conducting tube due to the modification of the magneto-mechanical coupling factor.

Although the basic properties and principal characteristics of the MDLs have not yet been presented, a rough idea about the performance of this set-up will be presented at this section. Experiments using this MDL arrangement have been performed, determining the dependence of  $V_o$  on magnetic field, displacement of a permanent magnet along the length of the pulsed current conducting tube and orthogonally to it, as well as stress and torsion applied on the set-up. In the experiments, we used a copper conducting tube having 30 cm length, 0.8 mm thickness and 15 mm diameter. The 300 turn search coils were made of 0.1 mm enameled copper wire. The tested magnetostrictive materials were ribbons, wires in the as-cast state and glass covered wires after high frequency annealing, all 15 m long.

Field dependence measurements illustrated sensitivity up to 1 mT. The response of the ribbon and the glass covered wire is smooth, while the response of the amorphous wire is influenced by the inner magnetic domain, exhibiting Large Barkhausen Jump, also observed in the MDL operation. The dependence of the MDL voltage output delay time between the search coil and excitation MDL region on the displacement of a moving magnet along the length of pulsed current conducting tube was linear. From this response, it can be seen that the sensitivity level is improved by a factor of 100, corresponding to the ratio between the diameter of the pulsed current conducting tube and the diameter of the MDL. Using conventional 1 Gs/s digital oscilloscope, the measurable time delays with this set-up were corresponding to 1  $\mu\text{m}$ . All other MDL set-ups used for position measurements had a sensitivity barrier of the order of 0.1 mm. We also believe that the 1  $\mu\text{m}$  sensitivity reaches the limits of magneto-mechanical and electromagnetic noise of the set-up.

This arrangement may be quite sensitive in moving magnet displacement sensing. Repeatability of  $\sim 3 \mu\text{m}$  and sub-micron sensitivity were obtained using laser interferometric calibration technique. Furthermore, the tensile stress and torsion dependence of this arrangement was found to be monotonic, but the repeatability of the measurement was not satisfactory because of the connections of the MDL with the pulsed current conducting tube.

Finally, magnetoelastic uniformity tests of different MDLs was determined illustrating a good uniformity by using amorphous wires or glass covered wires. Details of the response of this arrangement can be found in Chapter 3, where the various materials used for MDL will be discussed.

---

## 2.2.8 Circumferential MDL set-ups

---

A circumferential magnetostrictive delay line set-up is presented hereinafter, which offers improved characteristics for some given sensing applications. The tri-layer set-up consists of an inner cylindrical copper core, an intermediate thin insulating layer and an outer circumferential magnetoelastic thin film. Packaging reasons require a coating-insulating layer on top of the set-up. Different Fe-Ni compositions have been tested for the magnetostrictive film. Characterization of the devices showed that negative magnetostrictive film operates as a magnetostrictive delay line set-up, even without magnetic and heat treatment. Concerning positive magnetostrictive films, heat treatment was necessary to allow the propagation and detection of the elastic pulses.

The schematic of the magnetoelastic element is illustrated in Figure 2.23. A cylindrical conductor is used as the substrate for an insulating layer, on which a cylindrical magnetostrictive film is deposited. Passing pulsed current through the inner conducting wire results in transmitting pulsed circumferential magnetic field to the outer magnetoelastic film. Such field results in local micro-elongations or stresses due to the magnetostriction effect which, more or less, cancel each other due to the magnetoelastic uniformity of the outer film.

Local break of the magnetic symmetry results in a local break of the symmetry of the dynamic micro-strains, as depicted in Figure 2.24, thus generating an elastic pulse, which propagates along the length of the film, provided that such a propagation can take place. The propagating pulse can be received by means of a pulsed voltage output induced in a search coil at the one end of the device, due to the inverse magnetostriction effect. The time position of this pulsed voltage indicates the position of the magnet and its amplitude indicates the amplitude of the local magnetic field non-symmetry. This effect can be caused by a small permanent magnet travelling along the length of the device or by a local magnetic field anomaly. Therefore, such a device can be used as position/displacement sensor or distribution NDT sensor on magnetic surfaces.

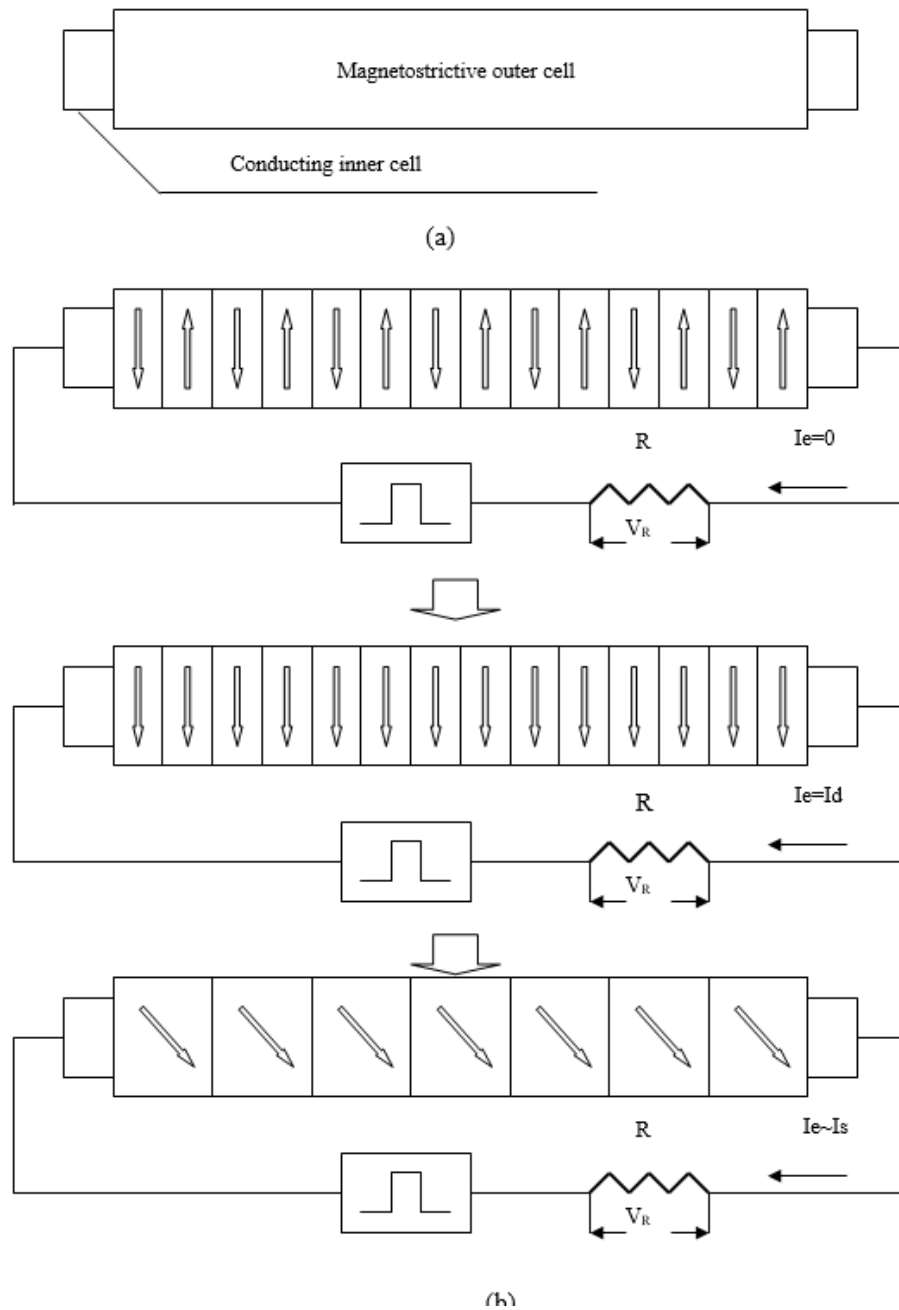


**Figure 2.23.** The schematic and the magnetization process of the circumferential MDL arrangement.

The realization of such a device took place in three steps. The first step was the development of the insulating interface layer between the conductor core and the magnetoelastic film. Although at the beginning this has been obtained by using a 0.1 mm copper wire thermally oxidised at  $\sim 550^{\circ}\text{C}$  for 10 minutes, resulting in a relatively thin oxide layer, with acceptable geometrical characteristics, for

repeatability and automatic production purposes, a magnetron sputtering device was used to deposit  $\text{SiO}_2$  film on the same 0.1 mm copper wire. The measurements of this oxide film thickness using cross section metallographic microscopy show a thickness of  $1 \mu\text{m} + 10 \text{ nm}$ , which is considered as acceptable.

The next step was the deposition of the magnetostrictive circumferential thin film, using the same magnetron sputtering facility. The first experiments were realised by depositing Fe-Ni alloys. The geometrical uniformity of the cross section of the films was also determined by cross section metallographic microscopy and was found to be  $1 \mu\text{m} + 20 \text{ nm}$ . X-ray diffraction structural characterization on the powder of the deposited magnetostrictive film indicated amorphous state. Elementary magnetoelastic measurements were performed in parallel with the structural characterization using Scanning Electron Microscopy (SEM) in order to determine the optimum conditions of films. It was found that the most significant structural problem was the generation of cracks on the magnetoelastic film. For the films having surface cracks, the elastic pulses could not propagate with acceptable repeatability and output gain. The best results (films without defects having some magnetoelastic response) have been found for films of thickness lower than  $0.8 \mu\text{m}$ . Details on thin film used as MDLs are given in Chapter 4.

The third and final manufacturing step was the coating of the magnetic films with a protective-insulating layer for packaging purposes. Trials for such deposition were realized by depositing  $\text{SiO}_2$  film. In such a development, a significant problem was the presence of “point” defects, which introduce stresses on the surface of the film. The absence of such defects was realized by controlling the coating deposition parameters, the key one being the vacuum conditions before the coating deposition. The best procedure of coating deposition was to realize it immediately after the magnetic film deposition. Bearing in mind that a heat treatment is necessary to minimize the coating-magnetic film interface stresses in order to obtain acceptable elastic wave propagation and detection, the final device was heat treated at  $\sim 450^\circ\text{C}$  for 10 minutes. Problems of overheating, could cause increase of those interface stresses.

Measurements were realized after setting a small Nd-Fe-B permanent magnet at the middle of the films in order to allow the generation of an elastic pulse. Most of the as-cast uncoated and coated films demonstrated poor magnetoelastic response. These properties were much improved by using heat treatment at  $300^\circ\text{C}$  for 1 h and consequent magnetic annealing at  $300^\circ\text{C}$  for 1 min and simultaneously passing 15 A pulsed current with 1% duty cycle and 1 ms period, through the inner copper wire.

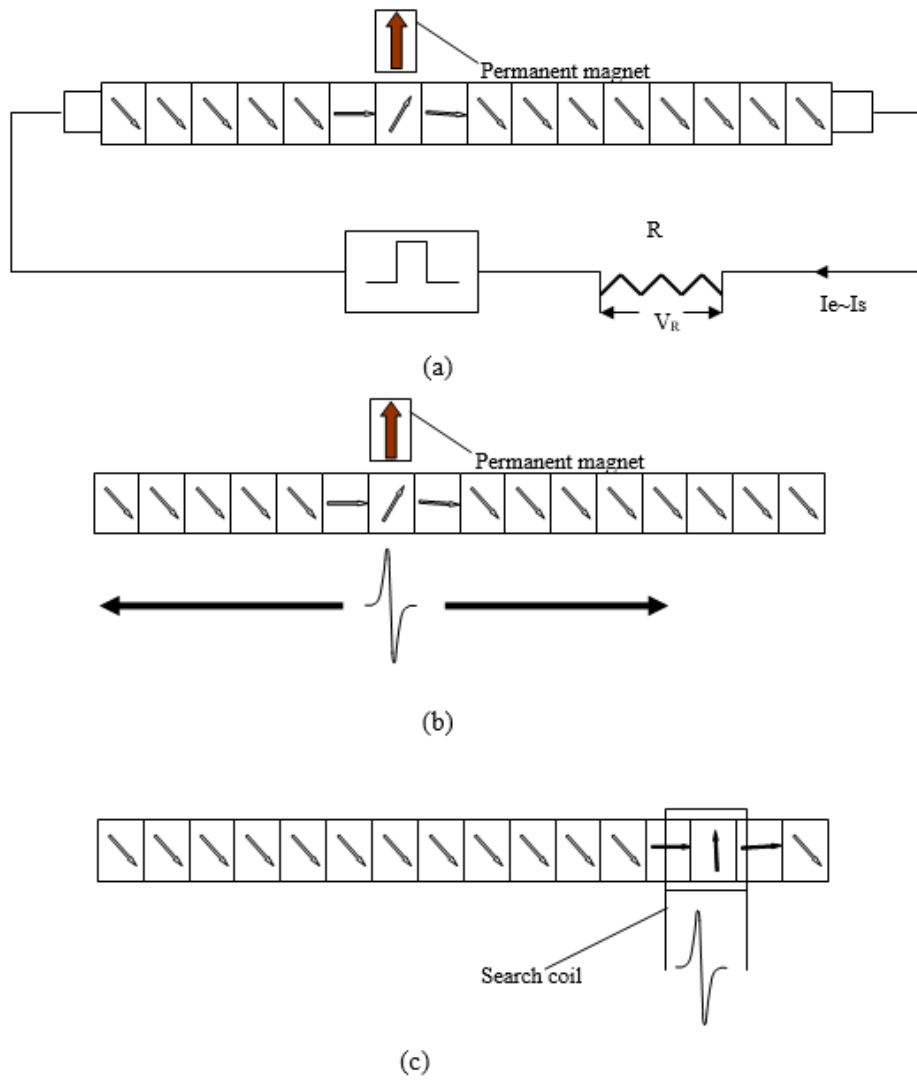


**Figure 2.24.** The magnetoelastic operation of the circumferential MDL arrangement.

The MDL voltage output dependence on the pulsed excitation field, for uncoated Fe, Ni and Fe50Ni50 films, illustrated a better response, although in all films a hysteretic behavior was observed. Similar response was observed for biasing field dependence measurements of the same films. The MDL tensile stress dependence of these uncoated films clearly illustrated the positive and negative magnetostrictive character of the tested films.

The response of the same magnetoelastic films after coating changed significantly. Some films, those with negative magnetostrictive behavior, operate even without heat and magnetic annealing. This is attributed to the different dependence of the positive and negative magnetostrictive elements on the tensile stress. Positive magnetostrictive elements tend to orient their magnetic moments towards the applied stress, while the opposite happens in the case of the negative magnetostrictive elements. The coating insulating layer of SiO<sub>2</sub> applies a tensile stress on these films. Therefore, the elastic signal in the case of positive magnetostrictive films becomes smaller, while the opposite occurs for the case of negative magnetostrictive films. Of course, heat annealing and consequent magnetic annealing help in different ways these two kinds of magnetostrictive films. In the case of positive magnetostrictive films it removes the interface stresses and additionally re-orientates the magnetic structure, increasing the magneto-mechanical coupling factor, while for the case of negative magnetostrictive films it affects only the magnetic structure. The optimum required frequency bandwidth and current consumption requirements have been found for each type of film. Finally, MDL resolution was measured following the definitions and procedures, illustrating a not significant difference for all tested samples.

---

### 2.2.9 Remarks and conclusions on the various MDL arrangements

---

Several MDL set-ups have been demonstrated in this chapter, covering all known MDL arrangements. Most of these arrangements have been conceived and studied in our research laboratory, while some (the circumferential MDL) have been re-developed and studied by us. In some cases, like the coily and the circumferential MDL set-ups, experimental results have been discussed concerning properties of MDLs or response of sensing arrangements, although these topics are covered in the next chapters of this work. These data have been given, in order to facilitate and enhance the understanding of the MDL arrangements, but also to “feel” which the basic parameters and properties of MDLs ought to be <sup>1</sup>. Thus, the basic properties of MDLs and the characteristics of various materials used as MDLs will be discussed in Chapter 3 and 4 respectively.

---

<sup>1</sup> For studying comprehension reasons experimental data are presented only once in the text

Furthermore, from the study of the MDL arrangements, it can be said that all possible parameters affecting the MDL operation which can be used for sensor applications are:

- i) The pulsed magnetic field  $H_e$ .
- ii) The biasing fields at the point of origin and the search point.
- iii) The mechanical properties of the magnetostrictive material.

Changing one and only one of the above mentioned parameters by a given physical size can result in a modification of the amplitude of the received pulsed voltage output. Various sensing elements have been developed, based on these parameters. They shall be demonstrated in the Chapters 5, 6 and 7, illustrating position, stress and field sensors respectively. Finally other MDL applications following the arrangements presented in this Chapter shall be demonstrated in Chapter 8.

# 3 MDL properties

In the previous chapter, the study of the basic MDL set-up and the description of the existing MDL arrangements revealed some of the properties which define the MDL operation and make apparent some of the parameters which help and characterize the proper MDL operation. These properties and parameters will be discussed in this Chapter. It should be kept in mind that  $\lambda(H)$  function is the crucial macroscopic characteristic which defines the MDL behaviour. Nevertheless, the  $M(H)$  function itself may also act independently, although it is related to the  $\lambda(H)$  function. The purpose of this Chapter is not to be used as a handbook, including all possible results concerning the MDL properties, but just to give indicative responses, thus offering a qualitative description of these properties. More analytical results can be found in the literature.

---

## 3.1 *The basic MDL properties*

---

The basic MDL properties namely, sensitivity, linearity and hysteresis partially define the quality of an MDL arrangement. All these properties are strongly related to the  $\lambda(H)$  and  $M(H)$  functions and are also somehow related to one another.

---

## 3.2 *Sensitivity*

---

Sensitivity of a given MDL arrangement is defined as the infinitesimal observable change induced in the search means or search coil following the smallest possibly applicable change of a parameter affecting the

MDL response. Such a typical definition is applied as the initial step of the MDL characterization. In fact, there are two practical ways to quantify the MDL sensitivity, since they play a significant role in the sensitivity determination. The first one is to measure the maximum possible amplitude of the detected pulsed voltage output.

The amplitude of the pulsed voltage output is practically of the order of a few tens of mV for a classical polycrystalline material as shown in Chapter 4, while sometimes reaching the limit of a couple of hundreds of mV, concerning the case of carefully prepared highly magnetostrictive amorphous ribbons or wires. The other way is to determine the noise level baseline of the electric output.

Usually, the worst case of noise level equals a few  $\mu\text{V}$ , while a proper electromagnetic shielding may result in a few nV noise level. Finally, the sharpness of the pulsed voltage output is a criterion affecting the MDL sensitivity, defined as the time needed for the MDL output to reach its maximum value. A typically acceptable pulsed output sharpness is  $100 \text{ mV}/\mu\text{s}$ .

---

### 3.2.1 Linearity

---

The MDL is far from being able to be characterized as a linear function. This strongly non-linear behavior is due to the non-linearity of the magnetization and magnetostriction process, as well as due to the acoustic properties of the MDL medium acting as an acoustic generator, waveguide and receptor.

The linearity in the MDL case is the monotonic and fitable dependence of the MDL pulsed voltage output on the parameters affecting its response. Normally, such a dependence as shown in Chapter 4 is usually monotonic and fitable, with the exception of some non-monotonic behavior in deep saturation of some types of magnetostrictive materials. Determining and fitting the MDL parametric dependence can offer the measurement of the uncertainty level of the given MDL set-up.

Such an uncertainty mainly depends on the pulsed or ambient biasing field at the vicinity of the MDL, without excluding mechanical action on it. Generally, MDLs are highly non-linear systems. As an example, Figure 3.1 illustrates a typical MDL dependence on pulsed field, concerning amorphous ribbon and fiber in their as-cast state as well as glass covered wire after high frequency stress-current annealing, where the absence of linearity is observed. The response of the amorphous fiber is more sensitive, for reasons related to the softness of its  $M(H)$  loop, resulting in relatively sharp  $\lambda(H)$  function.

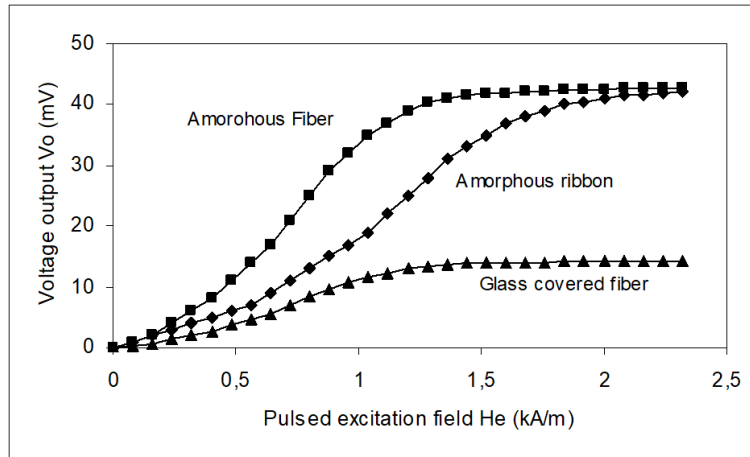


**Figure 3.1.** Typical MDL dependence on pulsed field.

### 3.1.3 Hysteresis

The third and most important property of the MDL response is the hysteresis, a highly non-linear effect defined as the difference on the MDL dependence on a parameter, when the amplitude of the given parameter increases or decreases.

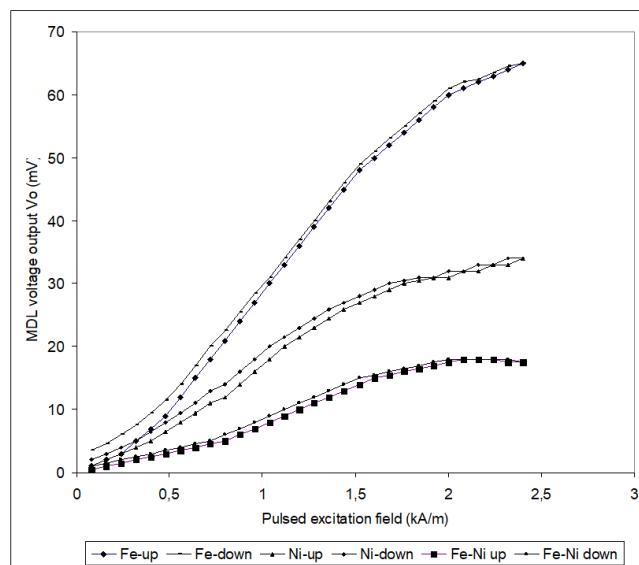


**Figure 3.2.** Typical hysteretic MDL response of polycrystalline Fe, Ni and FeNi wires, after heat treatment.

Hysteresis may appear in the dependence of the MDL output on the biasing and pulsed fields as well as on mechanical load. As an example, one parameter of hysteresis may be attributed to the difference of the

$V_o(I_e)$  function when increasing the pulsed current excitation peak value  $I_e$  up to a maximum value and consequently decreasing it to zero. Similarly, hysteresis may appear due to dc field change as well as to the applied stress, torsion or pressure on the MDL. The hysteretic behavior of the ferromagnetic materials is a part of the MDL hysteresis, so that it should be expected in all kinds of MDL materials and arrangements.

Surprisingly, in many magnetostrictive materials and arrangements, hysteresis has not been observable within the limits of our experimental facilities. The most commonly used magnetostrictive materials as delay lines, the amorphous ribbons, wires and glass covered wires illustrate zero hysteresis in the MDL response. This may be attributed to the forced operation of the MDL set-ups in the unhysteretic region of the under test materials, like the small angle domain rotation area of the magnetization loop. Generally, complete minimization of hysteresis can be obtained by avoiding Barkhausen jumps. Anyhow, determination of the region of un-hysteretic response of the MDL helps the designer and user of MDLs and MDL applications to obtain the optimum performance of the device under design.

Figure 3.2 illustrates a typical pulsed excitation field hysteretic MDL response of polycrystalline Fe, Ni and FeNi wires, after heat treatment in 300°C for 1 hr in Ar atmosphere.

---

### 3.1.4 Tailoring the basic properties

---

Magnetic characterization of soft magnetostrictive materials is the key-point in understanding their physics and using them for given applications [181,182]. Tailoring of their properties is mainly based on the anisotropy induced during various annealing processes.

Optimization of all the above mentioned parameters can be realized by tailoring the magnetostriction function  $\lambda(H)$  and the magnetization function  $M(H)$  and its parametric dependence mainly on frequency, stress and temperature. The main methods to optimize the magnetic and magnetoelastic properties of MDLs are the same three, as the ones used for the optimization of most magnetic materials.

The first one is the thermal treatment or thermal annealing, which can offer internal stress relief, provided that the annealing temperature, as well as the rhythm of increasing and decreasing the temperature have been carefully selected in order not to affect the structure (phase transformation), but only the

microstructure of the MDL material, such as defects, stresses etc. Such a treatment mainly contributes to the improvement of sensitivity and noise level.

Furthermore, magnetic annealing, i.e. thermal treatment in the presence of magnetic field may also contribute to the enhancement of the magnetic anisotropy and stabilization. Careful selection of the amplitude of the annealing field and most importantly its direction, contributes to a significant improvement of all basic MDL properties, like sensitivity, monotonic response and hysteresis.

Finally, in the last 20 years the stress-current annealing techniques are also used for tailoring the basic MDL properties. Current in inert or even in air atmosphere has a similar effect on the MDL to the thermal heating.

Additionally, the circumferentially induced magnetic anisotropy due to the current flow aids to some particularly interesting characteristics of the MDL like the absence of hysteresis. The simultaneous stress on the material during current heating also may introduce an anisotropy, which may contribute to the properties of the MDL.

Figure 3.3 illustrates the typically expected improvement of the response of amorphous ribbon after heat and field annealing in inert atmosphere and slow cooling-down process.

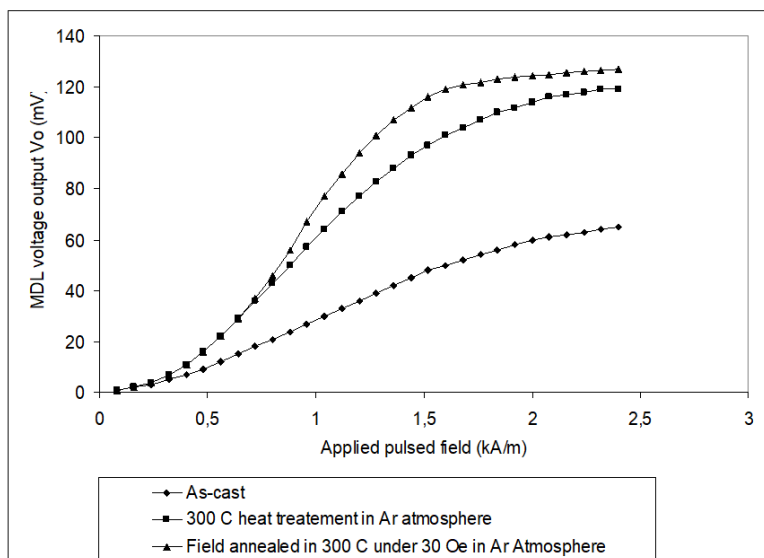


**Figure 3.3.** A typical improvement of the MDL response of FeSiB amorphous ribbon after thermal and field annealing.

---

### 3.3 Parametric dependence of the MDL response

---

The above mentioned MDL basic properties are affected and characterized by the MDL dependence on some crucial parameters, namely the field and temperature around the MDL, the tensile or torsional stress applied on the MDL, as well as the excitation pulsed field characteristics. These parameters will be presented hereinafter.

---

#### 3.2.1 DC Field dependence

---

The dc field dependence, i.e. the MDL pulsed voltage output dependence on the ambient dc field at either the elastic pulse excitation area or the receiving area, is the most well studied MDL parameter, since it is the most common parameter affecting the MDL response, in the most traditional coil-coil set-up. Figure 3.4 illustrates a couple of typical MDL waveforms under different biasing fields. A typical MDL dependence on dc biasing field can be seen in Figure 3.5, concerning as-cast amorphous Fe-rich wire.

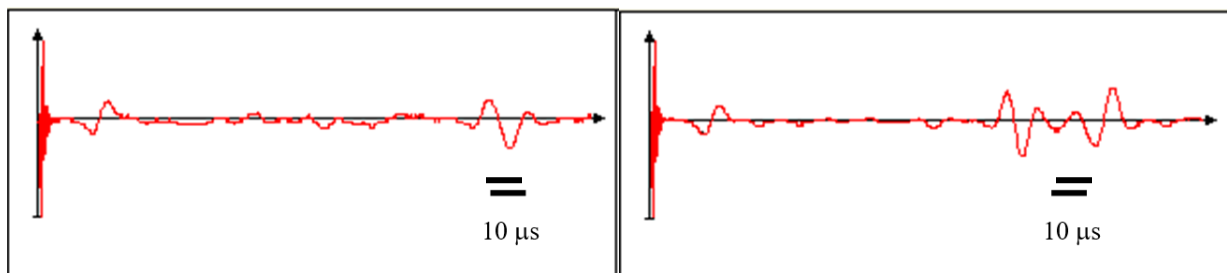


**Figure 3.4.** Typical MDL waveform outputs under various biasing fields. Left waveform corresponds to co directional bias and pulsed fields. Right picture illustrates opposing bias and pulsed fields. Horizontal axis corresponds to time.

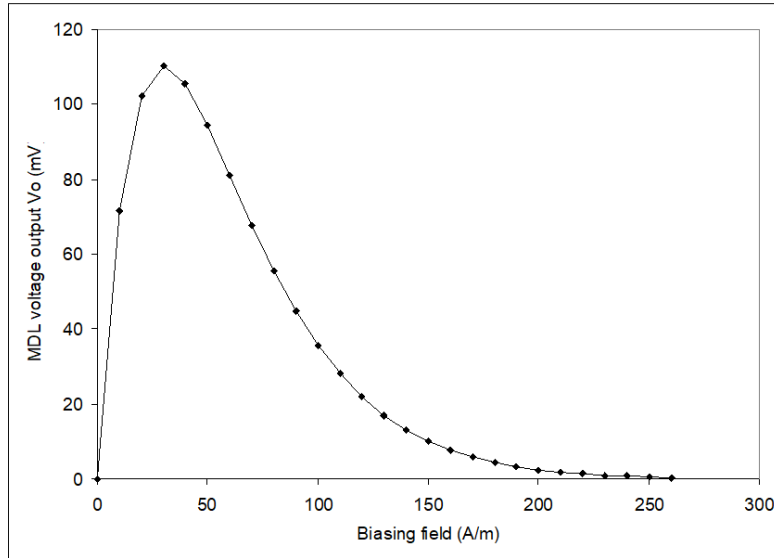


**Figure 3.5.** Typical MDL dependence on dc biasing field for heat treated amorphous Fe-rich wire.

The MDL response on field in this case, can be fitted by the following equation:

$$V_o(H) = V_o \cdot H \cdot e^{-\alpha_1 \cdot H} \quad (3.1)$$

where  $\alpha_1 > 0$  and  $V_1$  is the maximum response under no load. For the case of an amorphous wire, the coefficient  $\alpha_1$  was found to be  $\sim 1/10 \text{ (A/m)}^{-1}$ . The maximum deviation of the experimental data from the fitting equation 3.1 did not exceed 0.5 %.

The MDL dependence at the excitation point may differ from the one at the search point. This becomes observable in some magnetostrictive materials, like carefully prepared amorphous wires, as analyzed in the next chapter. Such a strong and non-monotonic MDL response normally makes the MDL behavior unpredictable and therefore non-useful for engineering applications. The presence of unexpected ambient fields modifies considerably the MDL response, thus destroying the read-out signals of the MDL sensor. The dependence of MDLs on the biasing field has been exhaustively studied in the past, concluding that there are only two ways to avoid such an effect: the first one is to magnetically shield the transducer and the other one is to measure and take into account the stray field presence (smart sensing

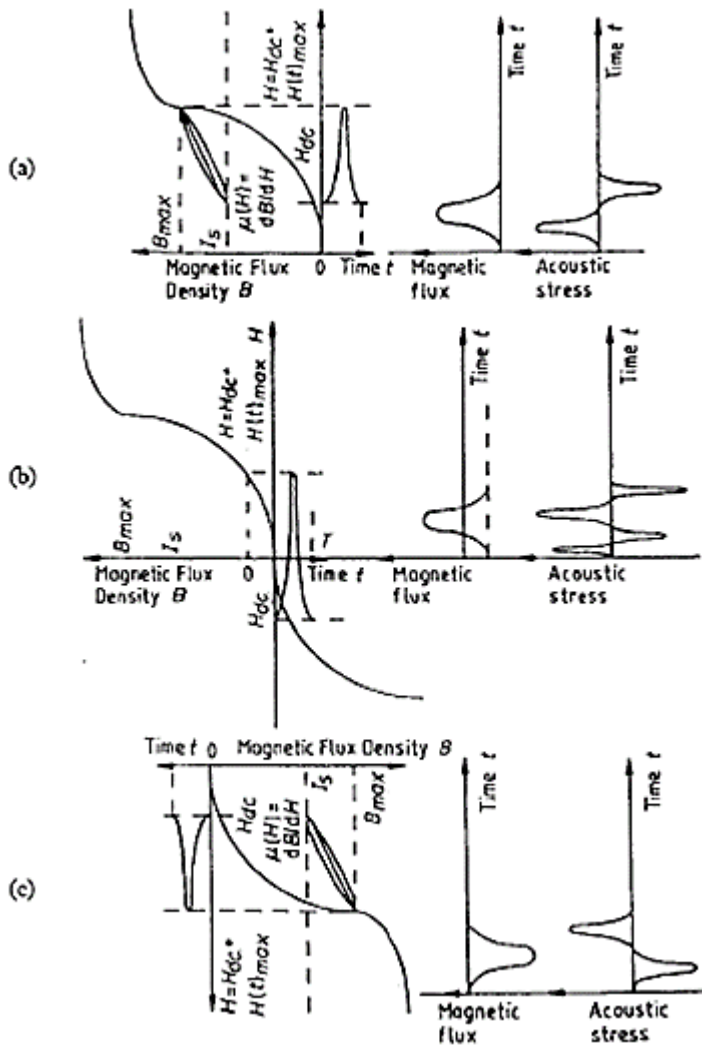


Figure 3.6. Analysis of the biasing field effect.

the acoustic pulse at the point of excitation due to the pulsed magnetic field applied longitudinally to the delay line is proportional to the first derivative of the square of magnetic flux, while the voltage output from the short coil at the end of the line, is proportional to the first derivative of the acoustic pulse. Three different cases can be distinguished:

1. DC field co directional to the pulsed magnetic field. Since a pulsed field is applied along the length of the line, a flux change and consequently an acoustic pulse is caused (Figure 3.6a).
2. Small - magnitude DC field opposite in direction to the pulsed field. The resulting pulsed flux change and the resulting acoustic stress are given in Figure 3.6 (b).

technologies). Instead, one could use either the outer or the inner part of the response in order to make use of the sensitive inner response for, as an example, magnetic non-destructive anomaly detection testing techniques, or the outer part of the response, after a threshold field biasing in order to make use of the long field range response. Studying the dc bias field response may help to understand the magnetic and magnetoelastic mechanisms of the under test magnetostrictive element.

Such dependence can be analyzed by following the MDL operation, as given in the previous Chapter. For simplification reasons it is assumed that the MDL has unhysteretic  $\lambda(H)$  response. It is also assumed that

3. Large DC field opposite in direction to the pulsed field. The resulting flux change and acoustic pulse are shown in Figure 3.6 (c).

Tailoring the dc field dependence can be obtained by using thermal treatment for hysteresis control, but mostly by using field or stress-current annealing in order to control the affecting biasing field range.

---

### 3.2.2 Pulsed field dependence

---

The pulsed field dependence, the MDL pulsed voltage output dependence on the pulsed excitation field or current, is significant not only for material characterization, but also for designing materials and devices for sensing applications. A typical response of the MDL dependence on the pulsed excitation field for a Ni wire after field annealing is given in Figure 3.7. It can be observed that the field range in the case of the dc bias field dependence is much smaller than the range of the pulsed voltage response. This is attributed to the domain wall motion in the case of the bias field effect and in rotation of magnetization in the case of the high bandwidth pulsed excitation field.

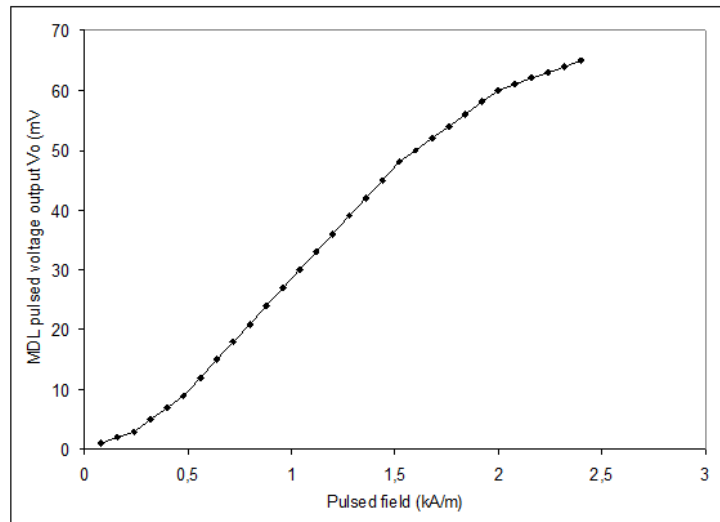


**Figure 3.7.** Typical MDL dependence on the pulsed excitation field for a Ni wire after field annealing in 300°C for 1 hr under 1 kA/m and Ar atmosphere.

This monotonic and unhysteretic behavior of some families of materials is responsible for the unhysteretic and sensitive response of sensors. Furthermore its sensitivity, i.e. how small pulsed field is required to saturate the MDL response is significant for a number of applications. Tailoring of such a response can be obtained by all three tailoring techniques presented above. Thermal treatment can improve hysteresis, while field and stress-current annealing can improve sensitivity and monotonic behavior. As analyzed in the previous Chapter, biasing and pulsed fields are crucial for the MDL response and their manipulation can serve for sensing application design and development.

---

### 3.2.3 Frequency dependence

---

Pulse width or frequency response has been defined as the dependence of the MDL pulsed voltage output on the frequency bandwidth of the pulsed excitation current.

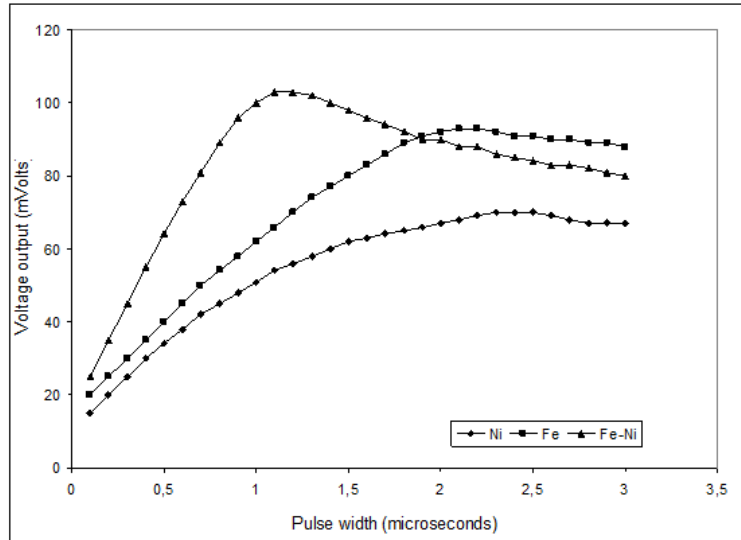


Figure 3.8. Typical frequency MDL response concerning as-cast Fe, Ni and Fe-Ni wires.

---

### 3.2.4 Stress dependence

---

The MDL stress dependence is defined as the MDL voltage output dependence on the applied tensile, compressive and torsional stresses along the length of the MDL, as well as on the pressure applied on the MDL. A typical response of the dependence of the MDL on applied load under various amplitudes of simultaneously applied biasing field is illustrated in Figure 3.9, concerning as-cast amorphous Fe-rich wires. Such stress dependence, in this case, can be fitted by the following equation:

$$V_o(\sigma) = V_o \cdot e^{-a_2 \cdot \sigma} \quad (3.2)$$

where  $a_2 > 0$ , and  $V_o$  is again the maximum response of the MDL. For this case, the coefficient  $a_2$  was found to be  $\sim 1/3 \text{ N}^{-1}$ . The maximum deviation of the experimental data from the fitting equation 1 was not more than 0.5 %, as for the case of the MDL field response.

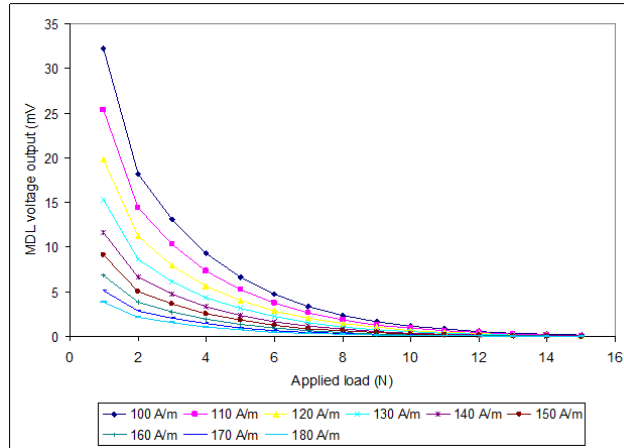


**Figure 3.9.** Typical response of the MDL dependence on applied load under various amplitudes of simultaneously applied biasing field.

### 3.2.5 Temperature dependence

The MDL temperature dependence illustrates the MDL voltage output change with temperature, the so called temperature coefficient in sensor technology. Generally, temperature dependence measurements showed a MDL voltage output stability up to 150°C. Accordingly, at this preliminary case study work, temperature coefficient has been considered as steady up to 150°C and therefore it has not been taken into consideration in the mathematic formalism of the MDL mode. A typical temperature response of MDLs is given in Figure 3.10.

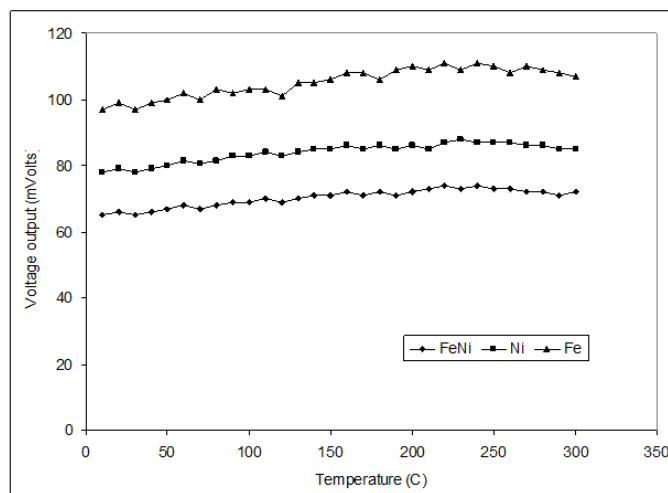


**Figure 3.10.** Typical temperature response of MDLs, for Fe, Ni and FeNi polycrystalline wires.

---

### 3.2.6 Temporal dependence

---

Temporal dependence is defined as the change of the MDL voltage output with time, keeping all the other parameters, such as field, stress and temperature stable. Temporal stability can be improved after aging the magnetostrictive material, by quenching. Generally, amorphous magnetostrictive ribbons and wires in the as-cast form have been found to be excellent in terms of temporal stability.

---

### 3.2.7 Response delay

---

Response delay is defined as the time needed for an elastic pulse to be detected and stored. Such a response delay is mainly controlled by the stability of the sound velocity of the magnetostrictive element, which will be studied separately in this Chapter. The methods for determining and stabilizing the sound velocity and the corresponding delay response have been analyzed, concluding that proper annealing and biasing field can result in delay response stabilization.

By the definition of the pulsed magnetic field MDL operation for a distance  $x$  from the receiving coil, the response delay consists of two time components: the first one is the  $x/v$ , where  $v$  is the longitudinal sound velocity of the MDL, resulting in different time delays for different elastic pulse points of origin. The other one is the pulsed current period, which is an offset delay time on top of the  $x/v$  component. The shorter the pulsed current period is, the better the MDL performance. However, shortening this period is limited by the  $x/v$  component, in order to avoid overlapping. A general method to determine the minimum required pulsed current period is as follows: considering the maximum and minimum distance between excitation regions and search regions as  $x_1$  and  $x_2$  respectively, the minimum possible pulsed current period  $T_{\min} = (x_1 - x_2)/v$ , in order to avoid any interference between acoustic pulses. Simultaneous transmission of pulsed current having this minimum period  $T_{\min}$  at excitation regions between these two extreme points  $x_1$  and  $x_2$  causes no interference among the acoustic pulses, provided that the distance between two adjacent and simultaneously excited excitation regions is large enough to avoid any superimposing of acoustic pulses.

As an example, considering the maximum distance between excitation and receiving regions 1 m, the maximum MDL response delay is less than 200  $\mu\text{s}$ , since longitudinal sound velocity of MDLs is about 5 m/sec. Furthermore, considering the maximum and minimum distance between excitation and receiving regions 1 m and 0.1 m respectively, the minimum pulsed current period is about 180  $\mu\text{s}$ .

---

### 3.2.8 Reflections, after-effects and signal dispersion

---

Elimination of reflections and after-effects improves the sensitivity and resolution of MDLs. Reduction of reflections can be obtained by high compliance termination of the magnetostrictive elements as well as by proper geometrical design of the MDL set-up. After-effect elimination can be realized by using optimum frequency response of MDLs after proper magnetic annealing. In many cases, it is important to measure the output signal dispersion, which defines the MDL resolution, which will be discussed separately in this Chapter.

Excitation pulses of a time width of the order of 1  $\mu\text{s}$  may often result in pulsed voltage outputs of the order of 15  $\mu\text{s}$ . The voltage output at the receiving coil was not only the one related to the applied pulsed current, but it was followed by a secondary, smaller in amplitude waveform, called after-effect waveform. Some theoretical explanations have been tried in the past, concerning scattering centres [39]. All of them agree with the fact that internal stresses in the delay line cause small reflections and therefore dispersion of the propagating magnetoelastic wave. So, the receiving waveform is followed by the after-effect waveform.

Apart from that the front part of the detected elastic wave is longer than the excitation pulse. This is due to the finite region of the MDL in which the magnetoelastic strain is caused. The size depends on the distance between conductor and delay line, and the magnitude of the pulsed current.

On the other hand, the receiving coil also plays a significant role, having a definite length and a quality factor, thus distorting the detected pulsed voltage output, as the resulting voltage is the convolution of the response of all the turns of the coil.

Stress relief process could improve the performance of the output waveform, due to the significant reduction of the internal stresses, thus resulting in a great reduction of the after-effect wave form. A significant improvement was observed for an MDL made of amorphous Fe-rich ribbon, heated in 300

degrees °C for 3 hours, in 90% Nitrogen, 10% Hydrogen, annealed afterwards in the same environment. Several MDL output waveforms have been presented in the literature, showing the generation of pseudo-transverse elastic waves following the main longitudinal propagating pulse. Such after effects are misleading if the original pulse is transverse. In such a case, a possibly generated pseudo-longitudinal pulse may arrive earlier than the initially generated pulse.

---

### 3.2.9 Experimental procedure of the determination of the MDL parametric response

---

Although determination of the magnetic properties of the materials used for MDLs, as well as their tailoring with respect to some parameters and applications has been well known and applied in research level so far, some other engineering characteristics have not been determined yet. The reproducibility, uniformity, resolution and finally uncertainty of the magneto-elastic behavior of these materials have not been approached yet as a generalized procedure by means of standardization. Magnetoelastic behavior determines the dependence of the generated micro-strains on the physical parameters affecting the behavior and their properties.

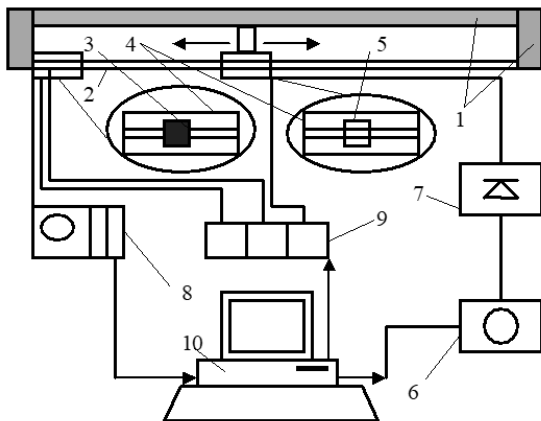


**Figure 3.11.** The computerized set-up for the characterization of magnetostrictive fibres. (1) Magnetoelastic sample, (2) search coil, (3) biasing coil for the search coil, (4) excitation coil, (5) biasing coil for the excitation coil, (6) mechanical terminations of the sample, (7) step motor for torsion on the sample, (8) step-motor and micro-positioner for tensile stress on the sample, (9) step-motor and linear translator for coil displacement, (10) arbitrary waveform generator, (11) RF amplifier, (12) digital oscilloscope, (13) computer, (14) triple power supply.

A computerized system has been proposed and implemented to study the behavior of soft magnetostrictive alloys in the shape of ribbons and fibers and develop a technique for complete

magnetoelastic characterization. Additionally, tailoring techniques using stress-current annealing processes can also be realized in the same set-up.

The simplicity of this system and the by-design straightforward determination of the magnetoelastic properties can make it the basic experimental set-up for the development of a new standard. The set-up of the system is illustrated in Figure 3.11 and 3.12.

The whole system can also work in vacuum. Testing the magnetostrictive material in vacuum, temperature control can be determined by design. Thus, sample annealing conditions can be determined with a higher degree of accuracy, attaining better levels of uncertainty. Signal post processing using wavelet techniques, can further improve on the overall performance of the system by means of reducing the output voltage noise and improving its integration procedure.

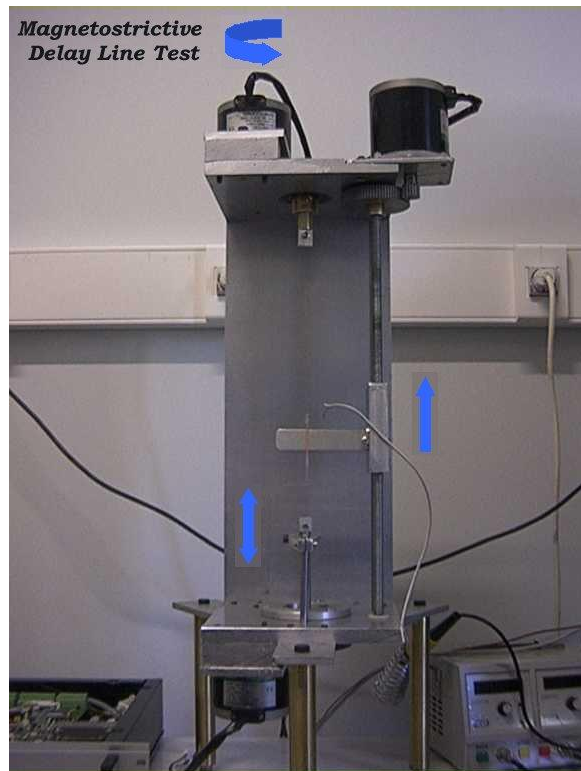


**Figure 3.12.** The MDL characterization system.

Inter-laboratory comparison tests have been performed at the Institute of Technical Physics, in Iasi, Romania and the Laboratory of Physical Metallurgy, National Technical University of Athens, Greece, using similar experimental arrangements. The reproducibility of the reported results was better than  $10^{-5}$ .

---

### **3.4 Magnetoelastic response and magnetoelastic uniformity**

---

The magnetoelastic uniformity (MEU) is defined as the fluctuation of the uniformity function  $V_o(x)$ , which in turn is defined as the dependence of the peak amplitude of the MDL pulsed voltage output  $V_o$  on the position of either the excitation or the search means, provided that one of these means remains steady in position. Such a measurement takes place under stable conditions of pulsed and DC bias magnetic fields

as well as in the absence of any kind of stress or varying stress on the magnetostrictive material acting as MDL. This unique approach of measuring the response of magnetostrictive materials is highly significant if the target is the use of magnetostrictive materials as magnetostrictive delay lines and thereafter as sensing analog multiplexers or simple sensing elements, since it defines the reproducibility of its response. Indicative results on the MEU of MDLs are reported, showing an improvement of the MEU after stress and current annealing, which decrease the local stresses induced during production of the material, as well as the effect of misaligned magnetic domains. A technique for fast magnetoelastic uniformity characterization capable to be used in industrial conditions is also proposed. A correction technique is finally proposed, according to which the output of the MDL can be calibrated in order obtain repeatable response.

---

### 3.3.1 Magnetoelastic uniformity

---

A typical experimental set-up for the recording of magnetoelastic uniformity is illustrated in Figure 3.13. The whole experiment can run automatically, as it can be interfaced with a driving computer. The optic bench offers mechanical stability against any undesirable movement during the uniformity function  $V_o(x)$  measurement. A typical  $V_o(x)$  response concerning an as-cast tested amorphous  $Fe_{78}Si_7B_{15}$  ribbon is illustrated in Figure 3.14. It can be seen that apart from the acoustic attenuation factor, the magnetoelastic uniformity suffers from a rather large uncertainty level, which is mainly attributed to the internal stresses of the material.

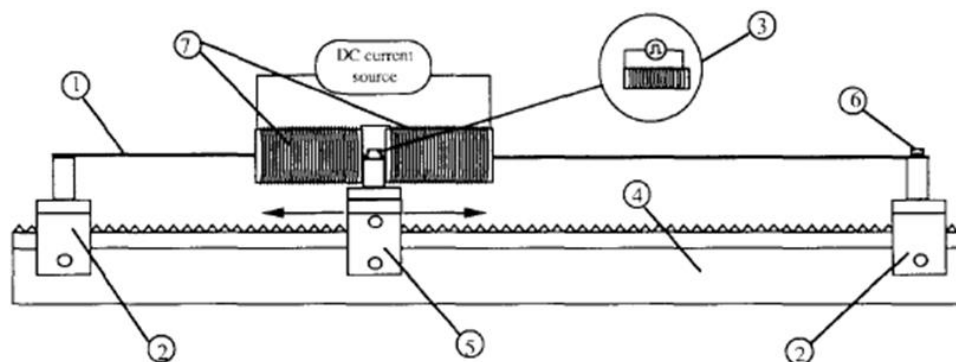


**Figure 3.13.** Experimental set-up for the measurement of the magnetoelastic uniformity. (1) MDL support, (2) fixed support, (3) exciting coil, (4) optic bench, (5) movable support, (6) detector coil, and (7) pair of coils for applying dc bias field.

Heat annealing of magnetostrictive materials, the so called stress relief process, improves the magnetostriction constant and reduces its internal stresses [24]. These stresses have enormous magnitudes and are unpredictably distributed in an as-cast magnetostrictive element. Additionally, the scattering centers, regarded as pinning and line defects, which cause secondary waveforms after the main pulse voltage for various kinds of magnetostrictive elements, are reduced after annealing [39]. Thus, all these can alter the acoustic behaviour of this material acting as MDL due to the unequal stiffness of the material along its length. Targeting the improvement of the MEU response, stress relief process was tried, as a means for a MEU possible improvement. Figure 3.14 shows the  $V_o(x)$  response of the previously as-cast tested amorphous  $Fe_{78}Si_7B_{15}$  ribbon after heating in  $350^{\circ}C$  for 1 hour in Ar atmosphere and consequent cooling with a rhythm of  $2^{\circ}C/min$ . An improvement of the MEU response can be seen, which unfortunately is not optimized.

Transverse or longitudinal magnetic annealing after stress relief process further improves the uniformity of magnetic domains for positive or negative magnetostrictive materials respectively [24]. So, targeting the improvement of such a response, the above mentioned as-cast  $Fe_{78}Si_7B_{15}$  ribbon was field-annealed in  $350^{\circ}C$  for 1 hour in Ar atmosphere and consequent cooling with a rhythm of  $2^{\circ}C/min$  in the presence of transverse field of  $800 A/m$ , since the  $Fe_{78}Si_7B_{15}$  ribbon is a positive magnetostrictive material. Its response is illustrated in Figure 3.16. A further improvement in the MEU response can also be observed, which unfortunately is not yet optimized.

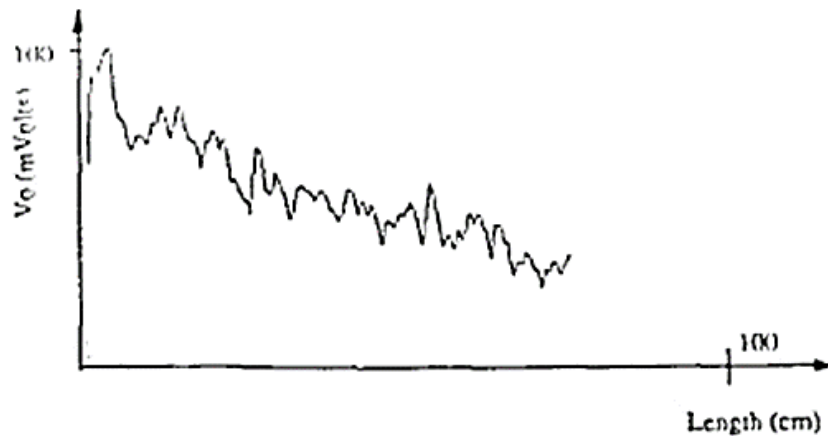


**Figure 3.14.** Typical  $V_o(x)$  response concerning an as-cast tested amorphous  $Fe_{78}Si_7B_{15}$  ribbon.

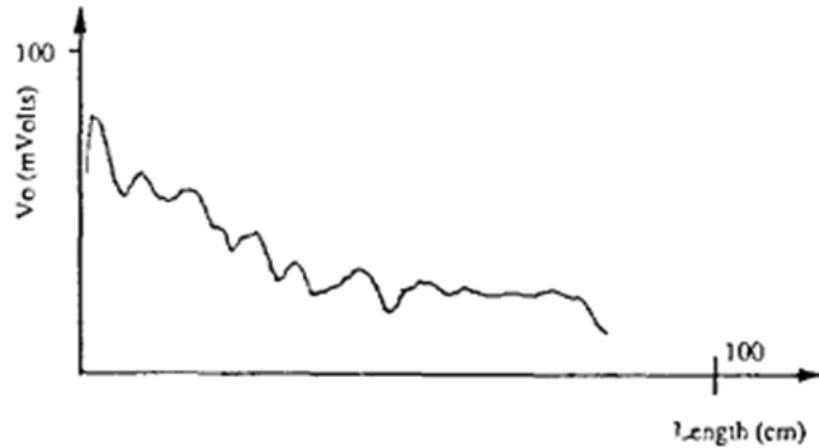


**Figure 3.15.**  $V_o(x)$  response of amorphous  $Fe_{78}Si_7B_{15}$  ribbon after 1 hr heating in  $350^\circ C$  under Ar atmosphere.

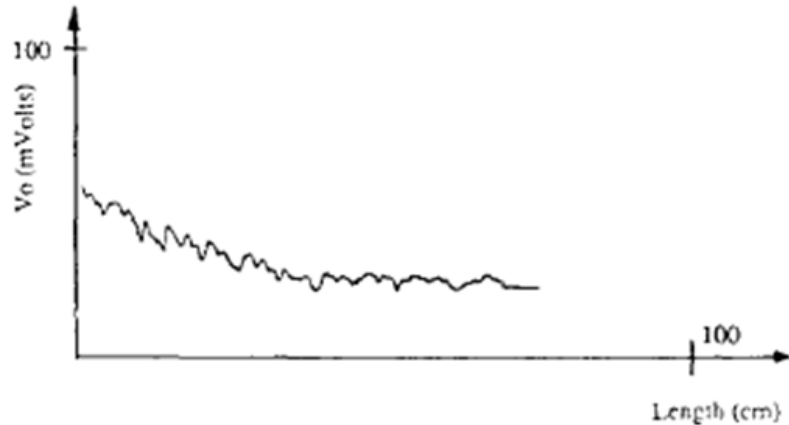


**Figure 3.16.**  $V_o(x)$  response of amorphous  $Fe_{78}Si_7B_{15}$  ribbon after 1 hr field annealing in  $350^\circ C$  and  $800 A/m$  under Ar atmosphere.

Finally, tensile stress in the line tends to make the magnetic domains uniform along the stress axis length, while current annealing results in fixing permanently this change after treatment. So, since the domain arrangement is more uniform, the magnetic flux density at the POs should be more uniform so that the flatness of  $V_o(x)$  should be improved. Thus, taking into account that flash-current annealing seems to offer similar results as the transverse magnetic field annealing and it is more proper for industrial applications, it was also tried, to observe its effect on the MEU response. Flash current annealing can be performed by stress-current annealing, typical values of stress, current and annealing time being 300-500 MPa, 100-500

mA for 30-300 seconds. Several results have been obtained, illustrating better or more uniform MEU response, but still not perfect.

In the contrary, amorphous wires offer a much better MEU response. Figures 3.17, 3.18 and 3.19 show the uniformity function of a  $\text{Fe}_{78}\text{Si}_7\text{B}_{15}$  wire tested as-cast, after stress relief process, obtained by passing 400 mA for 1 minute via the wire and after flash stress-current annealing under 400 mA for 1 minute under 500 MPa, for a line which was previously stress relieved in 350°C for 1 hour and then cooled down with 2°C/min. It was observed that the uniformity of the as cast wire was quite predictable especially in comparison to the tested amorphous ribbons of the same composition. Additionally to that stress relief process improves the sensitivity of the line due to the decrease of the internal stresses. Finally, a better sensitivity and uniformity was observed for the measurement under flash annealing, probably due to the more uniform orientation of the magnetic domains.

Similar results have also been obtained by testing magnetostrictive materials of many other compositions, shapes and crystalline structure. Taking into account that there are two types of usable shapes of magnetostrictive materials to be used as MDLs, one being the rectangular cross section, i.e. ribbon and the other being the circular cross section, i.e. wire, it can be concluded that in terms of magnetoelastic uniformity wires offer a significantly better MEU response. Only recently, some amorphous ribbons prepared by the planar flow instead of the spin-melt technique, offered a MEU response similar to the one of amorphous wires. This may be attributed to the following explanation: structural irregularities or scattering centers, called hereinafter irregularities, have a given periodicity in the material. So, the wavelength of periodicity of these irregularities is smaller in the planar flow quenched amorphous ribbons and the amorphous wires. In fact, such wavelength ought to be smaller than the excitation or detection region of the MDL, so that irregularities are covered or summed-up by the total length of the excitation or detection region. This becomes evident in the next section, where small irregularities have also been observed in amorphous wires, due to a different method of measuring the MEU response. It is noted, that polycrystalline magnetostrictive ribbons and wires present a rather good MEU response, better than the one of the spin-molten amorphous ribbons, but they suffer from other problems, like hysteresis and aging (temporal effect), so that they are not really used as MDLs.

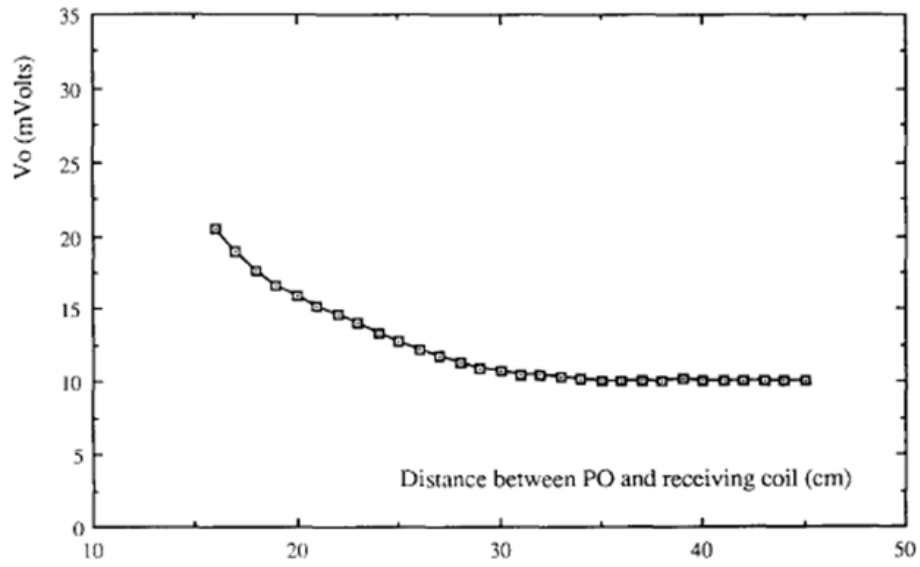


**Figure 3.17.** Uniformity of an as cast amorphous wire delay line.

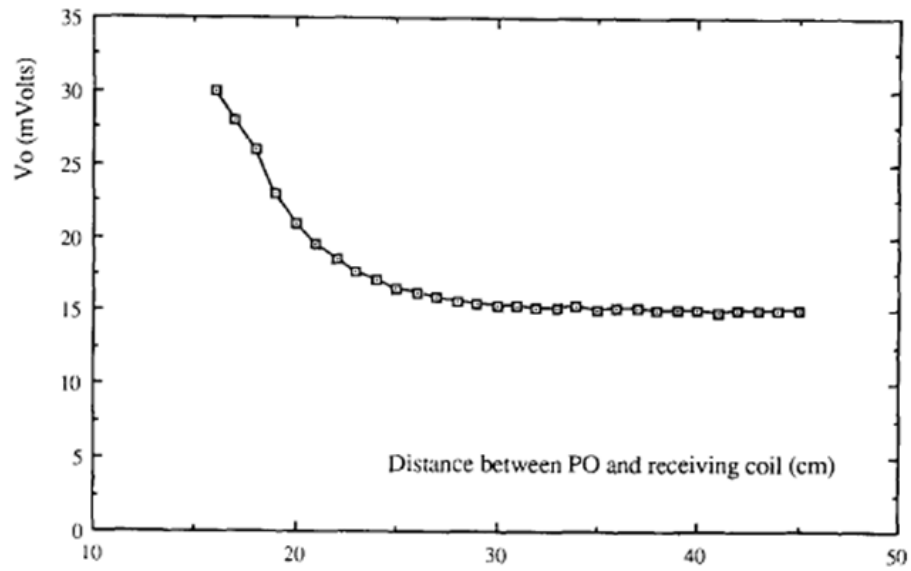


**Figure 3.18.** Uniformity of the line after stress relief process.

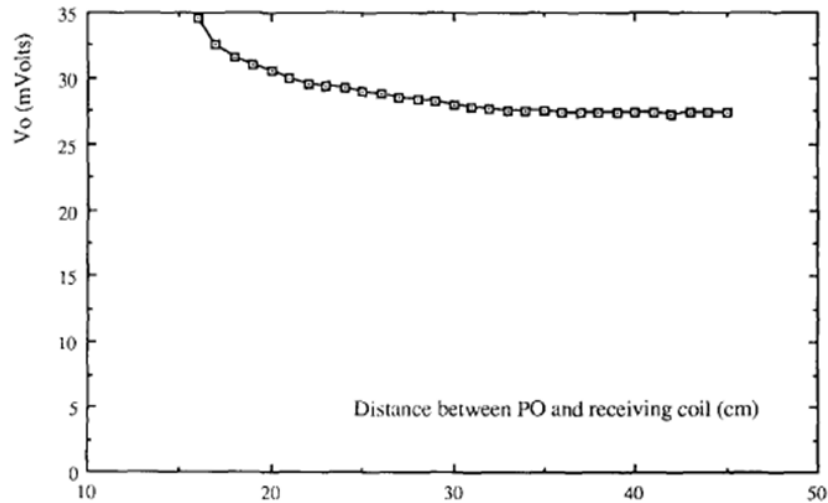


**Figure 3.19.** Uniformity of a stress-current annealed amorphous wire delay line.

---

### 3.3.2 Fast magnetoelastic uniformity determination

---

An alternative, inexpensive and fast method of determining the magnetoelastic uniformity of amorphous magnetostrictive ribbons and wires will be presented in this work. Such a method is based on the response of a magnetostrictive delay line (MDL) when pulsed field excites acoustically the whole line. Such a technique is not as informative as the classic MEU set-up, but it is much faster, thus allowing its industrial application.

The arrangement is illustrated in Figure 3.20. Such an arrangement comprises of exciting and receiving coils fixed in position inside a long quartz (or generally non-conducting and non-magnetic) tube. A long, uniform one layer coil is wound around this tube. This coil is short-circuited after winding. Pulsed current transmitted through the exciting coil, causes an acoustic stress in the MDL, which is detected by the receiving coil after a time relevant to the distance between exciting and receiving coil, but it also induces a pulsed current into the short-circuited long coil. Such a pulsed current within the short-circuited coil causes a pulsed magnetic field along the whole length of the MDL.

Assuming that the structure of the MDL (cross section area, magnetic material concentration, internal stresses etc) was uniform along its length, the produced neighbouring acoustic stresses along the MDL would be cancelled out, apart from the acoustic stresses at the regions of the MDL within the ends of the

long coil. In the case that an MDL had non-uniform structure at given regions, which results in nonuniformity of magnetoelastic waves, then acoustic stresses at those regions would not be cancelled out along the length of the MDL within the long coil, thus resulting in small elastic pulses propagating along the length of the MDL. These stresses would be received by the search coil as a train of voltage output irregularities being the indication of the nonuniformity of the MDL. In such an arrangement, as shown in Figure 3.19, can easily include a stress-current annealing facility.

The output of the receiving coil has two extreme pulsed signals, the one being the excitation pulsed signal coupled to the long coil and consequently to the receiving coil and the other one the voltage pulse induced at the receiving coil due to the main generated elastic pulse by the excitation coil. Between these two pulses the voltage waveform irregularities show the nonuniformity of the tested MDL. The smoothness and flatness of such a voltage waveform is the indication of the MDL magnetoelastic uniformity.

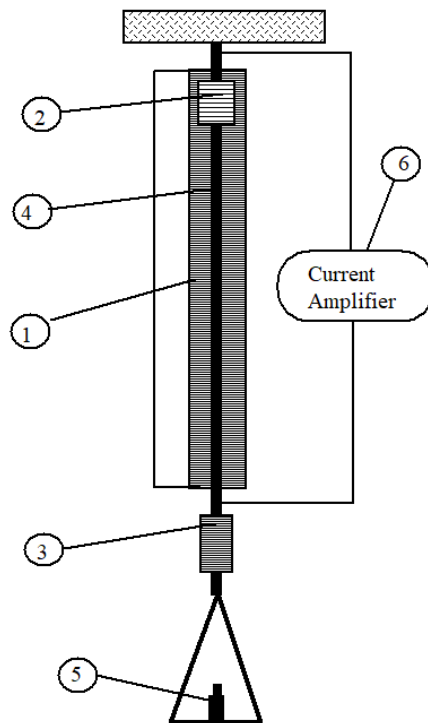


**Figure 3.20.** Arrangement of the device. (1) Magnetostrictive delay line (MDL), (2) Exciting coil, (3) Receiving coil, (4) Long, short-circuited coil, (5) Applied weight on the MDL, (6) Current amplifier.

Several ribbon and wire MDLs have been tested in order to observe their uniformity response and change, after stress-current annealing. Figure 3.21 shows the response of the receiving coil for a  $\text{Fe}_{80}\text{B}_{20}$  amorphous wire MDL in the as-cast condition and after stress-current annealing respectively. Stress-current annealing conditions for the illustrated results were 250 MPa and 500 mA for 3 minutes. Figure 3.22 illustrates the response of a  $\text{Fe}_{80}\text{B}_{20}$  amorphous ribbon MDL, which has undergone the same treatment as the above mentioned wire.

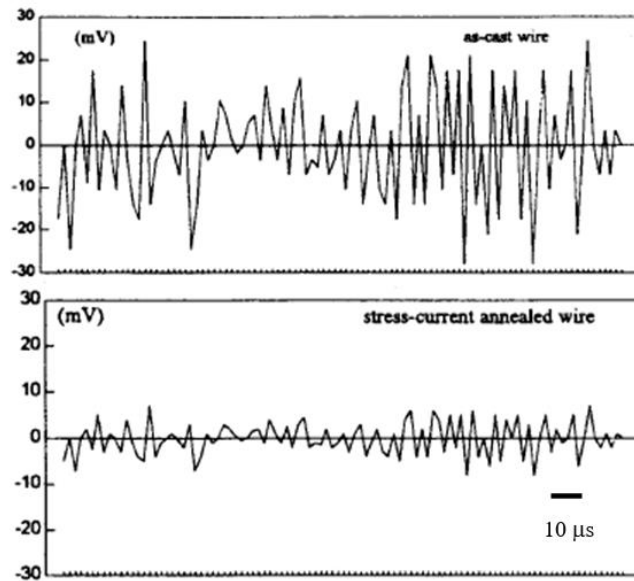


**Figure 3.21.** Fast MEU response of amorphous wire (horizontal axis in time).

Figure 3.23 illustrates non-uniformity in a torsionally annealed amorphous wire. Torsion annealing conditions were 10 turns/m and 500 mA for 3 minutes. From these experimental results it can be observed that the wire uniformity is much better than the ribbon one. The uniformity of both materials was improved after stress-current annealing, but not to perfection (flattening) for the case of ribbon MDL. It can be observed that induced stresses are observable even for the case of current annealed wires.

The results shown in this paper are in good agreement with results concerning nonuniformity function measured by the technique mentioned in the previous section. It should be also noted that the new method is more informative in principle than the previous one. In the previous method the exciting pulsed magnetic field was applied along a certain length of the MDL, which is called excitation length. This effect results in hiding MDL irregularities, appearing in lengths shorter than the excitation length. This can be observed indeed for the case of amorphous wires. In the results concerning measurement of uniformity of stress-current annealed wires due to our previous method no irregularities are observed obviously due to the averaging out of irregularities repeated in the excitation length itself. Instead, the new method can offer the observation of these irregularities as it can be seen in all related Figures, even for the case of stress-current annealed material.

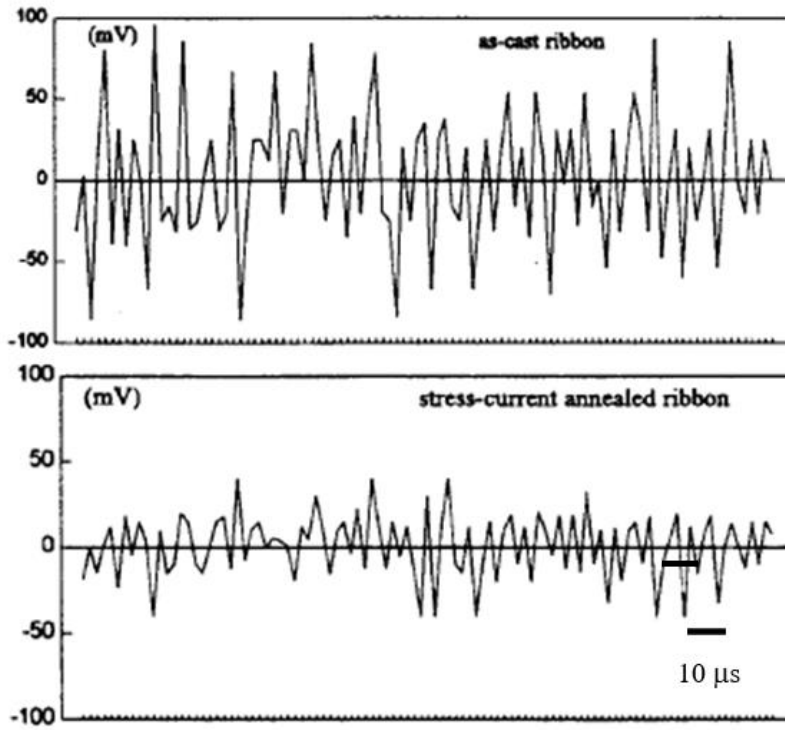


Figure 3.22. Fast MEU response of amorphous ribbon (axis horizontal in time).

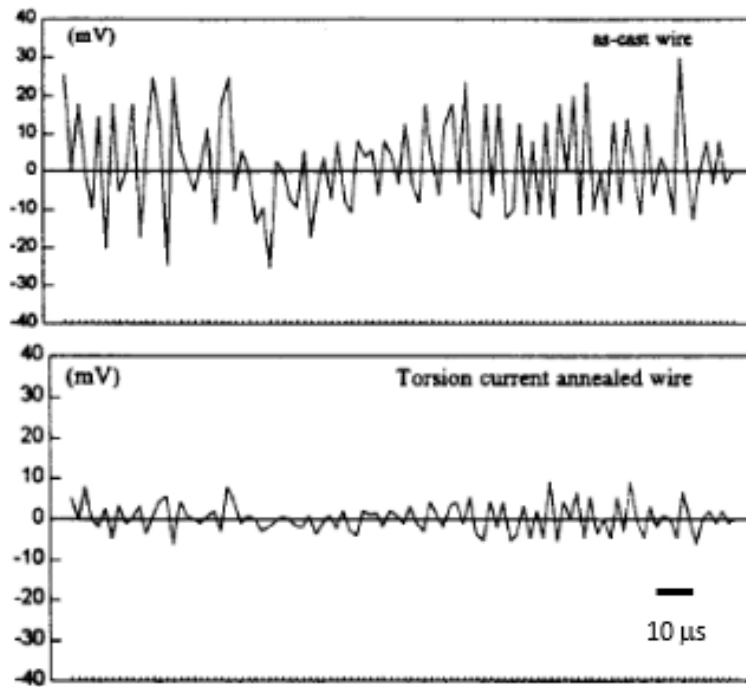


Figure 3.23. Fast MEU response in a twisted amorphous wire (horizontal axis in time).

The above-mentioned advantage of the new MDL uniformity characterisation set-up as well as the fast characterisation (200ms for 1 m MDL) makes this device attractive for industrial use of the characterisation of the uniformity of amorphous magnetostrictive ribbons and wires.

---

### 3.3.3 Normalization method and algorithm

---

The MEU response is not improved to perfection, even after stress-current annealing. However, even if a perfect or predictable uniformity function could be obtained, it could not ensure the unmistakable MDL operation as a perfect sensing analogue multiplexer or sensing element, since arbitrary, unpredictable variations of the geometry arrangements of the points of origin, like coil or packaging imperfections could occur, thus leading to undesirable and unpredictable acoustic pulse variations and non-uniformities. On the other hand, a correction of the readings because of the attenuation factor and other effects, like aftereffects, reflections etc is always needed.

There is an indication that a possible solution of the problem could be the use of weight factors to correct the readings of every sensing point of the delay line and such a solution is proposed in this section. These factors are defined with respect to a method, named normalization process. At this moment, it is believed that the outmost uniform response of the delay lines can be obtained by using this method. The experimental procedure to prove and implement this argument is as follows. The dependence of  $V_o$  on the peak amplitude of the applied pulsed current  $I_e$ , under the same conditions of DC magnetic bias field is detected for several excitation regions. All values of  $V_{oi}$ , for the given DC bias field (where the coefficient  $i$  declares the  $i^{\text{th}}$  excitation point), were divided by  $V_{ois}$ , corresponding to the value of the pulsed current  $I_{es}$  which saturates the MDL. As an example,  $I_{es}$  equal to 20 A leads well into saturation almost all magnetostrictive materials to be used as MDLs, even using the straight conductor perpendicular to the MDL arrangement. It was then found that the resulting values of  $V_{oin}$  (where  $V_{oin}=V_{oi}/V_{ois}$ ) vs  $I_e$  were identical for any point of excitation, so that the resulting fluctuation of  $V_{oin}$  becomes zero.

In the case of delay lines arranged so that they form a matrix of acoustic stress points of origin, using  $m$  delay lines and  $n$  conductors crossing them, the normalisation method is applied as follows: A saturating pulsed field  $H_{es}$  corresponding to the saturating current  $I_{es}$  (peak value typically equal to 20 A for the case

of conductor-MDL arrangement) is applied at the excitation regions, for all the points of excitation. The  $m \times n$  individual readings  $V_{osmn}$ , are used for storing in the memory of a computer the corresponding weight factors  $W_{mn}$ , which are equal to  $V_{osmn}^{-1}$ . One normalized function of  $V_{on}(I_e)$ , for any arbitrary selected point of excitation is also stored in the memory.

During the operation of the delay line, any reading  $V_{omn}$ , corresponding to a given position defined by the  $m^{\text{th}}$  delay line and the  $n^{\text{th}}$  crossing conductor is multiplied by the corresponding weight factor  $W^{mn}$  so that the value of the input  $I_e$  can be found by using the stored normalized value and  $V_{on}(I_e)$ . For an array of 100 delay lines and 100 crossing conductors, with 1 mm pitch for both the lines and the conductors, making thus 1 square meter sensing area, there are 10000 sensing points. If a 10-bit AD converter was used to read the corresponding outputs, about 40 KBytes would be needed to correct the readings, assuming that 2 Bytes are enough for any measured value, by using the normalization process. If such a method was not used, an individual read-out and correction of the readings by using individual look up tables would be needed, thus requiring far larger memory capacity (160 MBytes of memory), but more importantly, much longer time, thus making the measurements not real time readings.

---

### **3.5**      *Sound velocity and its uniformity*

---

For some MDL applications, apart from the magnetoelastic uniformity, the stability of the sound velocity is of great importance. In these applications, apart from the MDL pulsed voltage output, the time interval between excitation pulse and received MDL pulsed voltage output is to be detected. For these applications, the stability of the longitudinal and in some applications the transverse sound velocity of the material defines the precision of the sensor output. Of course, sound velocity measurement and characteristics are not only important for the characterization of the device based on the MDL technique, but also to study the material characteristics.

Several techniques have been presented in the past, referring to problems concerning the stability of sound velocity and describing the methods of determining it [13]. The major problem concerning the stability of sound velocity is the so called  $\Delta E/E$  effect. According to this effect, Young's modulus of some

magnetostrictive materials depends on the magnetic biasing field along the anisotropy axis, thus resulting in variation of the longitudinal sound velocity and consequently affecting the accuracy of the delay time measurement. Apart from that, the value of the sound velocity itself is important when the MDL technique is to be used for array sensor development. For these important reasons it is worth to determine the sound velocity and its characteristics, such as uniformity and parametric dependence, when magnetostrictive materials are to be used in MDLs and MDL applications. Among various techniques to determine the longitudinal sound velocity the coil-coil MDL arrangement has been selected for two main reasons: the first one is that most of the MDL applications utilize such an arrangement and therefore transmit elastic signals with the longitudinal sound velocity of the under test material and the second one is that this technique can be inexpensive and industrially applicable.

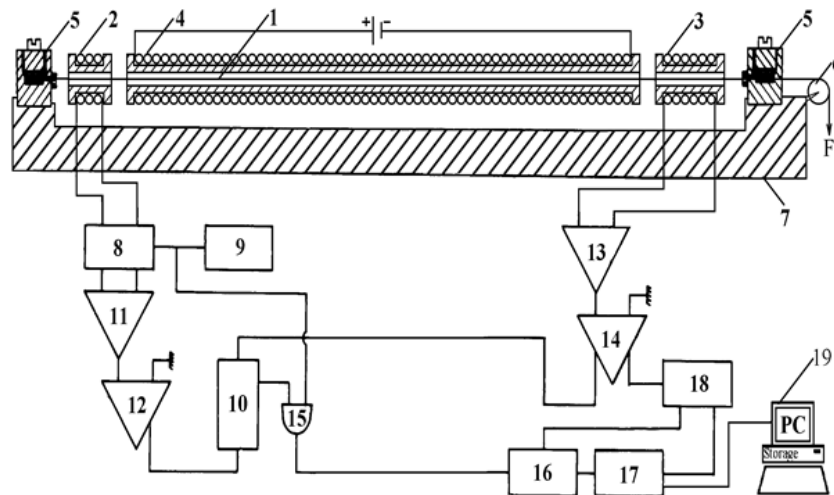


**Figure 3.24.** Electronic experimental set-up for the sound velocity measurements. (1) MDL, (2) Excitation coil, (3) Search coil, (4) Biasing coil, (5) Electrical conducts for current passing through the MDL, (6) Applied load on the MDL, (7) Optic bench, (8-18) Electronics for excitation and delay time measurement.

Magnetoelastic effects arise from the interaction between the magnetic moments and the mechanical structure of the material. Knowledge of the magnetoelastic properties dependence on different influence factors (external magnetic field, force, torque) offers the possibility to use such materials as new sensing elements. The change of the elastic modulus ( $\Delta E$  effect) in ferromagnetic materials originates from the rotation of the magnetization under the influence of applied magnetic field and stress. According to the  $\Delta E$  effect in these materials, the longitudinal sound velocity depends on the magnitude of the bias magnetic field and tensile stress applied parallel to the anisotropy axis.

The measurement system for longitudinal sound velocity is based on the magnetostrictive delay line principle. The basic diagram of the measurement system used for the determination of the longitudinal sound velocity value is presented in Figure 3.24. The amorphous wire (1) is fixed in a horizontal position and acts as a magnetostrictive delay line. Magnetoelastic waves are generated in the amorphous wire by a pulsed current in an exciting coil (2) set around one end of the wire having 2 mm length and 50 turns, made of 0.1 mm enamelled copper wire. The waves are propagating through the amorphous wire and they are detected at the opposite end by a receiving coil (3) having 3 mm length and 700 turns made of 0.04 mm enamelled copper wire. The amorphous wire was set in a bias coil (4) that generates the bias magnetic field along the axis of the wire. The tensile stress was applied at one end of the wire. A calibrated mechanical position meter is used to determine the distance between exciting and receiving coils. Pulsed current is transmitted to the exciting coil using a pulse generator (8). A 10 MHz oscillator was used to supply the necessary frequency for the pulsed current signal generator. In order to measure the time interval between the exciting and receiving pulses a time counter (16) was used.

The longitudinal sound velocity  $v$  is determined by  $v = L/T$ , where:  $L$  is the distance between the exciting and receiving coils centres and  $T$  is the time interval between the exciting and receiving pulses. The measurement system was calibrated using nickel wire as the magnetostrictive delay line. The uncertainty in the measurement of the dependence of the longitudinal sound velocity on the tensile stress and bias magnetic field comes only from the error of the time-counting system. This error is  $0.5 \times 10^{-7}$  s, resulting in a longitudinal sound velocity uncertainty of the order of 0.2 %.

Many different magnetostrictive materials have been tested and their longitudinal sound velocity has been determined. Among them, classical polycrystalline, Fe and Ni wires and tapes have been tested as well as amorphous ribbons, wires and glass covered wires in their as-cast form, as well as after heat annealing, magnetic annealing and stress-current annealing.

Since, amorphous materials play a significant role in terms of MDL applications, typical results concerning the longitudinal sound velocity as well as its dependence on the bias magnetic field and tensile stress values in  $\text{Fe}_{77.5}\text{Si}_{7.5}\text{B}_{15}$  amorphous wires, 125  $\mu\text{m}$  in diameter, tested in the as-cast state and after stress-relief process (thermally treated) are presented in this work. The heat treatments were performed at 300-370°C for 15 minutes to 1 hour, in a hydrogen atmosphere, in the absence of a magnetic field, in a non-inductive furnace ensuring a uniform heating of the wires all along their length.

Tensile stress and bias magnetic field were applied along the length of the amorphous wire. During the experiments the distance between the exciting and receiving coils centres was kept constant (500 mm). The amplitude, duration and period of the pulsed current were 14 A, 1  $\mu$ s and 2 ms respectively. The measurements made by increasing and decreasing the value of the bias magnetic field and tensile stress show the absence of hysteresis. The dependence of the longitudinal sound velocity in  $\text{Fe}_{77.5}\text{Si}_{7.5}\text{B}_{15}$

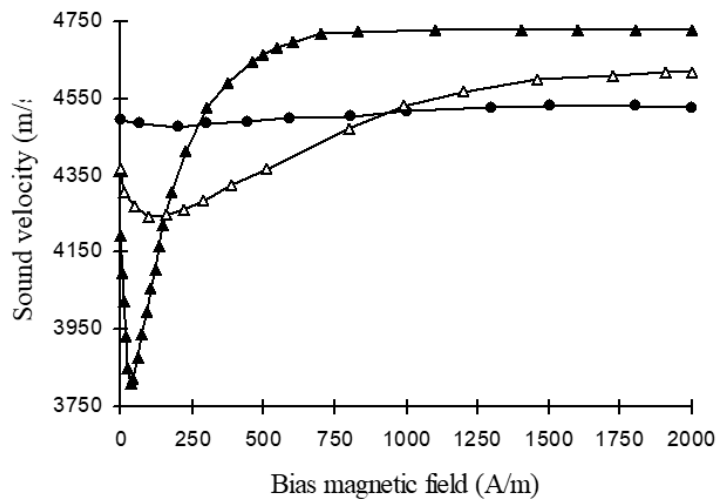


**Figure 3.25.** The dependence of the longitudinal sound velocity on the biasing field in  $\text{Fe}_{77.5}\text{Si}_{7.5}\text{B}_{15}$  amorphous wire tested in the as-cast state (bold circles) and after stress-relief process at 330°C (white triangles) and 370°C (black triangles) for 45 min and 15 min respectively.

amorphous wire tested in the as-cast state and after stress-relief process at 330°C and 370°C for 45 min and 15 min respectively on the bias magnetic field value is illustrated in Figure 3.25.

In the as-cast state, the change of the longitudinal sound velocity is negligible. For annealed samples, there is a strong dependence of the longitudinal sound velocity on the value of the bias magnetic field applied along the length of the wire, which is in good agreement with results concerning  $\Delta E$  effect. The value of the bias magnetic field corresponding to the minimum value of the longitudinal sound velocity decreases with increasing the annealing temperature. For annealing temperatures higher than 300°C, an abrupt decrease of  $v_{\min}$  is obtained at small magnetic bias field values. Thus, for a sample annealed at 300°C for 1 h,  $v_{\min} \approx 4400$  m/s (at 400 A/m) and for a sample annealed at 370°C for 15 min  $v_{\min} \approx 3810$  m/s (at 40 A/m). At saturation, the longitudinal sound velocity varies between 4585 m/s and 4720 m/s (depending on the treatment temperature). The changes observed in the longitudinal sound velocity for small bias field values are due to the modifications of the anisotropy energy during the heat treatment.

A strong dependence of the longitudinal sound velocity on the applied tensile stress was observed for annealed amorphous wires. The longitudinal sound velocity dependence on the bias magnetic field, for  $\text{Fe}_{77.5}\text{Si}_{7.5}\text{B}_{15}$  amorphous wire tested after stress-relief process at 370°C for 15 minutes tested under 0, 1.6, 5.7 and 12 MPa applied tensile stress is presented in Figure 3.26.

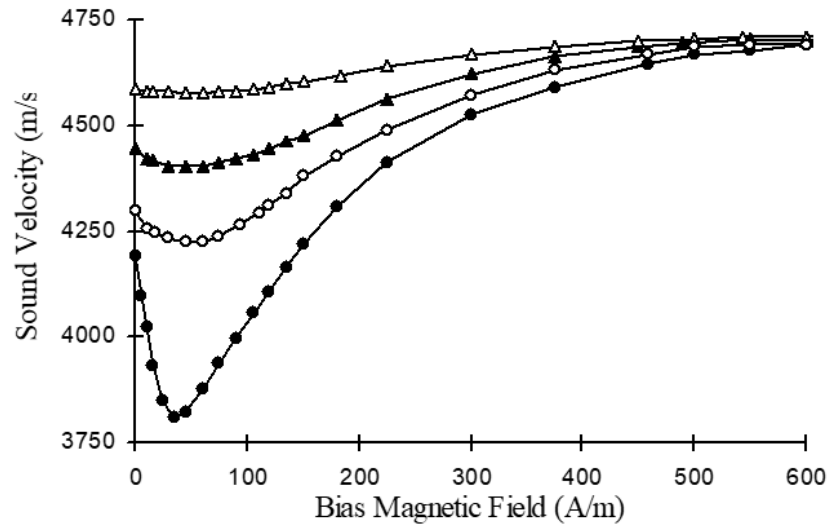


**Figure 3.26.** The longitudinal sound velocity dependence on the bias magnetic field, for  $\text{Fe}_{77.5}\text{Si}_{7.5}\text{B}_{15}$  amorphous wire tested after stress-relief process at  $370^\circ\text{C}$  for 15 minutes tested under 0 (black circles), 1.6 (white points), 5.7 (Black triangles) and 12 MPa (white triangles) applied tensile stress.

For bias magnetic field up to 300 A/m, the longitudinal sound velocity strongly increases with increasing the value of the tensile stress. For about 16 MPa and 600 A/m tensile stress and bias magnetic field respectively, the longitudinal sound velocity reaches the saturation value. The dependence of the longitudinal sound velocity on the applied tensile stress for  $\text{Fe}_{77.5}\text{Si}_{7.5}\text{B}_{15}$  amorphous wire tested after stress-relief process at  $370^\circ\text{C}$  for 15 minutes, under 0 A/m and 90 A/m bias magnetic field is presented in Figure 3.27. A monotonic dependence of the longitudinal sound velocity on the applied tensile stress is observed up to about 12 MPa.

These results prove that the use of as-cast amorphous materials offers the smallest possible field and stress dependence of the longitudinal sound velocity in magnetostrictive materials. Another problem that requires solution is the measurement and treatment of the local nonuniformity of the sound velocity. Improvement of the nonuniformity can result in highly accurate devices based on the MDL technique. For this reason, another experimental set-up has been developed, concerning the determination and improvement of sound velocity nonuniformity along the length of a magnetostrictive material.

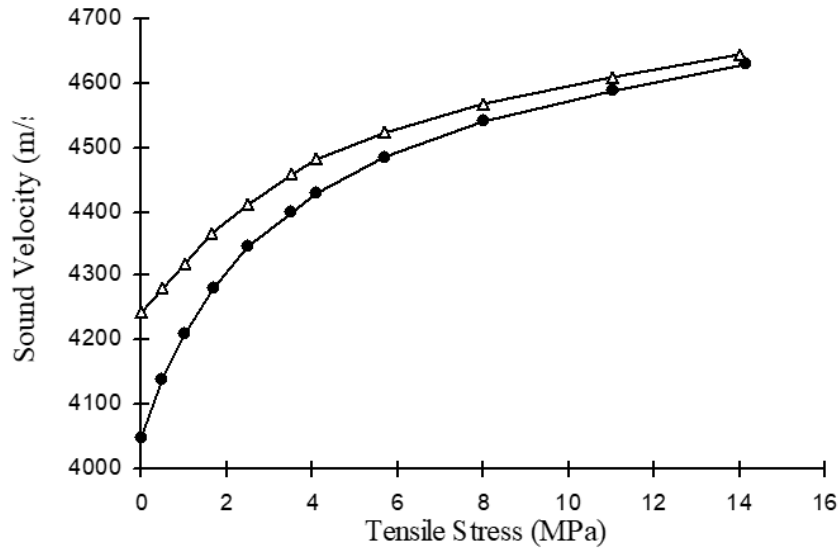


**Figure 3.27.** The dependence of the longitudinal sound velocity on the applied tensile stress for  $\text{Fe}_{77.5}\text{Si}_{7.5}\text{B}_{15}$  amorphous wire tested after stress-relief process at  $370^\circ\text{C}$  for 15 minutes, under 0 A/m (black circle) and 90 A/m (white triangle) bias magnetic field.

The determination of such a nonuniformity is obtained by using a pair of exciting and receiving coils fixed at a distance equal to 100 mm, under the same biasing field and able to travel along the magnetostrictive element. The local non-uniformities in longitudinal sound velocity decrease after heat annealing and stress-current annealing. This was expected, since both of these techniques help to decrease local stresses, which also affect Young's modulus, as well as to homogenate these stresses.

Of course, such a measurement is opposing the results concerning the stability of the sound velocity, as above mentioned. Therefore, a trade-off is required for choosing an as-cast magnetostrictive material or an annealed one. In the case of MDL sensing applications, where the delay time is measured, it is clear that sensitivity and sound velocity uniformity will be sacrificed for the stability of the sound velocity dependence on field and stress. Otherwise, the sensitivity of the device is lost. For applications where the delay time can be determined indirectly annealing the magnetostrictive material helps in sensitivity improvement.

---

### 3.6 MDL resolution

---

The MDL resolution is defined as the minimum distance between two, simultaneously excited, acoustic stress points of origin, which result in two discrete and not superimposing voltage output pulses. In other words, resolution is the closest distance between two coils or pulsed current conductors, used for MDL excitation means, generating two independent pulses at the receiving coil. Such a definition may be observed in Figure 3.28.

Improvement of the MDL resolution is necessary since this technique may lead towards the realization of inexpensive analog multiplexers and distribution sensors. As discussed in Chapter 2, the first contribution to the use of the MDL technique in practically applicable analog multiplexing is the replacement of coils at the excitation regions by current conductors, vertical or parallel to the MDL. By keeping the pulsed current duty cycle low, a thin conductor can be used for transmitting high peak magnitudes of exciting current.

Experiments established that with such a delay line arrangement, the optimum characteristics of the pulsed current causing a maximum value of acoustic stress on the line were 25 A peak amplitude and 3  $\mu$ s time width. The typical MDL resolution in the conventional coil-coil arrangement or the arrays set-ups described in Chapter 2 is of the order of 80 mm, which is not satisfactory for array sensors and analog multiplexer applications. Such a resolution can be improved down to 1 mm by following a careful design of magnetostrictive material and geometry of the MDL arrangement.

At the first place, careful design of the magnetostrictive material means proper tailoring of the  $\lambda(H)$  function of the magnetostrictive material, in order to make the  $\lambda(H)$  function sharper. Thus, the required amount of exciting pulsed field is reduced, resulting in a shortening of the effective length of the MDL, which is excited to generate an elastic strain. Such a tailoring can be obtained by inducing magnetoelastic anisotropy in the magnetostrictive materials. The anisotropy induction can be obtained by stress-current annealing or field annealing.

The typically easier way for anisotropy induction is the stress-current annealing. As previously mentioned, stress of the order of 100-700 MPa and current between 100 mA and 700 mA is proper for this type of annealing. Figure 3.29 illustrates the effect of stress current annealing on the MDL pulsed voltage output dependence on the applied excitation current. In this case,  $\text{Fe}_{78}\text{Si}_7\text{B}_{15}$  amorphous wires were stress current

annealed under 200, 300, 400 and 500 MPa, while the transmitted current was fixed at 500 mA (duration 3 minutes).

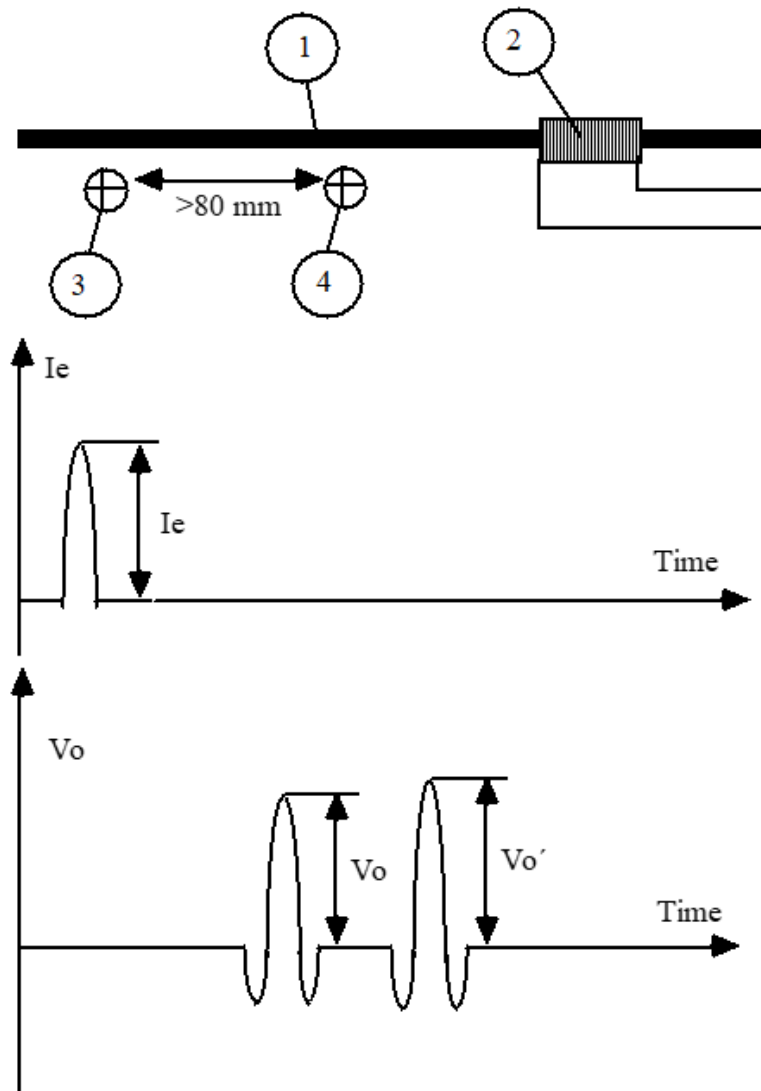


**Figure 3.28.** The MDL resolution is defined as the minimum distance between two consequent excitation points in order to detect two distinct voltage pulses. (1) MDL, (2) Search coil, (3) and (4) Pulsed current conductors. In most crystalline MDLs such a distance is 80 mm.

It can be observed that less excitation current is required for the case of the stress current annealed samples to obtain the same MDL pulsed voltage amplitude  $V_o$ , so that the effective MDL length is smaller in this case. Figure 3.30 illustrates the dependence of the voltage output  $V_o$  on the pulsed current width  $T$ . From all these results it is concluded that the MDL resolution is improved after stress current annealing

tailoring processes. In the given case, stress of 500 MPa under simultaneous dc current of 500 mA for 3 minutes gave the best results. This argument can be generalized for all positive magnetostrictive materials due to the experimental evidence. This is one way to tailor the properties of the magnetostrictive material targeting the sharpening of its  $\lambda(H)$  function.

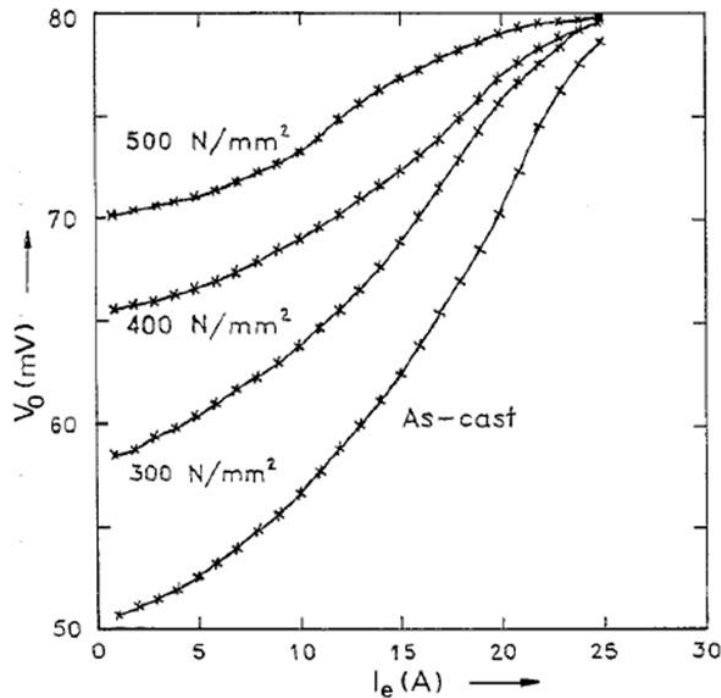


**Figure 3.29.** The effect of stress current annealing on the MDL pulsed voltage output dependence on the applied excitation current.

The other possible way to improve the MDL resolution is the tailoring of the geometry arrangement. For this purpose, one can make precise and thin excitation and/or search coils in order to improve the MDL resolution. As an example, the coils may be prepared as follows: A 1-3 turn flat coil with internal and external diameter of 0.15 and 0.16 mm respectively can be used to generate an elastic pulse, in order to further minimize the MDL effective length. Thus, modifying the number of turns of the receiving coil, one can determine the effect of the number of receiving coil turns on the MDL amplitude  $V_0$ .

For the currently presented experiment, the receiving coils have been prepared following the same technique as for the excitation flat coils (wet flat printed circuit board lithography). The dependence of

the MDL resolution and the amplitude of the voltage output  $V_o$  on the number of turns of the receiving coil are illustrated in Figures 3.31 and 3.32 respectively. Due to these indicative results, a resolution of 1 mm has been achieved by using a flat printed coil of 10 turns as receiving coil with internal and external diameter of 0.15 and 0.2 mm respectively, using a stress current annealed MDL in 500 MPa and 500 mA for 3 minutes. The optimized pulsed voltage output response with respect to the excited pulsed current is illustrated in Figure 3.33. In this Figure the absence of after effects and secondary waveforms can be observed, proving the effect of the material tailoring and geometry optimization on the MDL resolution. It is mentioned that these results are indicative, as all the results presented in this work, allowing either deviations from the typical values of the annealing and preparation conditions or deviations from the as-presented experimental procedure. But, in general, the methodology presented has been repeated and verified with inter-comparison tests, allowing to safely declare that stress current annealing and search coil geometry can improve the MDL resolution.

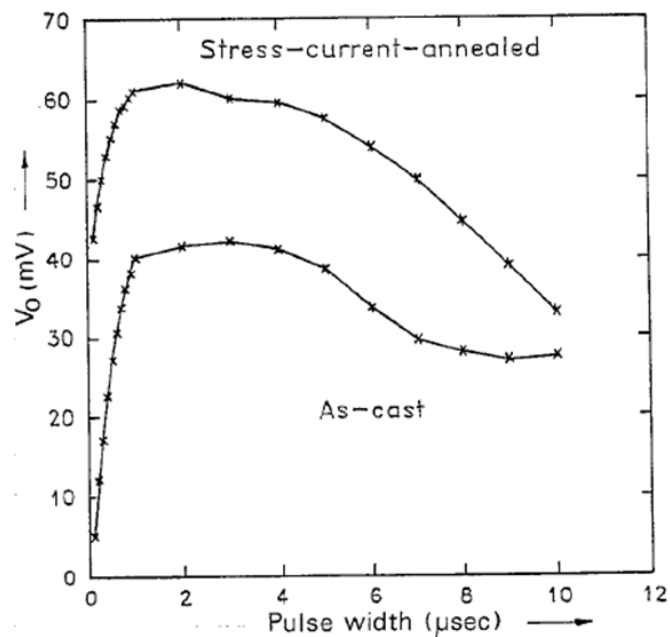


**Figure 3.30.** The dependence of the voltage output  $V_o$  on the pulsed current width  $T$ .

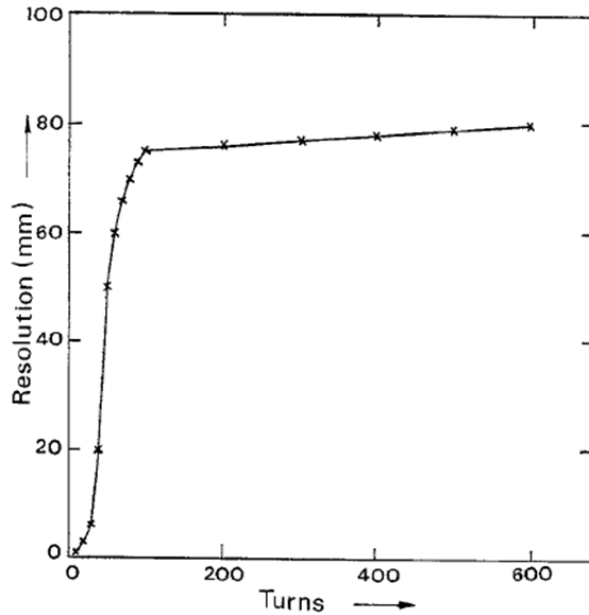


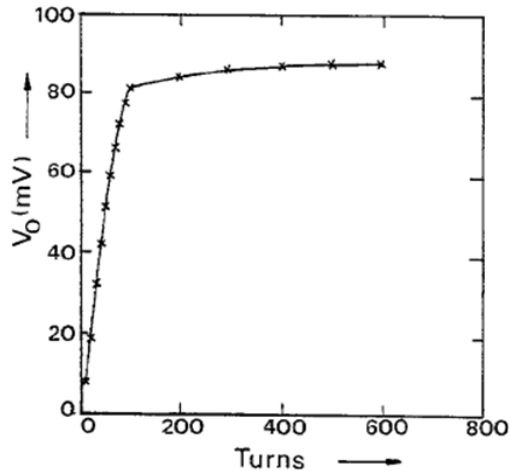
**Figure 3.31.** The dependence of the MDL resolution on the number of turns of the receiving coil.

Another way to improve the MDL resolution and other characteristics dependent on the magnetoelastic response of the magnetostrictive materials is to completely modify the MDL geometry, i.e. to develop a new kind of MDL.

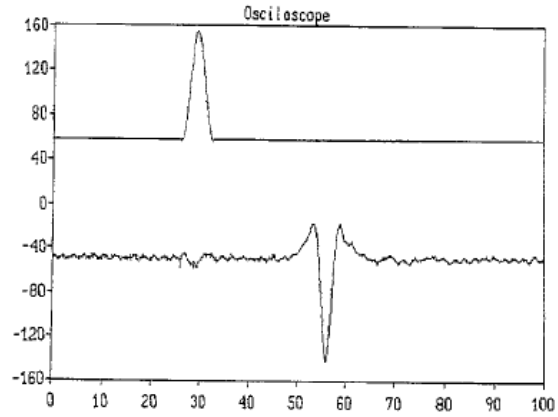
For this purpose and as an example the MDL arrangement presented in the previous Chapter was used, according to which a magnetostrictive material is used only for the generation and detection of the elastic pulse (see section 2.4 and Figure 2.14). In this set-up the magnetostrictive material is connected by using glue or soldering on a non magnetic or magnetostrictive acoustic wave guide, for example glass or ceramic at two distinct areas of it, in order to be used as excitation and detection regions of the elastic pulse respectively.

For the sake of the experiment Fe-rich amorphous wire specimen in the as-cast form has been used to be glued on a glass tube used as the acoustic waveguide. The diameter of the Fe-rich wire was 150  $\mu\text{m}$ , while the lengths used were 1, 2, 3 and 4 mm. The dimensions of the magnetostrictive material and the acoustic wave guide were of the same order to facilitate their coupling.

The pulsed response of such an arrangement indicates that the MDL resolution can be of the order of the length of the used magnetostrictive material. The non magnetic acoustic wave guide can also be tailored in order to minimize the elastic signal distortion.



**Figures 3.32.** The dependence of the amplitude of the voltage output  $V_0$  on the number of turns of the receiving coil.



**Figures 3.33.** Optimized MDL output with respect to the excitation pulse (y-axis in mVolts and x-axis in  $\mu\text{s}$ ).

---

### 3.5.1 MDL impulse response

---

In order to further understand the mechanisms of the magnetoelastic response of the MDLs, the impulse response characteristics may also be studied, although they are not categorized as a different property, since they can be studied together with frequency response and MDL resolution.

According to this experimental procedure the magnetostrictive material is polarized by the bias field so that the pulsed current saturates it. Exciting the MDL up to magnetoelastic saturation, the orientation of the magnetic dipoles along the length of the MDL is obtained. Then, having a very sharp falling edge of pulsed current, simulating the impulse response, the magnetic dipoles are driven from the saturation point down to an equilibrium angle.

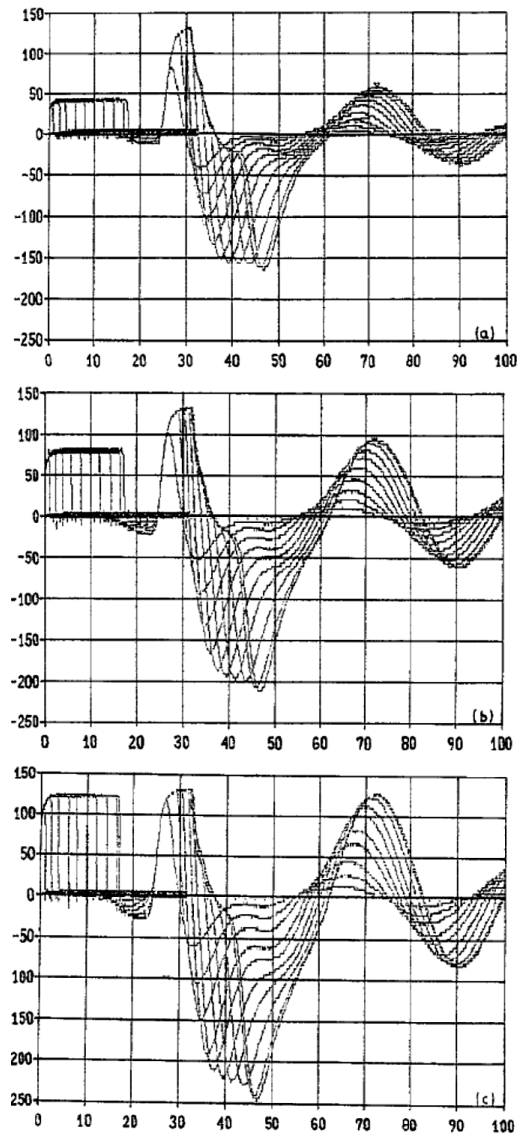


**Figure 3.34.** The MDL impulse response, for different pulse widths and amplitudes (y-axis in mVolts, x-axis in  $\mu\text{s}$ ). (a)  $H=0.8$  A/m, (b)  $H=1.6$  kA/m, (c)  $2.4$  kA/m.

The impulse response is illustrated in Figure 3.34 for different pulse widths and amplitudes. Under all circumstances the impulse response indicates that there is an exponentially decaying oscillation, with almost the same time constant of exponential decay and oscillation, described by:

$$V(t) = V_0 e^{-\frac{t}{T}} \cos\left(\frac{2\pi t}{T}\right) \quad (3.3)$$

$T$  is considered as a constant, which was found to be constant and equal to  $37 \mu\text{s}$  for the case of  $\text{Fe}_{78}\text{Si}_7\text{B}_{15}$  amorphous wires. This useful information indicates that under impulse response, the magnetostrictive dipoles of the material are subject to decaying oscillation around their point of equilibrium. Such an effect, apart from being useful to determine the equilibrium time of the magnetic dipoles, results in the undesirable elastic after-effects in the MDL response, so that they should be taken into account when MDLs are to be used for array sensor applications.

# 4 Materials for MDLs

Having analyzed the MDL operation, arrangements, properties and parametric dependence in the previous chapters, the materials for use in MDLs are analyzed hereinafter. At the first place, the classical polycrystalline metals and alloys are presented, although they are not advantageous with respect to other materials, like amorphous alloys, thin films and composite materials. In turn, amorphous alloys in the form of ribbons, wires and glass covered wires are presented: these materials cover the vast majority of MDL applications. Then, thin films and negative magnetostrictive materials are presented. Composite materials are finally presented although they have not yet been used as magnetostrictive delay lines.

---

## 4.1 *The classic poly-crystalline magnetostrictive wires and ribbons*

---

The most common polycrystalline metals and alloys usable as MDLs are the Fe and Ni wires, while rarely Fe, Ni and Fe-Ni ribbons may be also used. A typical MDL pulsed voltage output response, using Fe or Ni

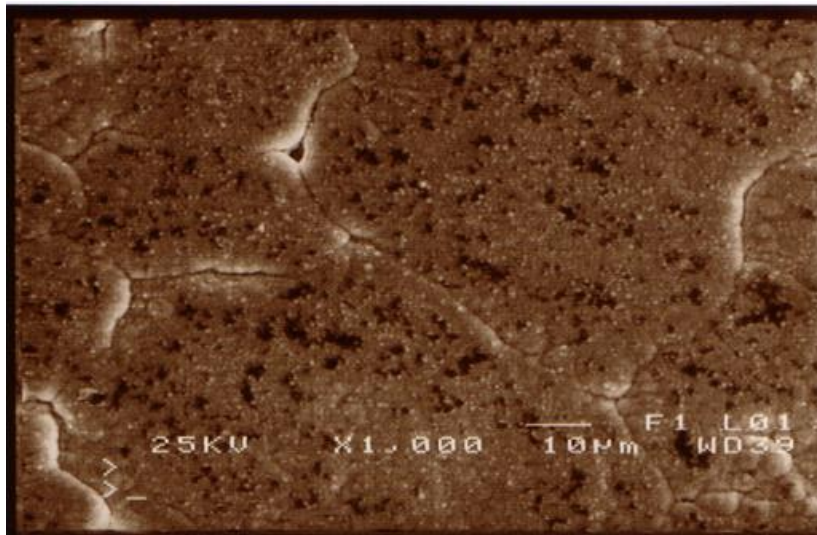


**Figure 4.1.** Microcracks on the surface of a magnetostrictive material prohibit the propagation of elastic waves.

polycrystalline wire as MDL can have a small or high noise level as well as small or high magnetic and acoustic aftereffects, depending on the microstructure and uniformity of the material, as well as the structure-stoichiometry and its uniformity. At first the presence of cracks in the material affects the ability of propagation of elastic waves. As an example, the microstructure illustrated in Figure 4.1 referring to a Ni ribbon almost prohibits the propagation of the elastic waves due to the clearly observed micro-cracks. Furthermore, scattering centers like the ones illustrated in Figure 4.2, referring to a Fe ribbon, may also affect the MDL response. They are responsible for partial reflections of the propagating elastic pulse, resulting in non-homogeneous superpositions of elastic waves along the length of the MDL, resulting in the non-uniformity effect discussed in the previous chapter.

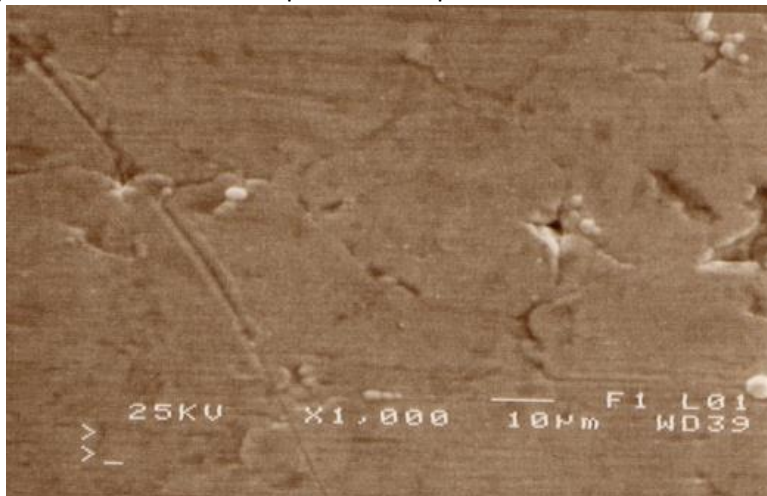


**Figure 4.2.** Scattering centers cause reflections and magnetoelastic non-uniformity.



**Figure 4.3.** Absence of defects results in a significant improvement of non-uniformity.

A rather uniform response is expected and observed in the case of a material illustrated in Figure 4.3, referring to a  $\text{Fe}_{80}\text{Ni}_{20}$  wire. The absence of micro-cracks is crucial for the uniformity and higher sensitivity of the magnetostrictive material. Finally, the presence of shape induced anisotropy shown in Figure 4.4, referring to  $\text{Fe}_{80}\text{Ni}_{20}$  ribbon, further enhances the magnetoelastic response and sensitivity. Such a microstructure may also enhance the Barkhausen noise of the magnetostrictive elements. Thus, the properly tailored magnetostrictive materials may exhibit a significantly small noise level, of the order of the fraction of a few  $\mu\text{Vs}$ , which is mainly attributed to the electromagnetic noise induced at the search coil. It is significant to notice the absence of secondary waveforms. Only reflections may appear in such an MDL without scratches and mechanical injuries.

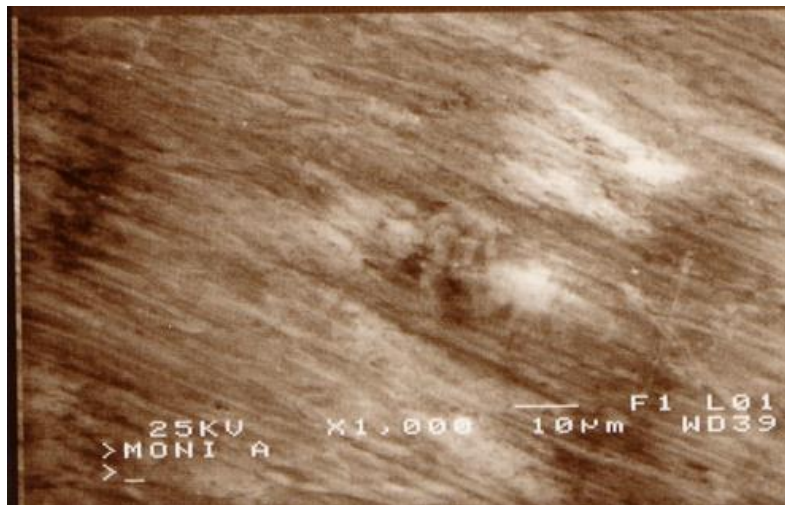


**Figure 4.4.** Shape induced anisotropy may occasionally help the improvement of the magnetoelastic properties.

The magnetic and magnetoelastic properties of these materials can not promote them as sensitive MDL materials in many MDL applications. Among these properties, hysteresis may be the worse observable property of these materials, as noticed in Chapter 3 (see Figure 3.3). Such a hysteresis makes these materials useless for voltage output dependent MDL applications, as illustrated in the next chapters of this work. Additionally, the observed sensitivity of the response of these materials on pulsed and dc biasing fields is poor, not allowing sensitive response and therefore not promising sensing behavior.

Nevertheless, in cases where the MDL operation and response is not dependent on the voltage output detection but on delay time dependence these polycrystalline materials appear to have a remarkably repeatable and steady response. The magnetoelastic uniformity of Fe and Ni wires illustrated a stability

equivalent to the amorphous wires, while their longitudinal sound velocity is almost constant. From these results, it can be seen that a remarkably uniform magnetoelastic response and a rather steady sound velocity with respect to the applied biasing field can be realized. This response suggests that polycrystalline MDLs can be used for delay time based MDL sensors, as it will be analyzed in the case of position sensors in Chapter 4. Taking into account that the cost of such polycrystalline materials, like Fe wires of 0.1 mm diameter can be found in the market in the cost ~30 Euros per kg or ~30 Euros per 10 km of MDL material, they apparently become attractive for the above mentioned application, provided that they do not suffer any mechanical stress during their use.

It is finally noted that the use of magnetostrictive polycrystalline alloys is not very common, since their magnetoelastic coupling factor and magnetostriction engineering constant  $\lambda_s$  are rather small in comparison to Fe and Ni polycrystalline wires or ribbons. They can be used in some particular cases, where the sign of magnetostriction plays a significant role.

---

## **4.2**      *The rapidly quenched magnetostrictive alloys*

---

In most of the developed applications, the use of amorphous alloys as MDLs offered repeatable results, since they are more sensitive and rigid than magnetostrictive polycrystalline materials (Fe, Ni, Fe-Ni). They combine high magnetostrictive and elastomagnetic sensitivity, high saturation magnetization and very attractive soft magnetic properties. On the other hand, since the magnetic and metallographic nature of these alloys has been satisfactorily investigated, their behaviour as MDLs can be determined due to the existing literature [12]. Some additional and indicative MDL properties of these alloys, out of a vast variety of experimental data, will be introduced and discussed hereinafter.

There are some practical reasons leading to the decision to choose these alloys. In our experiments, 20 or more Fe wires (0.1 mm diameter) were required in order to obtain an MDL with the same sensitivity as a single 125  $\mu\text{m}$  amorphous  $\text{Fe}_{78}\text{Si}_7\text{B}_{15}$  wire or a 0.025 mm thick and 1 mm wide ribbon delay line, under the same experimental set-up. Additionally, amorphous ribbons and wires are preferred to be used as acoustic

waveguides, since they are more rigid than crystalline materials, hence they can withstand larger amounts of applied forces on their surface.

Several amorphous ribbons and wires were sought in the existing literature and tested on the experimental bench. Among them, the Fe-Si-B family, such as the  $\text{Fe}_{78}\text{Si}_7\text{B}_{15}$  alloy, was finally chosen, because of its excellent magnetic properties and mechanical stiffness. The small concentration of carbon in this alloy, instead of lowering the MDL properties, increases its sensitivity under applied pulsed and biasing magnetic field. For an as-quenched amorphous  $\text{Fe}_{78}\text{Si}_7\text{B}_{15}$  alloy, the saturation magnetostriction is 30-100 ppm, saturation magnetization about 1 Tesla and its B-H loop offers very soft, unhysteretic and linear magnetic behavior. The elastomagnetic properties of this material are also significant; the relative permeability of this alloy varies with the applied stress along its length. This property was used for some of the proposed force transducers, as will be discussed in Chapter 7. A vast number of experiments has been performed concerning amorphous alloy ribbons, wires and glass covered wires, when operated as MDLs. In this Chapter, a few indicative results are given in order to illustratively demonstrate the operation of these alloys.

The obtained microstructure of amorphous  $\text{Fe}_{78}\text{Si}_7\text{B}_{15}$  alloys in their as-cast form, as illustrated in the TEM diffraction measurement of Figure 4.5, allows the existence of only local stresses due to the manufacturing method (either planar flow or in-rotating-water rapid quenching for ribbons and wires respectively). Such localized stresses could well be minimized by thermal heating, while magnetic anisotropy could be optimized by field annealing or stress-current annealing, provided that temperatures are smaller than crystallization temperatures. If crystallization or (more commonly) nano-crystallization has been caused in the material, the most usual effect is the counter-balance of the magnetostriction of the amorphous matrix and the nano-islands or crystallites (see Figure 4.6) by means of summing up positive and negative magnetostriction index, resulting in minimization of the magnetoelastic properties.

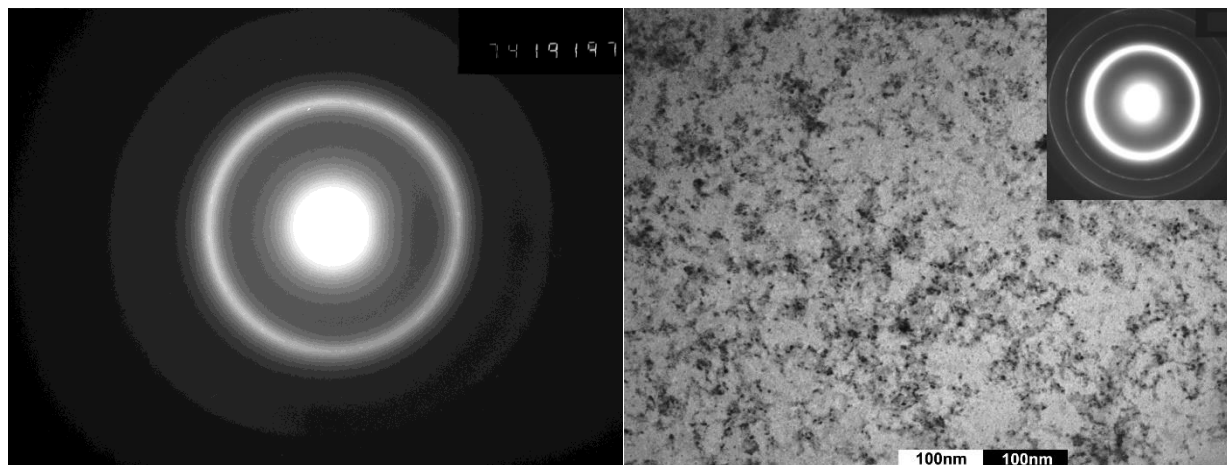


**Figure 4.5.** TEM diffraction pattern (left) suggests amorphous phases in Fe-rich ribbons, accompanied by repeatable and unhysteretic MDL response. Even partial nano-crystalline ribbon (right) resulted in small and hysteretic MDL response.

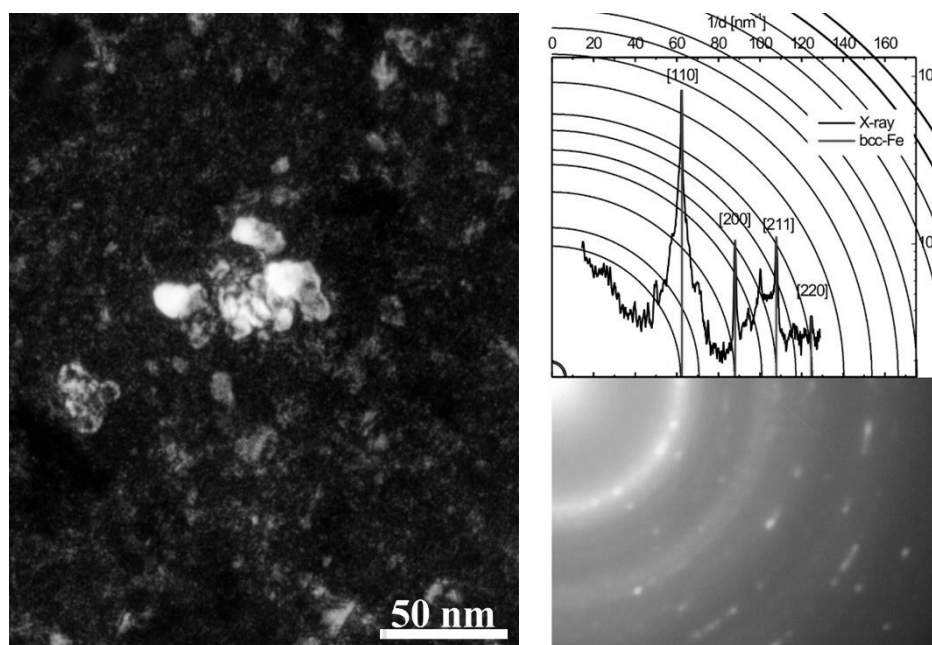


**Figure 4.6.** Nano-crystalline Fe-rich alloys cannot operate as MDLs due to the very small  $\lambda(H)$  function mainly due to the co-existence of positive and negative magnetostrictive phases.

---

### 4.2.1 Amorphous ribbons

---

Apart from some excellent magnetic and magnetoelastic properties, amorphous ribbons have some undesirable properties too, which must be effectively reduced or eliminated. All these properties, acceptable and not acceptable, are illustrated and discussed hereinafter. In many cases an engineer developing an MDL application has to develop MDLs of a width smaller than 1 mm out of a tape having width of 50 or even 100 mm. The way to develop narrow MDLs is mostly wet or dry lithography. Lithography introduces stresses, which affect the magnetoelastic uniformity and the other MDL properties of the alloy ribbon.

The most attractive property of Fe-Si-B alloy ribbons, and especially the  $\text{Fe}_{78}\text{Si}_7\text{B}_{15}$  composition, is the high level of response and mechanical robustness. On the other hand, it suffers from magnetoelastic uniformity response, as illustrated in the previous section. All the characteristics mentioned in the previous Chapter, namely magnetoelastic uniformity, sound velocity and sound velocity uniformity, hysteresis, linearity, response delay, dc magnetic field bias effect at both excitation and search region, reflections at the ends of the delay line, secondary waveforms, pulsed field amplitude and pulsed field duration and frequency response have been determined for various kinds of amorphous ribbons.

Since the basic idea behind all the proposed transducers is to measure the change of the magnetoelastic wave (either at the point of origin or at any point of the delay line as it propagates, or even at the receiving coil with respect to the applied displacement, force or pressure), these delay line characteristics are the ones that determine a possible MDL error. So, improvement of these characteristics improves the performance of the MDL.

One of the most severe problems experienced by using amorphous ribbon MDLs is their nonuniform magnetoelastic response (MEU), as defined in the previous Chapter. Experimental work has concluded that the fluctuation from the average value of the as-quenched, annealed and finally stress-current annealed after stress relief MDLs was 60-140%, 75-125% and 90-110% of a mean value respectively. Thus, nonuniformity was improved in the case of heat treatment, while a better result was observed in the case of a stress-current annealed delay line for which a stress relief process was previously applied. The normalization process has been successfully used in order to obtain optimization of the MDL response of the amorphous ribbons. Of course, a traditional method to eliminate the nonuniformity effect is the use

of more than one MDL [27]: the more MDLs, the better their uniformity function, since the differences between various excitation and/or search regions are averaged out.

On the other hand, as far as internal stresses are caused during the rapid solidification method of manufacturing of these alloys, the stiffness of the material along its length changes arbitrarily so that the strain caused by applying a longitudinal pulsed magnetic field is not predictable. Thus, after heating and annealing them, stress relief is obtained, so that the MDL behaves as a more uniform acoustic medium. But, even after the stress relief process, elastomagnetic waves are not uniform. The  $V_o(x)$  function can be further improved by making the magnetic domain orientation uniform. Such an orientation was achieved by stress and current annealing, which has similar results to the transverse magnetic field annealing. Heating and annealing delay lines could also induce additional internal stresses in the material. Such an effect can also be observed by the induced stress process on the MDL.

But even after stress relief and domain wall reorienting the elastomagnetic waves do not become absolutely uniform. This happens for a number of reasons:

1. Nonuniformity in the cross section area of the material. Since the material is produced by a rapid solidification process and made in ribbon form, the cross section areas are not uniform, causing a sort of difference in the acoustic pulse creation and propagation, when a pulsed magnetic field is applied. A fluctuation of the cross section area of the order of 10% has been reported for the case of ribbon alloys. This cross section area seems to be much more uniform, for the case of the FeSiB wires, due to the way of manufacturing.
2. Magnetic nonuniformity, i.e. variation in the percentage of the ferromagnetic material concentration along the length of the line. This effect causes different magnetic flux density at the various points of excitation.
3. Small changes of the distance between conductor and delay line cause fluctuation on the received voltage outputs which are about twice the ratio of the distance change.
4. Although the recently developed amorphous wires are not fully understood yet, there is an indication that the uniformity function is more uniform. For the moment, it is obvious that the normalization process is required when MDL techniques are used for analogue multiplexing.

A typical dependence of the MDL response  $V_o$  on the applied pulsed field amplitude  $H_e$  is illustrated in Figure 4.7. These data have been received by incrementing the pulsed field amplitude  $H_e$  upwards and downwards. The measurement of the MDL response of amorphous ribbons has been realized by using the

experimental set-up as illustrated in Figure 2.12, with a 12-bit A/D converter. The two recorded  $V_o(H_e)$  functions were identical, illustrating absence of hysteresis by using the 12-bit A/D converter. Furthermore, the response is almost monotonic although strongly non-linear, thus allowing mathematical fitting for look-up table calibration reasons.

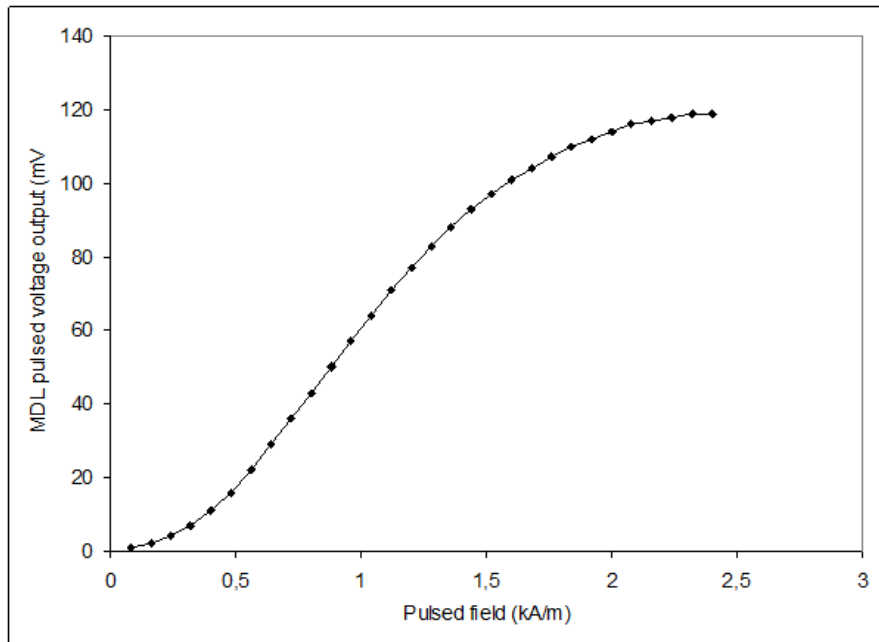


**Figure 4.7.** A typical dependence of the MDL response  $V_o$  on the applied pulsed field  $H_e$ .

The MDL response delay has been defined and discussed in the previous Chapter. It is the time needed for an acoustic pulse to be detected and stored. After the acoustic pulse is detected at the receiving point, the process of amplifying, sampling, holding and storing the peak value  $V_o$  in the memory of the computer takes place in less than  $10 \mu\text{s}$ . So, the time needed for storing the information out of 1 m of amorphous ribbons (and the other amorphous alloy MDLs) for one single pulsed current transmission is about 200 microseconds.

It has been experimentally observed that about 60% of the original acoustic pulse is reflected at a single reflection at the free end of an amorphous ribbon MDL. It has also been observed that after 5 reflections the level of the reflected signals in these materials is approaching the search coil noise level.

One method to avoid reflections of a non terminated delay line is to use a delay line longer than its sensing length, in order to receive any reflected acoustic pulses after receiving all the original and useful pulses. So, reflections are not taken for detection sampling and holding.

A method to reduce the reflections at the ends of a delay line is the use of damping material. In this way, acoustic waves are absorbed from it, while results become better if the thickness of the material increases progressively. The more absorbing material is applied, the smaller the reflection level, although no detectable results can be obtained when the termination is longer than 10 mm. Using 10 mm painted latex adhesive, it was observed that the first reflections can well be less than 1% of the original signal. Another method to reduce acoustic reflections is by using a multi-reflecting delay line termination. Thus, the elastic pulses are reflected at the multi-reflecting termination several times and finally, the reflected signal is hidden in the noise of the search coil. Combination of 3-edge multi-reflected termination and simultaneous use of damping material offered reflection level smaller than the MDL noise level.

The Van der Berg's idea [27] has been used in amorphous ribbon MDLs to eliminate reflections: using two MDLs, the one being free of terminations and the other stretched at its end results in two reflecting signals with opposite signs. Therefore, when they arrive at the receiving coil, they cause opposite pulsed voltage waveforms, cancelling each other. The observed voltage after-effect waveforms are quite significant in amorphous ribbons. Some explanations have been tried in the past, concerning scattering centres [39]. All of them agree with the fact that the internal stresses in the ribbon cause small reflections of the propagating magnetoelastic wave. So, the receiving waveform is followed by the after-effect waveform which lasts about 30 microseconds.

The time width of the main pulsed voltage waveform is not the same as the pulsed current one. This is due to the finite extend of the MDL excitation region, the size of which depends on the distance between conductor and delay line and the magnitude of the pulsed current. On the other hand, the quality factor of the receiving coil also plays a significant role. A typical time width of the front wave of the MDL pulsed output is 14  $\mu\text{s}$  for pulsed current time width of 3  $\mu\text{s}$ . Adding the secondary waveforms to that main MDL output, a total duration of 40-45  $\mu\text{s}$  has been observed. These numbers correspond to an as-cast amorphous ribbon.

It was believed that a stress relief process could improve the performance of the output waveform: internal stresses would be significantly reduced, thus resulting in a great reduction of the after-effect waveform. Indeed, secondary or after-effect waveforms have been eliminated for an MDL heated in 300°C for 3 hrs, in inert atmosphere, with a consequent 1°C/min slow cooling rate.

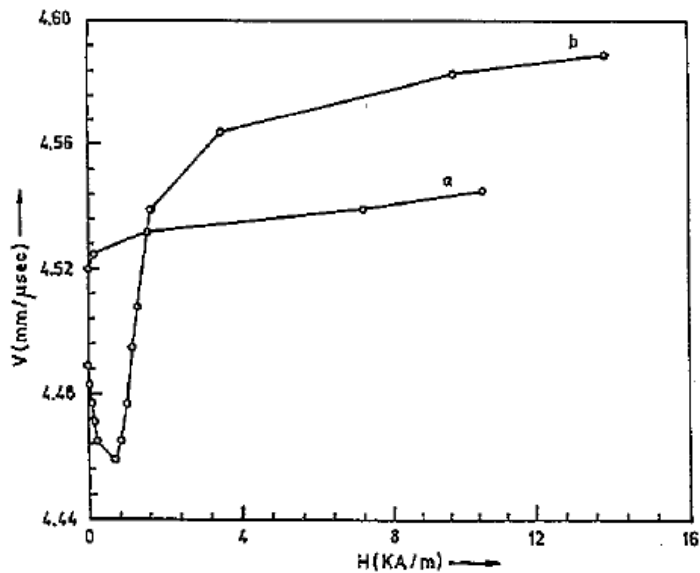


**Figure 4.8.** Longitudinal sound velocity dependence as-cast (a) and heat treated (300°C for 1 hr in Ar atmosphere) amorphous ribbons.

The typical MDL resolution of amorphous ribbons has been treated in a similar way as for the case of amorphous wires, as presented in the previous Chapter. At the moment, experimental observations suggest that a complete output waveform lasts about 44 microseconds, while this time width can be reduced down to 14 microseconds by applying stress relief techniques. Thus, adjacent, simultaneously excited points of origin must have a minimum pitch from 220 to 70 mm, dependent on the treatment of

the MDL. In fact, for the case of amorphous ribbon MDLs, we used a pitch equal to 80 mm, for delay lines after heat treatment. These levels of MDL resolution are clearly worse in the case of amorphous ribbons compared with amorphous wires, which have indicatively been analyzed in the previous Chapter.

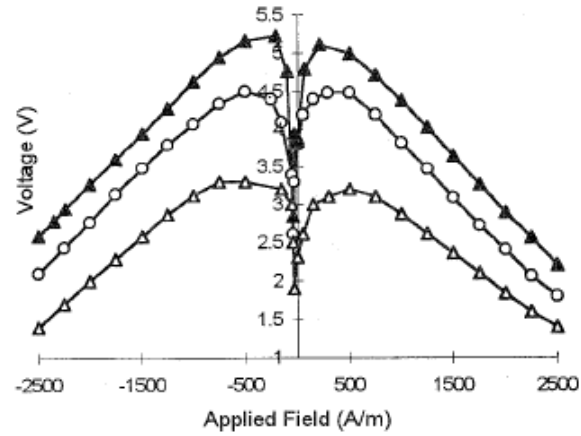
Improving the amorphous ribbon MDL resolution between adjacent, simultaneously excited conductors (called from now on, conductor arrays), demultiplexing techniques have to be used. This means that a number of conductor arrays, sequentially interrogated, close and parallel to each other could be used. So, after exciting the first array of conductors, the second is excited etc. The pitch between conductors, for two consequent arrays, defined as arrays having conductors in the closest possible distance and the time delay for pulsed current transmission being the shortest one, could be as small as the electronic technology can provide. A typical pitch of the order 1 mm between adjacent conductors has been achieved by using wet PCB lithography technology. Such a pitch has been used in the past for walkway gait analysis for Arthritis estimation.

For this application, the delay time between two sequentially excited conductor arrays should be long enough to avoid interference of the adjacent acoustic pulses with each other. So, a delay of about 16 microseconds would be enough since the main voltage waveform lasts about 14 microseconds and the pitch between adjacent conductors is 5 mm. In the walkway gait analysis, 128 arrays of conductors were used in order to have the desired resolution of 1 mm. In order to avoid interference between pulses at the

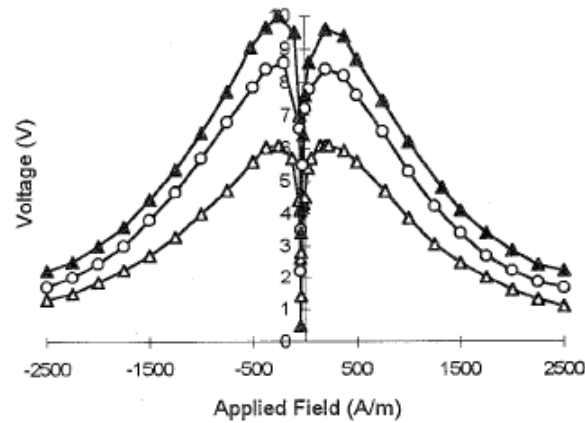
same conductor array, a minimum 256  $\mu\text{s}$  pulsed current period, corresponding to 1 m of MDL, was required for all the conductor arrays.

In general, if the desired pitch between consequent conductors is  $x$  mm, taking into account that 80 mm correspond to a minimum pitch for interference-free pulsed current MDL operation,  $80/x$  sequentially excited arrays of conductors are required. The delay between consequent pulses should be longer than  $(14+v/x)$   $\mu\text{s}$ , where  $v$  is the longitudinal sound velocity of the MDL. So the minimum period of the pulsed current waveform should also be larger than  $80(14+v/x)/x$   $\mu\text{s}$ . For this reason, sound velocity measurements are of importance for the MDL technique. An illustrative dependence of the longitudinal sound velocity of as-cast and heat-treated ribbon is shown in Figure 4.8.

The MDL pulsed voltage output is much dependent on the presence of a DC bias magnetic field.. A typical dependence of the MDL output on the absolute value of the dc biasing field at the excitation and the search region is illustrated in Figure 4.9a and 4.9b respectively. Similar results appear for the MDL dependence on the biasing field at the receiving region. Generally,  $V_o$  changes smoothly with respect to the external applied field, thus indicating a smooth magnetostriction and magnetization dependence on field. Indeed, Barkhausen jumps may appear only locally in amorphous ribbons. For the case of as-cast amorphous wires, as shown in the next section, large Barkhausen jumps are responsible for the non-continuation of the MDL pulsed voltage output on the biasing field. On the other hand, it was observed that for a DC field  $H_{dc}$ , applied at an angle  $\alpha$  to the axis of the delay line, the received voltage output becomes  $V_o \cos \alpha$ , where  $V_o$  is the voltage received under the same DC field  $H_{dc}$  applied on the direction of the line.



(a)



(b)

**Figure 4.9.** Typical absolute amplitude MDL voltage output dependence on the applied biasing field at the excitation (a) and search (b) regions, concerning as-cast amorphous Fe-rich ribbon. Measurements have been realized by exciting with pulsed excitation field He 200 A/m (white triangles), 400 A/m (circles) and 600 A/m (black triangles).

All these measurements have been taken for values of  $H_{dc}$  greater than a minimum field, corresponding to the maximization of the MDL response. For the case of Fe-Si-B amorphous ribbons it was found that this field equals to 0.35 A/cm. This field amplitude varies with respect to the annealing conditions of the material. Usually, maximizing dc bias field decreases with stress relief process and stress-current annealing process. As a general comment, it should be mentioned that the MDL dependence of amorphous ribbons on biasing field forms a smooth non-monotonic but fitable response. Such a response has a critical biasing field value  $H_c$ , where the magnetoelastic response is maximized, corresponding to the maximization of the first derivative of the  $\lambda(H)$  function. The value of  $H_c$  generally decreases with stress relief and stress-current annealing process.

The pulsed current waveform plays a significant role in the magnetoelastic wave for such an MDL operation, since the caused MDL pulsed voltage output is qualitatively proportional to the first derivative of the propagating elastic pulse. The pulse width response has been investigated for the case of amorphous Fe-Si-B ribbons. Pulse width response is defined [18] as the function of the peak voltage output  $V_0$  vs the time width of the pulsed current waveform. Frequency response is defined as the peak value of the voltage output vs the frequency of a sinewave signal transmitted longitudinally along the length of the line, which has a fixed amplitude. The pulse width response of the amorphous  $\text{Fe}_{78}\text{Si}_7\text{B}_{15}$  ribbons is quite similar to that of the crystalline Fe and Ni wires as illustrated in Figure 4.10.

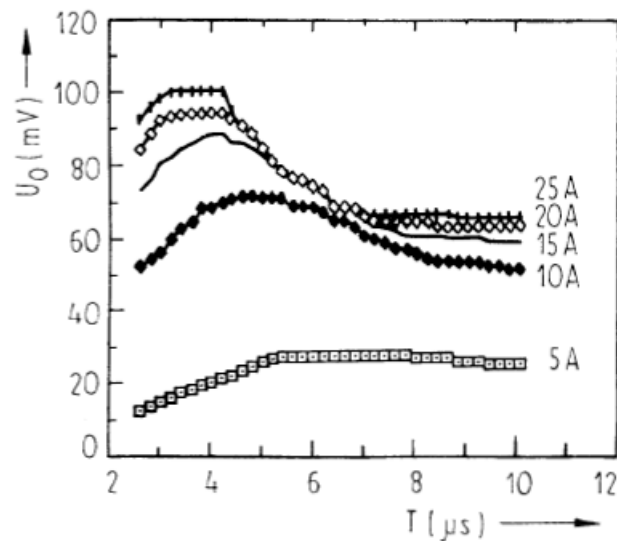


**Figure 4.10.** Pulse width dependence of the MDL for as-cast amorphous ribbons under different excitation currents.

It has been observed that the optimum pulsed current time width is  $1.6 \mu\text{s}$ . For pulsed current width greater than  $2.5 \mu\text{s}$ , the receiving signal starts to split up into two signals, because the time for mechanical relaxation is enough to split up the acoustic pulse at the point of origin this effect is undesirable for several delay line applications. Generally, these results are more or less similar to amorphous Fe-rich ribbons, but also to other magnetostrictive ribbons used as MDLs. In general, the MDL pulsed current/field width response has a maximum, corresponding to the time window, which allows the maximum motion of domain walls or the maximum rotation of magnetization.

---

## 4.2.2 Amorphous wires

---

Experimental data on amorphous magnetostrictive wires used as MDLs are reported and discussed. The reported results are also discussed and a comparison indicating the certain advantages and disadvantages of amorphous magnetostrictive ribbons and wires for each special application is given in order to allow the possible end user of these sensing ideas to select the most appropriate material in his special requested application.

The development of MDL and corresponding MDL based sensors using amorphous Fe-rich ribbons has offered some characteristics which satisfy some given applications. But there are some engineering problems still existing when they are to be used, like linearity and multiplexing resolution. In order to work towards the improvement of the characteristics of these MDL sensors, experiments using amorphous magnetic wires were performed. By using such materials a more linear response of the distribution sensors was obtained, while the indication of the control of the MDL multiplexing resolution has also appeared to be a reality, mainly by controlling the dependence of the magnetostriction factor  $\lambda$  on the applied field along the ribbon anisotropy,  $\lambda(H)$ .

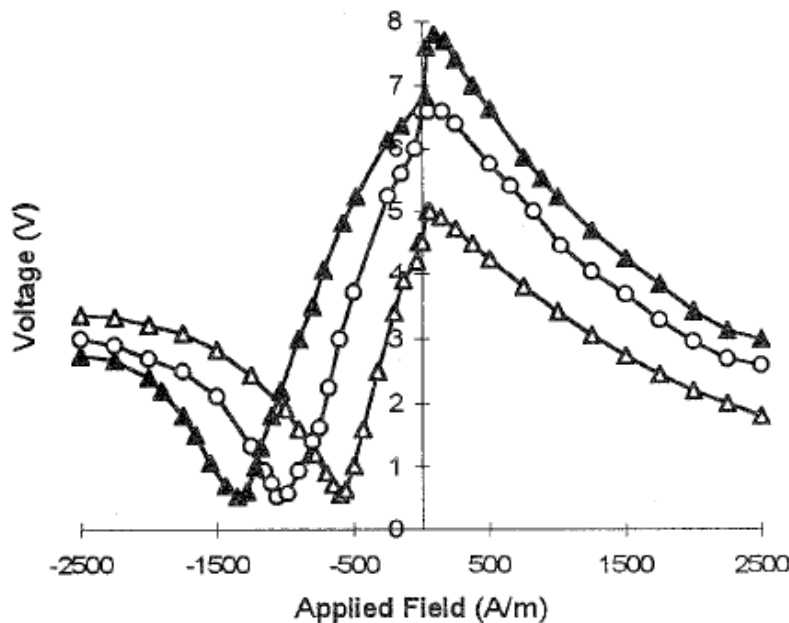


**Figure 4.11.** MDL voltage output dependence on biasing field, concerning as-cast Fe-rich amorphous wires. The presence of the large Barkhausen jump can be observed.

Among amorphous wires, the Fe-Si-B family offered the best sensitivity as for the case of ribbons. These materials have been tested and indicative results are provided in this work. Two experimental set-ups were developed to determine the response of amorphous wires used as MDLs: the one was used for the measurement of the pulsed and biasing field dependence and the other one for the stress dependence of the MDL.

The measurement of the dependence of the MDL pulsed voltage output  $V_o$  on the applied pulsed excitation field for as-cast, stress-relieved and stress-current annealed amorphous  $Fe_{78}Si_{7}B_{15}$  wires, illustrated an improvement of sensitivity after stress relief and after stress-current annealing, as for the case of amorphous ribbons. This was expected as discussed earlier.

A typical dependence of  $V_o$  on the biasing field is illustrated in Figure 4.11, concerning an as-cast amorphous  $Fe_{78}Si_{7}B_{15}$  wire. For this case, it can be seen that the MDL response is not a continuous function. This is attributed to the Large Barkhausen jump of as-cast amorphous  $Fe_{78}Si_{7}B_{15}$  wires. In these wires, the existence of an inner single domain along the whole length of the wire, results in bistable switching which is observable in the MDL receiving region for magnetization field dependence reasons, but also in the excitation region concerning discontinuity in the  $\lambda(H)$  function.

Such a response is influenced by heat treatment mostly due to increase of the Barkhausen jump effect. Stress-current treatment modifies the response of the amorphous wire; after this treatment, there is no Barkhausen jump and the bias field dependence becomes similar to that of amorphous ribbons.

A typical stress and torsion dependence of  $Fe_{78}Si_{7}B_{15}$  wires is illustrated in Figures 4.12 and 4.13 respectively. The response of these wires is very sensitive illustrating a difference in as-cast, temperature annealed and field annealed samples. As-cast wires illustrate a rather linear response, while annealed samples illustrate a non-linear but more sensitive stress dependence. This is attributed to the improvement of the magnetomechanical coupling factor of wires, which has also been observed for the same family of amorphous ribbons.

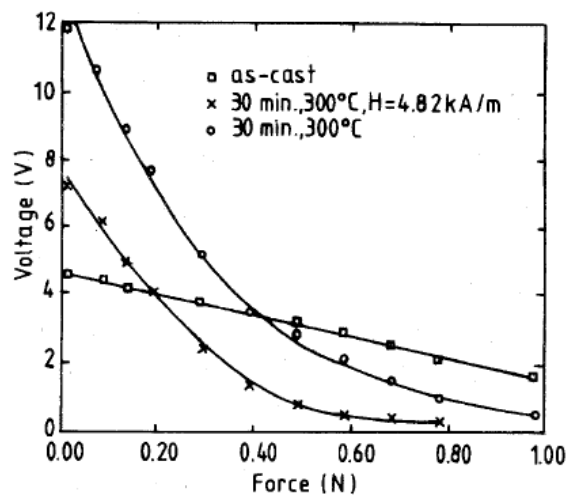
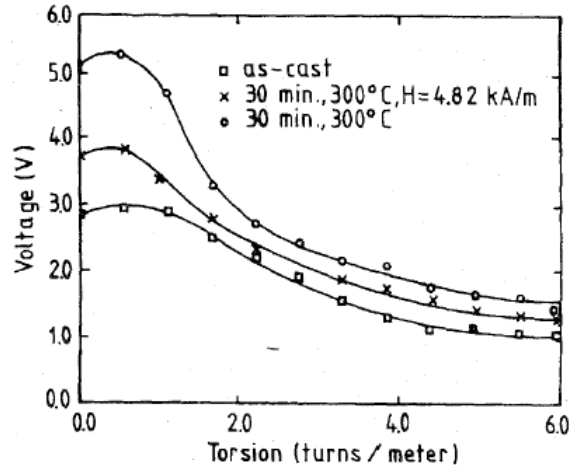
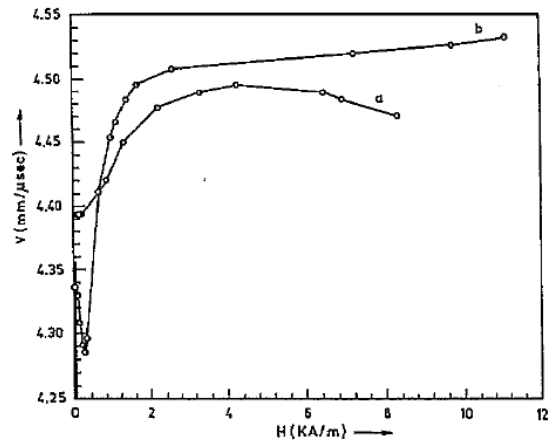


Figure 4.12. Stress dependence of amorphous wires used as MDLs.



**Figure 4.13.** Torsion dependence of amorphous wires used as MDLs.

A typical sound velocity dependence of as-cast and stress-relieved amorphous wires is shown in Figure 4.14, illustrating field dependence of the longitudinal sound velocity even in the as-cast form.



**Figure 4.14.** Sound velocity dependence of  $Fe_{78}Si_7B_{15}$  of as-cast (a) and stress-relieved (b) wires.

It has been experimentally established that the amorphous wires have almost uniform magnetoelastic response in comparison with ribbons. This means that their repeatability and their multiplexing accuracy is quite high and within the limits of the above mentioned accuracy, while of course the use of the normalisation process allows the same levels of uniformity, repeatability and multiplexing accuracy in the case of ribbons, under the assumption that a microprocessor controller is to be used.

As it was already discussed, the MDL secondary waveforms and the MDL resolution are much improved in the case of amorphous wires, compared to the response of amorphous ribbons of the same family. Furthermore, as shown in next chapters, there are cases where the amorphous wires offer a more linear response in sensing elements in comparison to amorphous ribbons.

From the experimental work, it has also been observed that the temporal stability of the response in an amorphous wire is of the same order of the corresponding stability as an amorphous ribbon. The deviation of the amplitude size is mainly due to random mechanical vibrations of the wire, while the involvement of domain wall instability is also present, resulting thus to a random instability distribution. The stability in amorphous ribbons and wires in the as cast form has been found to be of the order of 1% maximum. Thus, the sensitivity of these devices could not be better than 1% for direct readings for this kind. Using field annealed amorphous wires results in a reduction of the instability down to the order of 0.2%. This may suggest the absence of the Large Barkhausen jump for field annealed wires. Averaging out the sensor output does also result in a compensation of the instability output. For as-cast materials it is reduced down to 0.01%, while in the case of the field annealed materials it is reduced down to the least  $\frac{1}{2}$  digit of the used experimental set-up (12-bit Analogue to Digital Converter). The pulsed width response of the amorphous wires (Figure 4.15) is very similar to that of amorphous ribbons, having a maximum output at  $\sim 2 \mu\text{s}$ .

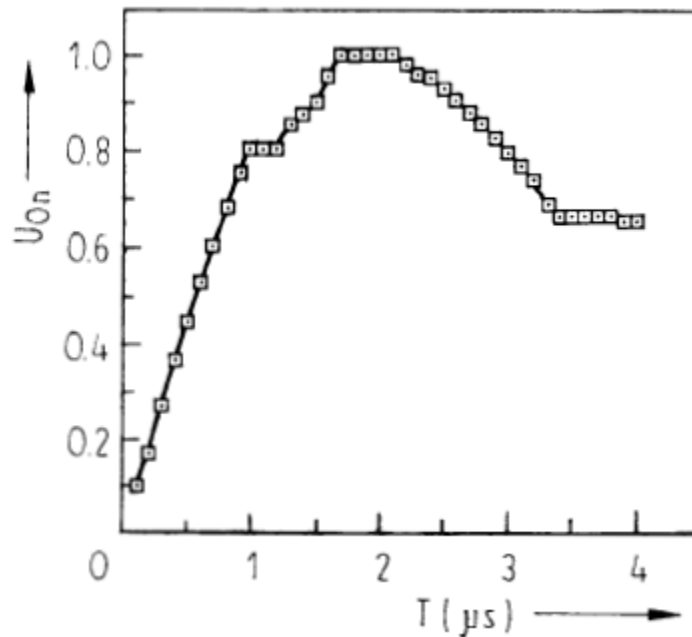


**Figure 4.15.** Pulsed current width normalized MDL response in amorphous as-cast wires.

The preference of wires with respect to ribbons and vice-versa will be discussed in each type of sensor based on the MDL technique separately. As an example, amorphous ribbons in the as-cast form are less sensitive in sound velocity changes than the amorphous wires, thus being more preferable for delay time based position sensors. On the contrary, amorphous wires are more sensitive to pulsed and bias field, thus being more preferable for voltage output dependent sensors.

It is clear though that cross sectional shape reasons may govern the decision of using either wires or ribbons. For example, if the MDL itself has to be stressed or torsioned, amorphous wires ought to be used. On the other hand, if the MDL has to be pressed, it seems that amorphous ribbons are more preferable. In the case that MDL has to be used as an untouchable waveguide, the use of either ribbons or wires may be suggested, depending on the application. For example, for field sensors with small range of measurement, amorphous wires very sensitive before the Large Barkhausen jump may facilitate for some given applications. On the other hand, long field range response of amorphous ribbons may allow their use in area field mapping.

Finally, stress-current annealing may significantly help to tailor the  $\lambda(H)$  function of amorphous wires, due to their cross sectional shape. This may allow the preferential use of amorphous wires for industrial sensing manufacturing and applications.

---

### 4.2.3 Amorphous glass covered wires

---

The operation of Fe-rich glass covered amorphous alloy wires as magnetostrictive delay lines is illustrated hereinafter. These wires can not demonstrate magnetoelastic wave propagation, since their signal vanishes fast due to the high interlayer stresses between glass coat and magnetic alloy core. We obtained magnetoelastic wave propagation and detection after glass removal and mainly after high frequency current annealing without glass removal. This is the reason why their MDL characteristics are presented more analytically than the other amorphous materials (ribbons and wires). The significance of glass covered amorphous wires is their anti-corrosion protection offered by the glass covering cell. The presence of the glass can also be used in some specific applications, where, for example, mechanical action like force is to be applied on the magnetostrictive wire surface, thus measuring force distribution and digitization.

Having the motivation to obtain the MDL operation from glass covered amorphous wires, GCA wires for short, their properties were investigated. The most challenging aspect was that, despite the fact that these wires have a magnetostrictive composition, they are not expected to show the usual magnetoelastic wave generation, propagation and detection in their as cast form, because of the tensile and quasi-torsional stresses induced at the surface acoustic wave propagation layer, which does not allow the propagation of elastic pulses generated in the magnetostrictive volume. The Fe-rich GCA wires, having the same  $\text{Fe}_{77.5}\text{Si}_{7.5}\text{B}_{15}$  composition of the more “classical” amorphous wires, a-wires for short, illustrate magnetostrictive properties, as the a-wires. This is proved by observing the modification of the B-H loop under applied stress. Thus, it would be expected that the GCA wires could generate magnetoelastic microstrain able to propagate as elastic wave.

In order to observe and determine the magnetoelastic wave generation, propagation and detection in these wires, which we will describe next. A 40 cm ceramic tube of 0.5 mm and 1 mm internal and external diameter respectively has been used in order to accommodate the GCA wire. A 10 turn coil made of 0.1 mm enamelled copper wire has been used for pulsed field excitation means. This coil was wound on a glass tube of 2.5 mm and 1.5 mm external and internal diameter respectively, able to be around the ceramic tube accommodating the GCA wire. Thus, this glass tube was able to be driven along the ceramic tube, in order to measure the magnetoelastic uniformity properties of the wire. A 30 mm long solenoid, made of 0.35 mm enamelled copper wire, was wound around a glass tube of 7 mm and 5 mm external and internal diameter respectively and has been used for applying biasing field along the region of the pulsed field used for excitation of the wire. A 1000 turn flux change receiving coil, made of 0.03 mm enamelled copper wire, has been wound along the one end of the ceramic tube. A fixed in position 30 mm solenoid, made of 0,35 mm enamelled copper wire, was wound around the receiving coil and fixed in position, used for applying biasing field along the region of flux change detection. A FET transistor based circuit was used for pulsed current generation, up to 20 A peak value, having a period of 1 ms and a duty cycle corresponding to pulsed current width from 0.1 up to 10  $\mu\text{sec}$ . The output of the receiving coil was connected to an oscilloscope for flux change observations. According to this, the magnetoelastic wave generation and propagation could be received by the receiving coil and observed in the oscilloscope. Hence, the dependence of the magnetoelastic wave behaviour on the exciting pulsed field amplitude and width could be determined as well as its dependence on the biasing field at either the point of excitation or the region of elastic wave receiving.

Fe-rich glass covered amorphous wire of the usual  $\text{Fe}_{77.5}\text{Si}_{7.5}\text{B}_{15}$  composition in the as cast form was initially used. No signal could be detected out of the receiving coil. Then, the glass cell was removed out of the GCA wire by using HCl solution of 0.001 N for 1 hr. The result was the appearance of a pulsed voltage output at the receiving coil. Actually, the magnetoelastic response of this wire was not uniform along the length of the material. This response was measured by moving the exciting coil along the ceramic tube under no biasing fields. The dependence of  $V_o$  on the distance between exciting and receiving means is given in Figure 4.16. This measurement proves that the glass coat does not allow the propagation of the magnetoelastic wave. Since our target was to use the GCA wires with the glass coat, we tailored the properties of GCA wires by high frequency current annealing. Passing high frequency current through the magnetic core, current transmission is limited at a given depth of the magnetic core, due to the skin effect.

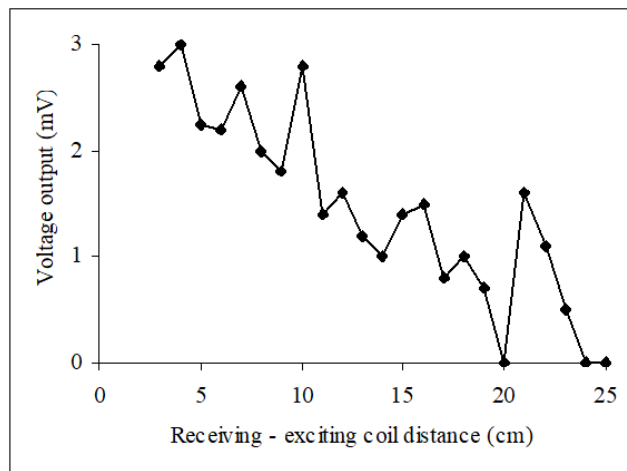


**Figure 4.16.** Magnetoelastic uniformity response for a glass removed CGA wire by chemical etching.

Such current heats up the glass coat – magnetic core interlayer, resulting in tensile and torsional stress relaxation at this interlayer. Indeed, after annealing with 10 MHz, 0.1 A current along the GCA wire for 1 minute, a pulsed voltage output at the receiving coil was observed.

The magnetoelastic wave characteristics for the high frequency magnetically annealed wires were measured, at a distance between exciting and receiving coil equal to 5 cm. The dependence of the voltage output amplitude,  $V_o$ , on the pulsed exciting field is illustrated in Figure 4.17. The dependence of  $V_o$  on the bias field at the exciting region is given in Figure 4.18. These experimental results prove that GCA wires can be used as magnetostrictive delay lines, having the advantage of the glass coat existence.

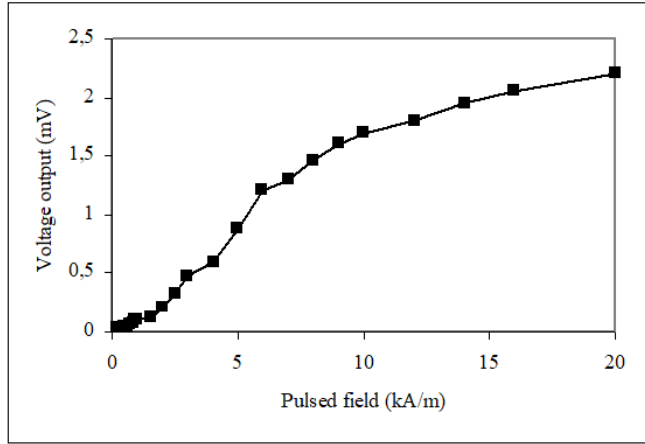


**Figure 4.17.** MDL voltage output dependence on the pulsed exciting current field for the GCA wire.

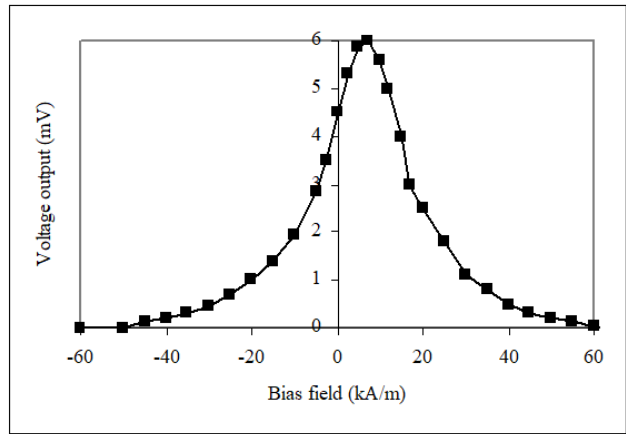


**Figure 4.18.** The MDL dependence of  $V_o$  on the bias field at the region of excitation.

The first effect under discussion is the explanation of the generation and detection of magnetoelastic waves along the GCA wire. It is clear that in the as-cast form of these wires, no magnetoelastic wave can be detected at the receiving coil, even if microstrains can be generated at the acoustic stress point of origin. Taking into account the tensile and torsional stresses induced at the interlayer surface between the glass cell and the metallic Fe-rich cylinder due to their production method, it is assumed that the generated microstrains at the region where pulsed field is applied are generally speaking small in size, with respect to the microstrain which could be generated at the same metallic cylinder, without such a glass surrounding cell and corresponding induced stresses. Such an even small in amplitude, generated microstrain is then to propagate along the length of the GCA wire, as a Surface Acoustic Wave (SAW) on

the Fe-rich metallic cylinder as acoustic waveguide. This SAW should be a longitudinal propagating wave, due to the shape of the acoustic wave guide, but it vanishes as soon as it is generated, due to the presence of the above mentioned stresses along the glass - metal interlayer, as it happens in a common MDL arrangement where the delay line is subjected to mechanical distortion.

The magnetoelastic response of the CGA wire tested after annealing in 10 MHz and 0.1A current along the wire for 1 minute was monitored and illustrated in Figure 4.19. Such a response is far better than the response of Figure 4.16, due to the uniform cover of glass on top of the magnetostrictive element and the uniformity of glass-MDL interlayer stresses.

The non-uniform response of the partial glass removal of Figure 4.16, in which the magnetoelastic signal equals zero for some distances between exciting and receiving MDL means, reappearing again at a higher distance between them, actually proves the above mentioned statements about the glass cell effect on the magnetoelastic behaviour of the GCA wires. Observing Figure 4.11, it can be seen that if glass exists at a given region of the wire, then it is impossible for a generated microstrain in this region to propagate along the wire. Figure 4.11 also indicates that, if a microstrain is generated at another region, it can propagate even if it meets along its travel path glass portion inducing stresses on the acoustic wave guide surface and thus distortion in its amplitude. These observations indicate that, if the interlayer tensile and torsional stresses induced by the GCA production method are minimized, a generated microstrain can propagate and be received as a magnetoelastic wave.

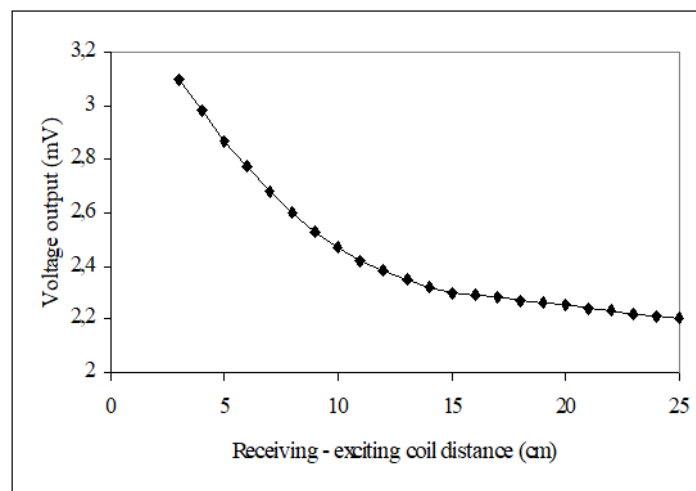


**Figure 4.19.** Magnetoelastic uniformity response for a complete glass removal GCA wire.

The most interesting result, though, is the realization of magnetoelastic wave generation, propagation and detection. The explanation is different than the latter mentioned process. Obtaining a smaller glass cell around the magnetic alloy core than the normal one, the amount of induced tensile and torsional stresses on the said interlayer is reduced, obtaining the acoustic wave propagation and detection. An interesting observation is that the magnetoelastic uniformity is similar to the function obtained in the complete glass removal samples, although the attenuation factor of this function and the MDL sensitivity is lower than in the complete glass removal case. This is explained by the existence of stresses at the interlayer. Improvement of such a signal can be realized by stress-current annealing in high frequencies of annealing current.

Actually, the experimental technique described in this paper can be used for observing the percentage of the glass removal process by scanning the magnetoelastic behaviour of the GCA wire. Having in mind that the optimum uniformity response is the one illustrated in Figure 4.19, the variation of the amplitude of  $V_0$  indicates the amount of glass existing on the amorphous alloy surface. Apart from the uniformity response it is also interesting to study the magnetoelastic wave sensitivity and characteristics. From Figures 4.17 and 4.18 it appears that the microstrain dependence of the GCA wires on the applied pulsed or biasing fields is less sensitive than the "classical" amorphous wires.

Considering that such a response concerns a GCA wire tested before annealing processes, this observation can be useful in terms of tailoring the magnetoelastic properties of these wires. Considering their use in sensors applications utilizing the MDL technique, their power consumption can be one order of magnitude lower than using the classical a-wires. Tailoring the microstrain dependence can also be used for MDL optimization by means of improving its spatial resolution and sensitivity.

Another significant although preliminary observation is the pulsed width response of the GCA wires. In Figure 4.20, it can be seen that this response, reflecting the bandwidth response [18], of the magnetoelastic behaviour of GCA wires can extend to the 10 MHz limit, set by the classical a-wires. This observation can lead to the use of higher frequency excitation pulsed fields, which can actually generate travelling surface acoustic waves of a higher frequency. The corresponding smaller wavelength of these waves may be able to travel even in the presence of the above mentioned stresses at the glass-alloy interlayer. Research work is also under way for this subject.

It can be said that the realization of magnetoelastic waves in the recently developed GCA wires after glass cell removal, apart from being an achievement by itself, it gave the indication of how to generate elastic

waves even in the presence of glass covering cell, namely being the partial or the complete removal of the induced stresses at the glass-alloy interlayer. Such a stress relief can be realized by annealing process, as above mentioned.

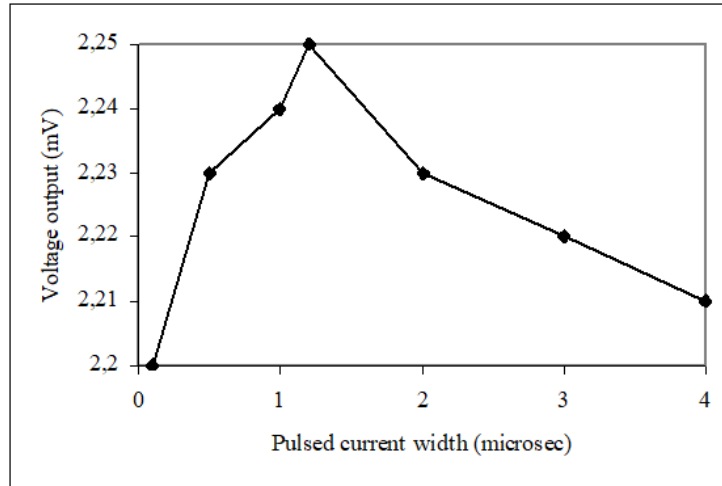


Figure 4.20. Pulsed width response of GCA wires.

Finally, a comparison of the magnetoelastic uniformity of as-cast amorphous ribbons and wires as well as high frequency annealed glass covered wires is illustrated in Figure 4.21.

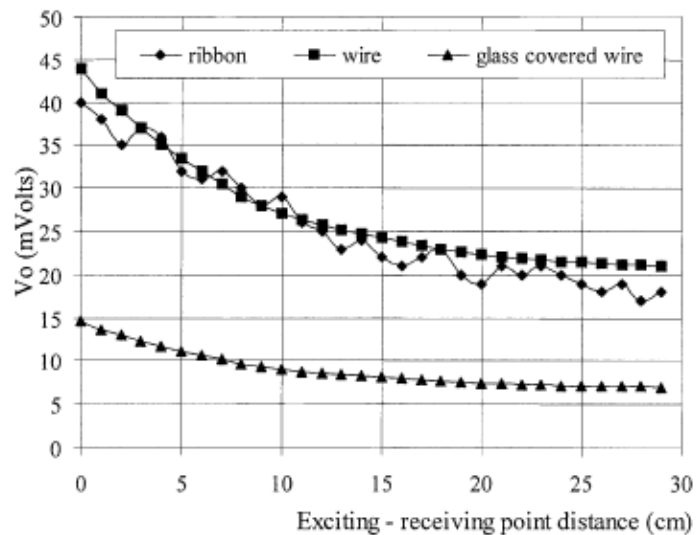


Figure 4.21. Magnetoelastic uniformity in as-cast ribbons, wires and high frequency annealed glass covered wires.

---

### 4.3 *Thin films*

---

Magnetostrictive delay lines have also been developed in thin film structure. A monolithic design has been achieved with the coils and the magnetoelastic element contained onto the same silicon substrate. Such a miniaturized device able to be used for MDL sensing applications was fabricated by using a multilayer-like technique.

The exciting conductor, the receiving coil and the MDL were fabricated using a conventional photolithographic technique. In order to use conventional magnetostrictive thin films and Fe-metalloid amorphous thin films as active magnetoelastic elements, the magnetoelastic properties which determine their performance were studied.

The realization of small size sensors with the magnetoelastic element and the electronic circuitry integrated in the same silicon wafer represents a considerable advantage of sensors based on thin films comparing to sensors based on magnetostrictive amorphous ribbons and wires.

Due to the fact that the Curie temperature  $T_C$ , the saturation magnetization  $M_s$  and the saturation magnetostriction  $\mu_s$  and their hysteresis response determine the magnetoelastic sensing applications, it is useful to study and evaluate these properties of the magnetostrictive amorphous and crystalline thin films used as MDLs.

These applications require high values of the saturation magnetostriction constant and magnetoelastic coupling factor in order to obtain dynamic, sensitive and versatile magnetomechanical sensors. Among all these properties concerning magnetoelastic sensing applications, the magnetomechanical coupling factor  $k$ , representing the elastic energy yielded by magnetic excitation and vice versa is the most important.

Among the crystalline materials, Fe and Ni wires are good candidates for delay line based sensors, as depicted in the first part of this Chapter. Furthermore, experimental data indicate that the magnetomechanical coupling factor  $k$  of Fe-Si-B amorphous alloys is higher than the one of Fe and Ni or other magnetostrictive materials.

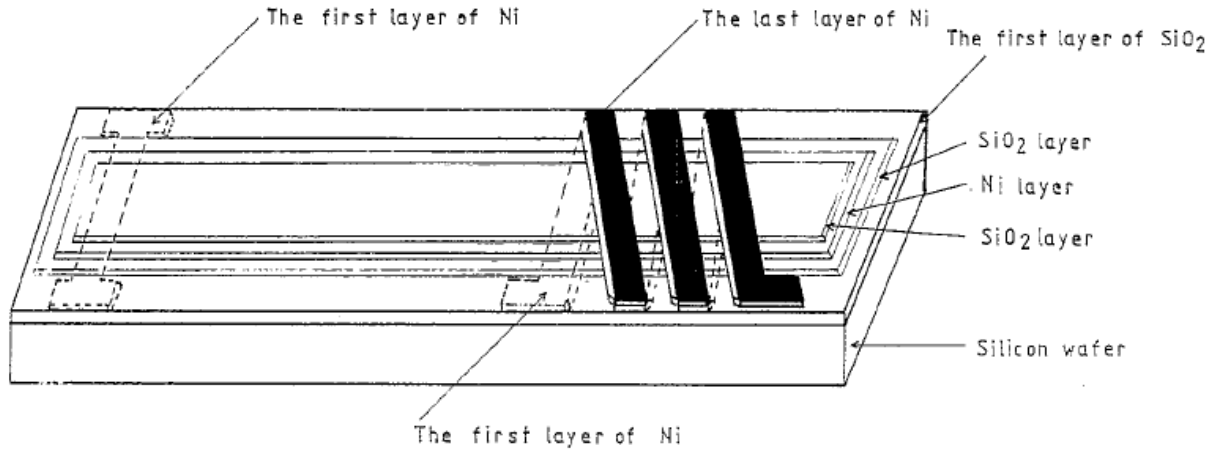


**Figure 4.22.** The configuration of the thin film MDL.

Low values of magnetic anisotropy constant  $k_u$  are required for large values of magnetomechanical coupling factor  $k$  in order to improve the performance of the sensors. It has been established that the magnitude of  $\Delta E$  effect depends on the ratio between the saturation magnetostriction constant  $\mu_s$  and the magnetic anisotropy constant  $k_u$ . If  $E_s$  is the Young's modulus in magnetically unsaturated state, the following equation is useful to compare delay line changes for different materials used as magnetoelastic elements:

$$\left(\frac{E}{E_s}\right) \left[1 + \left(\frac{9E_w \lambda_s^2}{2k_u}\right)\right]^{-1}_{min} \quad (4.1)$$

The magnitude of this effect depends on the alloy composition and the annealing history of the sample.

Another advantage of the use of amorphous thin films as delay line medium for magnetomechanical microsensors is their high mechanical strength. For these reasons, metallic glasses are used as active core magnetoelastic elements in magnetomechanical sensors-based MDLs.

The configuration of the magnetostrictive delay line presented hereinafter, fabricated on a 50 mm diameter silicon substrate, using a multilayer like structure, using Ni/SiO<sub>2</sub>, is illustrated in Figure 4.22. The reason why Ni magnetostrictive material has been selected as the MDL element was due to microfabrication compatibility reasons. 33 mm long magnetostrictive thin films have been used as MDLs, while an exciting straight conductor (EC) was deposited at the one end of the MDL and a receiving coil (RC) at the other end of the MDL. This geometry minimizes secondary waveforms out of the receiving coil. The

distance between EC and RC is important in the MDL miniature design, determining the delay time between exciting and receiving signals and consequently the detection of a discrete MDL output signal. It has been found that such a minimum distance between EC and RC is of the order of 30 mm.

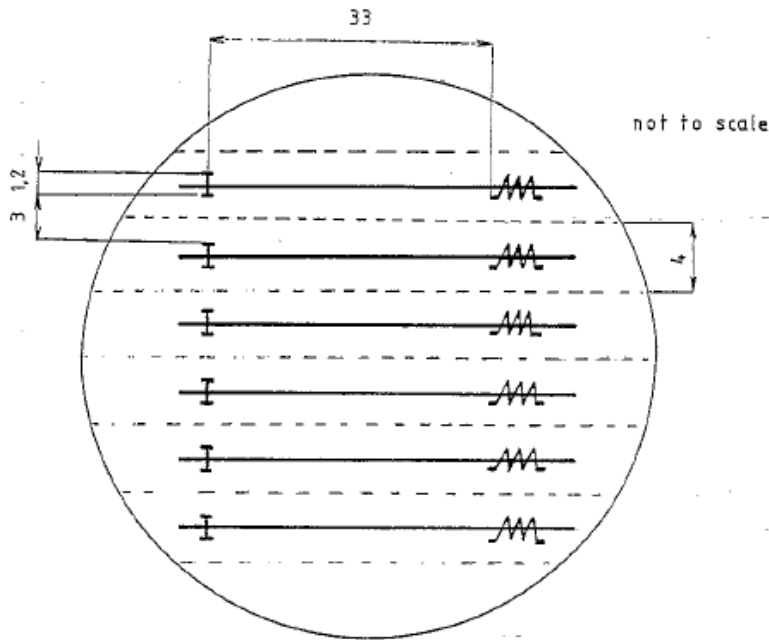


**Figure 4.23.** The 6 miniature MDLs silicon wafer schematic.

deposition and electron gun beam evaporation, respectively.

The lithography used to form the exciting and receiving coils as well as the MDL itself, was based on the ordinary positive photo resist application (Shirley AZ 1350J), an exposure using ultraviolet contact photolithography and development. The pattern was obtained by wet chemical etching, but it can also be obtained by dry lithography. The process sequence in the miniature MDL fabrication is illustrated in Figure 4.24.

Other elements, such as Fe and most importantly Fe-Si-B amorphous alloys can also be deposited instead of Ni, as MDLs. Indeed, Fe-based amorphous alloys have been developed. Among several experimental trials, the  $\text{Fe}_{70}\text{Si}_6\text{B}_{20}\text{C}_4$  composition demonstrated again the best performance within the limits of our processing facilities.

The silicon wafer schematic, including 6 miniature MDLs built on the same Si wafer, is illustrated in Figure 4.23, using multilayer-like structure deposition and photolithographic technique. The principle of operation of such an arrangement has been analyzed in Chapter 2.

The fabrication process of the MDL miniature is based on microelectronic technology. The insulating layers and metallic films were deposited by rf sputtering

The characterization was realized with respect to the main magnetic properties of technical importance, namely the saturation magnetostriction  $\mu_s$ , the magnetic anisotropy constant  $k_u$ , the Curie temperature TC and the saturation magnetization  $M_s$ . Magnetic measurements have been performed for both Ni and  $Fe_{70}Si_6B_{20}C_4$  alloy MDL. The films have been characterized by using glass substrates commonly used in thin film technology. Magnetostriction was measured by using capacitive-cantilever technique. The magnetic characteristics were measured by using torque magnetometry.

Large values of saturation magnetization are important for magnetostrictive materials used for MDLs. The value of saturation magnetization  $M_s$  of amorphous Fe-based thin films is considerably larger than the value of saturation magnetization of Ni polycrystalline thin films.

Furthermore, the hysteresis in amorphous substances is much smaller, therefore allowing larger values of magnetomechanical coupling factor.

The magnitude of the magnetic anisotropy constant decreases from  $7.0 \times 10^4$  for polycrystalline Ni thin films to  $3.1 \times 10^3$  for the amorphous  $Fe_{70}Si_6B_{20}C_4$  alloy

thin films. The difference between the anisotropy constants of these samples is attributed to the negligible

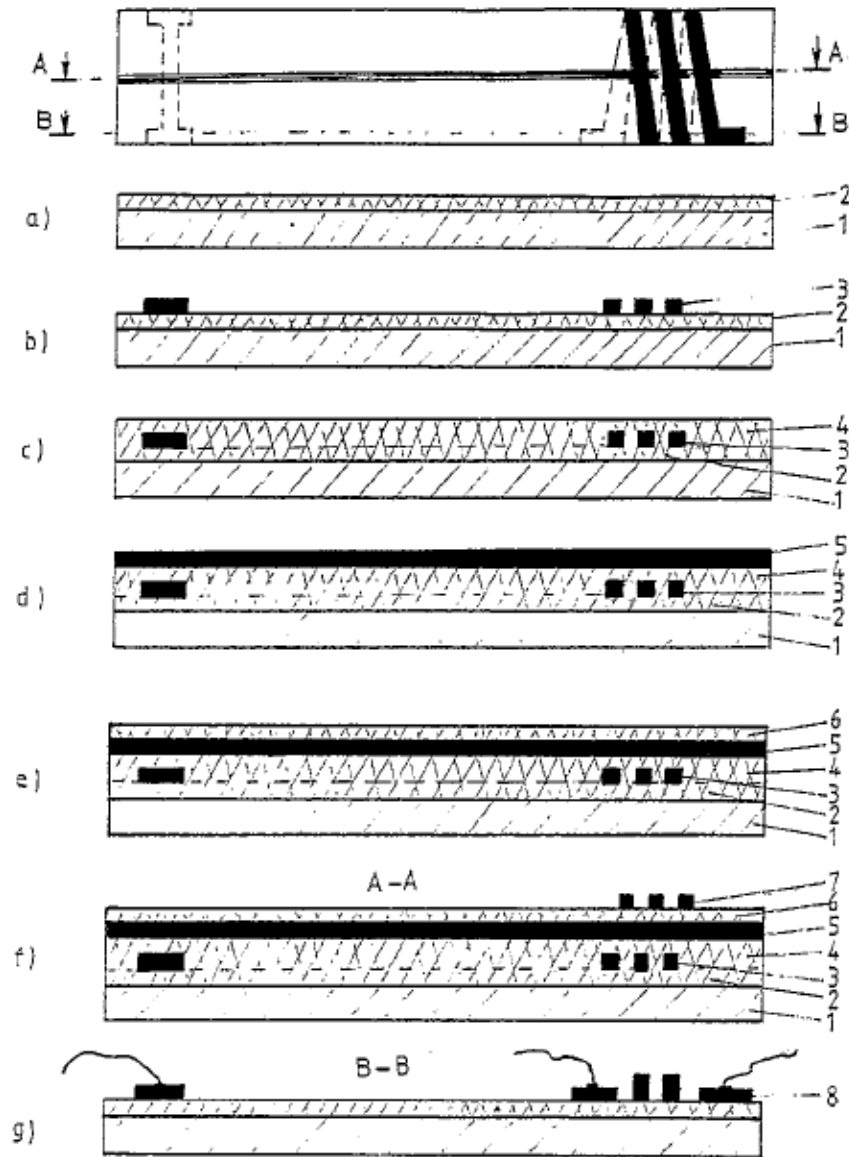


**Figure 4.24.** The process sequence in the miniature MDL fabrication.

values of magnetocrystalline anisotropy on metallic glass thin films. Typical linear longitudinal and transverse magnetostriction values of Ni alloy films are illustrated in Figure 4.25. The details of the structure of the films and the method of the determination of the dependence of  $\lambda$  on the applied field.

The magnetoelastic response of such a thin film concerning parametric control of pulsed and bias fields as well as stress dependence has been determined showing monotonic and non-hysteretic response. Suggestively, Figures 4.26 and 4.27 show the dependence of the MDL pulsed voltage output on the pulsed excitation current and the displacement of a  $\text{Nd}_1\text{Fe}_{12}\text{B}_1$  permanent magnet for a Ni MDL thin film.

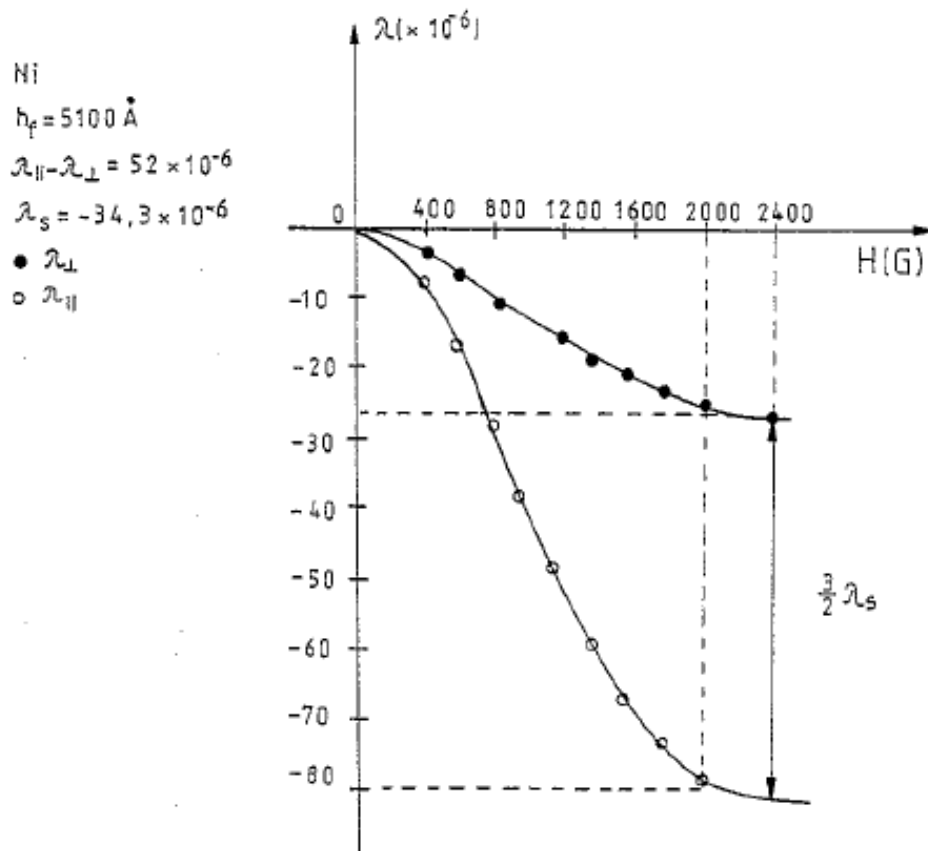


**Figure 4.25.** The linear longitudinal and transverse magnetostriction of Ni and  $\text{Fe}_{70}\text{Si}_6\text{B}_{20}\text{C}_4$  alloy films.

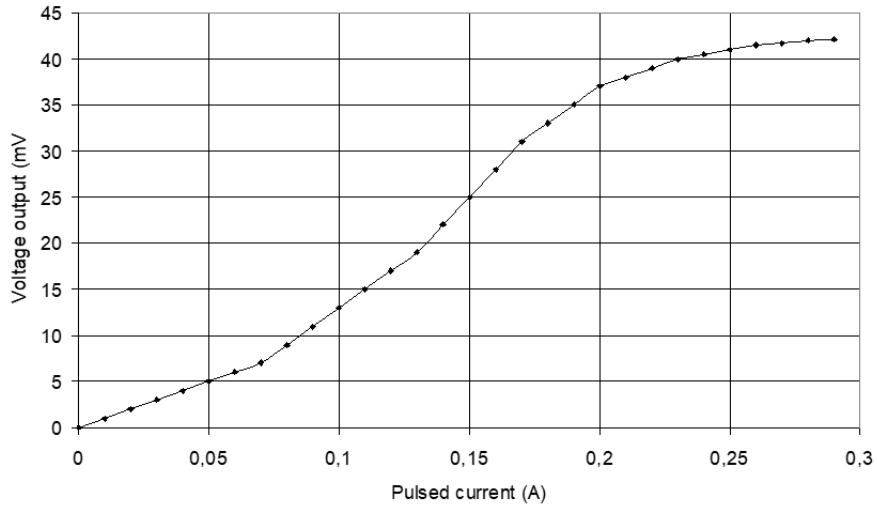


**Figure 4.26.** Thin film MDL output dependence on pulsed excitation current.

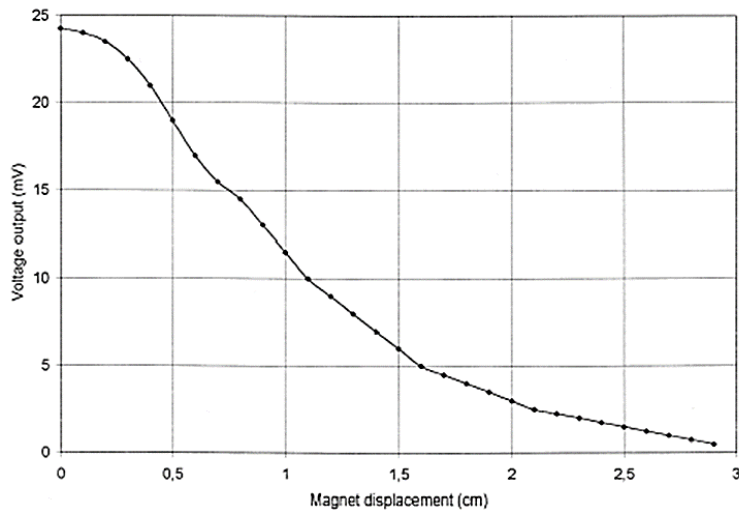


**Figure 4.27.** Thin film MDL output dependence on the displacement of a  $\text{Nd}_1\text{Fe}_{12}\text{B}_1$  permanent magnet.

An alternative way to detect the propagating elastic pulse in MDL thin films is the use of an MR element as illustrated in Figure 4.28. According to this arrangement, instead of using a miniaturized coil to detect the flux change, one may use magnetoresistive (MR) device in order to detect flux.

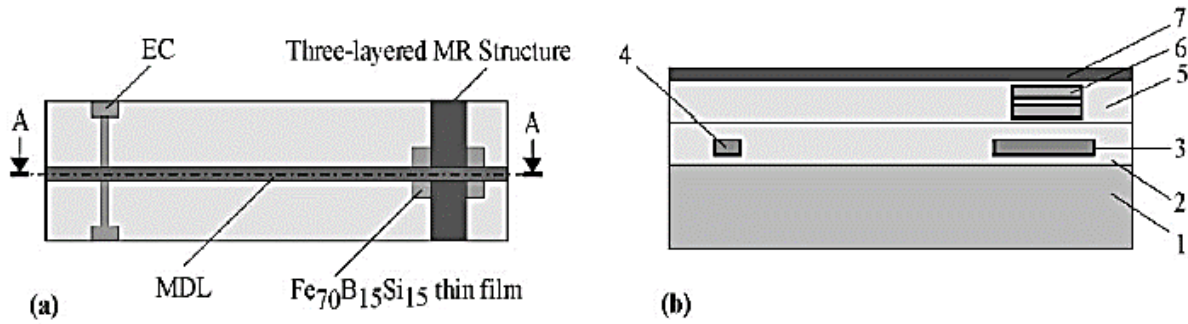


**Figure 4.28.** MDL thin film using MR element as search means. (a) Top view, (b) Side view. (1) Substrate or wafer, (2) Insulating layer, (3) Fe<sub>70</sub>B<sub>15</sub>Si<sub>15</sub> thin film, (4) Cu thin film acting as pulsed current conductor, (5) insulating layer, (6) Three-layered MR structure, (7) Fe<sub>70</sub>B<sub>15</sub>Si<sub>15</sub> thin film operating as MDL medium.

Apart from the classic MDL arrangement, the combination of inderdigital transmitter and electrostrictive materials with magnetostrictive materials may also be used. This is the “opposite” with respect to the arrangement illustrated in Figure 2.14. The schematic of the arrangement is illustrated in Figure 4.29. According to this arrangement, a Fe-rich thin magnetostrictive film is set on top of the acoustic waveguide used for elastic pulse, generation propagation and detection. The elastic pulse is a surface acoustic wave (SAW) generated due to an inderdigital transmitter acting on a piezoelectric or ferroelectric element. Such a SAW propagates along the electrostrictive material. When the elastic pulse arrives at the vicinity of the Fe-rich thin film, it is coupled with it, transmitting a part of the acoustic energy to the magnetostrictive film. The amount of the energy transmitted to the magnetostrictive film is proportional to the magnetization level of the magnetostrictive film. If the material is highly magnetized, the amount of acoustic energy transmitted to the film is reduced.

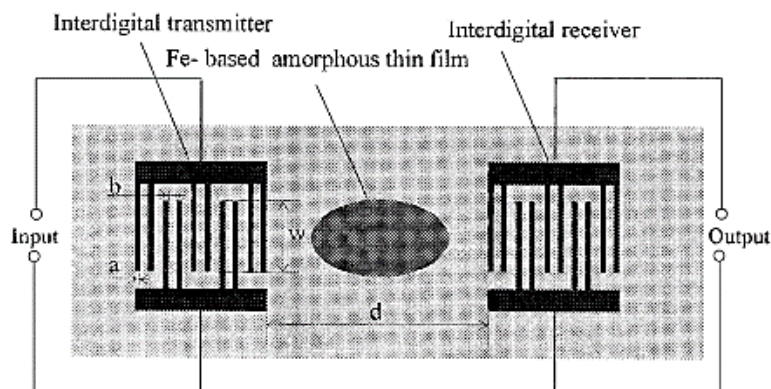


**Figure 4.29.** A thin film arrangement using an electrostrictive delay line, coupled with magnetostrictive material.

Thus, the propagating pulse, received by the interdigital receiver is small as the magnetostrictive material is not magnetized. If the magnetostrictive material is either stressed or biased with field, its magnetoelastic coupling factor changes and the propagating elastic pulse is modified (See Figure 4.30).

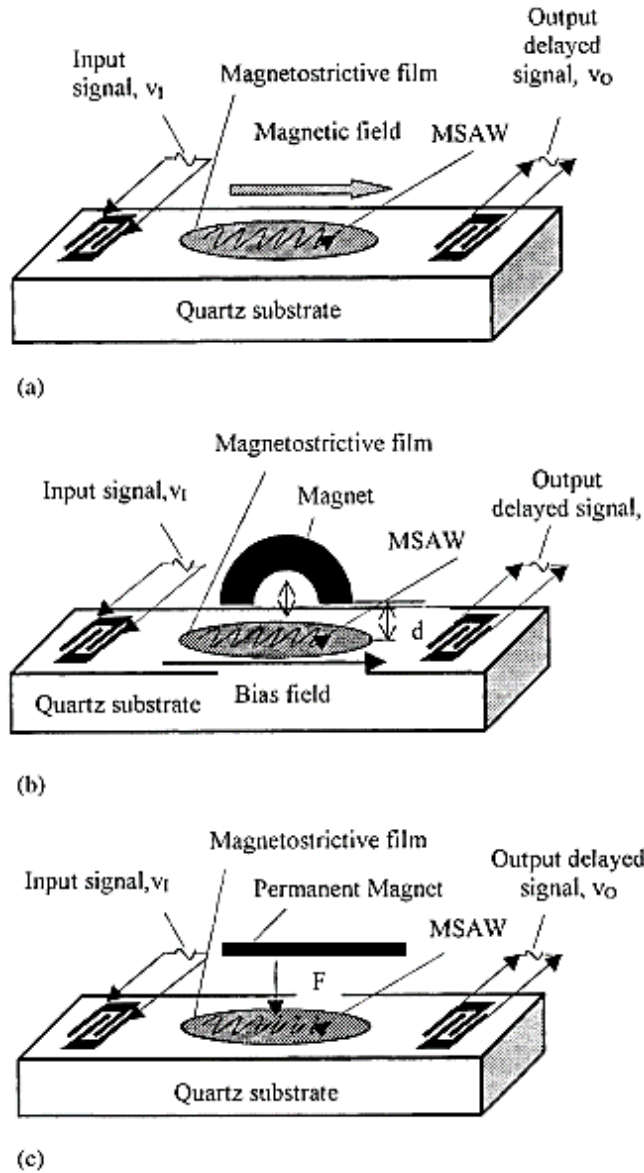


**Figure 4.30.** Operation of the SAW based thin film. (a) Operation of the electrostrictive delay line coupled with a magnetostrictive material, (b) effect of biasing field in the arrangement, (c) effect of applied load on the arrangement.

---

#### 4.4 *Negative magnetostrictive materials*

---

The sensing applications of negative magnetostrictive elements, used as magnetostrictive delay lines for sensor applications may be of importance. In particular, these applications correspond to the measurement of applying tensile stress, pressure and force, since the rest of characteristics ought to be similar to the response of positive magnetostrictive materials. The stress dependence of the above mentioned materials is presented and discussed in comparison with the more classic positive magnetostrictive delay lines.

The negative magnetostrictive materials used as MDLs are Ni, and Fe-Ni polycrystalline wires in the as cast form, after a stress relief process in 350 °C for 30 minutes or after flash stress current annealing using pulsed current of amplitude, duration and period equal to 1 A, 10 ms and 10 sec respectively. The sensitivity observed by increasing the excitation pulsed field reaches a saturation level, which is in agreement with the saturation field of the  $\lambda(H)$  function of the under test element. Such a sensitivity is generally increased with respect to the treatment of the material, especially after flash current annealing.

As above mentioned, the direct stress, pressure and torsion on the MDL should cause a different MDL response in negative and positive magnetostrictive materials. In this case the tailoring process caused an increase of the sensor response. In particular, stress relief process caused a decrease to the measurement span of the sensor, while the flash stress current annealing tailoring process didn't cause such a disadvantage, but it only improved the sensitivity.

The difference in negative magnetostrictive MDL (Ni wire) with respect to positive magnetostrictive wires (Fe-wire and Fe-Ni wire) is illustrated in Figure 4.31. The negative magnetostrictive material increases its response with stress, while the opposite takes place for the positive magnetostrictive materials.

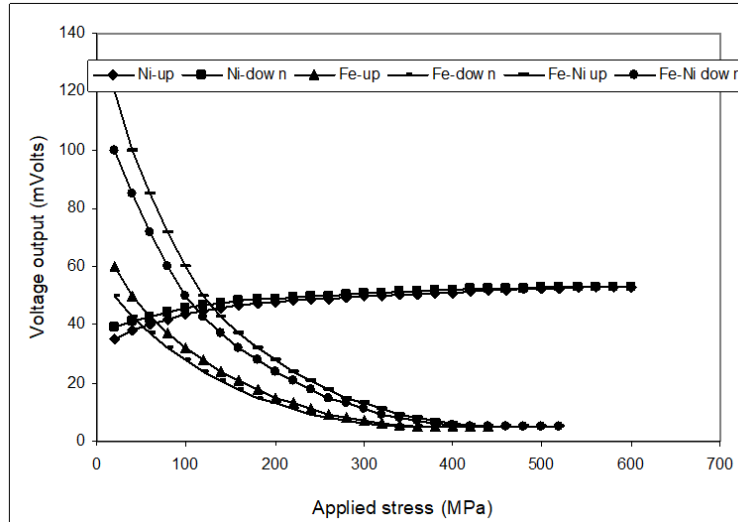


**Figure 4.31.** Stress dependence of Fe, Ni and Fe-Ni polycrystalline wires after flash annealing. Ni wire illustrated the expected increasing response, as negative magnetostrictive material.

In the case of the MDL basic arrangement into external biasing field, the tailoring process caused a different response to the sensor. The stress relief tailoring process increased the sensor's response and doubled the sensitivity, while the flash stress current annealing tailoring process didn't cause an important increase to the sensor's response but increased ten times its sensitivity for the corresponding input of intensity of the external biasing field. The usage of negative magnetostrictive elements as MDLs caused much improvement in many cases to their responses, especially when they are combined with a tailoring process to which the MDLs have been subjected. Generally, we could conclude that the flash stress current annealing tailoring process causes more beneficial effects to the above discussed sensors concerning their response than the stress relief tailoring process.

Using negative magnetostrictive materials for various sensor applications has shown a significant improvement for some types of sensors, especially for those measuring stress, torque or pressure. There are cases where negative magnetostrictive materials acting as MDLs have the same response as the positive magnetostrictive materials. Such an example is the case of the MDL acting as an acoustic waveguide. Applying pressure on a negative magnetostrictive FeCoSiB wire, results in a decrease of the corresponding MDL output to zero, as illustrated in Figure 4.32. On the contrary applying tensile stress on the same MDL, the pulsed voltage output increases, as illustrated in Figure 4.33.

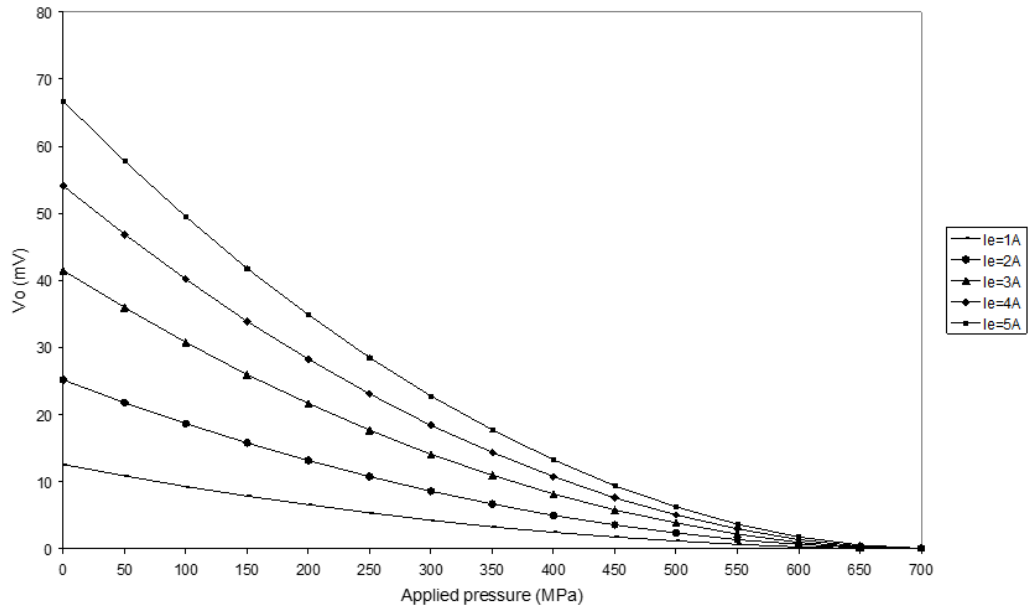


**Figure 4.32.** Applying pressure on a negative magnetostrictive MDL under various pulsed excitation currents  $I_e$  results in a decrease of the MDL output: the MDL acts as acoustic waveguide.

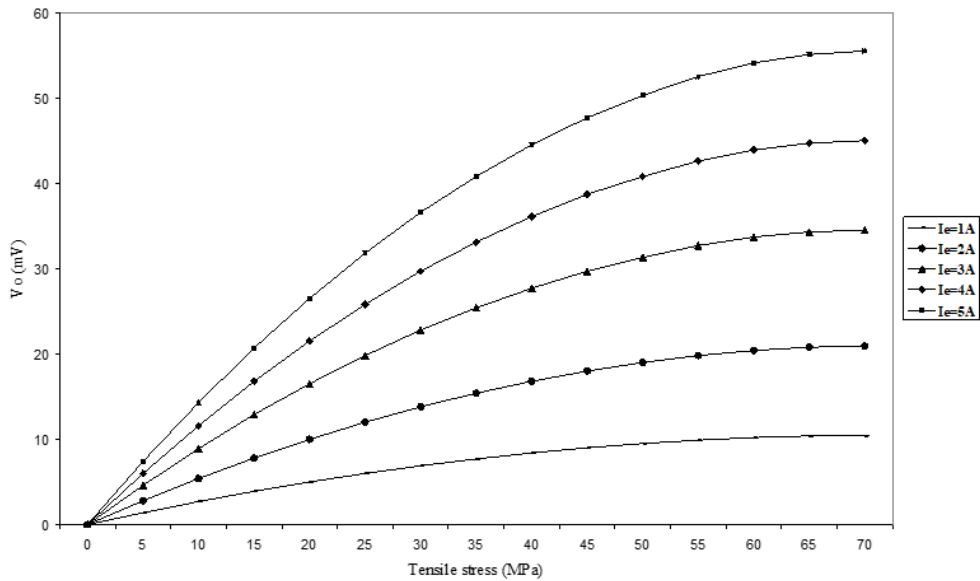


**Figure 4.33.** Applying tensile stress on a negative magnetostrictive MDL results in an increase of the MDL output.

---

## 4.5 *Composites*

---

Composite materials have not yet been developed in MDL arrangements, but it is possible that such materials will be developed in the future. These materials are magnetic or magnetostrictive parts with shape anisotropy, existing in a matrix of another non magnetic material. The magnetoelastic properties of such a material may appear either due to the rotation of the magnetic parts by external magnetic field without the requirement that these materials have to be magnetostrictive, or by the magnetoelastic properties these magnetic parts exhibit, so that the sea matrix of another non magnetic material receives the change of direction or dimensions of the magnetic parts and transmits it along the length of the composite. This matrix has to be soft enough to be sensitive to the motion of the magnetic parts. However, its stiffness results in damping the magnetic part change of state. A stiff polymer may be usable for such a material development.



# 5 Position sensors based on MDLs

Position sensors are widely used in production lines, testing laboratories and medical instrumentation. A vast variety of such sensor characteristics can be of interest, used in many different applications. The state of the art in reference position sensors is laser interferometers, offering an accuracy of the order of 100 nm per meter, while their high cost and sensitivity with respect to the required conditions of measurement makes them appropriate mainly for calibrating instruments and laboratory use. Although these sensors are sensitive, they are expensive and not able to operate in harsh environments.

A useful secondary standard position sensor is the lithographically printed plane surface, utilizing either magnetic or optic bars of sub-micron dimensions, their sequential counting by an appropriate head being the indication of position. Their accuracy is of the order of 10 micrometers per meter and they are often used not only as working standards in calibration laboratories, but also for industrial and medical applications, where a relatively high degree of accuracy is required. Reference lengths are also used for calibration procedures in micro positioners, displacement sensors and 3-d digitizers.

When a circular position needs to be measured, optical and magnetic encoders are used. When a linear position is to be measured, magnetic techniques are usually employed. Magnetic techniques are mainly inductive, such as the linear variable differential transformer – LVDT [3] and various other versions of closed magnetic circuits, in which the electric output of the system changes due to the displacement of the sensing core [4], which can be a permanent magnet, a soft magnetic element or a conductive means. Among these magnetic techniques the magnetostrictive delay line technique [5], named hereinafter the MDL technique, has been widely used for position measurement, offering good linearity and small hysteresis.

Apart from the above mentioned position sensors, when the accuracy required is not so high, candidate sensors have to have the advantage of a relatively low price. A number of such sensors has been presented in the past, mainly based on modification of magnetic circuit [1-3]. All sensing elements presented in this Chapter can be applicable and manufacturable in production lines. Their characteristics are competing

with the state of the art. At first, they are cordless, allowing their use in many applications. As an example, the typical position sensor, resulting from the motion of the pulsed current conductor and corresponding MDL response dependence with respect to its distance from the MDL is not presented as a position sensor, since it is a corded device and therefore it can hardly operate and compete as a position sensor.

---

---

## **5.1 Moving permanent magnet measurement**

---

---

This group of sensors refers to moving permanent magnet position measurement. There are three distinct families of such sensors. The first one is based on voltage output detection using distribution principles based on analog multiplexing techniques as discussed in the previous chapters. The second family is based on delay time measurement, without excluding voltage measurement for an additional dimension of position measurement. Finally, the third one refers to accelerometers using no excitation means to operate.

Each group of sensors is to be presented separately. After the basic description of each sensor, its response is given. Bearing in mind that the peak value of the receiving coil voltage  $V_o$ , is the output of all the proposed transducers, response of the sensors is the dependence of  $V_o$  on the relevant input, which corresponds to the position or displacement of a moving or movable permanent magnet.

---

### **5.1.1 Sensors based on MDL pulsed voltage output measurement**

---

This family of sensors is able to measure displacements up to 20 mm. They are based on the DC bias effect at either the elastic wave point of origin (PO) or the receiving coil of an MDL. They can be used as discrete sensors or as large integrated arrays. The size of these arrays is dependent on the length of the MDL (which can be about one meter). The principal idea of these transducers is based on the change of the peak of the received pulsed voltage output due to the change of the DC magnetic bias field, which is obtained by using moving magnet technique.

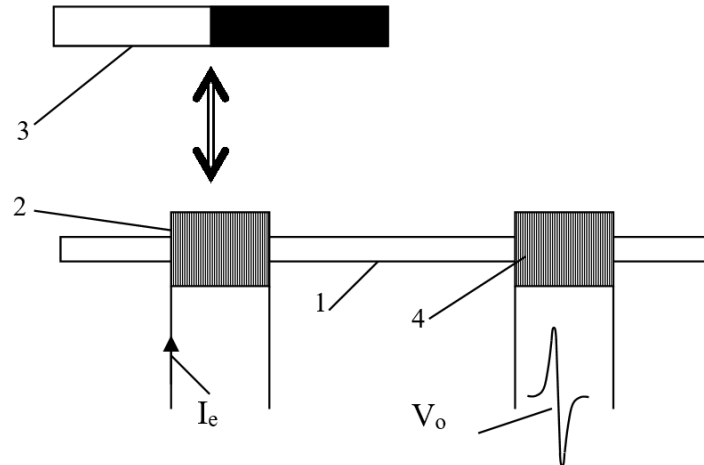


**Figure 5.1.** Moving magnet displacement sensor causes change of the elastic pulse at the excitation region. (1) MDL, (2) Excitation coil, (3) Search coil, (4) Moving magnet.

The basic arrangement of the first sensor of this group, which is based on the change of  $V_o$  due to the DC bias effect at the PO is shown in Figure 5.1. A coil used for pulsed current transmission is vertical to the MDL and a movable small field magnet is on top of the PO, serving as the sensing point. A small field magnet is fixed at the receiving coil, in order to maximize the voltage output.

Magnets are arranged so that their field is in the same direction as the pulsed magnetic field. According to this arrangement, when pulsed current is transmitted through the exciting conductor, the caused acoustic pulse magnitude and consequently the detected voltage peak is dependent on the distance of the magnet from the PO. This operation can be explained as follows: as the magnitude of the magnetic field out of the magnet is decaying with distance, the DC magnetic field and flux in the MDL are dependent on the distance between the magnet and the MDL.

If the existing magnetic fields around the MDL are known or controlled, the response of the sensor is dependent on the distance between the magnet and the MDL. This dependence may be monotonic, provided that the maximization of the MDL response has been obtained by an offset biasing field, for example by using a permanent magnet fixed in position.

A distribution displacement sensor may occur by using the arrangement illustrated in Figure 5.2. According to this arrangement a current conductor array used for pulsed current transmission is vertical to the MDL and movable small field magnets are set on top of the POs, which are the sensing points. A small field

magnet is fixed at the receiving coil, in order to maximize the voltage output. The magnets are magnetically parallel, since their field is in the same direction as the pulsed magnetic field.

According to this arrangement, when pulsed current is transmitted through the exciting conductor array, the caused acoustic pulse magnitudes and consequently the peaks of the detected train of pulsed voltages are dependent on the distance of each magnet from the corresponding PO. The operation of this arrangement runs as previously. It was experimentally found that positioning the magnets correctly can be done as follows: the magnet is in the desirable position, if the detected peak voltage  $V_o$  decreases as the magnet approaches the MDL, without inverting its sign.

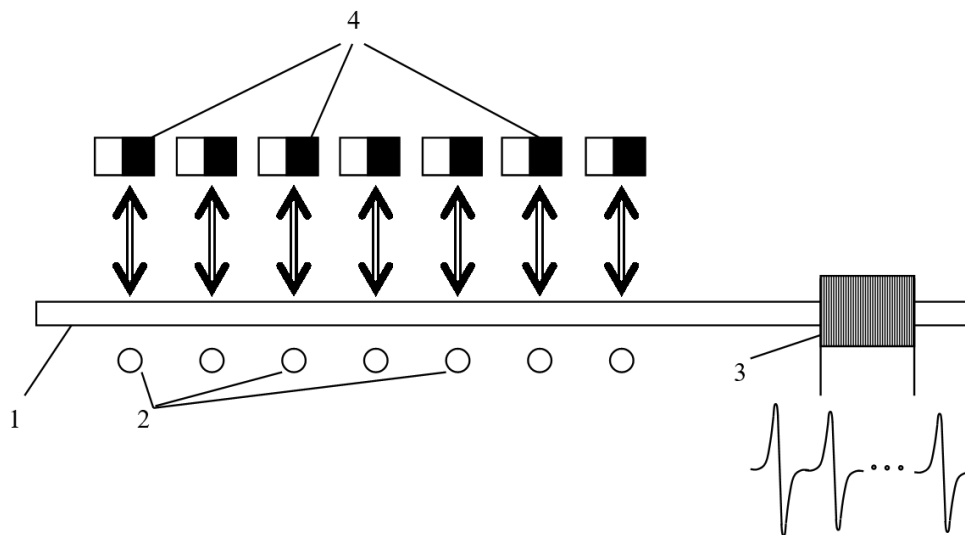


**Figure 5.2.** Distribution displacement sensor based on the sensing element of Figure 5.1. (1) MDL, (2) Array of pulsed current conductors, (3) Search coil, (4) Array of moving magnets.

The basic arrangement of a moving magnet position sensor is based on the DC bias effect at the receiving coil and the inverse magnetostriction effect, shown in Figure 5.3. A pulsed current conductor is placed vertically to the MDL. The search coil is now the sensing area, and a permanent magnet is on top of the search coil as the sensing core. Another permanent magnet is positioned at the PO, in order to maximize the detected response. This operation runs as follows: the MDL is excited by the pulsed current and the caused acoustic stress propagates in the MDL. It can be detected as a pulsed voltage induced at the search coil.

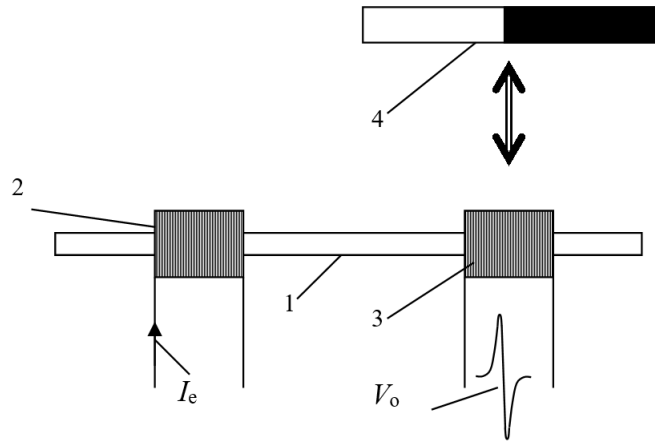


**Figure 5.3.** Moving magnet on top of the search coil changes permeability and flux at the measurement region. (1) MDL, (2) Excitation coil, (3) Search coil, (4) Moving magnet.

The magnitude of this pulse is dependent on the distance of the sensing core (the permanent magnet on top of the search coil) from the MDL. The closer to the delay line the magnet is the greater the magnitude of DC field is in the MDL at the sensing point. This dependence may also be monotonic provided that an offset biasing field at the sensing region is used as in the case of Figure 5.1.

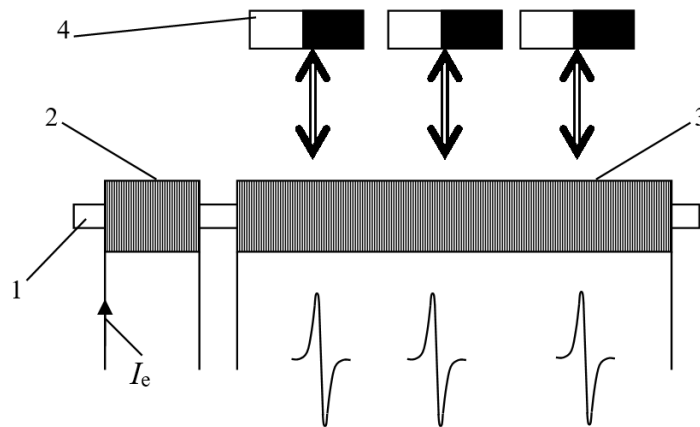


**Figure 5.4.** Distribution displacement sensor based on the sensing element of Figure 5.2. (1) MDL, (2) Array of pulsed current conductors, (3) Search coil, (4) Array of moving magnets.

A movable magnet displacement distribution sensor based on the DC bias effect at the search coil is shown in Figure 5.4. The same pulsed current conductor is used, set vertically to the MDL. A long coil is around the MDL, serving as search coil, and an array of movable, small field magnets is on top of the long coil, defining the sensing points of the integrated array. These magnets are now the moving displacement

sensing cores. The way to set-up this array is the same as for the sensor of Figure 5.2. The same small field magnet is also positioned at the PO, in order to maximize the detected response. This operation of the distribution sensor is as follows: the MDL is excited by the pulsed current and the caused acoustic stress propagates in the MDL. It can be detected as a train of pulsed voltages, out of the long coil. These pulses are caused at the sensing points due to the presence of the magnets. The magnitude of these pulses is dependent on the distance of the magnets from the MDL. The closer the magnet is to the delay line, the greater the magnitude of DC field is in the MDL at the sensing point. A monotonic response of the sensor can be also obtained by using the technique described above. The displacement of the small field magnets with respect to the MDL and the corresponding peak amplitude of  $V_o$  are the input and output of these types of displacement distribution sensors or sensor arrays.

Having discussed the dependence of  $V_o$  on the DC bias magnetic field at the PO and the receiving coil and using this information as a guide to understand the response of the sensors presented in this section, the dependence of  $V_o$  on the displacement of the moving magnet for the two types of sensors is given next. The experimental arrangements for getting the response of the first and second type of these sensors, corresponding to PO and search coil sensing areas respectively. The uncertainty of the micrometer calibrator was 1  $\mu\text{m}$ . The closest distance between the receiving coil and the magnet was offset to zero. A 5 cm long plastic support was used for attaching the magnet on the micrometer, in order to avoid any effect due to the presence of a ferromagnetic material, such as the steel bar of the micrometer.

The response of the sensors of Figures 5.1 and 5.3 has been realized for many different kinds of magnetostrictive elements serving as MDLs. Indicative results are shown hereinafter concerning amorphous Fe-rich ribbons and wires, which present the best performance for this type of MDL sensor. As an example, the dependence of as-cast amorphous  $\text{Fe}_{78}\text{Si}_7\text{B}_{15}$  ribbons MDLs on the magnet displacement is illustrated in Figures 5.5 and 5.6 respectively. Experimental data were obtained by increasing and decreasing the distance between the moving magnet and the MDL. The resulting curves were identical so that the hysteresis factor is negligible for these types of sensors, within the limits of the used experimental facilities. The response of these sensors was monotonic, for displacements up to 15 or 20 mm. The uncertainty of measurements was 2  $\mu\text{m}$  and it is believed that the use of a better calibration device can further improve the sensor uncertainty.

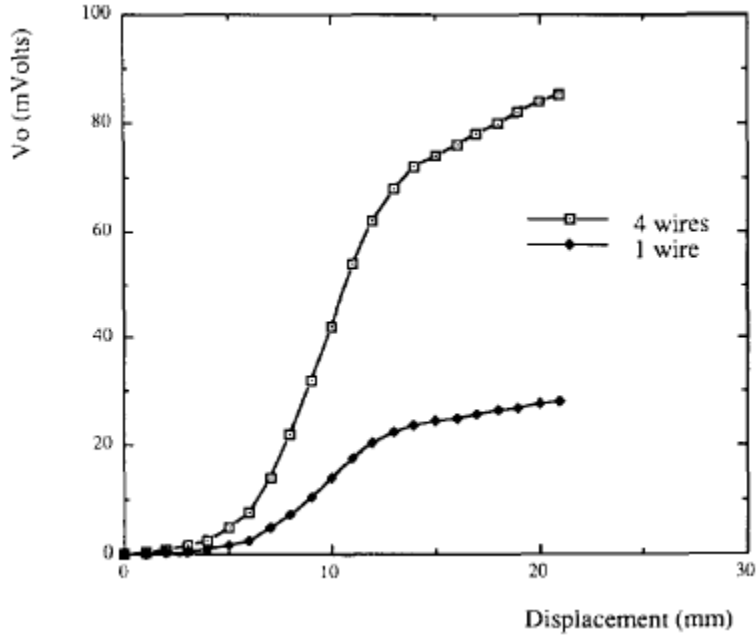


**Figure 5.5.** Response of the sensor of Figure 4.1 using as-cast amorphous  $\text{Fe}_{78}\text{Si}_7\text{B}_{15}$  ribbons.

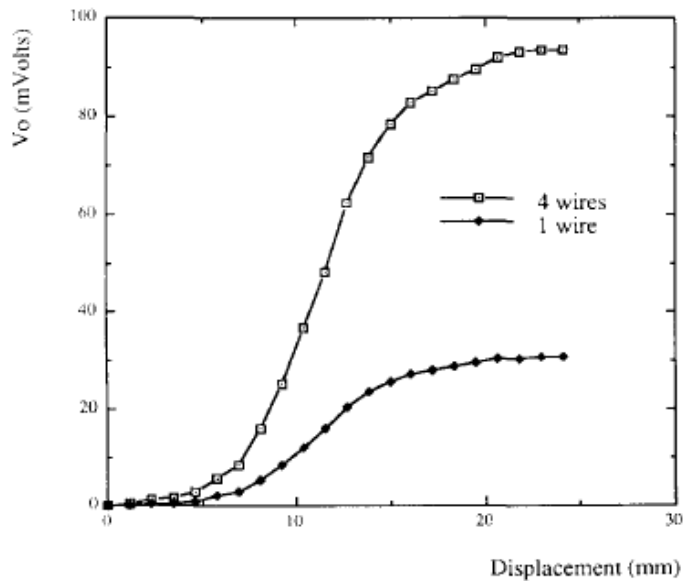


**Figure 5.6.** Response of the sensor of Figure 4.3 using as-cast amorphous  $\text{Fe}_{78}\text{Si}_7\text{B}_{15}$  ribbons.

The use of the amorphous FeSiB wires results in a more sensitive performance of these sensors, provided that the problem of the Large Barkhausen jump has been solved, in order to obtain a continuous dependence of  $V_o$  on magnet displacement. Such a problem is easily solved by the use of an offset magnet. Their better sensitivity and magnetoelastic uniformity compared to the properties of the amorphous

ribbons make them more attractive for this type of position sensors. Experiments showed that 125  $\mu\text{m}$  diameter  $\text{Fe}_{78}\text{Si}_7\text{B}_{15}$  wires showed 90% higher sensitivity than 2 mm wide and 25  $\mu\text{m}$  thick amorphous  $\text{Fe}_{78}\text{Si}_7\text{B}_{15}$  ribbons and 16 times better sensitivity than polycrystalline Fe and Ni wires.

These sensors can serve as distribution sensors, provided that magnetoelastic uniformity has been achieved and sensing points are far enough to ensure discrete MDL pulsed voltage outputs (MDL resolution properties). Such a typical monotonic and unhysteretic response is based on the magnetoelastic properties of the Fe-rich amorphous ribbon and wires and can be repeatable for these types of magnetostrictive materials.

The resolution for these types of sensors is up to  $80 \times 80 \text{ mm}^2$  and  $20 \times 20 \text{ mm}^2$  for the sensors of Figure 5.2 and 5.4 respectively. On the other hand, another array of delay lines-long coils can be used, positioned vertical to the first one, thus increasing the array sensor resolution. Obviously, the same pulsed current conductor can be used, turned 90 degrees in order to excite the second array of lines.

But, other types of MDLs, such as Fe-Co-Si-B or Fe-Co-Cr-Si-B ribbons or wires with relatively smaller magnetostriction constants may not illustrate a monotonic response. As an example, the response of Figures 5.7 and 5.8 is not monotonic, although unhysteretic. Thus, such a type of material cannot offer a proper moving magnet position measurement.

A technological advantage of these types of sensors is that the number of the required soldering connections has been reduced down to a number of the order of the delay line number. For the moving magnet sensors soldering connections are needed only for the existing pulsed current conductors (which is just one in the case of the long receiving coil sensor). So, with respect to the possible use of the FeSiB wires (easily achievable long substrates for the long coil), the cost of the transducers could be significantly reduced.

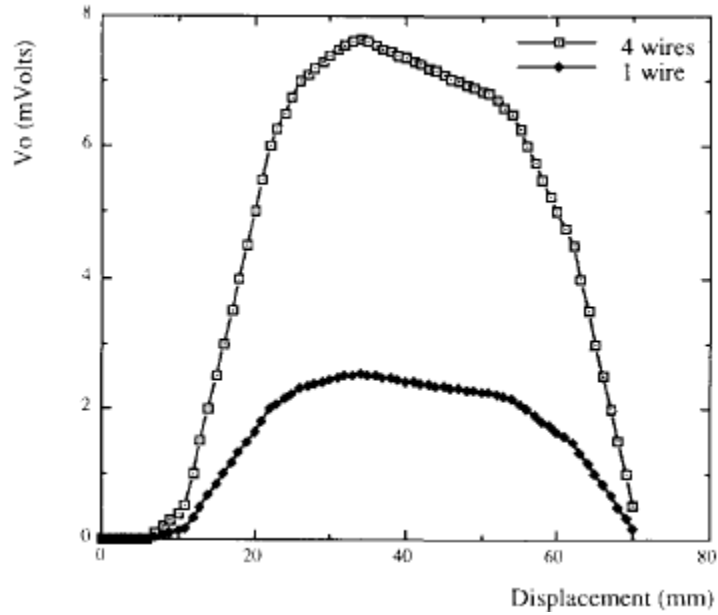


**Figure 5.7.** Response of the sensor of Figure 4.1 using FeCoCrSiB wire as MDL.

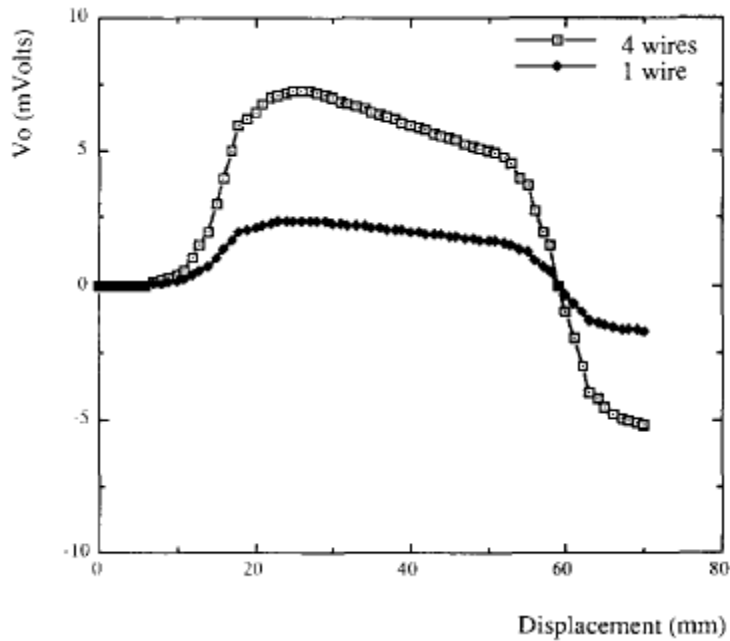


**Figure 5.8.** Response of the sensor of Figure 4.3 using FeCoCrSiB wire as MDL.

The first kind of this family of sensors can be easily manufactured. The manufacturing process could be divided into two parts, the one being the development of the MDL support, and the other developing the sensing core arrays. This can be done by using a movable mat (foam) and flexible arrays of magnets. Thus, using PCB technology, an order of one thousand discrete sensors per day or 100 distribution sensors,

having a matrix of 100x100 elements, can be feasible. Manufacturing the second kind of this family, the most important problem is the structure of the long receiving coils, requiring a special winding machine to manufacture them. We have developed such a winding machine and the speed of manufacturing long coil cannot be better than 100 meters per day. In fact the practical market of these sensors is laboratory or industrial dilatometers.

Furthermore, this type of sensor may well be a 3-dimensional digitizer, measuring the precise point of the sensing core, by using two MDL outputs of the four corresponding neighbouring microstrain points of origin and performing extrapolation techniques.

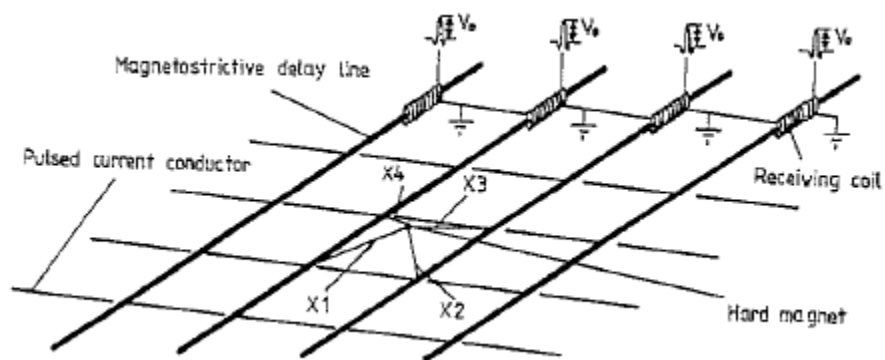


**Figure 5.9.** A 3-dimensional digitizer based on the sensor of Figure 4.1.

---

### 5.1.2 Sensors based on MDL delay time response measurement

---

Results on the characteristics of three position sensors based on magnetic delay line techniques are illustrated in this paper. These sensors are based on the linear motion of coils or magnets along the length of a magnetic delay line. The uncertainty of the first sensor has been improved up to 40  $\mu\text{m}$  per meter by applying bias field along its length, while the second cordless sensor has the worst accuracy of 100  $\mu\text{m}$  per meter.

The sensitivity of the third position sensor has been determined to be better than 10  $\mu\text{m}$ , provided that it is firmly shielded against ambient magnetic fields. The simplicity of these arrangements makes them interesting for industrial applications, where corded or cordless linear motion position sensors of relatively low cost are required. A basic principle of operation is illustrated in Figure 5.10.

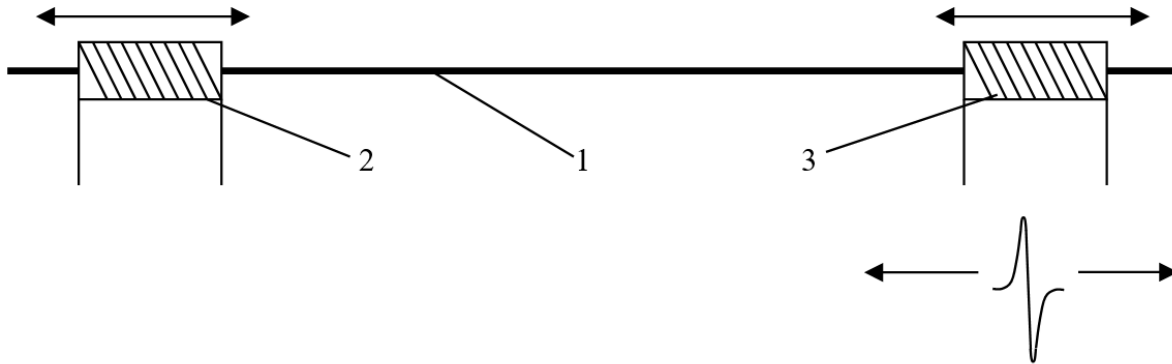


**Figure 5.10.** Moving either the excitation or the search coil results in a change of the MDL voltage output delay time. (1) MDL, (2) Excitation coil, (3) Search coil.

According to this arrangement, a magnetostrictive material is used as magnetostrictive delay line (MDL) in the form of a long ribbon or wire. This material is preferably an amorphous alloy and especially an amorphous wire due to the high degree of magnetomechanical coupling factor.

It also offers a high degree of repeatability of magnetoelastic properties. An exciting coil set around the MDL is used for transmitting pulsed current  $I_e$  and consequently generating a pulsed microstrain due to the magnetostriction effect, split up into two parts travelling along the MDL as pulsed acoustic waves.

The travelling acoustic waves generate a change of the magnetic flux at the corresponding regions of the MDL, due to the inverse magnetostriction effect. Such a flux change can be detected by a receiving coil set around the MDL, which can transduce the magnetic flux change along the MDL within its region into a pulsed voltage output.

The time delay between the exciting pulsed current  $I_e$  and the pulsed voltage output is proportional to the ratio of the distance between the two coils and the longitudinal sound velocity of the material used, assuming that such a velocity remains constant. Hence, having fixed in position one of the two coils and being able to move the other one, a position sensor can be realized, utilizing the position of the moving coil and the time delay between the exciting and detected signal as sensor input and output respectively.

---

### 5.1.3 Long coil position sensor

---

The first position sensor is illustrated in Figure 5.11a. In this case a long excitation coil is used for transmitting pulsed current and consequently pulsed field along the MDL. Assuming that the magnetostrictive alloy used is magnetoelastically uniform, pulsed microstrain due to the magnetostriction effect is generated only at the region of the material within the ends of the exciting coil.

Such an elastic pulse can be detected by a receiving coil as described in the previous arrangement. Setting a hard magnet along the exciting coil, preferably in the form of a ring, the symmetry of the pulsed microstrains breaks due to the additional biasing field caused by the magnet and a third pulsed microstrain between the above mentioned two microstrains is generated, also detected by the receiving coil as a pulsed voltage output. The delay time of this signal from the two other pulsed voltage outputs is the indication of the position of the magnet with respect to the two ends of the long exciting coil.

Thus, a position sensor can be realized, using the position of the magnet along the exciting coil and the output voltage of the receiving coil as input and output respectively. Experiments indicated that, for many magnetostrictive materials, it is better to use the long coil as search coil and another short coil or a conductor orthogonal to the MDL as the excitation means in terms of repeatability and continuity of the MDL pulse voltage output dependence on the motion of the moving magnet along the MDL.

In this case the sensing core is also the moving magnet and the effect used for sensing is the inverse magnetostriction effect. This arrangement can practically have the schematic depicted in Figure 5.11b, where the excitation coil causes currents in the short circuited long coil, the output of which determines the position of the moving permanent magnet due to the delay time at the search coil.

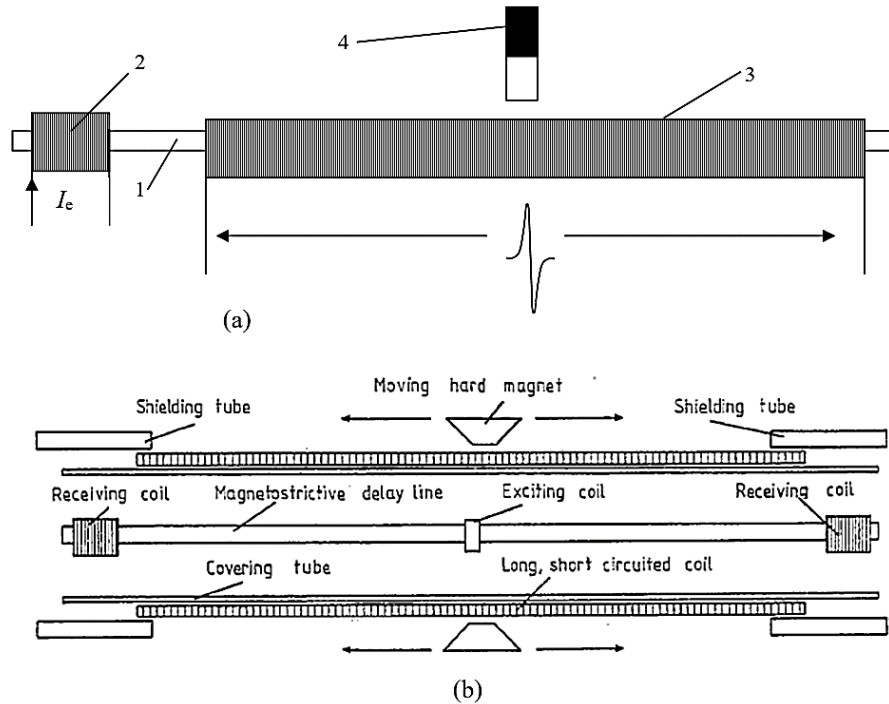


**Figure 5.11.** Moving magnet position sensor based on the delay time of the MDL output due to the displacement of the magnet along the long search coil. (a) the schematic operation, (b) a rather industrial schematic, representing the sensor structure. (1) MDL, (2) Excitation coil, (3) Search coil, (4) Moving permanent magnet.

The above described sensor have been tested against a calibrated optic bar position sensor secondary standard from Mitutoyo Ltd, with a sensitivity equal to  $1\ \mu\text{m}$  and an accuracy equal to  $6\ \mu\text{m}$  per m. Among various tested magnetostrictive materials, indicative results are hereinafter presented concerning  $\text{Fe}_{78}\text{Si}_7\text{B}_{15}$  amorphous wire after stress relief process in  $300\ ^\circ\text{C}$  for 1 hour. The response of the sensor is defined as the dependence of the detected delay time on the position of the moving magnet on top of the long coil. The typical response of this sensor ought to be just linear, except of cases where sound velocity could be modified due to the presence of magnetic anomaly. The measurement uncertainty has been determined to be  $100\ \mu\text{m}$  up to  $40\ \mu\text{m}$  per meter for the case of the long coil serving as excitation and search means respectively, while, in unchanged magnetic conditions and absent ambient field, the uncertainty reaches the levels of  $10\ \mu\text{m}$  per meter for the long coil serving as search coil.

The difference in uncertainty can be explained by the Large Barkhausen jump initiating unexpected noise and discontinuous MDL response, when the long coil is used as excitation means. Such a Barkhausen noise vanishes in the inverse magnetostriction effect after using offset magnet and therefore when the long coil is used as search means. An interesting combination of delay time and voltage MDL output measurement

is illustrated in Figure 5.12. The sensing element (1) is a magnetostrictive delay line (MDL) in the form of ribbon or fibre. A short excitation coil (2) is set around the one end of the MDL and an array of short, single layer coils (3), connected in series and named hereinafter “search coils”, is spread around the MDL along its length, used as the sensor output. A moving hard magnet (4), able to be displaced parallel to the sensing material, is the active core of the sensor. Without any loss of the generality, in this specific application the moving magnet was the end part of the hydraulic piston, having a magnetic pole orientation parallel to the length of the MDL. It is mentioned that the magnetic pole orientation of the active core of the sensor can be also vertical to the MDL, as it can be seen from the description of the operation of the sensor.

The serial output of the search coils is driven to an Application Specific Circuit – ASC (5), including the analogue and digital electronics for sensor excitation, signal conditioning and data acquisition & processing. The analogue part of the ASC includes the pulsed current circuit for the sensor excitation (6) and the amplification circuit of the output voltage pulse train (7). The digital part includes a digital oscillator/counter (8) for delay time detection, a fast analogue to digital converter – ADC (9) for the digitization of the output waveform and a microprocessor based circuit for data acquisition and processing. The data processing concerns the determination of the exact position of the moving magnet. Finally, the velocity and acceleration of the moving magnet can be determined by hardware or software calculation of the first and second derivatives of the moving magnet position. The excitation part of the sensor is packed up together with the ASC at the sensor termination, whereas the excitation coil is covered by a soft magnetic tube, for example permalloy, in order to properly shield the coil against ambient magnetic fields. The length of the sensor can vary by changing the number of search coils, thus allowing a variable sensor length, in a relatively inexpensive production technique.

The sensor operates as follows: Pulsed current of 1  $\mu$ s duration and 1 ms period is transmitted through the excitation coil. Then, the pulsed magnetic field along the length of the MDL generates an elastic pulse, propagating along the MDL length. As the elastic pulse propagates along the length of the MDL, it causes changes of magnetic flux at the intersections of MDL and search coils, thus inducing a voltage pulse train with pulse intervals corresponding to the distance between consequent coils. These voltage pulses are proportional to the ambient field along the axis of the search coils. In the absence of the moving magnet and low ambient field along the array of the short search coils, these voltage pulses are small in amplitude.

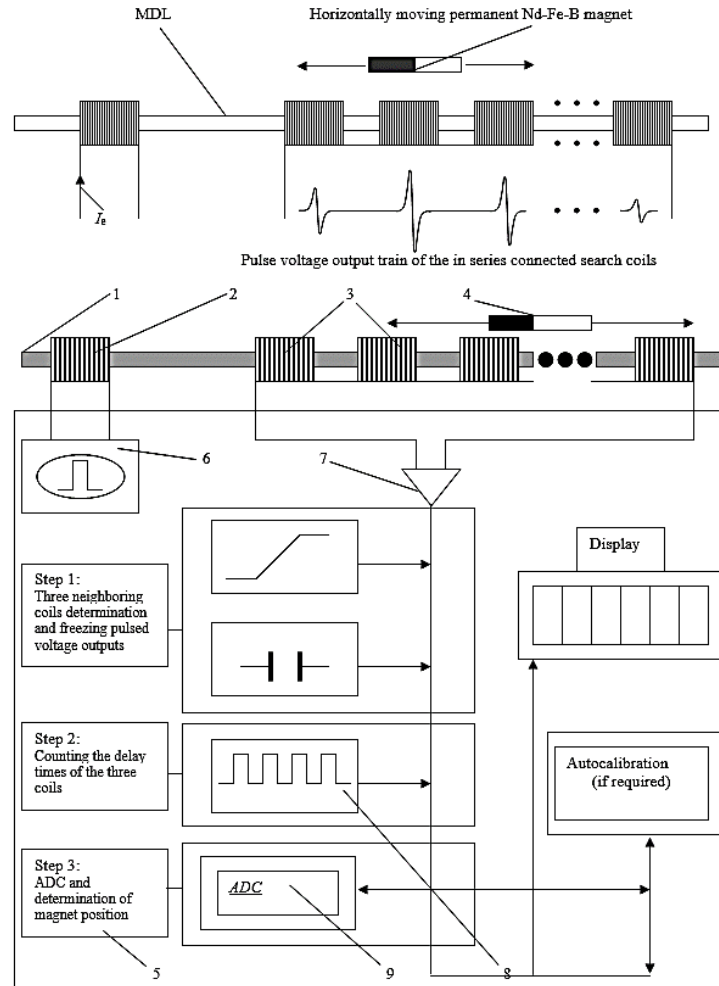


**Figure 5.12.** The position sensor. (1) Magnetostrictive delay line, (2) Excitation coil, (3) Array of search coils, (4) Moving magnet, (5) Application specific circuit, (6) Excitation circuit, (7) Analogue amplifier, (8) Oscillator/counter, (9), Analogue to digital converter.

In the presence of the moving magnet the voltage pulses of the neighbouring coils become larger. The closer the moving magnet is to a coil, the larger the corresponding voltage pulse, following the classical dependence of magnetostriction and inverse magnetostriction on the ambient field. Thus, if the moving magnet core is approaching three consequent receiving coils, the voltage output of these three coils overcomes a preset threshold and indicates that the magnet approaches the vicinity of these coils. Having tailored the magnetostrictive element in a way to retain a uniform and monotonic output response with respect to the ambient field along its length, the amplitude of the voltage pulses can be the indication of the distance of the magnet with respect to the three coils.

An algorithm, which can be used for the determination of the absolute position of the moving magnet, includes three steps. At the first step, a voltage threshold comparator determines and freezes the three consequent pulsed voltage outputs, which overcome a preset threshold. At the second step, an oscillator/counter circuit is used to measure the delay time of these three pulsed voltages, with respect to the excitation signal. Bearing in mind that the two outer pulses ought to be always smaller in amplitude compared to the middle one, it is known that the moving magnet is somewhere between the three coils. At the third step, the three frozen pulsed voltage outputs are measured by using the fast analogue to digital converter and the resulting digital words determine the relative position of the moving magnet with respect to the three coils. Using an EEPROM stored calibration look up table, concerning the dependence of the pulsed voltage output on the magnet displacement for the three pulsed output voltages, results in the determination of the position of the magnet with respect to the excitation coil. The three point measurement and the look up table are also the means for autocalibration procedures. Without such a unique look up table the sensor would not measure position and displacement in real time conditions. The amorphous magnetostrictive ribbons and fibres after proper treatment offered a uniform, sensitive and unhysteretic magnetoelastic performance along the length of the MDL, thus allowing the use of a unique look up table for all the search coils. A typical response of this sensor is illustrated in Figure 5.13, concerning  $\text{Fe}_{78}\text{Si}_7\text{B}_{15}$  amorphous wire as MDL and a small  $\text{Nd}_1\text{Fe}_{12}\text{B}_1$  permanent moving magnet.

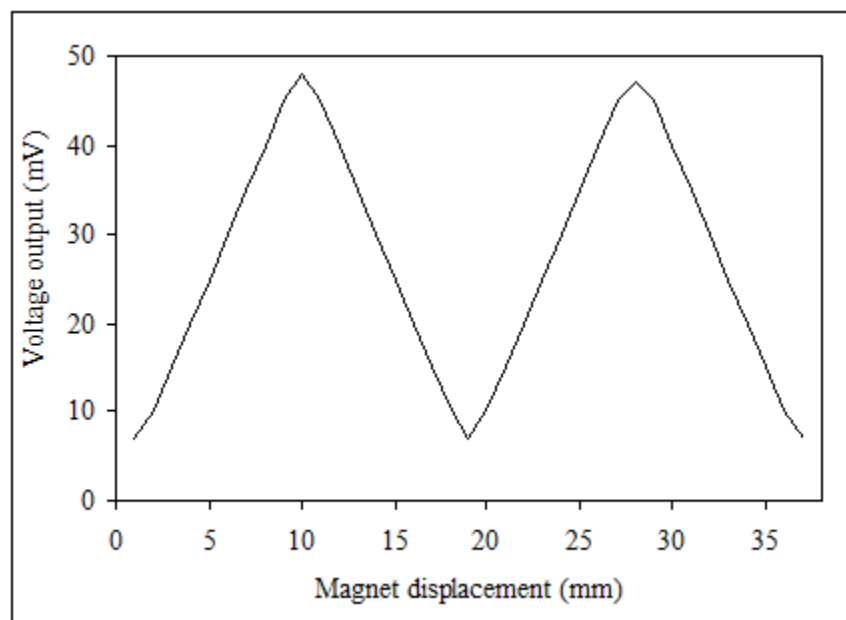


**Figure 5.13.** A typical response of the sensor illustrated in Figure 4.12.

---

### 5.1.4 Circumferential MDL and corresponding position sensor

---

In order to increase the manufacturing scale and the repeatability of properties, the human factor in production ought to be minimized. One way to obtain that is the development of devices able to be produced in automated production lines. In the case of MDLs, the thin film technology is a promising way of obtaining this target. Having the above mentioned targets as a motivation, a magnetoelastic device able to operate as MDL has been conceived. In the following text, the device is described as well as the manufacturing process is analyzed taking into account its microstructure and its ability or disability to operate as a MDL. Finally, the basic MDL characteristics are illustrated and discussed.

The schematic of the magnetoelastic element is illustrated in Figure 5.14. A cylindrical conductor is used as the substrate of an insulating layer which a cylindrical magnetostrictive film is deposited on. Passing pulsed current through the inner conducting wire results in transmitting pulsed circumferential magnetic field at the outer magnetoelastic film. Such a field results in local micro-elongation or stresses due to the magnetostriction effect which, more or less, cancel each other due to the magnetoelastic uniformity of the outer film.

Local break of the magnetic symmetry results in a local break of the symmetry of the dynamic micro-strains, as depicted in Figures 2.23 and 2.24, thus generating an elastic pulse which propagates along the length of the film, provided that such a propagation can take place. The propagating pulse can be received by means of a pulsed voltage output induced at a search coil at the one end of the device, due to the inverse magnetostriction effect. The time position of this pulsed voltage indicates the position of the magnet and its amplitude indicates the amplitude of the local magnetic field non-symmetry. This effect can be caused by a small permanent magnet travelling along the length of the device or a local magnetic field anomaly. Therefore, it can be seen that such a device can be used as a position/displacement sensor. Details of the development of this arrangement have been presented in Chapter 2.

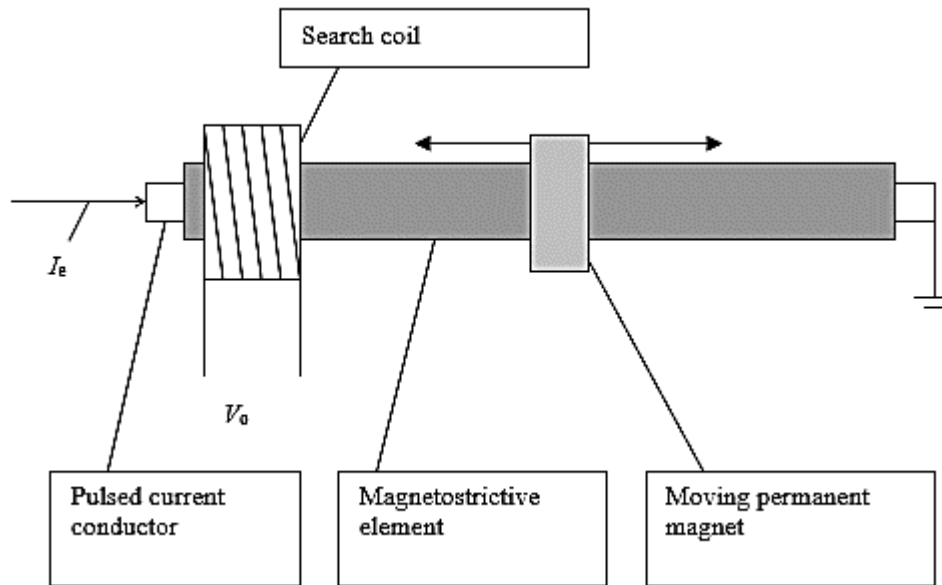


**Figure 5.14.** Circumferential MDL and corresponding delay-time based moving magnet position sensor.

Magnetoelastic measurements were realized after setting a small Nd-Fe-B permanent magnet in the middle of the films, in order to allow an elastic pulse to be generated. Most of the as-cast uncoated and coated films demonstrated poor magnetoelastic measurements. In fact positive magnetostrictive compositions illustrated MDL behaviour in the case of uncoated films, while coated negative magnetostrictive elements illustrated magnetoelastic response even without any treatment. These properties were much improved after heat treatment at 300 °C for 1 hr and consequent magnetic annealing at 300 °C for 1 min and simultaneously passing 15 A pulsed current with 1% duty cycle and 1 ms period, through the inner copper wire. Keeping the biasing field around the sensor stable, the transverse sound velocity may not change and therefore the response of the sensor may be linear.

Due to the relatively low amplitude of the transverse sound velocity in the magnetostrictive ribbons and wires, the set-up may offer an uncertainty of 50  $\mu\text{m}$  per meter within the limits of our experimental set-up, if magnetic conditions are so that no pseudo-longitudinal waves are generated. If such a generation takes place the longitudinal wave may arrive earlier to the search coil, resulting in a false measurement.

---

### 5.1.5 A new type of inexpensive and accurate position sensor

---

Targeting the decrease of the cost of the position sensor, its flexible and easy use, as well as maintaining or even improving the sensor characteristics, namely sensitivity, resolution and uncertainty better than 0.2 mm within a temperature range from -50 °C to 100 °C, linear and unhysteretic response by design and temperature operation range, a position sensor analyzed hereinafter has been conceived and developed.

The position sensor is illustrated in Figure 5.15 and based on the principle illustrated in the MDL arrangement of Figure 2.17. The sensing element (A) comprises of a magnetostrictive ribbon or wire (1), in the shape of an acoustic wave guide. This ribbon or wire is to act as the magnetostrictive delay line (MDL).

A pair of parallel conductors (2) is also set parallel to the MDL in a way to form one level and include the MDL between them. They are used to transmit pulsed current and therefore they are named pulsed current conductors. The two pulsed current wires and the MDL form a flat level, on top of which a soft magnetic ribbon or tape (5), parallel to the set-up of the magnetostrictive element and parallel conductors is set in order to act as a flux concentrator and an eddy current generator. The sensing core is a permanent magnet (7), which is moving parallel to the arrangement of the MDL – pulsed current conductors and soft magnetic material.

In Figure 5.16 the cross section of the sensing arrangement (A) is illustrated. The MDL (1) is surrounded by low density foam (6) holding the MDL in position without attenuating the propagating elastic pulse. The foam is set between the two pulsed current conductors (2) and suppressed by the soft magnetic material (5). Practically this foam may also be air, in order to avoid attenuation of elastic pulses. Insulating plastic film separators (8) may also be used to hold the sensing element in one piece. The movable permanent magnet (7) is outside of the cross section of the sensing arrangement (A), free to move along the length of the MDL. A conducting means (3) is used for the electrical connection of the one side ends of the two pulsed current conductors (2).

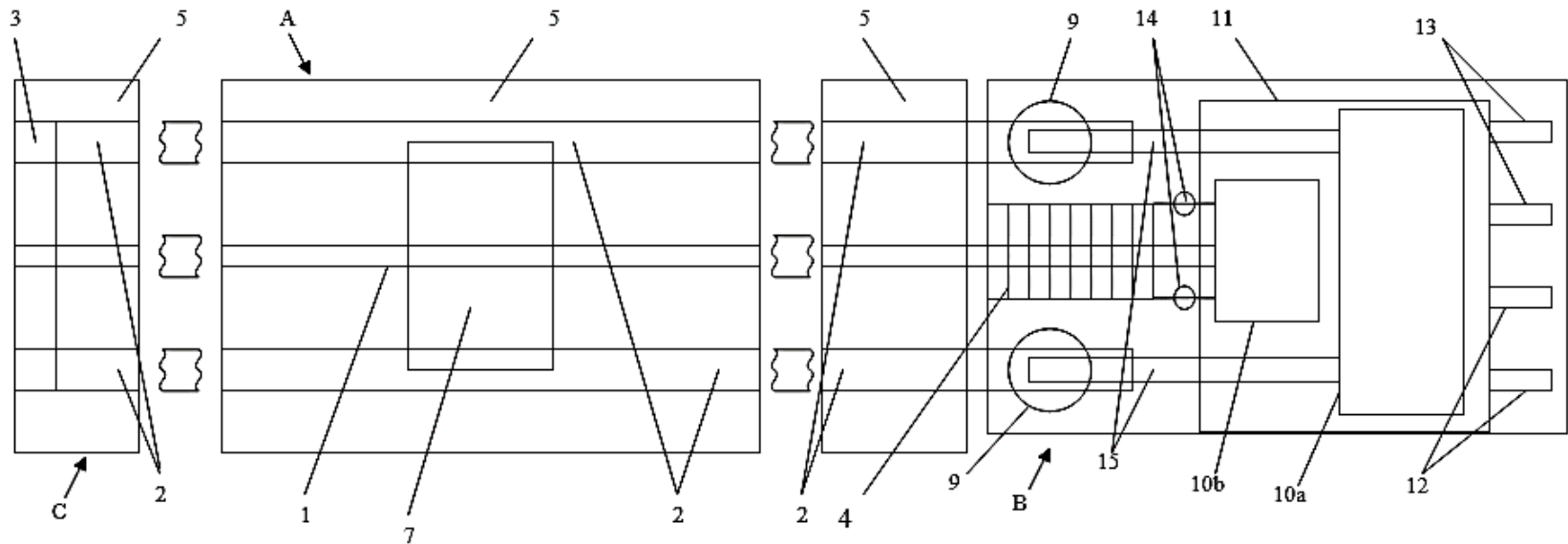


**Figure 5.15.** The schematic of the new position sensor. (1) Magnetostrictive delay line (MDL), (2) Pulsed current conductors, (3) Conducting connector for the pulsed current conductors, (4) Search coil, (5) Soft magnetic material, (7) Movable permanent magnet, (9) Conducting connection for the pulsed current conductor connection on the electronic board, (10a) Electronic pulsed current generation circuit, (10b) Electronic received signal conditioning circuitry, (11) ASIC integrating circuit for (10a) and (10b), (12) DC power supply pins, (13) Pins for the transmission of the conditioned signal out of the sensor, (14) Pins for the delivery of the searched signal from the search coil, (15) Pins for the pulsed current transmission to the pulsed current conductors. (A) Electromechanical part of the position sensor, named sensing element, including the MDL, pulsed current conductors, soft magnetic ribbon and insulating (preferably plastic) film separators, (B), Sensor electronic board including pulsed current conductor connection, search coil, pulsed current generation circuit and received signal conditioning circuitry and (C) Termination of the position sensor, hosting the conducting connector for the pulsed current conductors covering the end of the MDL.

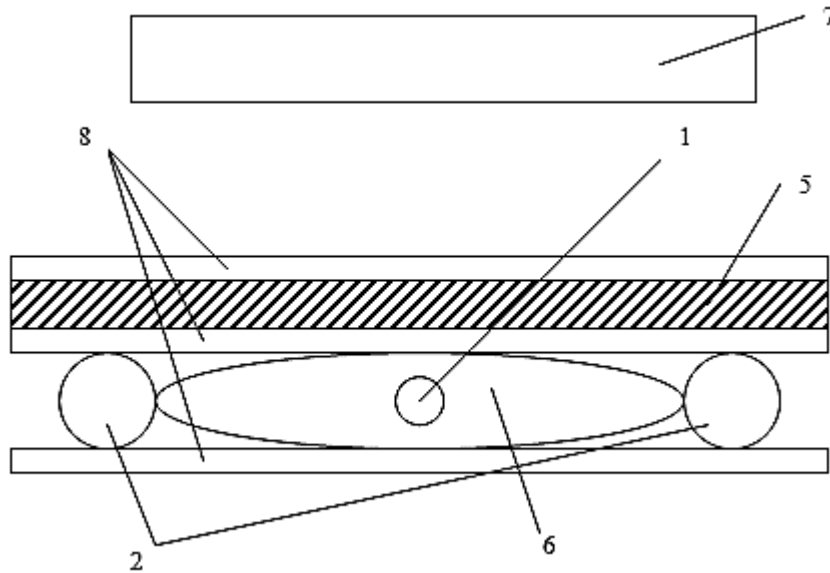


**Figure 5.16.** Cross section of the sensing element including the permanent magnet acting as sensing core. (1) Magnetostrictive delay line (MDL), (2) Pulsed current conductor, (5) Soft magnetic material, (6) Foam holding the MDL in position without attenuating the propagating elastic pulse, (7) Movable permanent magnet, (8), Insulating (plastic) film separator.

The other end of the sensing arrangement (A) is connected to the electronic circuitry (B), which includes the electronic circuitry (10a) for the transmission of pulsed current to the pulsed current conductors (2), the electronic circuit (10b) for the conditioning, digitization and transmission of the output signal and the search coil (4) used for detecting the propagating elastic flux due to the inverse magnetostriction effect. It is connected with the electronic circuit (10b) for the conditioning, digitization and transmission of the output signal. The two electronic circuits (10a) and (10b) may be included in a single chip, which has at least 8 input/output pins. From these, two pins (12) are used for the dc power supply, two pins (15) are used for the pulsed current transmission to the pulsed current conductors (2), two other pins (14) for the delivery of the searched signal from the search coil (4) to the electronic circuit (10b) and two pins (13) for the transmission of the conditioned signal out of the sensor. The electronic circuit includes two pins (9) for the electric connection of the free ends of the pulsed current conductors (2) with the two pulsed current transmission pins (15), as well as two pins for the electrical connection of the two output wires of the search coil to the two pins (14) which are driven to the electronic circuit (10b). The end of the MDL is preferably set inside the search coil (4), to avoid discrete reflections, which may cause undesirable secondary pulsed voltage outputs.

The sensing element operates as follows: Pulsed current is transmitted into the pulsed current conductor, invoking transverse pulsed magnetic field along the magnetostrictive element. Such a transverse pulsed magnetic field cannot generate an elastic pulse into the magnetostrictive element. However, the pulsed current induces eddy currents into the soft magnetic ribbon or tape. In the absence of the moving permanent magnet, they are equally spread into the soft magnetic material, provided that the soft magnetic material is electrically and magnetically uniform.

These eddy currents generate microstrains of the same amplitude along the length of the magnetostrictive element, if it is magnetoelastically uniform. Thus, the microstrains along the MDL cancel each other, apart from the edge of the magnetostrictive element or the soft magnetic material. Hence, two small in amplitude elastic pulses propagate along the MDL and are received by the search coil as two discrete pulses, defining the two terminations of the effective area of the position sensor.

In the presence of the moving permanent magnet, a certain amount of magnetic flux is induced at a given volume of the soft magnetic material. Such a magnetic flux changes the magnetic permeability at this volume and therefore changes the penetration depth of eddy currents at this given volume, which results in a different amplitude of eddy currents in this area of the soft magnetic tape or ribbon with respect to the rest of the body of the soft magnetic material. The difference between the eddy currents at the boundary between the magnetized and the non magnetized volume results in a break of the symmetry of eddy currents. Therefore, a pulsed current is locally generated, inducing a pulsed field along the length of the MDL. Thus, a longitudinal elastic pulse is generated propagating along the magnetostrictive element, which is detected by the search coil as a pulsed voltage.

The pulsed voltage is received with a delay time proportional to the distance between the permanent magnet and the search coil and inversely proportional to the longitudinal sound velocity of the MDL. Moving the position of the permanent magnet, results in a change of the delay time of the pulsed voltage output. Thus, the change of the delay time of the pulsed voltage output is the output of the sensing element, while the displacement of the permanent magnet is its input. The amplitude of the detected pulsed voltage may also inform about the proximity of the permanent magnet to the MDL, provided that the permanent magnet and its outside field distribution is known.

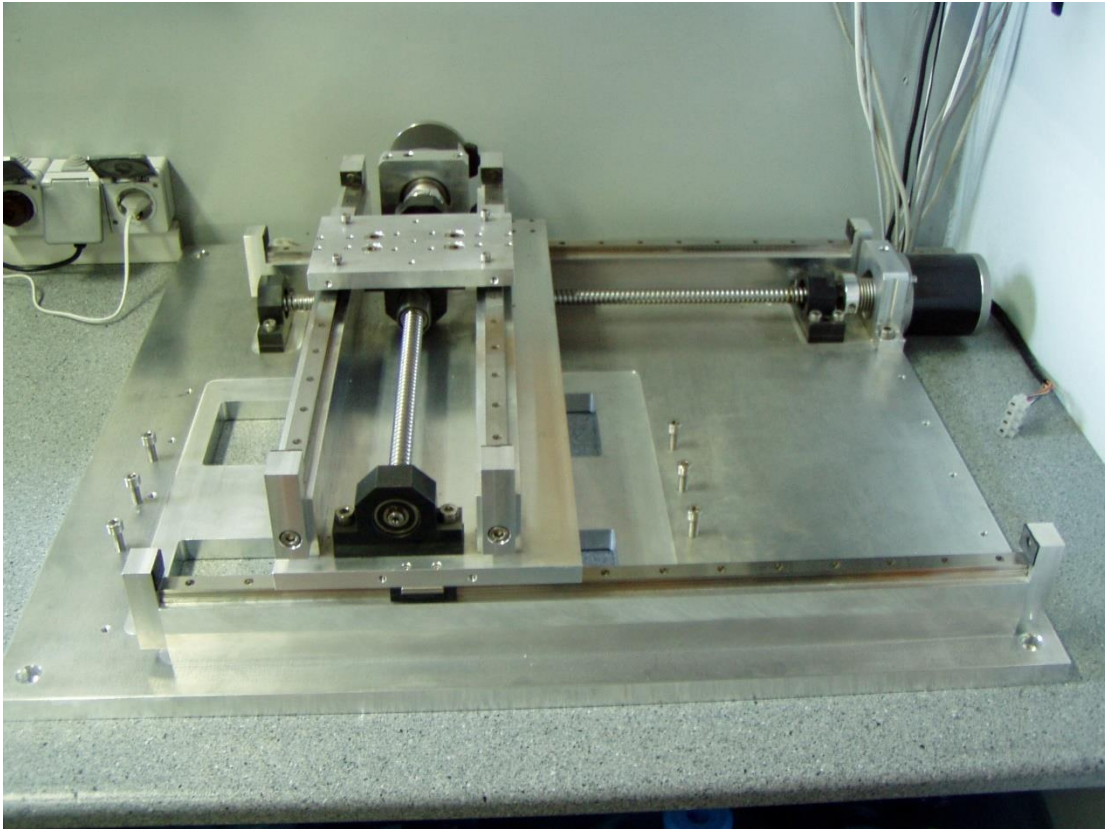


**Figure 5.17.** The set-up used for the determination of most of the developed position sensors.

The experimental set-up used for the determination of the sensor response is illustrated in Figure 5.17. A precision two-dimensional translating table has been constructed, offering mechanical sensitivity of  $5\ \mu\text{m}$ . The active area of the translating table was  $300\ \text{mm} \times 300\ \text{mm}$ . The rotating screws are movable by closed loop dc servo-motors driven by two independent Parker drivers. The drivers are controlled by a PC via a Delphi code. The under characterization sensor was adjustable on the table. A  $30\ \text{cm}$  long coil capable to transmit up to  $80\ \text{kA/m}$  was adjustable around the under test sensor in order to test the parametric effect to ambient magnetic fields. A flexible temperature blanket, consisting of a PC controlled Cr-Ni heater and a flexible heat isolator in the shape of a cylinder, surrounding the above mentioned long coil was used for applying temperature up to  $100^\circ\text{C}$ .

The sensitivity in temperature stability was better than  $0.1^\circ\text{C}$ . These two parameters, namely the ambient field and the temperature are the two most critical parameters in the sensor response. Therefore, the sensor characterization was realized taking into account these parameters. The sensing core was a

10mmX10mmX3mm Nd<sub>2</sub>Fe<sub>17</sub>B<sub>1</sub> permanent magnet, set at a 200 mm distance from the sensor, adjusted on the top moving table. Hence, the changing magnetic field along the length of the sensor was of the order of 300-400 A/m, thus simulating one of the worst situations of moving magnet position sensing, due to the very small changing field. A linear optical encoder has been used to measure the “near-true” value of the position of the top moving table. The certified sensitivity and uncertainty of the optical sensor was 1 μm and 10 μm/m respectively.

The electromechanical part of the sensor was realized, for practical reasons, by using an extruder with 1 m/s output speed ability producing a 5mmX0.7mm orthogonal cross section area assembly. In the middle of this cross section, a magnetostrictive wire of diameter less than 150 μm was set, surrounded by enameled Cu pair conductors of 250 μm diameter, parallel to the MDL. The distance between the pulsed current conductors was adjusted to 4 mm. The length of the sensor was adjusted to 20 cm.

Several types of magnetostrictive wires have been used as MDLs. The most sensitive of them were the amorphous Fe<sub>78</sub>Si<sub>7</sub>B<sub>15</sub> wires of 125 μm diameter and conventional polycrystalline Fe wires of 125 μm diameter. All wires have been tested in the as-cast form, after thermal annealing in 350°C for 1 hr in Ar atmosphere and after magnetic annealing in 8 kA/m and 350°C for 1 hr in Ar atmosphere. On top of the cross section assembly magnetic ribbons with low magnetostriction values have been glued, namely Fe<sub>74</sub>Co<sub>4</sub>Si<sub>7</sub>B<sub>15</sub> amorphous and Ni<sub>3</sub>Fe polycrystalline ribbons after transverse magnetic annealing in 8 kA/m and 350°C for 1 hr in Ar atmosphere. The electronic circuit of the sensor consisted of a discrete MOSFET current amplifier circuit used for pulsed current generation and excitation of the sensing element, as well as a voltage pre-amplifier. The reading of the peak pulsed voltage output time delay was realized by a PC controlled 12-bit flash A to D converter.

The experimental results exhibited significant differences between the different MDL wires and soft magnetic ribbons. In all cases, the dependence of the position of the moving permanent magnet with respect to the time delay measurement of the position sensor was an almost linear dependence of time. The major difference was the sensitivity in the voltage output allowing the relatively easier or more difficult detection of the delay time. It was observed that annealing and magnetic annealing improves the sensitivity of the sensor response for both wires. But it also resulted in the appearance of the hysteresis effect. The hysteresis effect increases and becomes un-predictable in the case of the magnetically annealed samples, when the sensor is subject to ambient fields. Covering the whole sensor by a metal cylinder, the field effect dependence almost disappeared for the case of both types of as-cast wires,

although the sensitivity was decreased, as shown in Figure 5.18. This effect was due to the non-linear dependence of the longitudinal sound velocity of the annealed samples on the ambient field.

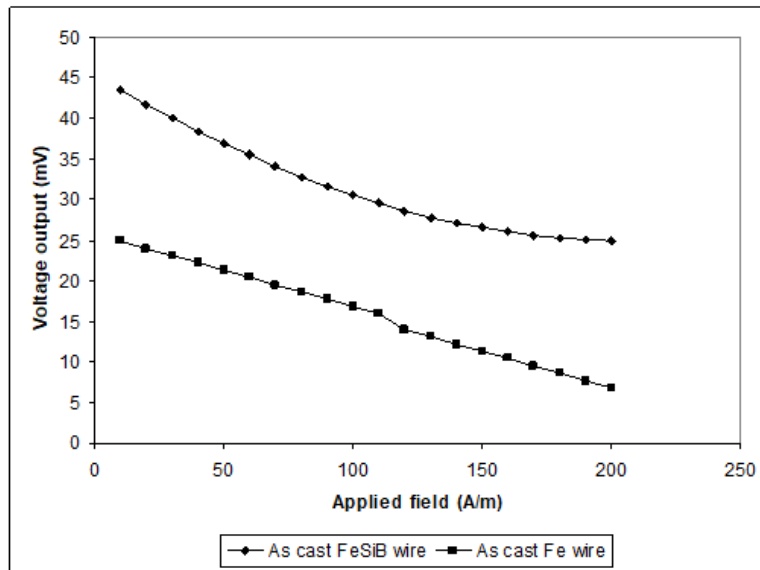


**Figure 5.18.** Field dependence of the sensor using amorphous FeSiB and Fe crystalline wires.

The temperature effect on the response of the different wires and ribbons is illustrated in Figures 5.19 and 5.20, concerning the amorphous  $\text{Fe}_{78}\text{Si}_7\text{B}_{15}$  and polycrystalline Fe wires. The temperature dependence is similar in all types of treatment of the wires. All these data also illustrate that the response of  $\text{Ni}_3\text{Fe}$  polycrystalline ribbons was more sensitive than that of the  $\text{Fe}_{74}\text{Co}_4\text{Si}_7\text{B}_{15}$  amorphous ribbons. The jittering effect of the electronic circuit was responsible for an additional increase of the total sensitivity by  $\sim 1 \mu\text{m}$ . Figure 5.21, illustrates the best achieved uncertainty, in the case of an as-cast amorphous  $\text{Fe}_{78}\text{Si}_7\text{B}_{15}$  wire, tested with magnetically annealed  $\text{Ni}_3\text{Fe}$  polycrystalline ribbon, achieving less than  $10 \mu\text{m}$  uncertainty. It is mentioned that the levels of uncertainty of polycrystalline Fe wire MDLs, tested with  $\text{Fe}_{74}\text{Co}_4\text{Si}_7\text{B}_{15}$  amorphous ribbons was not worse than  $25 \mu\text{m}$ .

The conclusions of these measurements were that use of amorphous Fe-rich wires in the as-cast form with magnetically annealed  $\text{Ni}_3\text{Fe}$  polycrystalline ribbons offers the best sensitivity, although inexpensive, commercially available polycrystalline Fe wires used as MDLs, accompanied by  $\sim 0$  magnetostriction amorphous FeCoSiB ribbons, offer a quite acceptable uncertainty of  $25 \mu\text{m}$ . Any change of the dimensions of the cross section of the sensor results in change of its response. Thus, the parametric control of the

geometry of the cross section of the sensing element and the composition of the MDL and the soft magnetic material results in different sensor applications, with respect to the strength of the moving permanent magnet as well as its distance from the sensor.

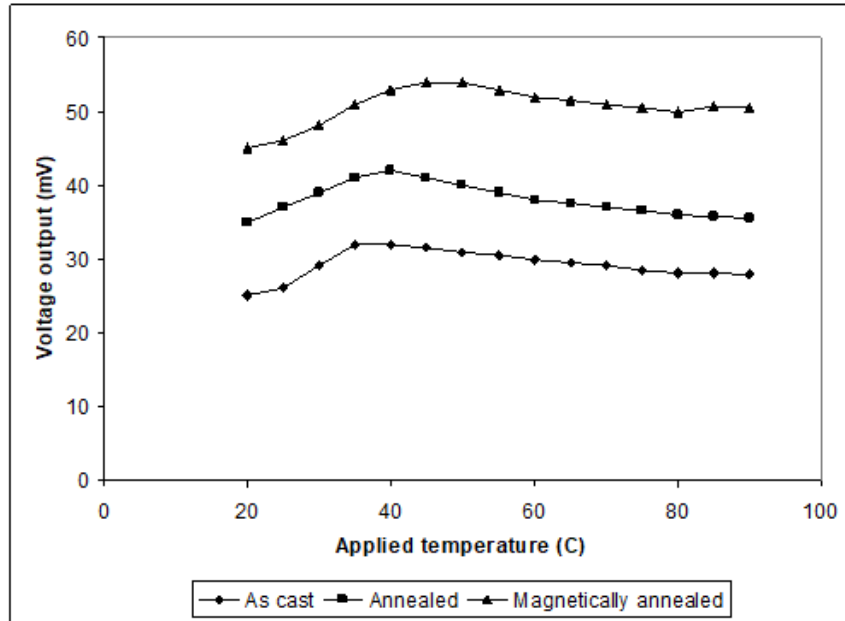


**Figure 5.19.** Sensor voltage output dependence on temperature concerning amorphous  $\text{Fe}_{78}\text{Si}_7\text{B}_{15}$  MDL and  $\text{Ni}_3\text{Fe}$  polycrystalline ribbon.

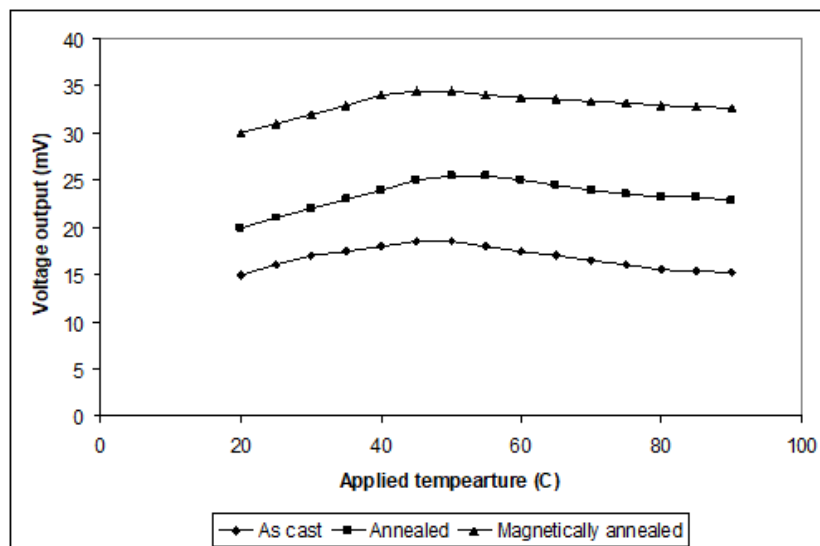


**Figure 5.20.** Sensor voltage output dependence on temperature concerning polycrystalline Fe MDL and  $\text{Ni}_3\text{Fe}$  polycrystalline ribbon.

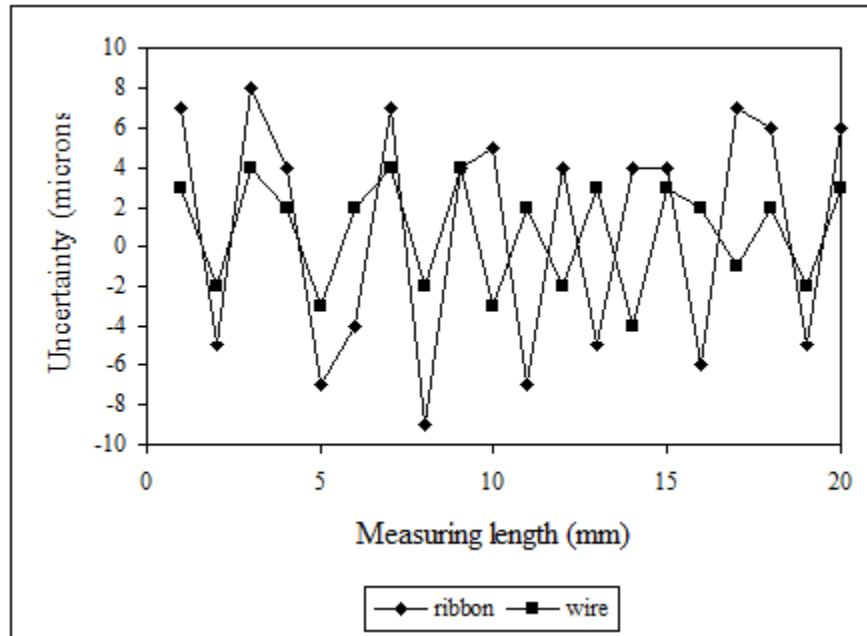


**Figure 5.21.** Uncertainty measurement of the position sensor using as-cast amorphous  $\text{Fe}_{78}\text{Si}_7\text{B}_{15}$  wire and magnetically annealed  $\text{Ni}_3\text{Fe}$  polycrystalline ribbon.

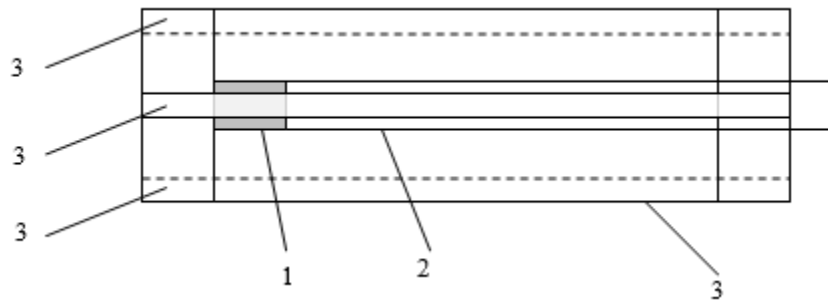


**Figure 5.22.** Application of the sensor in measuring position, velocity and acceleration of a moving pneumatic piston, with respect to a steady position sensor. (1) Moving permanent magnet at the end of the moving piston, (2) Moving piston, (3) Groove able to hold the sensor and the electronic board.

The above mentioned sensing element can be used as a position and displacement sensor in pneumatic devices, provided that the pneumatic device has a permanent magnet at the end of its the piston. In Figure 5.22, the application of the position sensor for the measurement of the position, velocity and acceleration of a moving pneumatic piston assembly is illustrated. The position sensing element can be fixed in position in one of the grooves (3), illustrated as channels on the surface of the cover of the moving piston (2). The

grooves (3) are also capable to keep in position the sensor electronic board of the position sensor, at the one end of the pneumatic piston.

The moving piston (2) also carries the moving permanent magnet (1) at the end of the moving piston. Experimental results with commonly available amorphous or polycrystalline magnetostrictive wires used as MDLs and commonly available Ni<sub>3</sub>Fe zero magnetostriction soft magnetic ribbons, illustrated a repeatable response in various sizes of permanent magnets and different distances between permanent magnet and soft magnetic material. Thus, a given arrangement of a magnetostrictive material and a soft magnetostrictive material, results in a repeatable and unhysteretic response for different types of pneumatic devices and pistons. Experimental results using the above mentioned magnetostrictive and soft magnetic material show an increase of the sensor sensitivity with the magnetic softness of the soft magnetic material. The best observed sensitivity corresponded to an almost zero magnetostriction Ni<sub>3</sub>Fe ribbon after magnetic annealing, resulting in a repeatability of 10 μm.

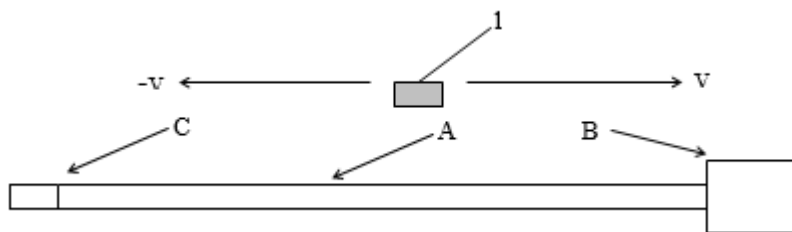


**Figure 5.23.** Application of the sensor in measuring the absolute ground velocity of a moving magnetic body, with respect to a steady position sensor. (1) Moving magnetic body parallel to the position sensor with velocity  $v$ , which is measured by the position sensor. (A) Position sensing element, (B) Sensor electronic board.

The position sensor can also be used for absolute ground velocity vehicle measurement. In Figure 5.23, the application of the sensor in measuring the absolute ground velocity of a moving magnetic body, with respect to a steady position sensor is illustrated. According to this arrangement, the position sensing element (A) as illustrated in Figure 5.15 together with the sensor electronic board (B) and terminal (C) are fixed in position.

A moving magnetic body (1) parallel to the position sensor travels with velocity  $v$ , being measurable by the position sensor. A similar set-up may also serve for the measurement of the velocity of a plurality of vehicles passing at the same time from the position of the sensing element, provided that a plurality of sensors is also used.

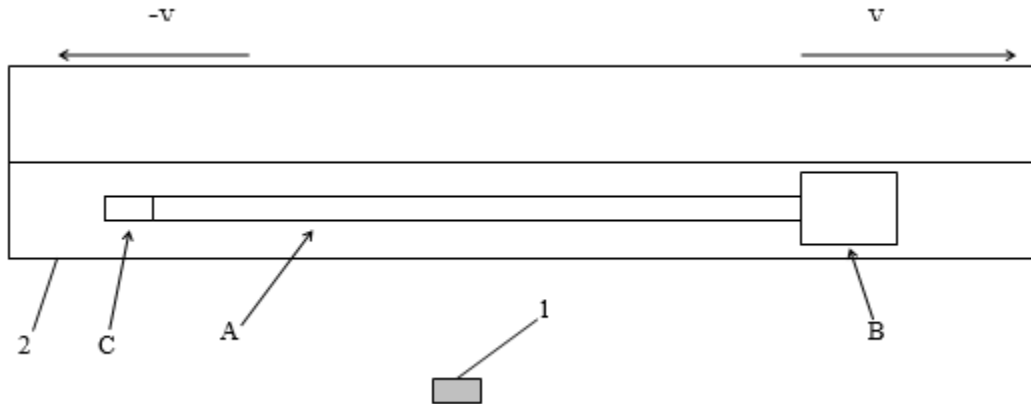


**Figure 5.24.** Application of the sensor in measuring the absolute ground velocity of a moving object with respect to a not moving permanent magnet. (1) Permanent magnet fixed in position, (2) Moving object parallel to the permanent magnet fixed in position with velocity  $v$ , carrying the position sensing element (A) and its electronics (B).

In Figure 5.24, the application of the sensor in measuring the absolute ground velocity of a moving object with respect to a not moving permanent magnet is illustrated. This sensor can be used for driverless driving of vehicles. According to this set-up, a moving object (2) with velocity  $v$  carries the position sensing element (A) and its electronics (B). Velocity  $v$  is to be measured by the position sensor. For this purpose, a permanent magnet (1) fixed in position is used. The dynamic motion of the permanent magnet can be determined by such a sensor, thus monitoring the velocity and acceleration of the permanent magnet. The detection can be realized by a proper electronic circuit. The limits of the velocity correspond to the speed of refreshing the readout signal of the magnetic flux receiver. The speed is related to the period of the pulsed current, the longitudinal sound velocity of the magnetostrictive material and the length of the sensor. Using a sensor of 1 m long, a pulsed current period equal to 1 microsecond and a longitudinal sound velocity of 5 mm/ $\mu$ s the maximum measurable velocity is 100 mm/sec. Consequently, the sensor can measure the acceleration of the motion as the first derivative of the velocity. The limits of the acceleration range measurement depend on the velocity range measurement and the period of the excitation pulsed current. Thus, the sensing element can detect the absolute ground velocity of a vehicle due to the magnetization of the vehicle caused by the ferromagnetic elements of various parts of it, mainly parts of the engine. The velocity of other vehicles may also be detected.

The sensing element can be also used to detect the level of liquids, provided that there is a permanent magnet on top of the under measurement liquid, which gives the input to the sensing element. In Figure

5.25, the application of the sensor in measuring liquid level is illustrated. Accordingly, the position sensing element (A), as illustrated in Figure 5.15, is set perpendicular in the liquid tank (2), with the sensor electronic board (B) and the sensor termination (C) at its end. The surface of the liquid level of the tank (3) allows a floater (4) on top of the liquid and movable parallel to the position sensing element (A) to stay on the liquid surface. Then, a permanent magnet on top of liquid (1) acts as sensing core.

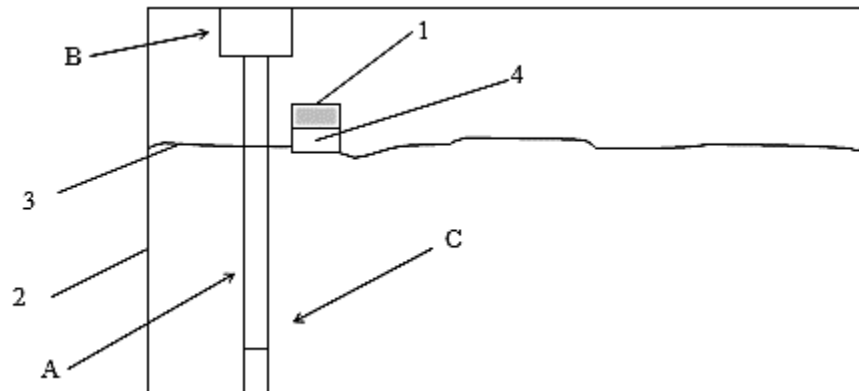


**Figure 5.25.** Application of the sensor in measuring liquid level. (1) Permanent magnet on top of liquid, (2) Tank with liquid, (3) Surface of liquid of the tank, (4) Floater on top of liquid. (A) Position sensing element.

The sensing arrangement (A) can be manufactured by many techniques, but the hereinafter presented principles of production illustrate the basic procedures of one of the least expensive methods of production, offering a robust sensor with repeatable characteristics. It requires the following raw materials:

- A magnetostrictive material, preferably in the form of cylinder and made of amorphous magnetostrictive wire of less than 150 micrometers diameter, is used. The magnetostrictive material should be annealed and magnetoelastically tested before being used in the production line for the magnetoelastic optimization and uniformity to be guaranteed.
- Pulsed current conductors preferably in the form of enameled copper wires with diameter less than 250 micrometers. The wires should be tested by the eddy current method or any other non destructive method to determine the uniformity of their resistivity.
- Soft magnetic material, preferably in the form of ribbon and made of amorphous non magnetostrictive alloy, having a thickness less than 30 micrometers and a width less than 5 millimeters. The soft magnetic material should be annealed and magnetically tested before being used in order to certify its magnetic permeability uniformity along the length of the ribbon.

- Low density foam to cover the magnetostrictive material in order to avoid bending and misattachment. Such a foam, having a Young's modulus much less than the Young's modulus of the magnetostrictive material does not absorb the elastic energy of the propagating elastic waves in the magnetostrictive material, thus allowing the maximization of the response of the sensor.
- Three housing ribbons, preferably in the form of plastic sheets, used as follows: the first one as the lower sensor substrate, the second one as intermediate layer between the MDL and the soft magnetic material and finally the third one as the upper sensor substrate. These plastic sheets should be tested preferably by dielectric uniformity tests in order to certify their thickness uniformity.

After the optimization and testing, these raw materials are used as raw materials to produce the position sensing element in the form of a long composite sheet, preferably by using the consequent following steps:

- The first housing ribbon sheet is de-wound and stressed by a roller.
- The two pulsed current conductors are de-wound, tested by eddy currents for the determination of the electrical resistivity uniformity and set parallel at a given distance.
- The low density foam is sprayed between the two pulsed current conductors and the magnetostrictive material is then de-wound, driven and set on top of the housing ribbon, in the middle of the two pulsed current conductors.
- The second housing ribbon is set on top of the pulsed current conductor and magnetostrictive material arrangement.
- The soft magnetic material is set on top of the arrangement and the third housing ribbon is set on top of the soft magnetic material.
- All the assembly is stressed under heat, thus fixing in position all the parts of the sensor.
- The whole assembly is wound and packed.

Alternatively, the sensing arrangement (A) may be manufactured, as presented in the experimental part of this paper, by using an extruder for housing the MDL and the parallel pair of pulsed current conductors and a second extruder for housing the soft magnetic ribbon.

Apart from this production line, the electronic circuitry (B) is assembled in one piece in another production line, including the magnetic flux receiver, as follows:

- The electronic circuitry for the pulsed current generation and transmission. The electronic circuitry may be either in the form of a through-hole printed circuit board or a surface mount technology printed circuit board or an application specific integrated circuit (ASIC).

- Electronic circuitry for the receiving signal conditioning, including buffer-amplifier, delay time measurement electronic circuit and signal conditioning and treatment. This electronic circuit may also be in the form of either a through-hole printed circuit board or a surface mount technology printed circuit board or an ASIC. Preferably, the two above mentioned electronic circuits are made in the same integrated circuit.
- The magnetic flux receiver, preferably in the form of search coil, is connected to the electronic circuitry for the receiving signal conditioning on a proper electronic substrate, preferably but not exclusively, in the form of printed circuit board. On the same electronic substrate the conducting layer for the pulsed current conductor connection also exists.

So, when a sensor of a given length is asked, the sensing element assembly is used and a length out of it is cut. Consequently, the one end of the position sensing element is connected to the electronic circuitry by means of connecting the pulsed current conductors and inserting the end of the MDL inside the magnetic flux receiver or the search coil. At the other end of the position sensing element, the pulsed current conductors are electrically connected by means of a conducting bar, which also presses the magnetostrictive material in order to keep it in position and eliminate any acoustic reflections.

The advantages of the arrangement are related to the existing state of the art in positioning measurement. The state of the art in the field of magnetostrictive delay line position sensors mainly refers to the following arrangement: a straight and usually cylindrical conductor is covered by a magnetostrictive material, which is usually in a tubular shape. When a pulsed current is transmitted through the conductor, a pulsed magnetic field tangential and circumferential to the tubular magnetostrictive material is generated. As long as there is no local magnetic field anomaly along the length of the magnetostrictive material and the magnetostrictive material is magnetoelastically uniform, the generated transverse microstrains are equal along the length of the magnetostrictive material. Therefore, the neighboring microstrains are cancelled out, apart from the ends of the magnetostrictive material, where the boundary conditions suggest the existence of non-cancelled microstrains, which propagate as elastic pulses and can be received as pulsed voltage outputs. In the presence of a local magnetic anomaly of a moving magnet for example, a transverse elastic pulse is generated in the region of the magnetic anomaly, propagating along the MDL. The delay time of the reception of this pulse determines the position of the magnetic anomaly.

Such a device does not fulfil the requirements of a position sensor able to detect the position of various kinds of moving magnets and various ranges of measurement. The most significant problem in such a device is that for some amplitudes of the magnetic biasing field, corresponding to certain hard magnetic

materials, geometries and distance from the magnetostrictive delay line, the above mentioned generated and propagating elastic microstrain results in the generation and propagation of pseudo-longitudinal elastic pulses. These elastic pulses travel with the longitudinal sound velocity, which is larger than the transverse elastic pulses velocity. Thus, under some given circumstances they can be received prior to the above mentioned transverse elastic pulses. Thus, the dependence of the time delay on the position of the magnet is not always a monotonic function and therefore this type of position sensor is not capable to monotonically detect the position of a vast variety of moving magnets and measurable lengths. Furthermore, experimental results have showed that this sensing element may suffer from non sufficient magnetoelastic uniformity, sensitivity and spatial resolution, despite the fact that the slower transverse sound velocity offers a by-design better sensitivity. This is due to the possible magnetic hysteresis appearing in this sensing element.

Additionally, to that, a rather laborious process is required to achieve uniform magnetostrictive thin films in a tubular shape of a proper thickness on top of a circular conductor, using physical deposition techniques. Thus, a batch production line process is to be used with relatively slow production rhythms and higher production cost. If the mechanical adjustment of the magnetostrictive tube is decided as a production line method, the sensor cannot be produced in a variety of lengths following an automated production line and it contains increased risk levels of failure and levels of sensor uncertainty. Thus, the sensor presented in this paper, offering solutions concerning the above mentioned drawbacks of the given state of the art has been conceived and developed.

Our sensor includes a couple of conductors as means of excitation, which are parallel and surrounding the magnetostrictive delay line. This flat conductor – MDL arrangement is covered at the one side by a soft magnetic tape or ribbon. Thus, in the presence of the moving magnet in the vicinity of this soft magnetic ribbon, the generated elastic pulse propagating along the length of the MDL is longitudinal. This propagating elastic pulse is also transformed to other modes of propagation like pseudo-transverse modes, thus generating transverse elastic waves. The advantage of this arrangement with respect to the given state of the art is that the longitudinal elastic pulses generate other modes of propagating pulses, but any other kind of secondary generated elastic pulse, like pseudo-transverse, will always have a sound velocity smaller than the longitudinal sound velocity. Thus, they will always arrive at the search point later than the initially generated longitudinal pulse. Therefore, the dependence of the delay time of the front wave of the arriving elastic pulse will be always proportional to the distance of the moving magnet from

the search coil and inversely proportional to the longitudinal sound velocity. Thus, such an arrangement can always detect the position of a variety of moving magnets and ranges of their displacements.

Apart from that, the soft magnetic tape or ribbon is firmly set on top of the flat conductor – MDL arrangement. Thus, the jittering of the moving magnet, being in a larger distance than the soft magnetic tape or ribbon from the MDL, causes a smaller jittering of the above mentioned pulsed eddy currents. The uncertainty of the position of the eddy currents is smaller than that of the position of the moving magnet. This allows a smaller uncertainty level of our sensor. Indeed, the obtained uncertainty of our set-up is of the order of 10  $\mu\text{m}$ , compared to the 100  $\mu\text{m}$  uncertainty level obtained with the given state of the art.

Furthermore, the production of our sensor is possible by implementing extrusion techniques and using magnetostrictive fibres as MDLs and enamelled copper wires as pulsed current conductors. Thus, the production line can be continuous, with a production speed of the order of 100 km/h, corresponding to the normal or minimum speed of an extruder. Furthermore, the quality of such an extrusion-based production line is not decreased by the increase of the extrusion speed. On the contrary, following an increase of the production speed up to a typical limit of 300-350 km/h, the uniformity of the flat conductor-MDL structure is maintained or even improved. Thus, the production line is automated and the cost of the sensor is almost labor independent. Additionally, the use of polycrystalline conventional Fe-rich fibers can result in further decrease of the cost of the sensor.

This sensor does not require a return cable to obtain pulsed current transmission. This role is achieved due to the presence of the two pulsed current conductors. Thus, a simple electrical connection of the two ends of the pulsed current conductors at the one side of the sensing element, by using a conducting element, is enough to result in an electric circuit able to transmit pulsed current by connecting the other two free ends of the two pulsed current conductors with the pulsed current electronic circuitry. Furthermore, the diameter of the magnetostrictive wires used as MDLs, which is of the order of 100 – 150  $\mu\text{m}$ , allows the use of commercially available CD driver reading coils. The use of these coils was not possible in the sensing element of the prior art. Thus, the electronic circuitry comprised of two chips, one for pulsed current transmission and one for voltage output detection and conditioning, as well as the receiving coil, can allow a low cost electronic circuit board.

Finally, the control and tailoring of the properties of the significant parts of the sensing element, such as the magnetostrictive fiber acting as the MDL and the soft magnetic tape or ribbon, allows the repeatability

of the operation of our sensor and the above mentioned uncertainty of the moving magnet position measurement.

---

### **5.1.6 Accelerometers based on dynamic moving magnet displacement**

---

Acceleration measurements are important in many cases, especially considering applications for the automotive industry. Requirements for repeatable and secure response of accelerometers with low consumption are important in this highly increasing sensor market, an example being their use in airbags.

The major demand of this kind of sensors is the determination of reaching or not a certain level of acceleration threshold, over which the sensor activates an actuating mechanism, like an airbag, which is a kind of on/off operation. Apart from the calibration procedure, it is important to test the sensor under various conditions, the most important of which being the time dependence of the sensor response, the durability against vibration, temperature and humidity.

The parameter of electromagnetic compatibility and interference (EMC-EMI), mainly in very low as well as in telecommunication frequencies is also important. It is understood that an accelerometer for airbag applications, good enough in terms of accuracy and durability, having though the disadvantage of being sensitive to mobile phones would not be appreciated.

A magnetostrictive delay line (MDL) set-up for the detection of acceleration was demonstrated, requiring no excitation means for the sensor, usually needed for the generation of elastic wave within the magnetostrictive element. The conventional operation of MDLs involves the use of two coils, one for the elastic wave generation due to the magnetostriction effect and the other one for the elastic wave detection due to the inverse magnetostriction effect. We have performed experimental work to determine the sensor response, linearity, hysteresis and total uncertainty.

Also, we performed experiments in determining the time, vibration, temperature and humidity dependence. Finally, we obtained results in the field of EMC-EMI testing in dc magnetic field, concerning ambient field compatibility, as well as in 1 GHz field, corresponding to mobile communication interference.

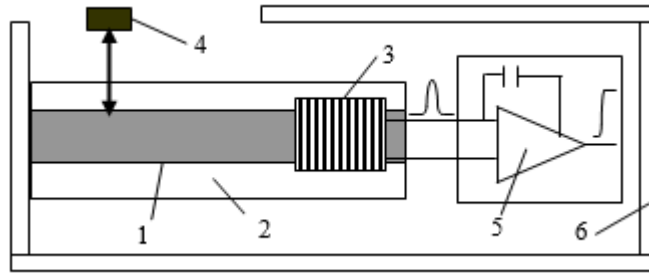


**Figure 5.26.** Accelerometer schematic arrangement. (1) Magnetostrictive delay line, (2) Glass substrate, (3) Detecting coil, (4) Permanent magnet, (5) Pulsed voltage integrator, (6) Field screening soft magnetic material.

The schematic of the new accelerometer is illustrated in Figure 5.26. A long magnetostrictive element (1) acting as the MDL is set on a glass substrate (2). A short, multi-turn detecting coil (3) is set at the one end of the MDL. A permanent magnet (4) is set on top of the MDL, having a fixed pole orientation with respect to the MDL. An electronic integrator (5) detects and integrates the output of the detecting coil. The whole set-up is covered by a soft magnetic material (6), except of the region of the permanent magnet, for electromagnetic field screening purposes. Displacement of the permanent magnet results in a corresponding change of the magnetic flux component along the length of the magnetostrictive element at the short intersection of the material and the permanent magnet. Consequently, a microstrain, proportional to the first derivative of the flux change and the displacement is generated within this region, due to the magnetostriction effect.

Provided that such a microstrain change has a bandwidth response corresponding to the MDL bandwidth of the magnetostrictive material, this material acts as a surface acoustic waveguide. Therefore, it allows the propagation of the microstrain along its length, and it can be detected by means of a pulsed voltage output via the detecting coil (3), due to the inverse magnetostriction effect. Such a voltage output is proportional to the first derivative of the propagating microstrain. Therefore, the integrated voltage output of such a signal is proportional to the second derivative of the displacement of the permanent magnet. This magnitude corresponds to the acceleration of the permanent magnet. Use of an electronic integrator at the output of the detecting coil can result in the fast determination of the acceleration magnitude of the moving magnet.

**Table 5.1.** Range of acceleration due to displacement and time duration.

Time duration	Displacement	100 $\mu$ sec (10 kHz)	10 $\mu$ sec (100 kHz)	1 $\mu$ sec (1 MHz)	0.1 $\mu$ sec (10 MHz)
	1 $\mu$ m	10 <sup>-5</sup> g	10 <sup>-3</sup> g	1 g	10 <sup>2</sup> g
	10 $\mu$ m	10 <sup>-4</sup> g	10 <sup>-2</sup> g	10 g	10 <sup>3</sup> g
	100 $\mu$ m	10 <sup>-3</sup> g	10 <sup>-1</sup> g	10 <sup>2</sup> g	10 <sup>4</sup> g
	1000 $\mu$ m	10 <sup>-2</sup> g	1 g	10 <sup>3</sup> g	10 <sup>5</sup> g

Taking into account that the frequency bandwidth of the MDL operation can vary from 10 kHz up to 10 MHz and the range of magnet displacement is from 1  $\mu$ m to 1 mm, the resulting range of measurable acceleration can be from 10<sup>-5</sup> g up to 10<sup>5</sup> g, as shown in Table 5.1. Keeping in mind that a practically safe displacement of a permanent magnet is 1 mm, by means of repeatable experimental procedure, the measurable acceleration range is from 10<sup>-2</sup> g up to 10<sup>5</sup> g.

The sensor was set on a support base, free from vibration, by using spike mechanical isolation. The magnetostrictive material was a 1 mm wide, 5 mm long and 25  $\mu$ m thick Fe<sub>78</sub>Si<sub>7</sub>B<sub>15</sub> amorphous ribbon, tested in the as cast form and after 300°C heat annealing under 8 kA/m magnetic field along its length, to optimize its performance by maximizing the magnetomechanical coupling factor. The 100 turn, 1 mm long detecting coil was made of 0.05 mm enamelled copper wire. The permanent magnet was an Alnico 5 mm X 0.1 mm X 0.1 mm rectangular piece, placed 1.5 mm apart from the FeSiB ribbon. It was fixed on a speaker-like magnetic actuator, using a non-magnetic glass tube separator to avoid interference with the magnetic material. We used three different speaker coils able to supply dynamic displacement from of 1  $\mu$ m up to 1 mm of the Alnico magnet. The magnetic actuator was powered using a stereo power amplifier, fed by an arbitrary signal generator, allowing pulsed displacements, having a time width from 10 ms up to 0.1  $\mu$ s. A typical sensor response is illustrated in Figure 5.27, with the use of FeSiB ribbon annealed under magnetic field, under 1 mm displacement and 1  $\mu$ sec duration time. This was the optimum response obtained within the limits of our experiment.

The response was obtained for pulsed magnet displacements equal to 28 mm and pulse width about 1  $\mu$ sec, where a maximum sensitivity was observed. The sensor response was monotonic within the range of the measured acceleration and it was determined by increasing and decreasing the applied duration of

the pulsed displacement, thus allowing determination of hysteresis, which was found to be negligible within the limits of the experimental set-up.

Measurements concerning the time stability of the sensor have been performed. The set-up was set at a given pulsed magnet displacement, of 1  $\mu\text{s}$ , in a period of 1 ms, for one week. The observed variation of the sensor output was less than 1 mV. We have also performed an aging process, by repetitive heat annealing at 380°C. The observed variation was also determined to be less than 1 mV. Therefore, the temporal dependence of the accelerometer was determined to be less than 1 mV.

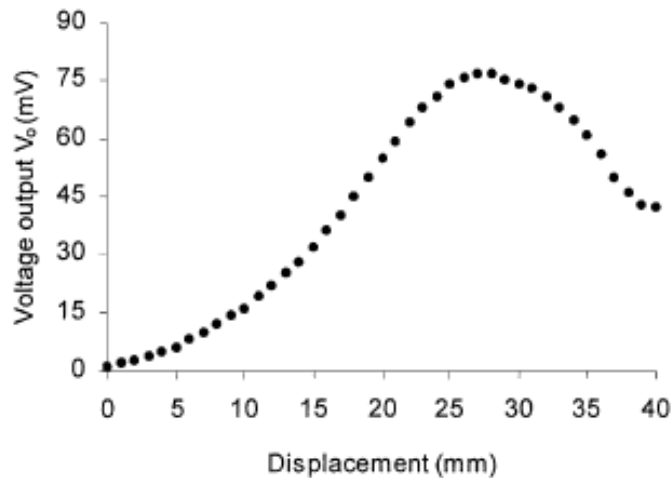


**Figure 5.27.** The response of the sensor.

Experiments on temperature and humidity dependence have also been realized, inserting the whole experimental set-up except of the electronic apparatus into an oven, able to reach 400°C. Following the same repetitive procedure as in temporal dependence, we observed negligible dependence on humidity, but large dependence on temperature.

The temperature dependence is illustrated in Figure 5.28, being in agreement with the magnetization dependence of the material on temperature. The observed variation of voltage output can be limited to 1 mV, for temperatures up to 200°C, increasing drastically after that point.

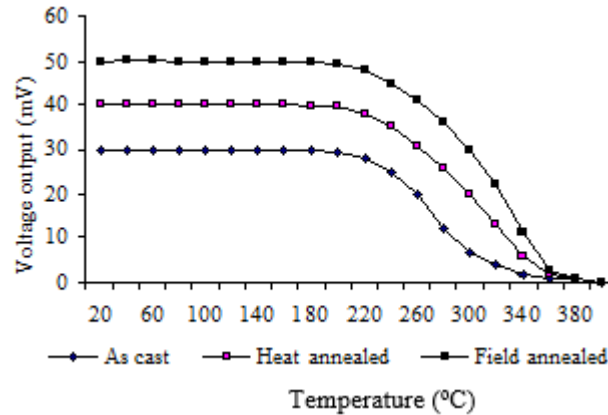


**Figure 5.28.** Temperature dependence of the accelerometer.

Experiments on the electromagnetic compatibility of the sensor have also been performed, in two ranges of frequencies. The first one concerned very low frequencies and the other one in the region of 1 GHz corresponding to the ambient field and the mobile communication interference respectively. The interference concerning the dc field was greatly affecting the behaviour of the sensor, when the soft magnetic material, covering the accelerometer was not in place. This dependence of the accelerometer output on the ambient field is shown in Fig. 5.29, concerning a typical pulsed displacement of 1 mm and duration of 1  $\mu$ sec. The reason of such a large dependence is the change of the biasing point of the  $\lambda(H)$  function with the change of the ambient field. This voltage output is strongly dependent on the direction of the ambient dc field, due to the uniaxial anisotropy in FeSiB ribbons. After having set a permalloy around the sensor apart from the area of the moving magnet, as illustrated in Fig. 5.26, we observed its influence on the sensor response, resulting in a voltage output not larger than 1 mV, as shown in Fig. 5.29.

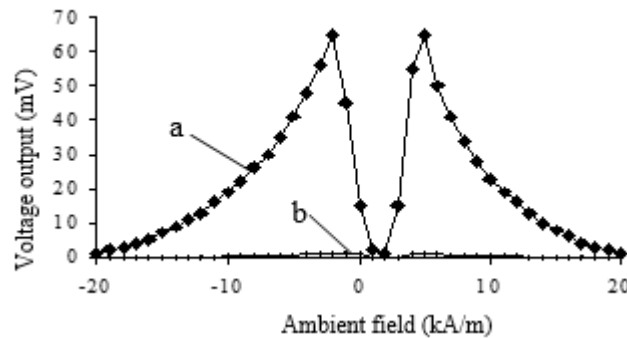


**Figure 5.29.** Accelerometer output dependence with (a) and without (b) magnetic shielding.

The interference in the range of 1 GHz was introducing a noise of the order of only 1 mV. The reason is that such a high frequency exceeds the upper limit of the frequency response, which is up to 10 MHz in most magnetostrictive materials, so that the expected microstrains due to the alternating interfering field are negligible in size. These measurements allowed the conclusion that the uncertainty of the accelerometer is of the order of 1 mV, allowing an acceleration threshold check with an accuracy of + 1%. Having in mind that the most severe problem of such a sensor is the electromagnetic interference with dc ambient fields, we determined different bandwidth responses concerning field and stress effect on the whole arrangement. Hence, an FFT circuit could be incorporated to avoid the undesirable effect of ambient fields at the vicinity of the arrangement. We have also conducted experiments concerning the dependence of the accelerometer response on the displacement of the moving magnet. Such a dependence concerning 1  $\mu$ sec duration of displacement is illustrated in Fig. 5.30, indicating that 1 mm is the optimum displacement of the moving magnet, maximizing the sensor output, corresponding to the frequency dependence of the FeSiB ribbon, where 1  $\mu$ sec duration of pulsed field requires 400 A/m changing field for optimum response.

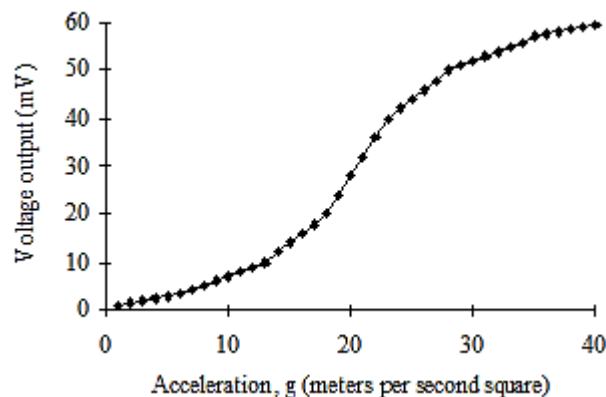


**Figure 5.30.** Accelerometer output response dependence on the maximum displacement of the moving magnet.

The sensor is also sufficient for practical application in terms of power consumption. As it does not require excitation means to operate, the power consumption is limited to the requirements of the signal conditioning circuit. Using common surface mount devices for that circuit, power consumption of the order of nW is enough for signal conditioning. The sensor packaging for the realization of the laboratory prototype has been obtained using conventional macroscopic techniques. Instead of using a glass support, we used fibre glass in printed circuit board form of 2 cm X 0.5 cm X 0.5 cm, in order to use one face as the

board for the electronic circuit and the other one for sensor packaging. The copper free surface was used to host the magnetostrictive ribbon of 2 cm length, 2 mm width and 25 microns thickness.

The hand made coil around the fibre glass and the ribbon was electrically connected with the electronic conditioning circuit. This circuit was a couple of op-amps in one chip, used for buffer and integrator process and was made using surface mount technology. The whole set-up was covered by permalloy of rectangular cross section. The moving magnet was connected mechanically, using epoxy resin. Therefore, the total dimensions of the circuit were limited to 2.2 cm X 0.7 cm X 1 cm. This arrangement could also be developed in a more sophisticated way. Involvement of thin film technology could result in the consequent development of the magnetostrictive material, detecting coil, moving magnet and the electronic circuit, so that the device is more accurately repeatable.

---

## **5.2 *Moving soft magnet measurement***

---

We hereinafter present a family of displacement sensors, based on the MDL technique, able to detect the displacement or the position of a soft moving magnet, changing the magnetic circuit at the region of origin of the elastic pulse. Integrated arrays of sensors can be obtained due to the acoustic delay line technique and they can be used as tactile arrays, digitizers or devices for medical applications like gait analysis, while the absence of hysteresis and low cost of manufacturing make them competent in this sector of sensor market. The range of measurement is small, thus making these sensors also usable as dilatometers. A number of small displacement sensors can be found in the literature. Strain gauges are such an example, while silicon diaphragms offer a relatively larger range of measurable displacement [1]. Optical methods are also useful when high accuracy measurement is required. Magnetic sensors based on inductive techniques are most commonly used when larger displacement [5,6] is to be detected. All the above mentioned devices have a common disadvantage: although they are sufficiently accurate and linear, they cannot be easily formed in arrays, since discrete sensors are to be used. Therefore, the whole structure becomes expensive and impractical for given applications. Aiming the manufacture of a not expensive, but accurate array sensor, we have developed the hereinafter presented device. Although its response was not linear for the whole range of displacement, it offered 8-bit analogue to digital conversion accuracy at a linear region between 0.5 and 1.5 mm.

The first sensor is shown in Figure 4.31a. A soft magnetic material is used as the active core AC of the sensor and is placed close to the MDL-pulsed current conductor crossing point PO. If the core AC is absent, the magnetic flux density in the MDL is maximized. Approaching the core AC, the magnetic flux density in the MDL is decreased due to the magnetic coupling between core and MDL. From the geometry, one can arrive at the following conclusion: the closer the core AC is to the MDL, the less magnetic flux in the delay line exists, resulting in a decrease of  $V_o$ . The displacement of the active core AC could be calculated with respect to the detected output  $V_o$ . It was experimentally observed that the presence of the core AC results in a change of the caused acoustic pulse for MDL-AC distance less than 2 mm. In the arrangement of Figure 5.31b, presence of the core AC increases the magnetic flux at the MDL.

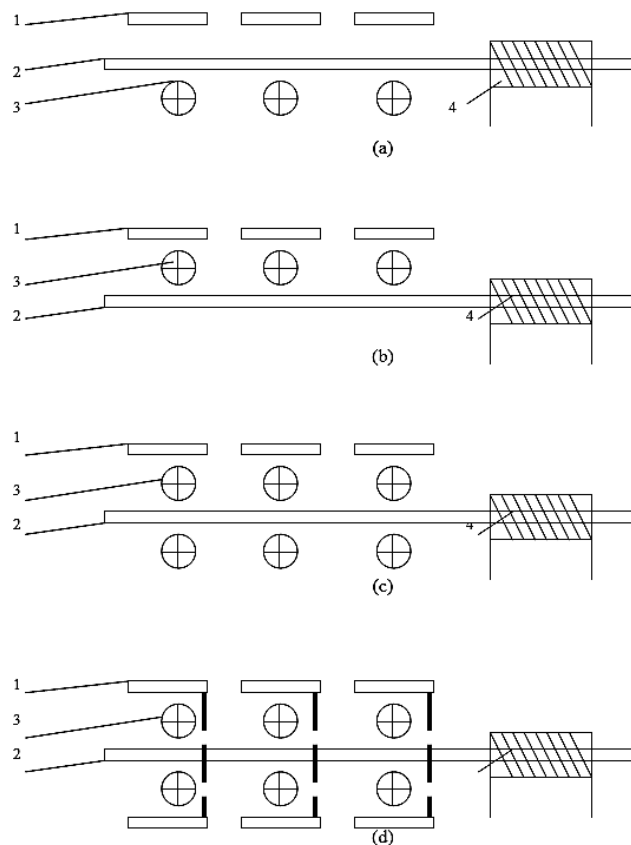


**Figure 5.31.** Measuring the displacement of soft magnetic materials. (1) Soft magnetic core, (2) MDL, (3) Pulsed current conductor, (4) Search coil.

Combination of Figure 5.31a and 5.31b results in the sensing device shown in Figure 5.31c: two pulsed current conductors are placed above and below the delay line at the crossing point PO. They are connected at the ends, so that the amplitude and direction of the pulsed current in both of them is the same. In the

absence of the magnetic core AC, the magnetic field due to the conductor above the delay line is opposing the magnetic field due to the one below the MDL. So, for an ideally symmetrical arrangement, the magnetic flux at the PO in the absence of the core AC is always zero. If the active core is in a small distance from the MDL (less than 2 mm), magnetic coupling between the MDL and the core is obtained, the pulsed magnetic flux has a non-zero value and the resulting amplitude of  $V_o$  depends on the distance between the core and MDL. So, as the distance between core AC and MDL decreases, the unbalance of the magnetic flux of the conductors inside the MDL increases, resulting in an increase of the caused elastic pulse.

Finally, another sensor arrangement of this group is shown in Figure 5.31d. In this case, two cores AC are used above and below the MDL respectively. They are joined together using a connecting strip CS in order to keep the distance relative to each other fixed. Both active cores AC are involved in altering the resulting output  $V_o$ . Two symmetrically arranged conductors are used for applying pulsed current in the same way as depicted in Figure 5.31c. When no displacement is applied, cores AC are at their maximum and minimum distances from the MDL respectively, resulting in a maximum flux at the PO and consequently a maximum output  $V_o$  at the search coil.

As the arrangement of the two cores moves down the pulsed magnetic flux in the MDL decreases to zero, since pulsed flux and consequently  $V_o$  decrease to zero as the two cores AC approach symmetrical positions with respect to the delay line. Moving further the pair of active cores AC the flux in the MDL starts increasing so that the amplitude of the output voltage  $V_o$  increases. The gap between the two active cores AC results in changes of the response of the sensor. The response of the sensor can be predictable under the assumption that pulsed current conductors are kept at a fixed distance from the delay line. The maximum amplitude of the output voltage increases as the distance between the MDL - conductor decreases. In our set-up, this distance was equal to 0.1 mm.

The dependence of  $V_o$  on the distance between the core AC and the MDL-pulsed current conductor assembly was determined for various values of pulsed current peak amplitudes  $I_e$ . Figures 5.32 a, b and c illustrate indicative response of the sensing elements of Figures 5.31 a, c and d respectively. Figure 33 shows the response of the sensor of Figure 5.31d under various values of the distance between the two active cores at constant value of  $I_e=13.63$  Amperes. Experimental results were taken by decreasing and subsequently increasing the above mentioned displacement. The measured output was the same for both cases, indicating the absence of hysteresis for 12-bit analogue to digital conversion accuracy measurements. The response of the sensor does not change for distances between MDL and active core

AC greater than 5 mm. The response of the sensor of Figure 5.31c is fairly linear between 0.5 and 1.5 mm. The sensitivity of the device was also measured by observing the minimum change of the voltage output corresponding to a minimum displacement of the active core. So, the defined sensitivity was found to be  $10 \mu\text{V}/\mu\text{m}$ .

The qualitative theory given in the description of the sensors is in good agreement with the experimental results. The amplitude of  $V_o$  in sensors of Figures 5.31a and c decreases monotonically as the active core AC moves away from the MDL. The reason for that has been explained in the second chapter “description of the sensors”. Sensor sensitivity is high for regions of displacement 0.5 to 2 mm and low for regions 0 mm - 0.5 mm and 2 mm - 4 mm.

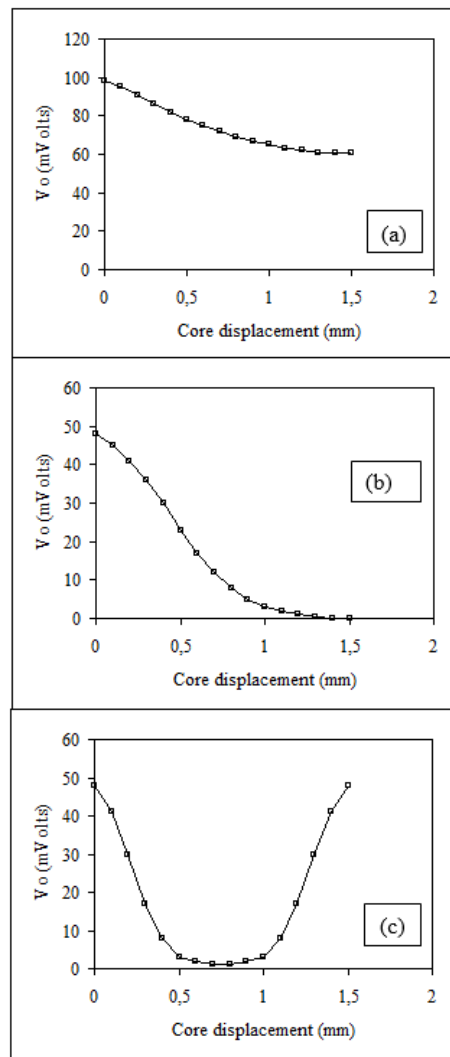


**Figure 5.32.** Response of the sensing elements illustrated in Figure 4.31.

Such an effect is due to the nonlinear behaviour of the microstrain function of the MDL, as well as to the nonlinear magnetic coupling between MDL and active core: such a coupling does not decrease linearly as the distance between core and MDL increases. The non-monotonic response of the sensor of Figure 5.31d is explained by the microstrain function  $\lambda(H)$  of the MDL. The dependence of  $\lambda$  on the applied field  $H$  is symmetrical with respect to  $\lambda$  axis and the value of  $\lambda$  for any field  $H$  equals to the value of microstrain for the given field  $H$ . Hence, the caused acoustic pulse and the received voltage output  $V_o$  follow the same law. Decreasing the gap between the two active cores, results in a sharper response as shown in Figure 5.33 because pulsed flux unbalance is obtained for a shorter displacement of the core's assembly.

The lack of hysteresis may be explained by the fact that we used annealed soft magnetic materials as MDL and active cores. This annealing reduces the coercive field  $H_c$ , which is mainly responsible for the hysteresis in the magnetoelastic behaviour due to the  $\lambda(H)$  function of the materials. According to measurements of the hysteresis of the  $\lambda(H)$  function, it is within the limits of the accuracy of the analogue to digital converter, thus resulting in non readable hysteresis in the output of the sensor.

Although one can obtain a simple and inexpensive distribution transducer by using these sensors, there are some drawbacks to it, the most important of which is the integrated sensor array nonuniform response: such a response was detected for the same displacement of the active core, under fixed conditions of pulsed current excitation and DC bias field at different sensing points along the length of the MDL, although delay lines were tested after stress and current annealing. Early experiments show that a normalization process can be applied here to standardize the sensor response.

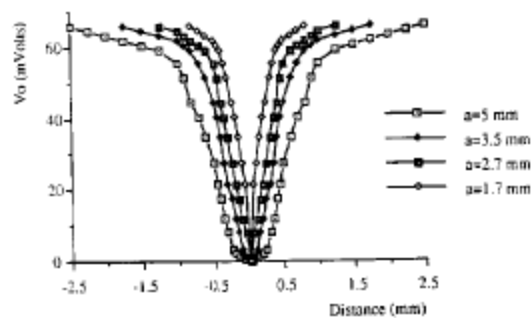


**Figure 5.33.** Response of the sensing element shown in Figure 4.31d under various distances of the sensing cores.

Alternatively, the FeSiB amorphous wires may be used as MDLs to reduce the nonuniformity and increase the resolution of the transducer. In fact, we performed measurements using  $\text{Fe}_{78}\text{Si}_7\text{B}_{15}$  amorphous wires concerning the sensing arrangements presented in this section. The results illustrated a surprisingly linear response for all set-ups.

The balanced structure of the sensing element of Figure 5.31c is the most crucial matter concerning the manufacturing process of this type of sensors. Such a balanced structure can be constructed as described in the experimental set-up description. The single sensing elements can be easily repeated in one or two dimensions, thus allowing one or two dimensional integrated distribution sensors, which can be manufactured using a relatively simple method. It is worth to mention that the balance structure of Figure 5.31c, arranged in a two-dimensional sensor, could be efficiently used as a tactile array device, in order to detect the presence of ferromagnetic bodies close to it. In that case, any sensing point of the array operates as an "on-off" sensor using a threshold voltage comparator. So, the sensor detects either a ferromagnetic material is close to the balance structure surface or not. For this type of operation there is no need for nonuniformity corrections. For applications where the relative distance between ferromagnetic bodies is to be determined, the sensor of Figure 5.31d can be used.

The active cores AC can be made of Metglas 2605SC ribbon, directly applied to a springy material, which can in turn be glued or stuck on the balance structure. Other methods for such an implementation are still under investigation. Finally, in order to convert this type of small displacement sensor to a load cell or a pressure gauge, the displacement caused on a spring has to be converted to a force  $F$ . As a first approximation, it may be assumed that the response of the spring corresponds to its linear region of operation. Thus, a force  $F$  results in a displacement  $a$ , of the support of the core, which is given by  $F=Ka$ , where  $K$  is the Hook's coefficient of the spring.

Another possible application of these sensing elements is the measurement of angle of soft magnets. The arrangement is illustrated in Figure 4.34. A  $\text{Fe}_{77.5}\text{Si}_{7.5}\text{B}_{15}$  amorphous ribbon is used as the MDL (1). A 750 turns receiving coil (2), located at the end of the magnetostrictive delay line is used to detect elastic pulses in the form of a pulsed voltage. Two parallel copper wires, (3) and (4) respectively, are used to transmit an equal amount of rectangular current pulses for the delay line excitation. A magnetoelastic ribbon (5), having a typical surface of  $15 \times 5 \text{ mm}^2$ , is used as the active core of the sensor.

The operation of the sensor is as follows: Pulsed current is transmitted through the parallel conductors. Since the MDL is set in the middle of the distance of these two conductors, the induced pulsed fields from

the two conductors are opposing each other and the resulting elastic pulse is almost zero. Placing a soft magnetic tape on top of the conductor – MDL intersection, results in a break of the symmetry of the above mentioned pulsed fields.

Therefore, an elastic pulse is generated in the MDL, propagating along the length of it, which is detected as a pulsed voltage at the search coil. The magnitude of the generated elastic pulse is dependent on the relative position of the soft magnetic material set on top of the pair of the pulsed conductors. The more length of the pulsed current conductors is covered by the soft magnetic tape the larger the pulsed output signal is. This happens because the magnetomechanical coupling factor between the excitation conductors and the delay line changes by the rotation of the soft magnetic tape acting as a sensing core. Hence, considering the soft magnetic tape as the sensing core and the rotation of it as the input of rotation in the system, the pulsed voltage output corresponds to the rotation sensor output.

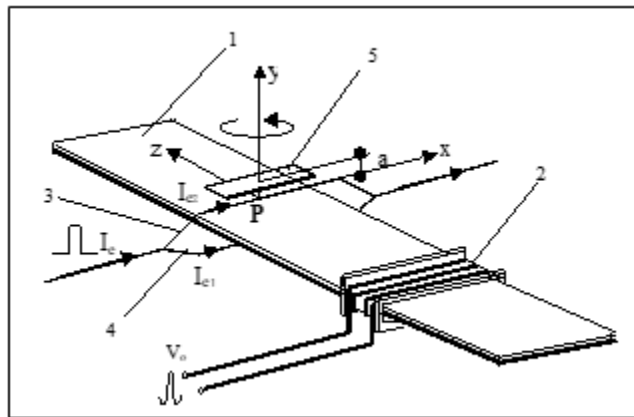


**Figure 5.34.** Basic diagram of the absolute and incremental angular position sensor working according to the MDL principle. (1) MDL, (2) Search or Receiving coil, (3) Balanced pulsed current conductors, (5) Soft magnetic tape.

The response of the sensor is illustrated in Figure 5.35. The rotation of a passive core around the Y axis of the Cartesian coordinate system with the origin in P, produces a permeability modulation resulting in a sinusoidal variation of the output voltage of the sensor of the type presented in this figure. The mathematical function obtained by filtration and approximating the response characteristic of the sensor is given by:

$$V_0(x) = A \sin \frac{\pi(x-x_c)}{w} + A_0 \quad (5.1)$$

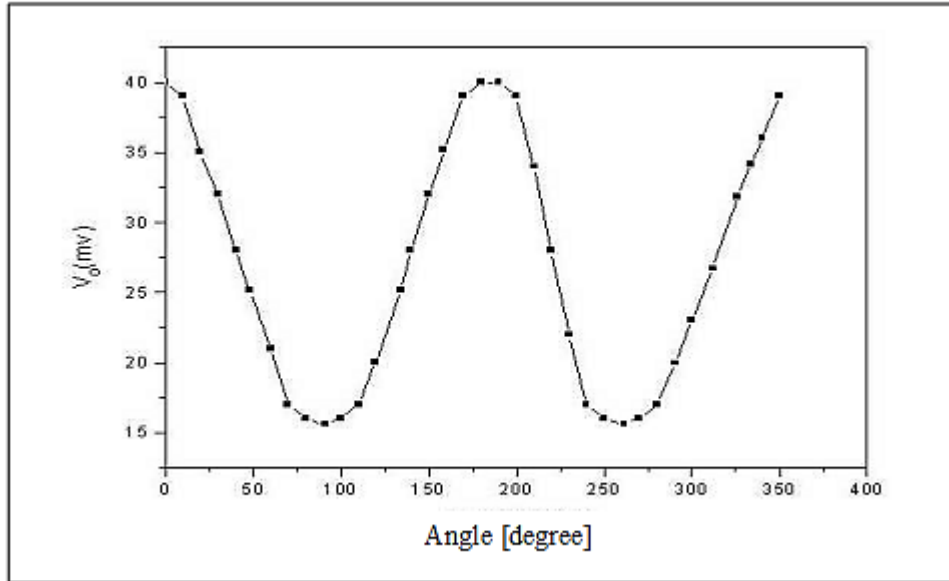


**Figure 5.35.** The response of the absolute and incremental angular position sensor.

The sensing elements of Figure 5.31 may lead to the realization of a 2-dimensional tactile array as illustrated in Figure 5.36, where the sensing core may be a soft magnetic element or elements moving on the surface of the balanced MDL structure.

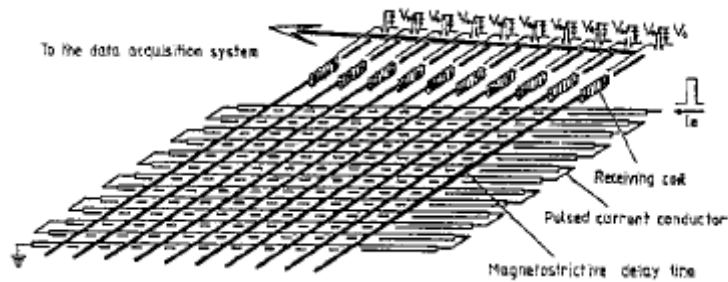


**Figure 5.36.** A 2-dimensional tactile array based on the sensing principles demonstrated in Figure 5.31.

---

### 5.3 *Moving non magnetic conducting disk measurement*

---

A new kind of displacement sensor is proposed hereinafter, based on the generation of eddy currents on a moving conducting disk, set over an amorphous wire magnetostrictive delay line. These eddy currents are caused by the presence of a straight conductor parallel to the MDL. Pulsed current transmitted through the conductor, causes eddy current loop in the conducting disk, which in turn causes an acoustic pulse above the delay line.

Studies on the characteristics of the sensor show a variety of possible applications and a reproducible response. In the following sensor we propose a more sophisticated sensor arrangement, using a cordless active core, presenting its response and characteristics. Its possible applications as a digitiser, displacement distribution sensor and eddy-current quality sensor are also illustrated.

The arrangement of this sensor is shown in Figure 5.37. A detecting coil is around the MDL at the one end of it. MDL is well terminated by latex adhesive. A small field magnet bar is set close to the MDL in order to maximize the output of the detecting coil. A pulsed current conductor is set parallel to the MDL, so that in the absence of the movable disk, the output of the detecting coil equals zero.

Approaching the conducting disk close to the MDL-conductor arrangement, eddy currents are caused on the disk. Keeping unchanged the pulsed current and the biasing field along the MDL, the amplitude of the pulsed eddy current in the disk increases with the decrease of the distance between disk and MDL.

These eddy currents cause pulsed magnetic field along the length of the MDL, at a region of the MDL called from now on the sensing point, which in turn causes a pulsed voltage output, induced in the detecting coil. The amplitude of this pulsed voltage is the output of our sensor. The delay time between voltage output and exciting pulse defines the position of the conducting disk. The higher the eddy current, the higher the magnitude of the detected voltage output. Displacement of the conducting disk, along the MDL results in a change of the delay time between the exciting pulse and the detected voltage.

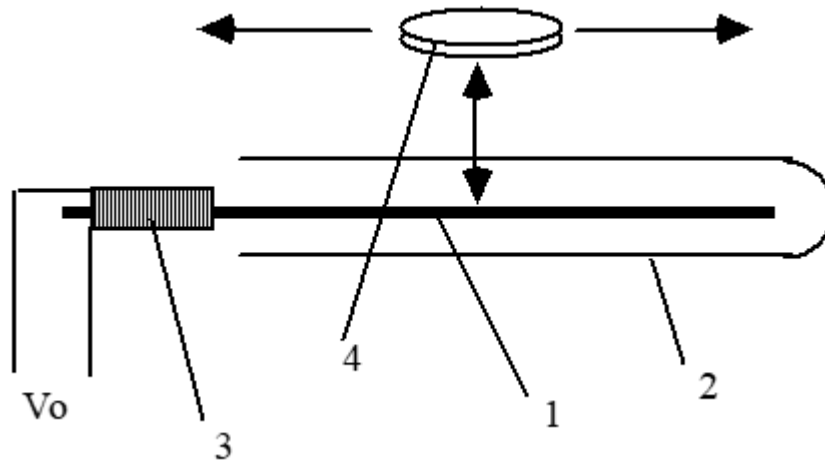


**Figure 5.37.** Arrangement of the moving conducting disk position sensor. (1) MDL, (2) Pulsed current conductor, (3) Receiving coil, (4) Moving conducting disk.

A micrometer with 5 cm long plastic (non-ferromagnetic) tube was used to displace the conducting disk. A 125  $\mu\text{m}$   $\text{Fe}_{78}\text{Si}_7\text{B}_{15}$  amorphous wire was used as a delay line. The MDL was tested in the as-cast condition and after stress-current annealing. Annealing conditions were 200  $\text{N}/\text{mm}^2$  and 500 mA for 3 minutes. A 0.25 mm enamelled copper wire was used as a pulsed current conductor. A 25 mm diameter, 2 mm thick aluminium disk was used as the active core of the sensor. The 300 turns detecting coil was made of a 30  $\mu\text{m}$  enamelled copper wire. A 14-bit A/D converter was used for detecting the peak value of voltage output  $V_o$ . A 100 MHz pulse generator/counter was used to detect the delay between the exciting pulsed current and the voltage output pulse.

A typical dependence of the amplitude of the voltage output  $V_o$  on the distance between the moving disk and the MDL is given in Figure 5.38. A number of results have been obtained for this arrangement concerning various materials used as MDLs or conducting disks. These results were obtained for increasing and decreasing the distance between the conducting disk and the MDL. The resulting curves were identical, showing the absence of hysteresis within the accuracy of our experimental apparatus. From these results, it can be concluded that such a sensor can detect displacements from 0 to 5 cm, with sensitivity dependent on the measuring electronic system. The use of a commercially available 14-bit A/D converter resulted in 3  $\mu\text{m}$  sensitivity.

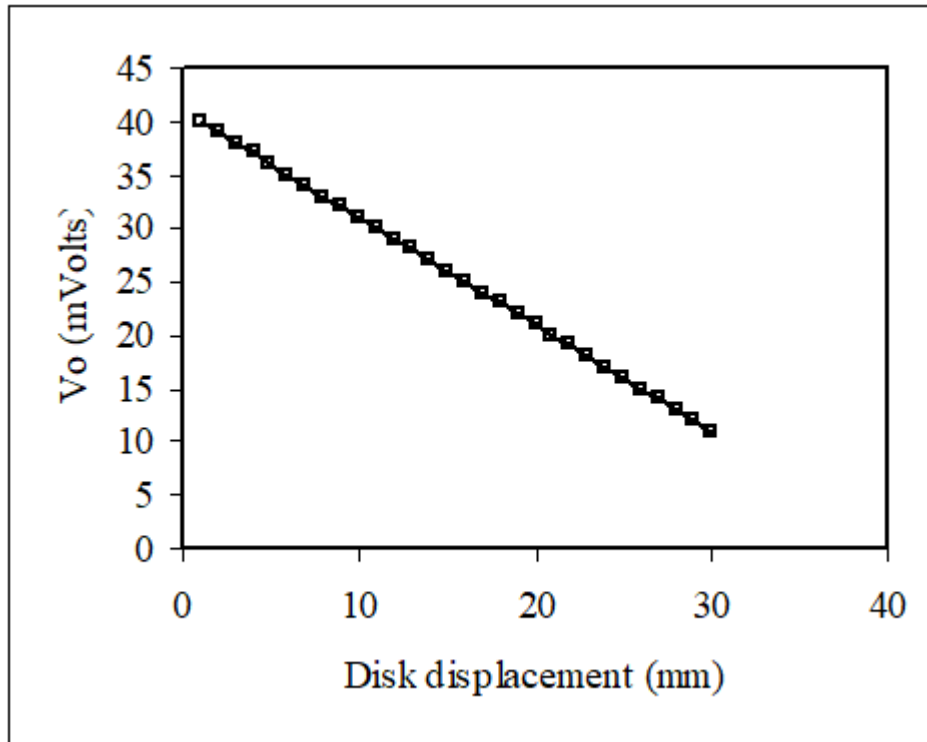


**Figure 5.38.** The response of the sensor moving conducting disk position sensor.

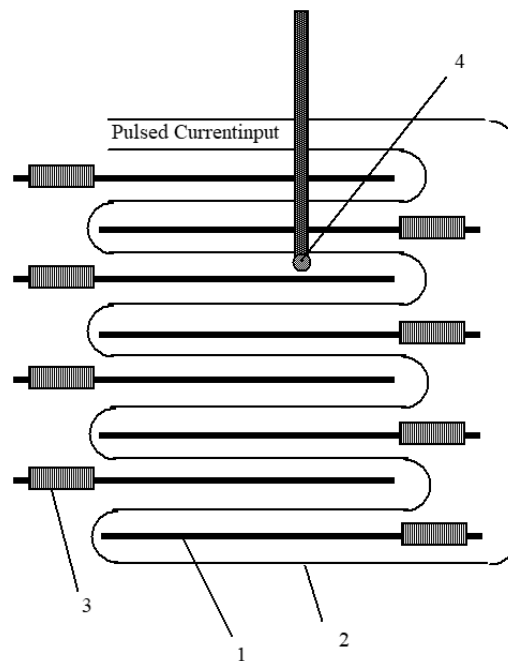


**Figure 5.39.** A two - dimensional digitiser based on the MDL technique and the displacement of a conducting disk.  
 (1) MDL, (2) Pulsed current conductor, (3) Receiving coil, (4) Moving disk.

One can use more than one active core (conducting disk) along the length of an MDL, making thus an integrated displacement distribution sensor as illustrated in Figure 5.39. The resolution of such a sensor is defined as the minimum distance between two active cores, in which discrete voltage outputs can be obtained. For our experimental apparatus this distance was 8 cm. Such a sensor could detect the position of the movable conducting disk in three dimensions. Preliminary results show that the digitizer has an isotropic behaviour in three dimensions. This means that displacement of the sensor in the Y or Z direction results in the same output voltage. Within the limits of the used experimental set-up, the sensitivity of measurement was found to be 0.1 mm in a range of 10 cm.

Another application of such an idea is an eddy current sensor for quality tests. Having fixed the position of a conducting disk, the pulsed voltage output defines the amount of eddy current in the disk. This is an indirect source of information of the resistivity of the disk. Tests among various diameters and kinds of coins are in good agreement with respect to their resistivity. Work is under way to further implementation of this device. The applications can be numerous, an important one being the security systems.

From the experimental results, it can be seen that using stress-current annealed amorphous wire MDLs one can obtain a more sensitive response of the sensor, due to the increase of the magnetomechanical coupling factor of the amorphous wire.

# 6

## Stress sensors based on MDLs

Stress measurement at a given point can be obtained by using position or displacement techniques and consequently transducing displacement into a stress magnitude. It can also be measured directly by low compliance mechanical sensors, such as pressure diaphragms, strain gauges, load cells or torque meters. The MDL technique under pulsed current – magnetic field operation has been used to the forming of stress sensors and distributed stress sensor arrays.

The proposed sensors have been divided into five groups, with respect to the major operation and kind of measurement involved. The first group is tensile stress and tensile stress distribution sensors and they are based on the change of the magnetic circuit at the elastic pulse point from origin, named PO, due to the stress applied on a sensing core. In this topology, MDL remains free of mechanical stresses.

The second and third groups are pressure gauges and force digitizers respectively, based on the change of the propagating acoustic pulse along the length of the delay line, when a force is applied at a point of it. The fourth category is load cells and torque meters based on the modification of the properties of the MDL, when stress or torsion is applied directly on it. Finally, the fifth category is a sensor able to measure the thickness of thin films in-situ, based on the coil-less MDL set-up as illustrated in Chapter 2.

Each group of sensors is to be presented separately in this chapter. After the basic description of each sensor, its response is given. Bearing in mind that the peak value of the receiving coil voltage  $V_o$  is the output of all the proposed transducers, response of the sensors is the dependence of  $V_o$  on the relevant input.

## 6.1 Tensile stress sensors

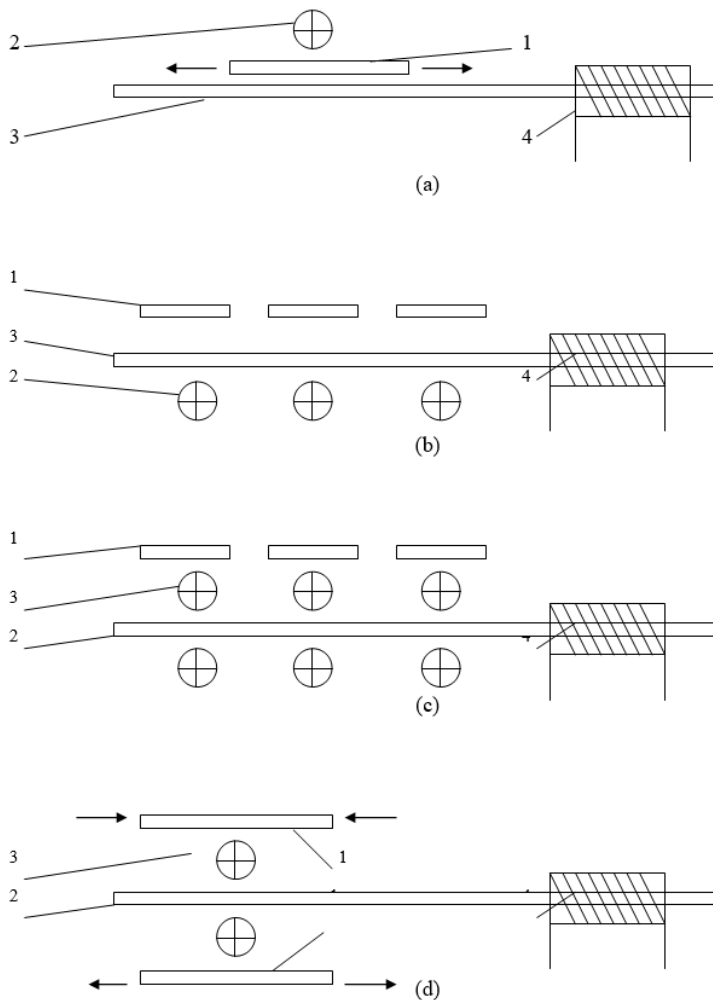


**Figure 6.1.** The schematics of various tensile stress sensing arrangements. (1) Sensing core, (2) MDL, (3) Pulsed current conductor, (4) Search coil

This group is based on the elastomagnetic properties of the magnetostrictive ribbons or tapes. As for a magnetostrictive element in the form of tape, ribbon or wire, the relative permeability is dependent on the tensile or compressive stress along its length: such stresses act as an effective field along the length of the magnetostrictive material. Such a field is regarded either in the same or the opposite direction, if the material is positive or negative magnetostrictive material respectively. Such a stress or effective field magnetizes the material, either by domain wall displacement or by domain rotation. Therefore, in a positive magnetostrictive material, tensile stress results in orientation of the magnetization towards the stress while compressive stress orients the

magnetization normal to the applied stress and on the plane of the tape or the film. Thus, tensile and compressive stresses decrease and increase respectively the magnetic permeability in positive magnetostrictive materials. The opposite happens in the case of negative magnetostrictive materials, where tensile and compressive stresses increase and decrease respectively the magnetic permeability.

In this type of sensors the MDL is supposed to remain free from stresses under any circumstances. This sensor family uses the set-up in which array conductors vertical to the MDL are used. The basic idea is the change of the magnetic circuit at a sensing point, defined by the elastic pulse point of origin PO, which is in turn defined as the crossing point of the MDL and the pulsed current conductor. For the present group of sensors, the change of the magnetic circuit takes place by changing the magnetic characteristics of the magnetic sensing core S, and more specifically by decreasing the relative permeability due to the applied stress on the core S, which is firmly positioned relative to the delay line.

The first type of this group is shown in Figure 6.1a. The active core S is placed at a fixed distance from the delay line, between the pulsed current conductor and the line. This arrangement is initially studied in the static case, in order to simplify the understanding of its operation. Assuming that DC current is applied to the conductor of Figure 5.1a, a magnetic field is caused having a circular path in the absence of the core S and the MDL. The presence of the active core S and the delay line modify the path of the magnetic lines.

Only if the delay line is present, a number of magnetic lines is kept in it, as it is a magnetic material, causing a change of their path: a greater number and a longer distance of magnetic lines is now parallel and inside the elementary cross section areas of the line. This qualitative explanation suggests that the magnetic field and flux density in the delay line is greater than the one in the same area of free space before setting the delay line in position. If now the active core S is set in between delay line (at a fixed distance from it) and conductor, the magnetic circuit changes again. Core S operates as a magnetic screen, so that a number of magnetic lines which entered the MDL are now attracted by S.

The number of these lines is dependent on the magnetic characteristics (permeability) of the core S and the MDL, as well as the geometry of the arrangement. So, in the presence of the core S, the number of magnetic lines at any cross section area of the delay line, is less than the one when having only the MDL in position. By applying a stress on the active core S, its relative permeability and consequently its ability to attract (screen) magnetic lines decreases.

So, if the saturation magnetization of the MDL is not reached, the ability of the MDL to attract magnetic lines increases: the magnetic flux density at any cross section area of the delay line increases. So, the more tensile stress on the core S, the greater is the value of magnetic flux density in the delay line. A similar magnetic behaviour is followed, if pulsed current (with a fixed peak value  $I_e$ ) is transmitted at the conductor, although the magnetic flux inside the delay line for applied DC current  $I_e$  is not equal to the flux caused by pulsed current with peak  $I_e$ . But, although a DC current causes no acoustic stress in the delay

line, pulsed current causes an acoustic pulse, which can be detected as pulsed voltage (peak amplitude  $V_0$ ).

So, for the arrangement of Figure 6.1a and for pulsed MDL operation, it can be concluded that the applied tensile stress at the active core S results in an increase of the peak voltage  $V_0$  at the receiving coil. This fact may term the arrangement of Figure 6.1a as a tensile stress transducer, having the applied stress and the receiving peak value  $V_0$  as its input and output respectively. The same principle of an array of conductors crossing an array of MDLs could be applied here, resulting in a tensile stress distribution transducer.

Figure 6.1b shows another type of sensor. In this case, the active core S operates in a slightly different way. In the presence of it, the magnetic circuit and consequently the magnetic flux at the sensing point changes because the core S attracts some of the magnetic lines, although the MDL operates now as a magnetic screen. So, coupling between core S and MDL results in an increase of the magnetic flux in the delay line with the increase of the tensile stress along the active core, causing thus another type of tensile stress sensor. Figure 6.1c is a mixture of the arrangements of Figures 6.1a and 6.1b.

The balanced structure of Figures 2.8 and 2.9 is also used here. As pulsed current  $I_e$  is transmitted in the same direction in the two conductors, in the absence of the core S, there is zero magnetic flux in the delay line and consequently zero voltage output is detected. When core S is positioned at a distance from the line, then, the magnetic circuit changes: if core S is placed in a fixed position from the MDL, the flux density in the line is not zero any more. Observing the magnetic circuit of the arrangement, it can be concluded that applying tensile stress on the core S results of a decrease in the coupling between core and line, so that the magnetic flux in the line decreases.

So, increasing the stress on the core the voltage output at the receiving coil decreases. As it will be shown in the experimental results section for this type of sensor, a voltage output from a maximum value down to zero was obtained, for zero and maximum tensile stress on the active core respectively, which means that its relative permeability effectively becomes equal to one.

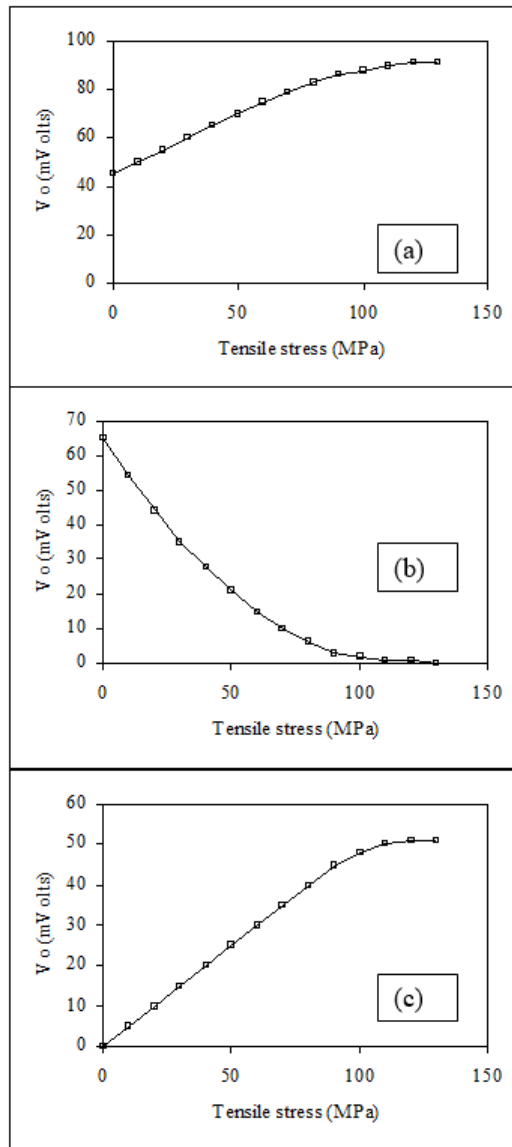


**Figure 6.2.** Typical response of the tensile stress sensing arrangements illustrated in Figure 6.1.

Another sensor is proposed in Figure 6.1d, which also uses the balance structure set-up. Two cores  $S_1$  and  $S_2$  above and below the delay line respectively are fixed in equal distances from the MDL. The one core ( $S_1$ ) remains unstressed, while a tensile stress can be applied to the other one ( $S_2$ ). When no stress is applied at the core  $S_2$  the magnetic flux inside the delay line is zero. If tensile stress is applied on core  $S_2$ , the magnetic flux inside the line becomes non zero, since the relative permeability of the core  $S_2$  decreases (change of the magnetic circuit). This arrangement offers zero voltage output when no tensile stress is

applied on  $S_2$ , which increases with the applied stress on it. If tensile stress is applied on the core, the magnetic circuit changes because the ability of the core to attract magnetic lines decreases. Consequently, if the MDL is not saturated, more magnetic lines are kept in it. The maximum possible number of these lines under fixed peak value of pulsed current and DC bias field is obtained for the maximum possible tensile stress applied on the active core, resulting in the minimum possible permeability of it, concerning the Fe-rich positive magnetostrictive amorphous alloys.

The response of the sensors of Figures 6.1a, 6.1c and 6.1d has been studied by using various different families of positive magnetostrictive ribbons and wires. Indicative results are hereinafter presented, showing data of  $Fe_{78}Si_7B_{15}$  amorphous ribbons, which represent the most dramatic dependence of magnetic permeability on stress. Input and output of the system is the applied tensile stress on the magnetic active core and the peak value of the detected voltage output  $V_o$  respectively.

The dependence of the  $V_o$  on the tensile stress applied on the ribbon under various values of exciting pulsed current  $I_e$  was measured. Figures 6.2a, 6.2b and 6.2c show the response of the sensors of Figures 6.1a, 6.1c and 6.1d respectively. The sensing element of Figure 6.1a and 6.1b could be regarded as similar to the simple strain gauge. It is observed that concerning the response of Figure 6.1a, the gain of full-to-zero applied tensile stress is 2.5 to 1. This fact makes this type of sensor more attractive than strain gauges in terms of sensitivity (strain gauge gain about 0.1 - 0.3 %), although the disadvantage with respect to the strain gauge is its nonlinearity. It was observed that the response of the sensor shown in Figure 6.1c fits an exponential dependence:

$$V_o(\sigma) = V - c\sigma_{omax} \quad (6.1)$$

where  $V_{omax}$  is the maximum value of  $V_o$ . In the case of  $Fe_{78}Si_7B_{15}$  amorphous ribbons the coefficient  $c$  equals to  $3.5 \text{ MPa}^{-1}$ . Thus, the normalized function  $V_{on}(\sigma)$  is given by:

$$V_{on}(\sigma) = \frac{V_o(\sigma)}{V_{omax}^{-c\sigma}} \quad (6.2)$$

Concerning the response of the sensor illustrated in Figure 6.1d, it fits another exponential function:

$$V_o(\sigma) = V - c\sigma_{omax} \quad (6.3)$$

where  $V_{omax}$  is the maximum value of  $V_o$ . Coefficient  $c$  is the same as above. So, the normalized response of this sensor is:

$$V_{on}(\sigma) = \frac{V_o(\sigma)}{V_{omax}^{-c\sigma}} \quad (6.4)$$

All these results were taken by increasing and decreasing the applied tensile stress on the ribbon and the reported output was the same for both cases, so that the resulting hysteresis appeared to be small.

---

### 6.1.1 A low compliance beam structure force sensor based on this the sensor topology

---

The main idea of this sensor is based on the opposite orientation of the magnetic domains of a Fe-rich positive magnetostrictive amorphous ribbon, when it is stressed and compressed. The principal idea is shown in Figure 6.3. A balanced structure is used for this type of sensor (two pulsed current conductors are in equal distances above and below the MDL, transmitting identical pulsed current waveforms). Two identical magnetoelastic ribbons  $S_1$  and  $S_2$  are in equal distances above and below the MDL. When pulsed current is transmitted through the two conductors, and the ribbons are unstressed or uncompressed, the acoustic stress and consequently the detected voltage output is zero.

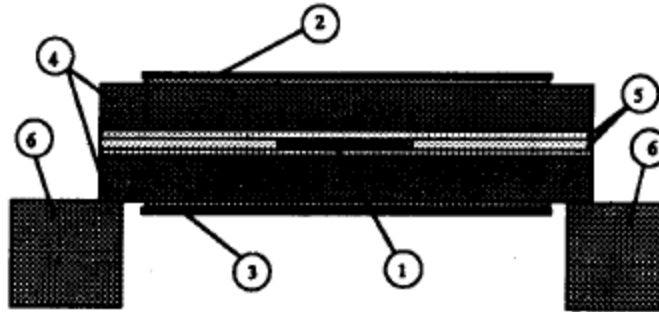


**Figure 6.3.** A low compliance beam structure force sensor. (1) MDL, (2) and (3) Ribbon sensing cores to be stressed and compressed respectively, (4) 1.5 mm thick non magnetic support of the sensing cores, (5) Three-layer support for the MDL, (6) Beam support.

Applying tensile stress and compression on  $S_1$  and  $S_2$  respectively, the magnetic domains are oriented as shown in Figure 6.3, the magnetic circuit changes, there is not equilibrium of magnetic flux in the MDL any more and the detected voltage output becomes not zero. This principal idea can be applied for a beam structure sensor, so that an applied force could result in stress and compression of the cores  $S_1$  and  $S_2$  respectively.

As an example Vitrovac 7605 was used as the magnetoelastic ribbon. Two, 10 mm long, 5 mm wide cores were glued by epoxy resin, on two, 50 mm long, 10 mm wide, 1 mm thick, fibre glass supports. They were glued in order to apply no stress and/or compression on them. Only one surface of the ribbons was glued on their support. The fibre glass supports were completely etched. A 1 mm wide straight copper line was set on each support to be used as a pulsed current conductor.

Two, 23 mm long, 10 mm wide, 0.1 mm thick fibre glass pieces were used as the middle layer of the balanced structure. The balanced structure was made in order to have the unstressed and/or uncompressed cores on its outer surface. The total thickness of the structure was 2.2 mm. A 0.7 mm wide FeSiBC ribbon, made by Hull University, was used as an MDL. The whole structure was fixed on two 10x10 mm, 1 mm thick, fibre glass supports. Nothing else was connected or glued on the beam.

The distance between PO and receiving coil was 30 cm. Two small field magnets were close to the PO and the receiving coil, in order to maximize the response of the device. Maximizing the voltage output was done as follows: pulsed current was transmitted through the one conductor, and one magnet was approached at the PO, so that the detected voltage was maximized. After fixing this magnet, the other one was approached and fixed at the receiving coil to obtain the same goal. Load in the form of steel balls was applied on top of the surface, so that the core above the MDL was compressed and the other one stressed. The weight of each steel ball was 0.21 N.

The response of the sensing element is illustrated in Figure 6.4, for excitation pulsed current amplitude  $I_e=9.9$  Amperes. In this case, Vitrovac 7605 was used as magnetoelastic ribbon. Data were taken by incrementing and decrementing load on the beam structured sensor. The resulting curves were identical, indicating absence of hysteresis within the limits of the experimental set-up. The most interesting observation out of this experiment is that the response of the sensor is almost linear for load from 5 N to 25 N. This means that nonlinearities of the magnetic operation are cancelled out probably because of stressing and compressing two identical cores in a mirror arrangement.

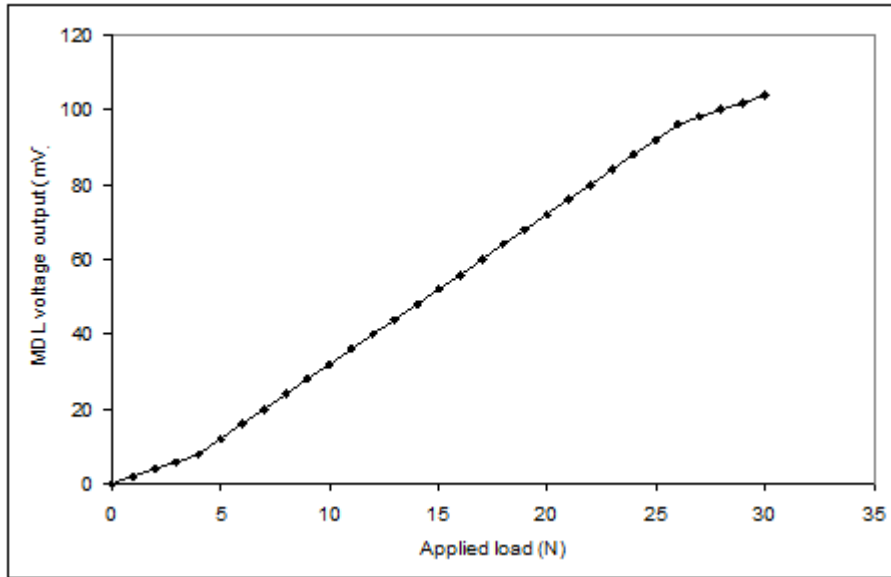


**Figure 6.4.** The response of the sensor of Figure 5.3, using Vitrovac 7605 magnetoelastic ribbon.

### 6.1.2 Improvement of the sensor: a 2-dimensional stress sensing element

A two or three dimensional force sensor, based on this sensing principle, is proposed here. The basic diagram of a two dimensional force sensor is presented in Figure 6.5.

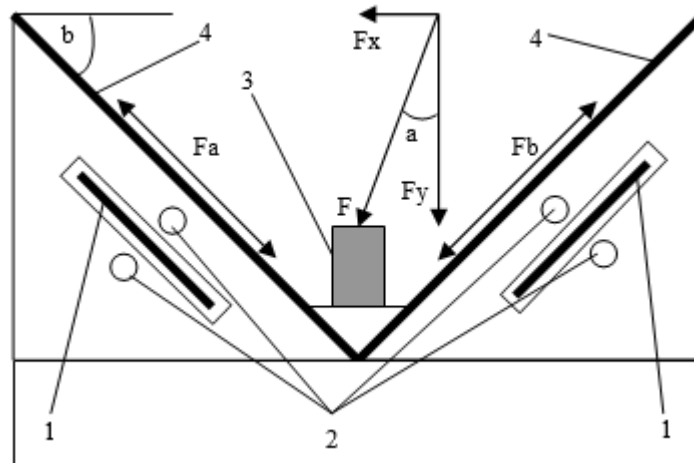


**Figure 6.5.** Basic diagram of a two-dimensional discrete force sensor. (1) MDL (2) Pulsed current conductor. (3) Point of applied force F (4) Active core.

By defining the X and Y axes as the horizontal and perpendicular directions respectively, a two dimensional force F can be analysed in two components  $F_x$  and  $F_y$ :

$$F_x = F \cdot \sin a, F_y = F \cdot \cos a \quad (6.5)$$

The components of the forces  $F_x$  and  $F_y$  result in two force components on the left sensing core,  $F_1$  and  $F_2$  respectively, while they also result in two force components on the right sensing core,  $F'_1$  and  $F'_2$  respectively:

$$\begin{aligned} F_1 &= F_y \cdot \sin b = F \cdot \cos a \cdot \sin b \\ F_2 &= F_x \cdot \cos b = F \cdot \sin a \cdot \cos b \end{aligned} \quad (6.6)$$

$$\begin{aligned} F'_1 &= F_y \cdot \cos b = F \cdot \sin a \cdot \cos b \\ F'_2 &= F_x \cdot \sin b = F \cdot \cos a \cdot \sin b \end{aligned} \quad (6.7)$$

These couples of forces result in two forces  $F_a$  and  $F_b$  on the left and the right sensing cores respectively:

$$F_a = F_1 - F_2 = F \cdot (\cos a \cdot \sin b - \sin a \cdot \cos b) = F \cdot \sin(b - a) \quad (6.8)$$

And

$$F_b = F'_1 + F'_2 = F \cdot (\sin a \cdot \cos b + \cos a \cdot \sin b) = F \cdot \sin(a + b) \quad (6.9)$$

So, the tensile stresses at the two sides,  $\sigma_a$  and  $\sigma_b$  are given by:

$$\sigma_a \cong 8F_a \text{ and } \sigma_b \cong 8F_b \text{ (in MPa and } F_a, F_b \text{ in N)}$$

in the case of a 5 mm and 25  $\mu\text{m}$  thick active core. These two stresses are unequal and therefore they cause two different MDL pulsed voltage outputs. The cores are pre-stressed to operate for tensile and compressive stresses. By using the principle of the structure of Figure 5.1c, the normalized function of the peak  $V_o$  function, applied for the stresses  $\sigma_a$  and  $\sigma_b$ , gives the normalized functions  $V_{oan}$  and  $V_{obn}$ , which have an exponentially decaying response at the left and right part of the core as follows:

$$V_{oan} = e^{-c\sigma_a} = e^{-8cF_a} \text{ and } V_{obn} = e^{-c\sigma_b} = e^{-8cF_b} \quad (6.10)$$

where  $c$  is a constant coefficient. So,  $F_a$  and  $F_b$  can be calculated by knowing the normalized values  $V_{oan}$  and  $V_{obn}$ , which can be in turn calculated by measuring the corresponding measurements  $V_{oa}$  and  $V_{ob}$  as well as the related maximum values  $V_{oa,max}$  and  $V_{ob,max}$ . So,  $F_a$  and  $F_b$  are given by:

$$F_a = F \cdot \sin(b - a) = -\frac{\ln(V_{oan})}{8c} = -\frac{\ln\left(\frac{V_{oa}}{V_{oa,max}}\right)}{8c} \quad (6.11)$$

and

$$F_b = F \cdot \sin(b + a) = -\frac{\ln(V_{obn})}{8c} = -\frac{\ln\left(\frac{V_{ob}}{V_{ob,max}}\right)}{8c} \quad (6.12)$$

Thus,  $F_x$  and  $F_y$  can be calculated by the above equations.

### 6.1.3 Manufacturing the tensile stress sensors

The structure and the cost of the transducers are presented for the most well integrated stress sensor as illustrated in Figure 6.1c. Figure 6.6 shows the arrangement of a single sensing point. It can be observed that the tensile stress on the active core is caused by converting the applied force  $F$  using a bridge structure. The delay line air channel was made from three layers of 0.1 mm thick epoxy glass plane surface, connected together either by under heat compression or by epoxy resin. Two long rectangular cross section bars, made from fibre glass glued on top of the channel parallel to the delay line air channels to avoid pressure on them, were set on top of the MDL air channel to prohibit any touch of the MDL caused by any large force  $F$  applied on the device. Another approach for making such a structure is to machine a thicker epoxy glass plane surface, in order to make the channels between these long bars, thus offering a stiffer sensor structure. Such a structure is repeated in two dimensions: Air channels, parallel to each other are made for positioning an array of  $k$  delay lines and a number of  $(k+1)$  long bars are on top of them (either by glueing them on top of the air channels or machining the top epoxy glass level of the air channel sandwich). The long bars may have a structure along their length, like the one shown in Figure 5.6: rectangular pieces of

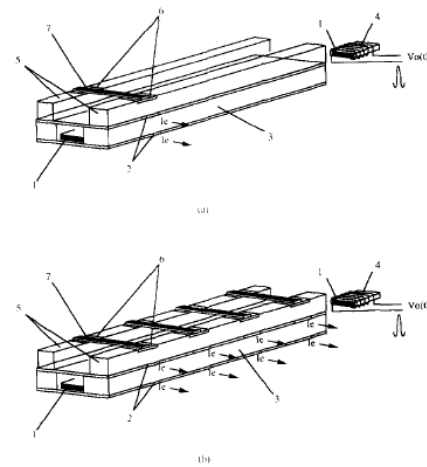


**Figure 6.6.** Sensor arrangement. (a) Discrete tensile stress sensor; (b) one-dimensional sensing array. (1) MDL, (2) Pulsed current conductors, (3) MDL 3. Delay line support, (4) Search or receiving coil, (5) Epoxy glass ribbons, used as supports of the active core, (6) Copper for soldering the active core, (7) Active core.

copper are set on top of the bars. The purpose of using these copper pieces is for soldering the ribbon active cores.

The ribbons are pre-stressed under a small tensile stress, i.e. 10 MPa before soldering, in order to avoid any change of geometry after the manufacturing process. A disadvantage of the soldering pre-stressed ribbons is that they become less sensitive in terms of magnetic permeability. After pre-stressing the strips, their positioning on top of the copper surface and soldering on the copper surfaces creates discrete sensing cores: each ribbon section between two long bars, withstands the same amount of tensile stress, which is equal to the initially applied stress. Any applied force  $F$  causing a tensile stress on it does not cause any stress or movement at the neighbouring ribbon sections, defined by the neighbouring long bars. An advantage of using pre-stressed ribbons is that the tensile stress, applied on the ribbon, caused at any sensing point due to any force is predictable.

In the case of the sensor of Figure 6.1 the pulsed current conductor can be fixed on top of the ribbon strip. It must be electrically insulated from the ribbon strip, although experimental observations show that there is almost no change of the response of the sensor if the long strip and the conducting surface are in touch. This can be explained by the fact that the resistivity of the copper is negligible compared to the one of the ribbon. This is one way to create the sensing points of the sensor. Another one is to use a long copper support for square active cores. So, by glueing the active cores on the copper support, we could use the active core support as the exciting pulsed current conductor. This type of sensor is not ideal in terms of long operation life time and accuracy of response, because the force  $F$  is also applied on the exciting conductor, so that any displacement caused on it results in non predictable changes of the magnetic flux in the delay line.

Manufacturing process of the sensor shown in Figure 6.3 is divided in two parts. The first one is the balance structure and the second one the sensing core structure. The balance structure can be realized by following wet etching lithography techniques for printed circuit boards. The method of making the sensing core structure is as above mentioned. The method of making the long strips is by machining an epoxy glass surface and positioning afterwards the small copper pieces, used for soldering the ribbon strip. Finally, the two plane structures are glued or connected by heating and pressing together. Following such a process, the sensor shown in Figure 6.7 can be built, by using two long bar-ribbon strip structures. Using such a structure in order to apply stress on the active core, the tensile stress can be calculated with respect to the applied force  $F$ .

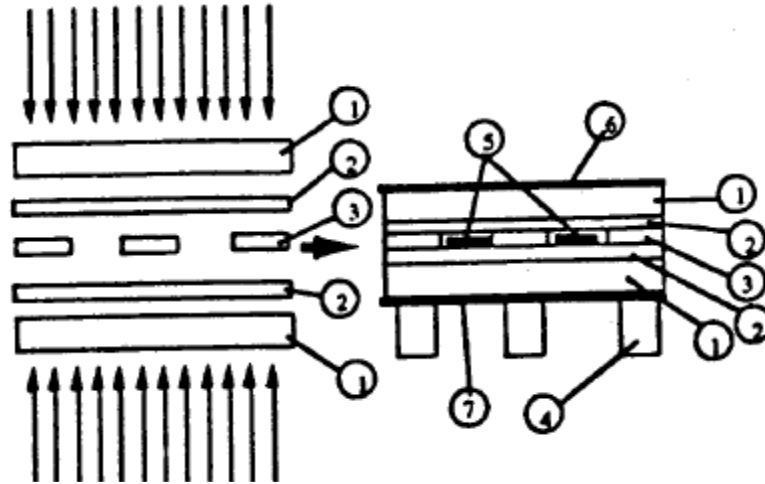


**Figure 6.7.** Basic procedure for manufacturing the beam force sensor. (1) 1.5 mm thick fiber glass bar orthogonal to the delay line, (2) 0.1 mm thick fiber glass planes, (3) 0.1 mm thick fiber glass bars for making the MDL channels, (4) Fiber glass bars parallel to the MDL, (5) MDL, (6) Compressible ribbon, (7) Stressable ribbon.

---

## 6.2 Pressure gauges

---

The idea of this type of sensor is based on the fact that the original elastic pulse is affected by any pressure applied on the elastic pulse point of origin PO or any other point of the MDL.

The basic idea of this sensor is shown in Figure 6.8. According to this arrangement, a delay line is positioned on a channel. The pulsed current conductor was made by etching a 0.1 mm thick fibre glass PCB layer in order to leave only a 1 mm wide straight copper line on it. This layer was the lowest and unmovable part of the MDL channel. Positioning the pulsed current conductor like that, we succeeded to avoid any change of the relative distance between conductor and delay line.

Applying no force on the channel, and transmitting pulsed current through the conductor, the detected output is  $V_0$ . If PO is the sensing point (point to apply pressure), then any force applied on it, should affect the acoustic signal. The way to apply a force on the MDL runs as previously: with respect to the same geometry, a force  $F$ , on the upper surface of the channel can cause a pressure on the MDL. It is expected

that the acoustic pulse should decrease as the applied force increases and should vanish under a minimum value of pressure, for given values of  $I_e$  and DC bias fields.

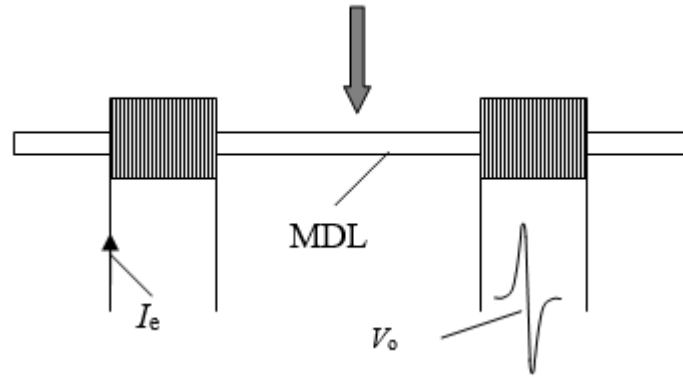


**Figure 6.8.** The basic principle of the MDL pressure gauge.

Magnetostrictive amorphous ribbons have been tested for geometry purposes. Among various experimental results, an indicative response is hereinafter illustrated concerning  $Fe_{78}Si_7B_{15}$  as-cast amorphous ribbons. The dependence of  $V_o$  on the applied force at the sensing point for these ribbons under various values of applied pulsed current  $I_e$ , is given in Figure 6.9.

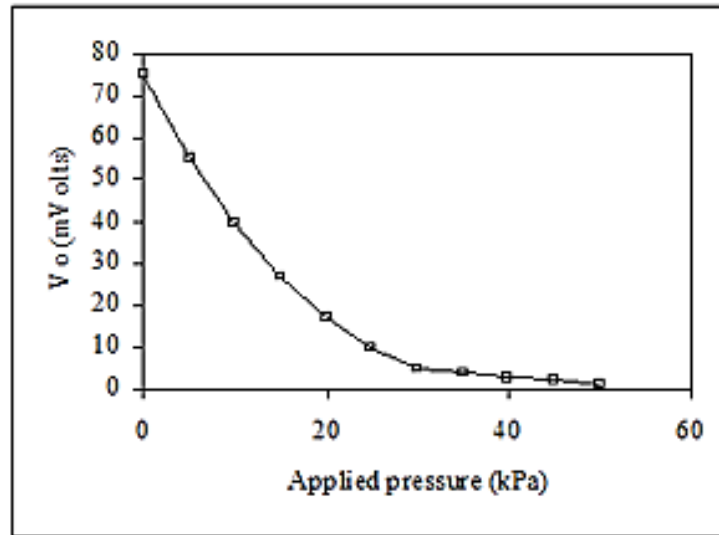


**Figure 6.9.** Response of the MDL pressure gauge.

It is observed that the output signal was decreased from its maximum value  $V_o$  down to zero, for a range of forces from zero up to 3 N respectively. For the given arrangement with the sensing point 40 cm far

from the receiving coil, the smallest detectable force was 0.1 N. The detected  $V_o$  was found to be exponentially dependent on the applied load:

$$V_o(F) = V_o e^{-c_p F} \quad (6.13)$$

where  $V_o(F)$  and  $V_o$  are the peak values of the MDL output under load and the maximum MDL output respectively. Coefficient  $c_p$  for the tested ribbons was determined equal to  $\sim 0.35 \text{ N}^{-1}$ . The exponential response of the sensor can be explained by the fact that tension and compression of an acoustic stress, propagating in a rectangular cross section solid waveguide, decay exponentially with the surface tension or the applied force on the surface of the waveguide.

The experiment was carried out by increasing and decreasing the magnitude of the applied force  $F$ . The resulting output was the same for increasing and decreasing the applied load, showing that the hysteresis of the sensor is negligible within the limits of the experimental set-up. It is noted that this sensor is named pressure gauge, since it transfers the applied load in pressure, dependent on the area the said force is applied to.

The problem of the nonuniformity still exists in this type of sensor too and can also be solved by the methods presented in Chapter 3, especially by following the law of normalization.

---

### 6.2.1 Distribution pressure sensors based on this principle idea

---

This kind of discrete pressure sensor could be used as the basis for a force distribution sensor. The reason is as follows: it is assumed that two forces  $F_1$  and  $F_2$  are applied on two sensing points  $A_1$  and  $A_2$ , defined by the crossing points of the MDL and two conducting wires  $C_1$  and  $C_2$ , vertical to the MDL as shown in Figure 6.10, in distances  $x_1$  and  $x_2$  from the receiving coil respectively. The elastic pulse caused by the conductor  $C_1$ , changes due to the two forces  $F_1$  and  $F_2$ , so that the pulsed voltage output at the search coil is related to  $F_1$  and  $F_2$ . The elastic pulse caused by the conductor  $C_2$ , changes only due to the force  $F_2$ .

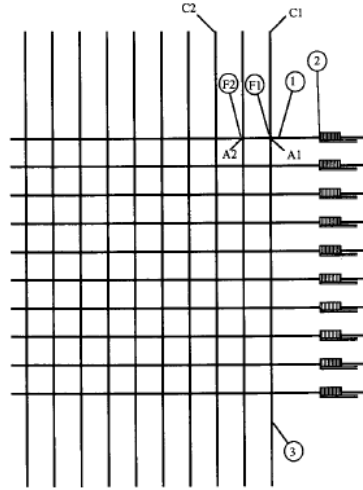


**Figure 6.10.** A pressure distribution sensor based on the MDL pressure gauge. (1) MDL, (2) Search coil, (3) Pulsed current conductor.

From the experimental results, the pulsed voltage output  $V_o$  follows an exponential dependence on the applied force  $F$  at the sensing point or the elastic pulse point of origin; taking into account the attenuation factor of the given MDL material as  $b$ , the propagating elastic pulse  $S(t, F_1)$  caused at a PO at a distance  $x$  from the receiving coil is given by:

$$S(t, F_1) = S_o \left( t - \frac{x}{v} \right) e^{-bx} e^{-c_p F_1} \quad (6.14)$$

where  $S_o(t)$  is the elastic pulse caused by the pulsed current at the PO under no applied force and  $v$  is the longitudinal sound velocity of the MDL. So, the magnitude of the acoustic stress  $S'_t$ , originated at the sensing point  $A_2$  that arrives at the sensing point  $A_1$  is given by:

$$S'_t = S_{o2} \left( t - \frac{x_2 - x_1}{v} \right) e^{-b(x_2 - x_1)} e^{-c_p F_2} \quad (6.15)$$

At this point  $S'_t$  is also to change due to the force  $F_1$ . Thus, the magnitude of the elastic pulse originated at  $A_2$  passing also through  $A_1$  and finally arriving at the receiving coil,  $S_2(t)$  is given by:

$$S_2(t) = S_{o2} \left( t - \frac{x_2}{v} \right) e^{-b(x_2)} e^{-c_p (F_1 + F_2)} \quad (6.16)$$

Thus, the corresponding peak voltage output  $V_{o2}(F)$ , assuming that the attenuation is negligible, is given by:

$$V_{o2}(F) = V_{o2} e^{-c(F_1 + F_2)} \quad (6.17)$$

where  $V_{o2}$  is the detected peak output corresponding to  $A_2$  under zero applied forces. In a similar way, the magnitude of the acoustic stress originated at  $A_1$ ,  $S_1(t)$ , arriving at the receiving coil, is given by:

$$S_1(t) = S_{o1} \left( t - \frac{x_1}{v} \right) e^{-bx_1} e^{-c_p F_1} \quad (6.18)$$

and consequently, the corresponding value of  $V_{o1}(F)$ , assuming that the attenuation is negligible, is given by:

$$V_{o1}(F) = V_{o1} e^{-cF_1} \quad (6.19)$$

where  $V_{o1}$  is the peak voltage output corresponding to  $A_1$ , in the absence of any applied force. From these equations we have:

$$F_1 + F_2 = \frac{\ln\left(\frac{V_{o2}}{V_{o2}(F)}\right)}{c} \quad (6.20)$$

and

$$F_1 = \frac{\ln\left(\frac{V_{o1}}{V_{o1}(F)}\right)}{c} \quad (6.21)$$

So, by measuring  $V_{o1}$ ,  $V_{o2}$ ,  $V_{o1}(F)$ ,  $V_{o2}(F)$ ,  $x_1$  and  $x_2$ , one can detect  $F_1$  and  $F_2$ . There is a restriction concerning the magnitudes  $F_1$  and  $F_2$ : they have to be less than the load vanishing the output signal.

This method could also be applied for a number of sensing points  $m$ . Thus, having positioned  $m$  conductors  $C_m$  at  $m$  different positions of the delay line, so that  $m$  sensing points  $A_m$  are defined along the length of the line, the  $A_j$  sensing point is defined as the region of the MDL on top of the  $C_j$  – MDL intersection, as shown in Figure 6.10. Having stored the output signal  $V_{oj}$  in the absence of applied load and detecting the corresponding  $V_{oj}(F)$  under load  $F$ , when the array is in use, the corresponding relation between  $V_{oj}(F)$  and  $V_{oj}$  is given by:

$$V_{oj}(F) = V_{oj} e^{-c(F_j + F_{j-1} + \dots + F_2 + F_1)} \quad (6.22)$$

Thus

$$V_{o1}(F) = V_{o1} e^{-c(F_1)}$$

$$V_{o2}(F) = V_{o2} e^{-c(F_2 + F_1)}$$

$$V_{o3}(F) = V_{o3} e^{-c(F_3 + F_2 + F_1)}$$

.

$$V_{ok}(F) = V_{ok}e^{-c(F_k+F_{k-1}+\dots+F_2+F_1)}$$

$$V_{om}(F) = V_{om}e^{-c(F_m+F_{m-1}+\dots+F_2+F_1)}$$

and therefore, the corresponding values of the forces  $F_m$  are given by:

$$F_1 = \frac{\ln\left(\frac{V_{o1}}{V_{o1}(F)}\right)}{c}$$

$$F_2 = \frac{\ln\left(\frac{V_{o2}}{V_{o2}(F)}\right)}{c} - F_1$$

$$F_3 = \frac{\ln\left(\frac{V_{o3}}{V_{o3}(F)}\right)}{c} - (F_2 + F_1)$$

$$F_k = \frac{\ln\left(\frac{V_{ok}}{V_{ok}(F)}\right)}{c} - \sum_{j=1}^{k-1} F_j \quad (6.23)$$

$$F_m = \frac{\ln\left(\frac{V_{om}}{V_{om}(F)}\right)}{c} - \sum_{j=1}^{m-1} F_j \quad (6.24)$$

By applying such a procedure, the force distribution can be determined as follows: place pulsed current is transmitted at the conductor closest to the receiving coil  $C_1$  and the force  $F_1$  is calculated. Afterwards, conductors  $C_2, C_3, \dots, C_m$  are sequentially excited and forces  $F_2, F_3, \dots, F_m$  are correspondingly calculated. All this procedure can be applied in the assumption that applied forces are small enough not to cause the detected output signals to vanish.

The total dimensions of a discrete sensor could be kept down to 3 cm long, 1 cm wide and 1 cm high one, by having the one end of the MDL inside the receiving coil. A major target is the use of a solid structure of the MDL - conductor arrangement, which involves the use of such substrates with given Young's modulus to avoid the acoustic pulse distortion during its propagation.

This simple type of sensor can compete in sensitivity with other types of pressure gauges and strain gauges. Such a force sensor has a sensitivity of 0.1 V/N without electronic signal conditioning.

---

### 6.3 Force digitizers

---

The principal idea of a single force digitizing element is shown in Figure 6.11. An MDL (1) is positioned on an epoxy glass substrate (2) of a rectangular cross-section area. An exciting conductor (3) is placed orthogonal to the MDL close to the one end of it. A short coil (4) is placed around the MDL at the one end it, close to the exciting conductor. The two ends of the MDL are well terminated by using latex adhesive (5) in order to eliminate any reflections. So, by applying a pulsed current, transmitted through the conductor, a pulsed voltage is received from the short coil, also named in this case original pulse, having a peak amplitude  $V_o$ .

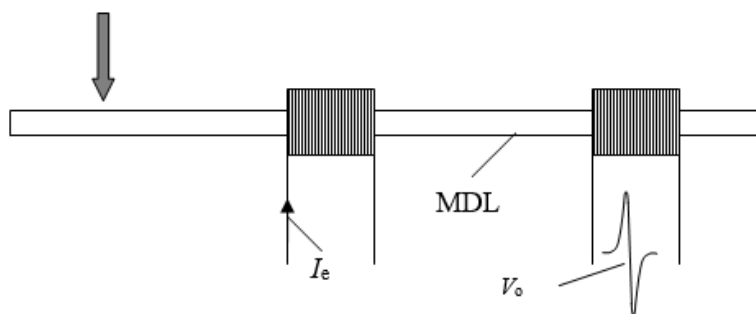


**Figure 6.11.** Schematic of the force digitizing sensing element.

A smooth-ended stylus of any kind of material can be used to cause the reading information. If it attaches to and presses the delay line at any position at least 3 cm away from the exciting conductor, in order to avoid any interference with the original pulse, an acoustic reflection is caused at this point. The magnitude of such a reflection depends on the force applied on the MDL as well as on the material forcing the MDL. The reflected acoustic pulse is also detected by the short coil and the delay time between the peak value of the original and the reflected signal defines the distance between conductor and digitizing point, while the amplitude of the reflection is monotonically related to the applied force. Such a principle can be used for sensing the applied force at a single sensing position of a delay line.

Magnetostrictive amorphous ribbons and wires have been tested for such a sensor. Various experimental results indicated that amorphous ribbons demonstrated the most repeatable sensor performance, for geometry reasons. An indicative dependence of the reflected voltage output  $V_r$  on the applied load concerning  $\text{Fe}_{78}\text{Si}_7\text{B}_{15}$  as-cast amorphous ribbon and a  $5 \times 15 \text{ mm}^2$  loading epoxy glass area is illustrated in Figure 6.12. It is observed that the reflected signal starts from zero and increases to its maximum value  $V_{r0}$  following an exponential dependence:

$$V_r(F) = V_{r0}(1 - e^{-c_r F}) \quad (6.25)$$

where  $c_r$  is a constant dependent on the material used as a substrate and the MDL material.  $V_{r0}$  is close to the amplitude of  $V_o$ , provided that the attenuation factor and the distance between load and receiving coil are relatively small. For the given arrangement and used materials, concerning sensing point 40 cm from the receiving coil,  $c_r$  equals  $6.5 \text{ N}^{-1}$ , while the smallest detectable load was 1 mN.

Taking into account the attenuation factor  $b$  of the MDL, the force digitizer response can be given by:

$$V_r(F) = V_{r0} e^{-bx} (1 - e^{-c_r F}) \quad (6.26)$$

where  $x$  is the distance between loading point and receiving coil. The exponential response of the sensor is also explained due to the exponential decay of a propagating elastic pulse in a waveguide.

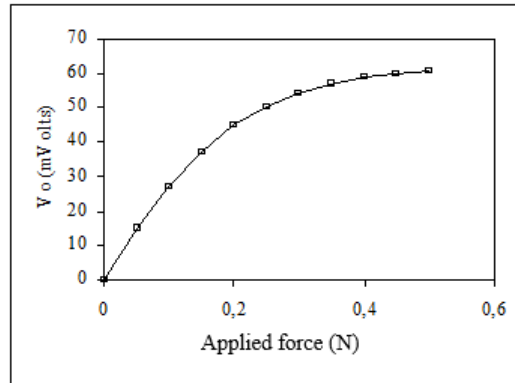


**Figure 6.12.** The reflection response on force of the force digitizing sensing element of Figure 6.11.

Since the operation of such a sensor is based on acoustic reflections, the response of the sensor is expected to be absolutely reversible, since the MDL loading is operated in the elastic region of the Hook's law corresponding to its linear stress-strain response, thus resulting in non-hysteretic response. Actually, an absence of hysteresis was observed within the limits of the experimental set-up (12 bit analog to digital conversion), but it is predicted that no hysteresis can be measured in such a system provided that the MDL is loaded in the elastic and reversible region of the stress-strain response. As soon as such a limit is overpassed, the response of the sensor is not expected to be non-hysteretic anymore. In fact, overloading the MDL results in a permanent reflection signal, which is the result of plastic deformation or permanent local stresses in the material.

Although the materials used for this type of sensor suffer from magnetoelastic nonuniformity, the sensor is free from this problem. The reason is the mode of operation according to which the reflected signal is only due to the mechanical properties. As long as the MDL operates in its linear region of the stress-strain response, the sensor response is to be uniform. The response of this sensor is an exponential function of the applied load. So, by knowing the values of the coefficients  $b$  and  $c_r$ , the load  $F$  can be calculated from the MDL output  $V_r$ , corresponding to the reflected signal. Considering the attenuation factor negligible, the load  $F$  is given by:

$$F = \frac{\ln\left(\frac{V_{ro}}{V_{ro}-V_r}\right)}{c_r} \quad (6.27)$$

The spatial resolution of the sensor can easily reach the 0.1 mm in the MDL axis. Since, the longitudinal sound velocity of the MDL is of the order of  $\sim 5 \text{ mm}/\mu\text{s}$ , a 0.1 mm spatial resolution is achievable by using a 100 MHz oscillator and a delay time counter.

If a two dimensional load digitization is desired, an array of MDLs can be used. In this case, the spatial resolution in the other direction is dependent on the width of the MDL. For this purpose, amorphous wires can be used instead of ribbons. Monitoring the response of  $\text{Fe}_{78}\text{Si}_7\text{B}_{15}$  as-cast amorphous wires, one can also observe the absence of hysteresis and the exponential response of the sensor output.

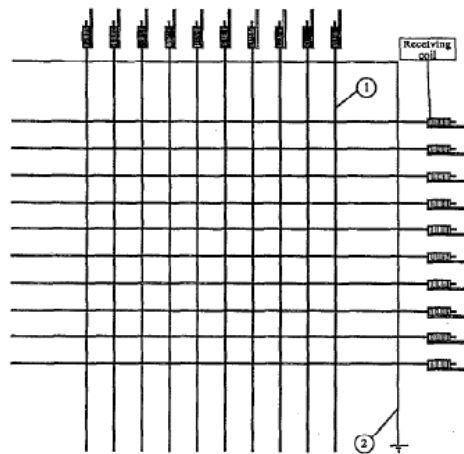


**Figure 6.13.** Force digitizing array sensor. (1) MDL, (2) Pulsed current conductor.

Spatial resolution may be significantly improved by using another array of MDLs perpendicular to the initial one, excited by the same conductor turned by  $90^\circ$ , as illustrated in Figure 6.13. A detail of such a structure is given in Figure 6.14. Of course, following such a structure, spatial resolution is not uniformly spread on the digitizer surface. The repeatability and life time of such an arrangement depends on the MDL substrate, the layer used to transducer the applied load on the MDL surface and the MDL itself.

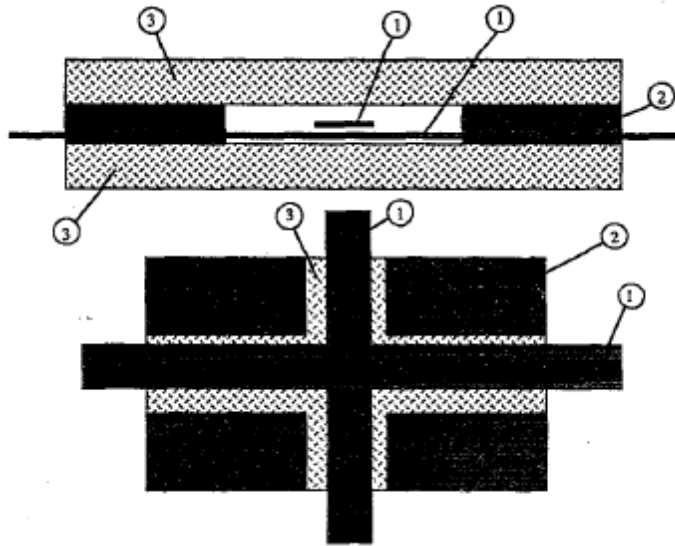


**Figure 6.14.** Detail of the sensing element of the digitizer: ( 1) MDL, (2) MDL substrate, and (3) substrate used to apply transform pressure to the line.

Such a digitizer also offers some other advantages. A critical advantage is the ability of this cordless digitizer to simultaneously detect the position and the amplitude of a load applied on a surface. The delay time of the reflected signal defines the position of the applied load, while the amplitude of the detected reflection pulse determines the amount of this load. One application of such a digitizer can be a signature recognizer, by observing not only the path of signing but also the pressure applied at each point of the signature in real time, which is a certain characteristic of any individual person. Another advantage is its size. It can be extended as large as an A<sub>0</sub> page size, without significant increase of its cost. The limitations of the size of the digitizer are the maximum length of the MDL, allowing negligible or small attenuation, and the attenuation factor itself.

One technique to physically eliminate the acoustic attenuation factor is the use of receiving coils in both ends of the MDL. Doing that, the voltage outputs  $V_{r1}$  and  $V_{r2}$  at the two coils respectively, corresponding to one single reflection are generally un-equal due to the attenuation factor. But,  $V_{r1}$  and  $V_{r2}$  are given by:

$$V_{r1}(F) = V_{r0}e^{-bx}(1 - e^{-c_rF}) \quad (6.28)$$

and

$$V_{r2}(F) = V_{r0}e^{-by}(1 - e^{-c_rF}) \quad (6.29)$$

where  $V_{r0}$  is the same for both coils due to the MDL operation in the linear region of the stress-strain curve, provided that the two coils are identical. But  $x + y = L$ , where  $L$  is the distance between the two coils. Thus,

$$V_r(F) = \sqrt{V_{r1}V_{r2}} = V_{r0}e^{-\frac{bL}{2}}(1 - e^{-c_r F}) \quad (6.30)$$

On the other hand, there are some limitations for this force digitizer. One target as in the case of the pressure gauges is the use of a solid structure of the MDL - conductor arrangement, facilitating substrates with a given Young's modulus to avoid the acoustic pulse distortion during its propagation. Thus the life time of the sensor is increased. Another limitation is the typical limitation of all MDL sensors, which is the delay in detecting a signal, corresponding to the velocity of the propagating elastic pulse.

Using amorphous wires as digitizers in the as-cast state and after stress-current annealing can result in an increase of sensitivity, but mainly in a more accurate exponential fitting of the reflected elastic pulse dependence on the applied load.

All the reported experiments concern the response of a single sensing point of the digitizer. A vital information missing from the results of this single point response experimental set-up is the response of the wire along its length, under a given pressure on it. For this purpose the following experiment was performed. A stainless steel cylinder of 10 mm diameter and 10 mm length, fixed at the end of a spring with its axis orthogonal to the MDL axis in order to roll it on the MDL surface. Displacing the free end of the spring downwards one could modify the applied pressure on the MDL. A displacement  $x$  of the spring resulted in a force  $F=kx$  on the MDL, where  $k$  is the constant of the spring. The spring-pressing cylinder system was fixed on a linear motion system in order to move it along the MDL. The delay line was set on a flat surface so that adjustment of the spring deformation was resulting in uniform force applied on the MDL. The position of the pressing cylinder was detected by using a position detector of 1  $\mu\text{m}$  sensitivity and 6  $\mu\text{m}/\text{m}$  accuracy. A 100 Msamples/second digital oscilloscope was used to detect the delay of the peak of  $V_r$ . It was found that the delay time between the two detected voltage outputs was linearly dependent on the distance between exciting conductor and pressing cylinder, with undetectable error within the limits of our experiment. So, using 100 M samples/second sampler one can repeatably obtain a 0.1 mm resolution of the MDL axis. We have also run experiments concerning stress current annealed wires for various forces from 0.1 N to 1 N and we found that the dependence of the  $V_r$  amplitude on the

distance between the pressing cylinder and the receiving coil was flat for distances between the pulsed current conductor and the rolling cylinder from 5 cm up to 90 cm.

---

## **6.4**     *Load cells and torque meters*

---

Load cells and torque sensors have a significant share in the international sensor market. Many instrumentation arrangements can be realized with respect to them, in industrial, medical and laboratory environments. New sensing principles and devices offering better characteristics and/or lower cost are welcome in this competent field. Advances in magnetic materials allow engineers to work towards this direction, mainly taking advantage of the magneto-elastic properties of the recently developed soft magnetic materials with tailorable properties. The robustness and miniaturization of these sensors are two of the key points for the viability of these devices. Considering material technology for sensor development and characterization, one has to take into account two main families: silicon and magnetic sensors. Bearing in mind the zero displacement required for sensors based on magnetic materials to detect stress, the development of stress centre sensors based on magnetic materials is in the of our focus. Searching for applications of such magnetic materials, we mainly paid attention to the development of sensors based on the MDL technique. Targeting the development and the possible use of amorphous wires in load and torque sensing applications, we have developed load meters and torque sensors based on the MDL technique. The implementation of the given circular cross sectional type of the wire has been selected for symmetry reasons of load and torsion application. The use of amorphous alloys has been selected for mechanical robustness purposes. These sensors are also compared to load cells and torque meters based on the magneto-inductive principle.

---

### 6.4.1 The load cell

---

The schematic of a load cell using the MDL technique is illustrated in Figure 5.15 and its operation in Figure 6.16 (a). A metallic outer cell (1) is used for sensor encapsulation as well as for transducing the applied force to the sensing material. This cell has preferably but not exclusively a cylindrical shape, with a means of fixing the used wire at its two ends, one end being fixed in position (2) and the other being adjustable (3). The non-movable fixture (2) has a coil which is used for excitation and receiving purposes and covered

by permanent magnetic cylinder (4) and a soft magnetic alloy (5) for shielding purposes, both of them being free from stress in order to control the biasing field at the elastic pulse region of origin and avoid the effect of the ambient field on the wire. The exciting-receiving coil (6) is used for pulsed current transmission at the corresponding region of the magnetostrictive wire, which causes the generation and propagation of an elastic wave by means of the magnetostriction effect propagating along the length of the wire.

The wave is reflected at the two ends of the wire so that it can be detected by the same coil due to the inverse magnetostriction effect. The other fixing means (3) can be adjustable with respect to its micro-position regulation. The pre-stressed magnetostrictive wire (7) is fixed at the two fixing means, the tensile stress along its length being controllable by the fixing means (3). The outer cell also

hosts the electronic circuitry used for the excitation of the magnetostrictive wire (8), obtained by a pulse generator (i.e. an LM 555) and a high frequency bandwidth FET, as well as the circuitry for the detection and conditioning of the sensor output (9), which is obtained by means of a positive and a negative peak holder of the MDL pulsed voltage output  $V_o$ . The input of the sensor is the applied force  $F$  on the outer cell, while its output is the sampled and held positive and negative peaks of the MDL pulsed voltage output  $V_o$  at the output of the signal conditioning circuitry (9).

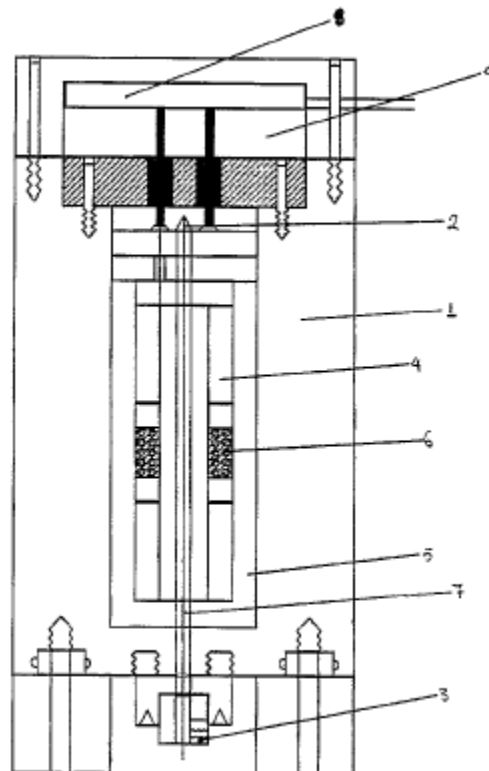


**Figure 6.15.** Schematic of the load cell and torque meter sensing element.

Under no applied load, the pre-stressed magnetostrictive wire demonstrates a reduced magneto-mechanical coupling factor due to the tensile stress along its length and consequently the generated pulsed voltage output across the ends of the receiving coil is not the maximum possible. The physical meaning of the magneto-mechanical coupling factor is the ease or difficulty of the magnetic dipoles of the magnetostrictive wire to rotate following the externally applied magnetic field. When a pressing or compressive force  $F$  is applied to the cell, it causes a reduction of the tensile stress along the length of the wire. So, the magneto-mechanical coupling factor of the wire increases and the MDL pulsed voltage output increases respectively. The saturation of the sensor in this case occurs when the microstrain due to the compressive load  $F$  releases all the pre-applied tensile stress on the wire. In such a case the MDL pulsed voltage output cannot increase any more. If a load in the opposite direction,  $-F$ , is applied on the cell, additional tensile stress is caused in the outer cell and consequently along the length of the magnetostrictive wire, which further reduces its magneto-mechanical coupling factor, resulting in a further reduction of the sensor output. The saturation of the sensor in this case occurs when the tensile stress in the wire is maximized, so that the magneto-mechanical coupling factor is minimized or even reduced to zero. Due to the monotonic response of the magnetostrictive wire under stress, it is predicted that applying positive and negative force on the load cell results in a respective increase and decrease of the sensor output.

---

### 6.4.2 The torque meter

---

The schematic of the torque meter using the MDL technique is illustrated in Figure 5.15 and its operation in Figure 6.16 (b). A three-part outer cell (1) is used for the sensor encapsulation as well as for transmitting the applied torque to the sensing material. These three cells are preferably but not exclusively cylinders, connected with a horizontal bronze bearing (2) in order to allow torsional stress to be applied on the magnetostrictive wire. The outer cylinder supports the ends of the sensing material by means of two threaded holes. A stress-free magnetostrictive wire (3) is fixed at the two ends of the outer cell by means of two fixing screws (4), allowing the controllable realization of tensile stress along the length of the wire. The outer cylinder also contains the exciting/receiving coil (5), which is covered by a permanent magnetic cylinder and a soft magnetic alloy (6) for shielding purposes, in order to avoid the ambient field effect on the wire. The use of the exciting/receiving coil is identical to the above mentioned coil of the load cell

based on the MDL technique. The outer cells also contain an electronic circuitry for the excitation of the MDL wire (7) and the circuitry for the detection and conditioning of the sensor output. Both circuits are the same as for the above mentioned load cell based on the MDL technique. The input of the sensor is the applied torque  $T$  on the two outer cells, while the output is the sampled and held positive and negative peaks of the MDL pulsed voltage output  $V_o$  at the output of the signal-conditioning circuitry.

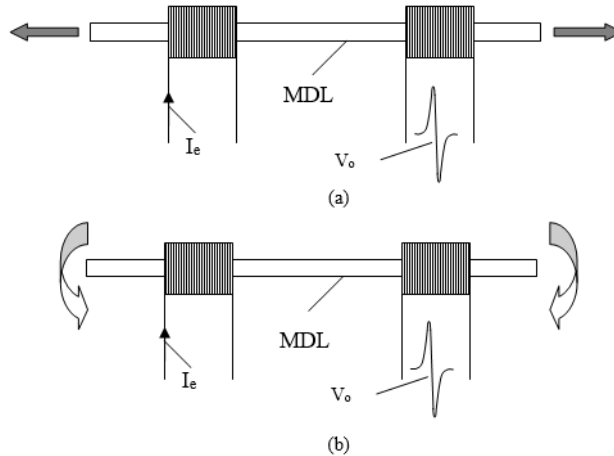


**Figure 6.16.** Operation of the load cell (a) and torque meter (b).

Under no applied torque, the unstressed magnetostrictive wire displays a maximum magneto-mechanical coupling factor and consequently the generated pulsed voltage output at the ends of the receiving coil is the maximum possible one. When a clockwise or anti-clockwise torsion  $T$  is applied to the outer cells of the sensor, it causes a reduction of the magneto-mechanical coupling factor due to the reduced ability of the magnetic dipoles of the wire to be oriented towards the direction of the externally applied field. Thus, the pulsed voltage output of the MDL decreases. Theoretically speaking, no saturation of the sensor can occur in this case, because the magneto-mechanical coupling factor reduces asymptotically to zero: the ability of the magnetic dipoles to be oriented towards the direction of the externally applied field does not vanish as in the case of the externally applied tensile stress.

The effect of stress in both cases of load cell and torque meter can be seen as an effective field applied along the axis of the applied stress, provided that the material is positively magnetostrictive and opposite in sign if it is negative magnetostrictive. Thus, more stress causes a magnetic state closer to saturation for

positive magnetostrictive materials and the opposite for the case of negative magnetostrictive materials. Thus, saturation can be reached for tensile stress, but never for torsional stress.

---

### 6.4.3 Experiments

---

The tested materials, as above mentioned, were magnetostrictive wires. Among various tested compositions the Fe-rich positive magnetostrictive amorphous wires illustrated the best performance. Indicative results are hereinafter shown, concerning Fe<sub>78</sub>Si<sub>7</sub>B<sub>15</sub> wires in the as-cast form, after stress-relief process via thermal treatment in 300°C for 30 minutes in inert atmosphere, as well as after magnetic annealing under the same temperature conditions and the simultaneous presence of magnetic field of ~5 kA/m along the length of the wire. Field was kept during 1°C/min slow cooling.

An indicative dependence of the load cell response on applied force, using amorphous Fe-rich wire is illustrated in Figure 6.17. Figure 6.18 illustrates a comparison of the load cell response for ribbon, wire and glass covered wire. Figure 6.19 shows a typical torsion dependence of an amorphous as-cast wire, while Figure 6.20 shows a comparison between amorphous wire and a glass covered wire, used for torsion measurements. In all cases the sensor response is monotonic and unhysteretic within the limits of the experimental set-up, while in the case of the as-cast tested wire, a surprisingly linear behaviour may be observed. From these results it can be seen that the torque meter response remains monotonic and unhysteretic, despite the non-monotonic behaviour of Fe-rich amorphous wires under torsional stress. This happens because wires have been pre-torsioned before being used above a torsion threshold, after which the torsional stress dependence of MDLs becomes monotonic.

Since the only stressed parts of the load cell are the outer cell and the magnetostrictive wire, any applied force on the outer cell of the sensor results in tensile stress only on these two elements:

$$\sigma(F) = \frac{F}{S} = \frac{F}{\frac{\pi}{4}((d_e^2 - d_i^2) + d_w^2)} \quad (6.31)$$

where F is the applied force,  $\sigma$  is the applied tensile stress, S is the sum of the cross section of the outer cell and the sensing wire,  $d_e$  and  $d_i$  are the external and internal diameters of the outer cell and  $d_w$  is the diameter of the magnetostrictive wire. Since  $d_w \ll d_e, d_i$ , the above mentioned equation becomes:

$$\sigma(F) = \frac{F}{S} = \frac{F}{\frac{\pi}{4}(d_e^2 - d_i^2)} \tag{6.32}$$

The range of the applicable force  $F_{max}$  on the load cell can be calculated, taking into account the maximum applicable stress for repeatable stress results on such wires is  $\sigma_{max}$ :

$$F \frac{\pi x(2d_e + x)}{4} max_{max} \tag{6.33}$$

where x is the thickness of the outer cell of the load cell.

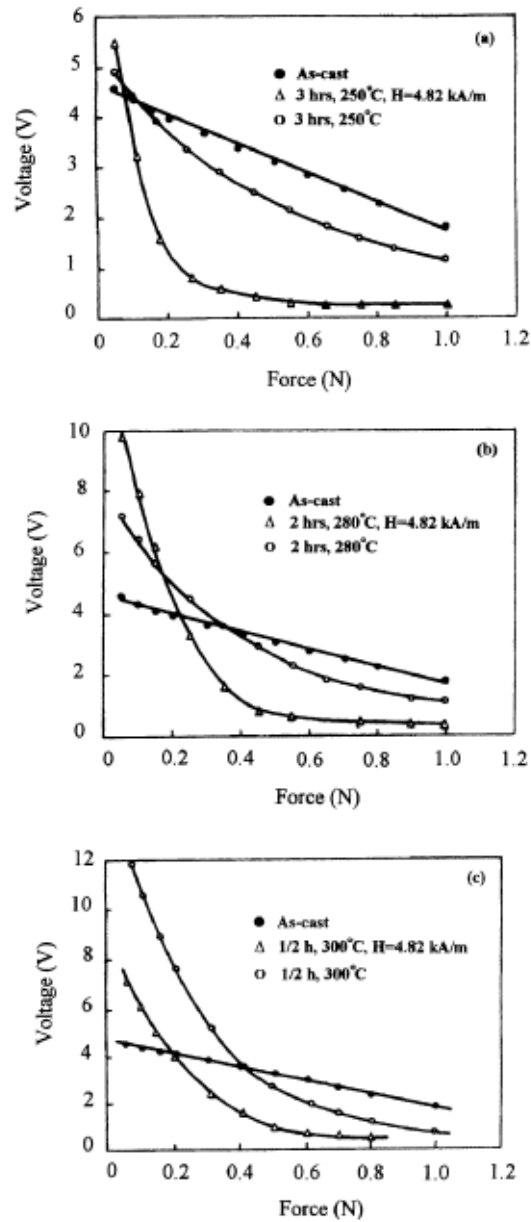


Figure 6.17. Load response of amorphous Fe-rich wires after different treatment.

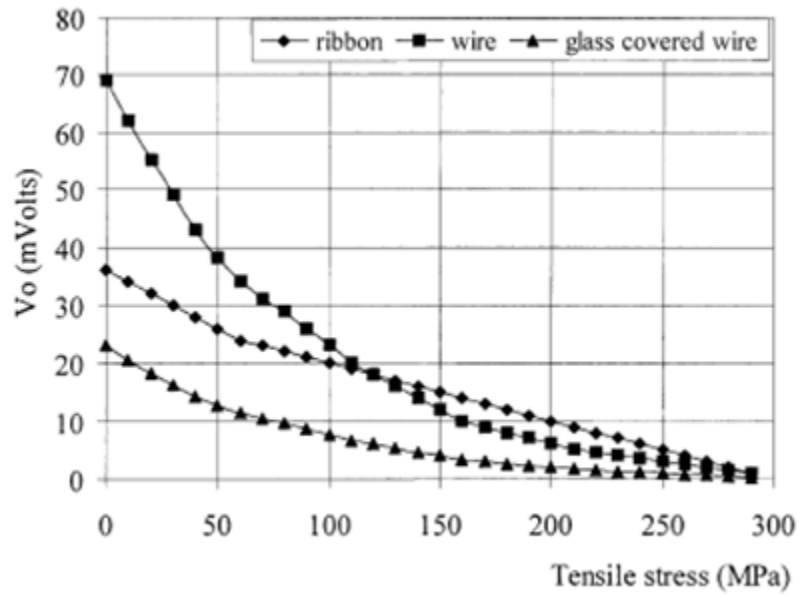


Figure 6.18. Dependence of the MDL pulsed voltage output  $V_o$  on the applied stress using amorphous ribbon, wire and glass covered wire.

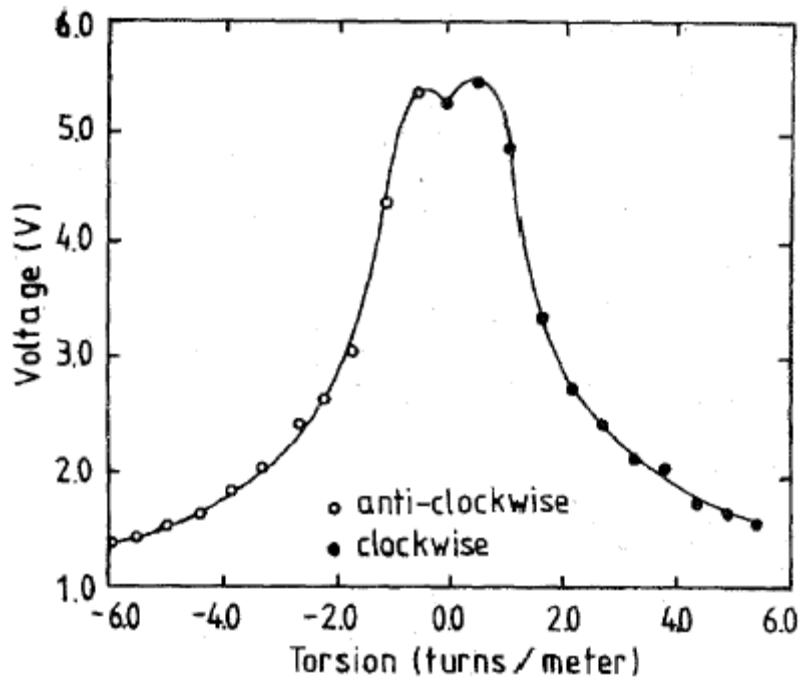


Figure 6.19. A typical MDL response on the applied torsion using amorphous wire.

As an example if  $\sigma_{\max} \sim 300$  MPa, then for  $d_e = 20$  mm and  $x = 1$  mm results in  $F_{\max} \sim 10$  kN. This tensile stress is transduced to the magnetostrictive wire and responsible for the change of the magnetomechanical coupling factor. The response of the as-cast and annealed wires follows a linear and exponential dependence respectively:

$$V_{ac}(F_w) = V_o - aF_w e^{-bF_w} \quad (6.34)$$

and

$$V_a(F_w) = V_o e^{-bF_w} \quad (6.35)$$

where  $V_{ac}(F_w)$  and  $V_a(F_w)$  are the as-cast wire and annealed wire dependence on force,  $V_o$  is the MDL response under unstressed conditions,  $F_w$  is the force applied on the wire and  $a, b > 0$ . Such behaviour can be understood, considering the applied force  $F_w$  as an effective field, polarizing further the magnetostrictive material towards its axis. The applied force in the case of the linear response can be calculated from  $F_w = \frac{V_o - V_{ac}(F_w)}{a}$ , while in the case of annealed wires the applied force can be respectively calculated from  $F_w = \frac{\ln V_o - \ln(V_a(F_w))}{b}$ . Both expressions can be given by analog or digital electronic circuitry for read-out purposes.

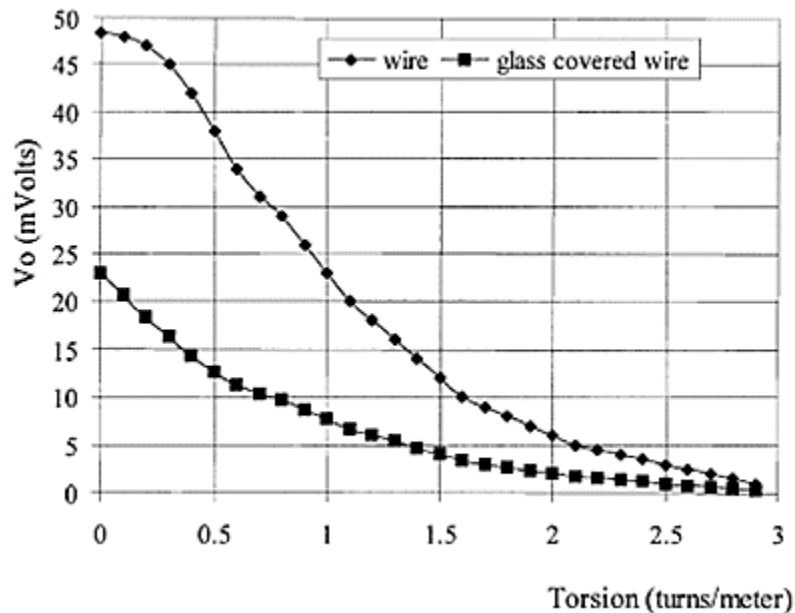


**Figure 6.20.** Dependence of the MDL voltage output  $V_o$  on the applied torsion using amorphous wire and glass covered wire.

The control of the range of the measurable load, by controlling the diameter and thickness of the outer cell is a major advantage of this cell. Furthermore, an auto-calibration procedure may also be realized by monitoring the pre-operation applicable stress on the wire.

The sensitivity of the load cell is  $\sim 50$  N/V for the as-cast wire, improved to  $\sim 10$  N/V for field annealed wires. The sensitivity of the torque meter is  $\sim 1^\circ/\text{mV}$ , improved to  $\sim 0.2^\circ/\text{V}$  after a field annealing. This sensitivity can be further improved by oversampling techniques. The main reason explaining the sensitivity improvement after magnetic annealing is the magnetic noise reduction due to the more uniform arrangement of the magnetic domains in the outer cell of the wire. The stress dependent sensitivity vanishes for stresses on the wire larger than 500 MPa or  $\sim 5$  N for a wire diameter  $\sim 0.12$  mm. The sensitivity of these materials in stress is much higher, does not need bringing techniques and therefore is advantageous with respect to the given state of the art of resistive strain gauges.

The repeatability and reproducibility of these sensors mainly depends on the properties of the used magnetostrictive materials. These properties have been analyzed in a previous Chapter. The robustness of the materials is also a major parameter, dominating the sensor lifetime, mainly dependent on the magnetostrictive material lifetime. Therefore, although the annealed amorphous Fe-rich wires are advantageous in terms of sensitivity, in some cases where high lifetime and repeatability in harsh environments are required, the use of as-cast Fe-rich wires is suggested. An addition of  $\sim 2\%$  Cr may help in the anti-corrosive protection of these wires. The glass covered magnetostrictive wires may also be the solution for high sensitivity and lifetime, since they are able to operate as MDLs after high frequency current annealing, as analyzed in a previous Chapter.

The sensors consumption is of the order of 10 mW in the case of as cast  $\text{Fe}_{78}\text{Si}_7\text{B}_{15}$  wires, which is improved to  $\sim 2$  mW after stress-current annealing. The sensor consumption drops below 100  $\mu\text{W}$  for carefully field annealed amorphous wires. This is achieved by tailoring, i.e. making sharper, the  $\lambda(H)$  function of the wires. A major problem of the sensors is their strong dependence on ambient magnetic fields. This problem may be reduced by shielding, but it can be eliminated by using a smart sensing system, in which the field is calculated simultaneously with the applied stress and then, the field contribution is deduced from the total sensor response. According to this technique, the MDL set-up is also operated in another magnetic mode or other magnetic modes, namely magneto-inductive or domain wall nucleation and propagation arrangement, so that the reading of two or three physical inputs respectively can be measured simultaneously.

A major competitor of the MDL based stress sensors is the magneto-impedance (MI) technique. Results obtained by using the MDL and the MI technique in wires [216] illustrated that the force or tensile stress response is more sensitive in MDLs and torque response is more sensitive in the MI technique. A disadvantage of MDLs may be regarded the presence of coil, thus making difficult and probably more expensive the implementation of this technique for stress sensor production.

---

## 6.5 *Thin film thickness sensors*

---

The fifth and final type of stress-mass sensors based on the MDL technique is a thin film thickness measurement, during film production. According to this new set-up, the MDL arrangement can be miniaturized in the micrometer scale, without the use of coils and air gaps, following the coil-less MDL set-up presented in Chapter 2, thus allowing a simple and cost effective manufacturing process. Measurements of thin film thickness during manufacturing are important for many reasons and applications. The state of the art concerning in situ thin film thickness sensors is the oscillating quartz technology. The frequency of an oscillating quartz is decreased as the thin film thickness grows up. The MDL set-up able to be used as a thin film thickness sensor is illustrated in Figure 6.21 and may correspond to the MDL coil-less arrangement illustrated in Chapter 2 (Figure 2.21). In this set-up two rectangular magnetostrictive elements (1) are set at the two ends of a glass substrate (2), which has two long parallel cuts, thus being able to act as long acoustic waveguide with rectangular profile. Two pairs of copper ribbons (3) are connected by silver paint (4) aside the magnetostrictive elements. The whole set-up can be controlled by a PC by generating and detecting the pulsed voltage input and output respectively.

In order to model the behaviour of the sensor and without any loss of the generality, a sputtering thin film chamber is considered as the thin film development chamber. Introducing the sensor in the chamber and starting to make vacuum, the pulsed voltage output response starts to increase until a maximum amplitude  $V_{om}$ . This maximized response is due to the presence of a minimized number of gas atoms within the vacuum chamber, beating the glass substrate, acting as acoustic wave-guide surface. Then, introducing the plasma gas, the pressure starts to increase up to a nominal amplitude  $V_{on}$ , which is lower than the unloaded sensor response in free atmosphere.

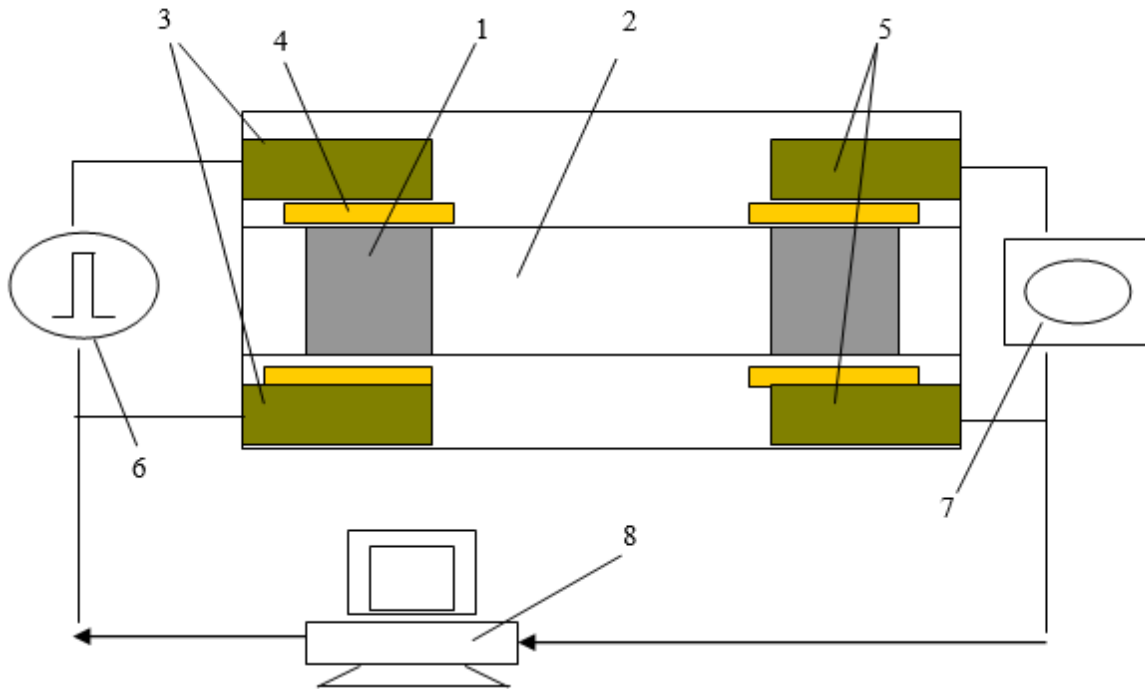


**Figure 6.21.** Schematic of the thin film thickness sensor based on the MDL technique. (1) Magnetostrictive element, (2) Glass substrate, (3) Current conductors at the excitation region, (4) Silver paint, (5) Current conductors at the sensing region, (6) Pulse generator, (7) Oscilloscope, (8) PC.

When the procedure of the thin film development starts, atoms of the target beat the deposition substrate as well as the glass substrate of the sensor. Beating the magnetostrictive elements is prohibited by using a metal mask. Thus, atoms are connected on the glass substrate, affecting the characteristics of the waveguide surface, resulting in the distortion of the propagating signal and the detected output. Beating atoms cover sequentially more and more this surface, until an atomic layer is created. Until the moment all atoms cover a single, atomic layer of deposition, the pulsed voltage output response is expected to decay approximately with the same rhythm, down to an amplitude of  $V_{o1}$ , corresponding to a full single atomic layer. Then, deposited atoms start to generate the second atomic layer, thus decreasing the voltage output down to  $V_{o2}$ , before starting the third atomic layer. Concerning the second layer, the rhythm of the signal decaying is expected to be smaller than the first one but also steady, while in the third one it is even smaller but also steady, this procedure being continuous until the deposition stops. The continuous lines indicate the signal decrease in consequent atomic layers. Since the development of the  $(n+1)^{\text{th}}$  atomic layer does not start as soon as the complete development of the  $n^{\text{th}}$  atomic layer, but a little bit before, it is

expected that the sensor peak output response decreases exponentially with respect to the thickness of the deposited thin film on it, fitting the series of the above mentioned straight lines.

A Leybold sputtering thin film manufacturing facility was used for the characterization of the sensor. The calibrating means was the system quartz oscillator sensor, thus allowing a secondary standard characterization procedure of + 1 nm uncertainty level. Our sensor was made by using hybrid thick film technology: The glass substrate of 0.3 mm thickness, 2 mm width and 7 mm length was glued under heat reflow on alumina support. Two rectangular  $\text{Fe}_{78}\text{Si}_{17}\text{B}_{15}$  magnetostrictive ribbons of 25 microns thickness and 2 mm width and length, were connected on the two ends of the glass substrate, also using a heat reflow process. The four Cu ribbons of 0.5 mm thickness 2 mm width and 4 mm length were similarly connected on the edges of the glass substrate and magnetostrictive elements. Silver paint was used to secure connections. The reflow heat was 350°C, in order to obtain stress relief of the magnetostrictive elements, resulting in a higher degree of magneto-mechanical coupling factor. The whole sensor arrangement was set next to the quartz oscillator, to avoid any secondary effects due to deposition non-uniformities.

The input of the MDL sensor was controlled by a computer and a HP arbitrary waveform generator, driving an amplifier able to transmit pulsed current of up to 1 A p-p amplitude, 1  $\mu\text{s}$  duration and 1 ms period. The pulsed output of our sensor was driven to an HP digital oscilloscope and then to the computer. Controlling the waveform generator and the oscilloscope output was realized by the HP VEE software package. The characterization of the sensor was obtained by plotting the dependence of the amplitude of the MDL sensor response on the quartz oscillator response, by taking independently the two responses with respect to time. The conditions for getting the sensor response concerning the deposited material were Si, Fe and SiFe target. The response of the sensor is illustrated in Figure 6.22.

This new arrangement improves the state of the art in MDL design for sensing applications as it requires small power consumption to operate. Having a peak current excitation of 0.1 A, the power consumption is less than 1 mW during excitation. Provided that the duty cycle of excitation is about 1:1000, the total power consumption is of the order of 1  $\mu\text{Watt}$ . Using such a set-up, the MDL structure becomes simpler and repeatable in manufacturing without the use of coils and air gap separation. This set-up is also competent in terms of response repeatability. The involving parameters, such as pulsed field and sensor geometry, which determine the operation of such a delay line are controllable by the thickness of the magnetostrictive element. The experiments on force, stress, field and magnet displacement show a monotonic decrease of

the output signal from 100% down to zero. Controlling such parameters by magnetic annealing and geometrical arrangement, one could approach a linear or quasi-linear response. Preliminary experiments indicate a different bandwidth response concerning field and stress effect on the whole arrangement. Hence, using a fast Fourier transform (FFT) procedure, the separation of the two measurands could be obtained, thus allowing the manipulation of the undesirable effect of ambient fields at the vicinity of the sensor. Considering the ambient field shielding process, the use of a permanent magnet ribbon below the magnetostrictive element could strongly bias the MDL set-up and therefore minimize the effect of other smaller fields. Another possible arrangement for such a sensor could be the use of only one magnetostrictive element for generating and detecting the magnetoelastic wave, by using the reflected wave in the glass acoustic waveguide.

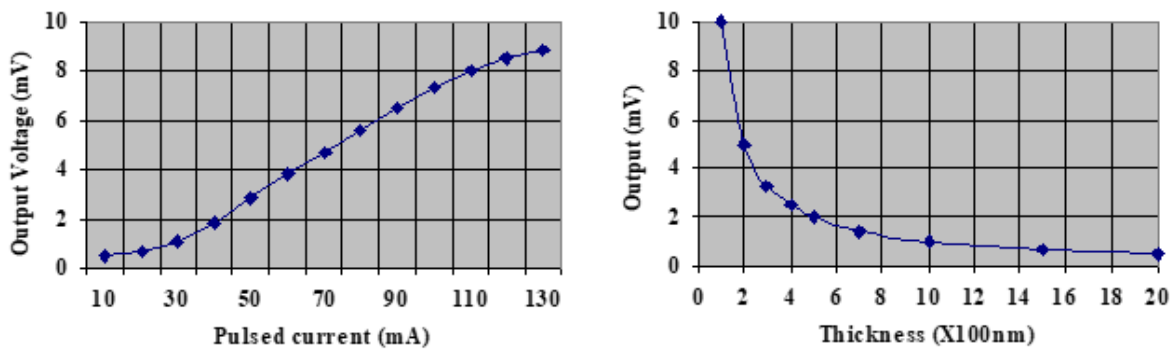


Figure 6.22. The response of the sensor of Figure 6.21.



# 7

## Field sensors based on MDLs

The sensors presented hereinafter refer to a magnetic field sensing principle, based on the MDL technique and especially on the change of the MDL response due to the biasing magnetic field. Sensors based on this idea can also be formed in arrays in order to measure the distribution of a magnetic field along the axis of an MDL or in two or three dimensions. Experimental results are reported showing an uncertainty of 1 nT. It is also illustrated how such a sensing device can be used as an integrated magnetic field distribution sensor with the mapping area of such a field up to 100 cm x 100 cm. Having the motivation to develop a magnetic field integrated sensor array, we decided to employ the magnetostrictive delay line (MDL) technique, because of its real time multiplexing characteristics and the absence of hysteresis by using certain kinds of magnetostrictive materials.

The principle of operation of a single magnetic field sensing element is as follows: pulsed current is transmitted through a pulsed current conductor set orthogonal to the MDL. Consequently, the pulsed current is translated to pulsed magnetic field along the MDL at the acoustic stress point of origin. Thus, an elastic pulse propagating along the two directions of the MDL is generated due to the magnetostriction effect and detected by the MDL detecting coil. The amplitude of the detected pulsed voltage output depends on the pulsed magnetic field and the bias field at the point of origin and the receiving coil. Having fixed the magnitude of pulsed magnetic field and the bias field at either the excitation or the receiving coil, the amplitude of the detected pulsed voltage output  $V_o$  depends on the unfixed magnitude of the bias field. This dependence can offer the possibility of a magnetic field sensor using as input and output the magnetic field along the MDL and the amplitude of  $V_o$  respectively.

From this principle, an one-dimensional magnetic field array sensor can be created: an array of pulsed current conductors vertical to the MDL transmits pulsed magnetic field at the MDL-conductor intersections creating thus a train of discrete elastic pulses propagating along the length of the MDL. Such a train is detected by the receiving coil by means of a train of voltage pulses. Keeping the pulsed current amplitude and the bias field at the receiving coil stable, the amplitude of each voltage pulse depends on the bias field

at the acoustic stress point of origin of the corresponding elastic pulse. Thus, a one-dimensional magnetic field array sensor can be realised by using as input and output the bias field at each acoustic stress point of origin and the corresponding response of the search coil respectively.

Additionally, a two-dimensional magnetic field array sensor can be realised by using the arrangement illustrated in Figure 2.11. The array of pulsed current conductors intersects an array of MDLs vertical to each other. The train of voltage pulses at each receiving coil is the result of the generation and propagation of elastic pulses at each intersection of MDL-pulsed current conductor. The dependence of the discrete pulsed voltage outputs on the corresponding applied bias field results in a two-dimensional magnetic field sensor.

From experimental observations, it has been observed that pulsed voltage output can be sufficiently detected and processed via the normalization process for distances between the acoustic stress point of origin and the receiving coil greater than 100 cm. Hence, it can be assumed that a one-dimensional array sensor can have a mapping area of the order of 100 cm. Thus, two dimensional mapping tables can be realised according to this technique, having a mapping area of the order of 100 cm x 100 cm. Experimental results also showed that a distance between two consequent MDLs can be of the order of 5 cm, without magnetic and elastic interference. Such a 5 cm distance, although defining the best resolution of such an array of MDLs, does not define the resolution of magnetic field mapping. This is due to the law of continuity of magnetic field allowing the implementation of computational techniques by using the measured magnetic field values at the MDL-pulsed current conductor intersections as boundary conditions. The given geometry and the known magnetic and electric properties of MDLs allow for the accurate definition of the magnetic field of a given surface.

Furthermore, according to the above mentioned arrangements, a three - dimensional magnetic field distribution sensor can also realise comprising a plurality of the above defined two dimensional magnetic field distribution arrangements and further comprising a plurality of magnetostrictive delay lines, passing normally through the thereby formed arrangement of MDLs and pulsed current conductors. Each one of those normal magnetostrictive delay line passes as close as possible to each one of the crossing points defined by the above arrangement of MDLs and pulsed current conductors. Each of the above mentioned one, two or three dimensional magnetic field array sensors can be used to detect AC magnetic field, provided that the excitation current is set to have a period half of the period of the detected AC magnetic field.

In these set-ups the maximum magnetic applied dc field was  $2.5 \cdot 10^3$  A/m. Various magnetostrictive materials have been tested in this set-up. Among them the Fe-rich amorphous ribbons and wires illustrated the best performance due to their higher magnetoelastic coupling factor. Indicative results will be presented concerning 1 mm wide and 25  $\mu\text{m}$  thick  $\text{Fe}_{78}\text{Si}_7\text{B}_{15}$  amorphous ribbons tested after stress and current annealing. Annealing conditions were 200 N/mm<sup>2</sup> stress, 500 mA current for 3 minutes. Indicative results will be also presented referring to  $\text{Fe}_{78}\text{Si}_7\text{B}_{15}$  amorphous wires (a-wires for short), tested in the as cast form and after heat and magnetic annealing. Heat annealing conditions have been 300 °C for ½ hours, 250 °C for 3 hours, 280 °C for 2 hours and 200 °C for 4 hours. Magnetic annealing conditions have been  $\sim 5$  kA/m along the length of the a-wires during heating in the above mentioned temperatures.

The MDL output waveform change with applied bias field at the receiving coil using an amorphous wire is illustrated in Figure 6.1. Numbers 1 to 10 indicate the amplitude of the applied bias field opposing the pulsed excitation field multiplied by 100 A/m. Such a response illustrates the change of the MDL pulsed voltage output in sign.

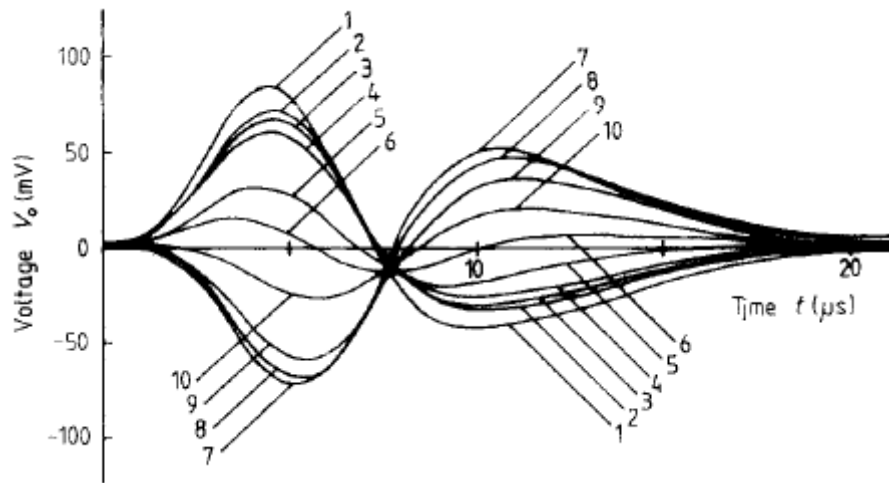


**Figure 7.1.** MDL output waveform change with applied bias field at the receiving coil, using amorphous wire. Numbers from 1 to 10 indicate the amplitude of the applied bias field opposing the pulsed excitation field multiplied by 100 A/m.

The dependence of the pulsed voltage amplitude  $V_o$  on the applied dc magnetic fields at the excitation and detection regions is illustrated in Figure 7.2, concerning amorphous ribbon in the as-cast form.

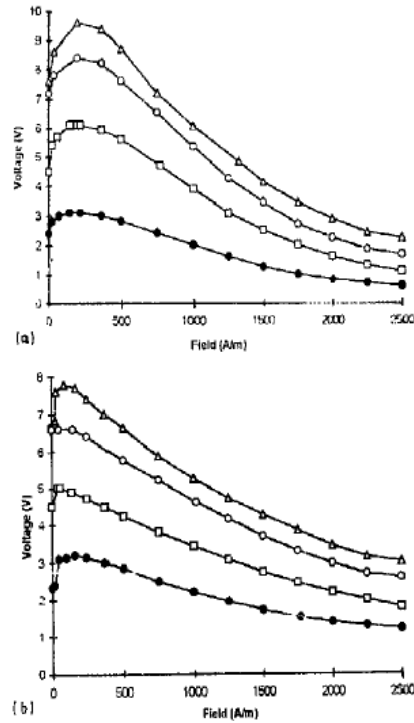


**Figure 7.2.** MDL voltage output dependence on dc bias field applied at the excitation (a) and search region (b).

A careful cancellation of the earth's field results in the calibration curves of amorphous ribbons in the as-cast form under various amplitudes of excitation current  $I_e$  as shown in Figure 7.3. The response of an amorphous ribbon in the as-cast form, after heat treatment in 300°C for 1 hr in Ar atmosphere and after stress-current annealing under 500 MPa, 0.5 A for 10 minutes is shown in Figure 7.4. The smooth response of both Figures may suggest the use of amorphous ribbons in MDLs as field sensors. Amorphous wires, although having a sensitive response, may not be promising as MDLs cores for field sensing due to their Large Barkhausen jump.

Absence of hysteresis was observed within the limits of our experimental arrangement for the tested ribbons and a-wires. A hysteresis factor must exist though, which should be detectable with a more sensitive measuring system. The almost unhysteretic response of the sensor is explained due to the relatively small hysteretic behaviour of the dependence of the microstrain  $\lambda$  on the applied field  $H$ .

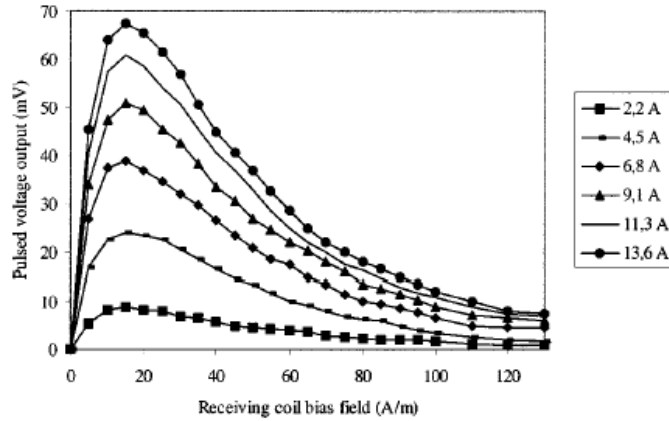


**Figure 7.3.** MDL field sensor response using amorphous ribbon in the as-cast form and after annealing.

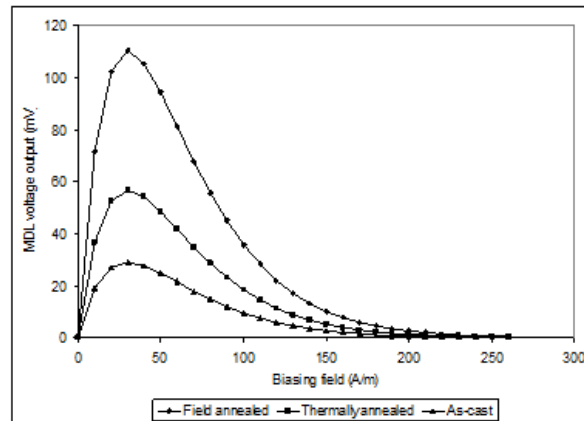


**Figure 7.4.** MDL field sensor response using amorphous ribbon after stress-current annealing and various excitation currents.

The uncertainty measurement of the sensor has been realized using a standard current source supplying the biasing coil. According to these experiments and taking into account a 5<sup>th</sup> degree polynomial correction factor for the whole range of measurement, the uncertainty of the ability of the MDL in measuring field is of the order of 10 nT with a noise level of 1 nT.

Magnetoelastic nonuniformity is obviously important for this type of sensor and can be reduced or bypassed by the annealing techniques and the normalization process respectively. The resolution of this device depends on the width of the delay lines and the pitch of the wire conductors. The obtained

resolution is 1 cm x 1 cm, since 1 cm is enough to avoid the magnetic coupling between adjacent delay lines. The size of the whole sensor can be of the order of 1 m x 1 m.

The proposed magnetic field sensor can also detect an alternating field: bearing in mind that the period of the exciting pulsed current is 1 ms, one can detect the bias components every 1 ms. Such a pulsed current period results in a sensor ability of measuring alternating magnetic field, with a frequency less than 500 Hz. Further reducing the period of the exciting pulsed current one can detect higher frequency fields. In our experiments a sensor operation with pulsed current period equal to 100  $\mu$ s (10 KHz) was obtained. In that case, ac field up to 5 KHz can be measured within the above described uncertainty.

Results have also been obtained concerning the dependence of the sensor pulsed voltage output on the angle of the bias field with respect to the MDL axis, as illustrated also in Chapter 3. According to these data the MDL can read with a linear dependence the biasing dc field on  $\cos\alpha$  with the same accuracy as in the case of dc biasing field parallel to the MDL.

Finally, from the structure of the sensing element it appears that the most possible application is magnetic mapping of plane surfaces, such as laboratory tables, production lines dependent on terrestrial field etc.

---

## 7.1 *Another field sensor array*

---

Trying to face the spatial resolution problem of the MDL field sensors, we used the arrangement presented in Figure 7.5.

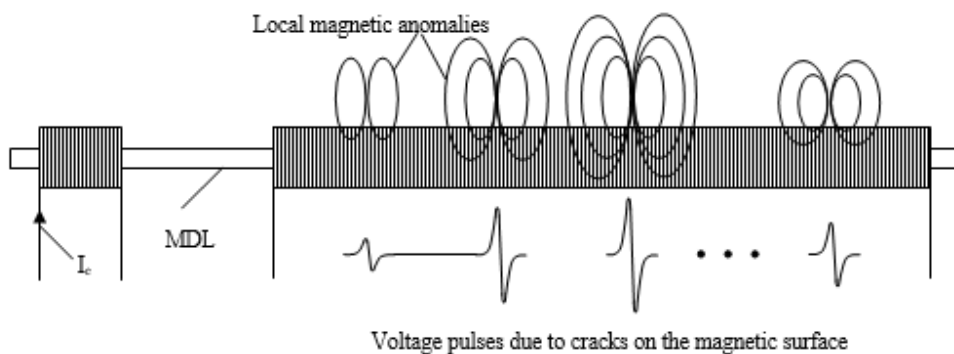


**Figure 7.5.** A long coil MDL array field sensor.

According to this arrangement a long receiving coil with a small - theoretically infinite - diameter with respect to its length is set around the MDL in order to generate an elastic strain along the magnetized length of the material. Correspondingly, a short excitation coil is set around the MDL at the one end of it, in order to receive the propagating acoustic signals. Assuming that the MDL is magnetoelastically uniform, in the presence of a magnetic field uniformly applied along the length of it, the pulsed voltage output gives peaks only at the ends of the long exciting coil, named terminating MDL output pulses. In the presence of non-uniform magnetic fields along the length of the MDL, the delay line is locally biased at different biasing points of the  $\lambda(H)$  function, so that different microstrains are generated at the terminating output pulses. Hence, the described symmetry is now broken, resulting in non-zero voltage response between the two terminating output pulses at the receiving coil. The voltage output enclosed between the two terminating MDL pulses is the transduced information of the existing magnetic field along the axis of the delay line. Digitizing such a voltage response, one can obtain a spatial resolution dependent only on the accuracy and resolution of the reading digitizing oscillator, which is typically of the order of 0.1 mm.

In order to make such an idea operational, a number of problems of the sensing principles should be solved. The main parameters and characteristics involved in the performance of the device are linearity and repeatability. Using the sensor in one of the two monotonic areas of its response, the detected output may accurately be related to the applied field. The repeatability of the sensor has to do with the magnetoelastic uniformity and repeatability. Satisfying these two parameters, one can obtain standardized types of wires to be used for field sensing applications.

Facing the problem of the range of measurement, one has to tailor the  $\lambda(H)$  function in order to meet a monotonic response up to the maximum amplitude of the measurable field. An example for such a tailoring process is the heat annealing, the magnetic heat annealing, the flash current annealing and the stress current flash annealing.



# 8

## Applications of MDLs

---

### 8.1 *Non destructive testing using MDLs*

---

The magnetic and electromagnetic non-destructive testing techniques and devices based on the magnetostrictive delay line principle are mainly three. The first is based on surface crack and defect detection on ferromagnetic surfaces by measuring the corresponding magnetic anomaly distribution. The second is the measurement of eddy currents generated around the cracks and defects on a magnetic or non-magnetic metallic surface. The third technique is measuring the surface magnetic permeability of ferromagnetic substances. Finally, the methods of measuring the properties of magnetostrictive ribbons and cylinders used as MDLs, such as magnetoelastic performance and longitudinal sound velocity as well as their uniformity measurements are also discussed.

---

#### 8.1.1 The state of the art

---

A number of non-destructive testing (NDT) techniques have been developed in the past by research laboratories and industries working in this field [183]. The main target of all these techniques is the determination of cracks and defects on the surface or in the body of a given item. The most widely applicable and important NDT techniques are those referring to metallic surfaces and substances, either being magnetic or non-magnetic [184].

Among the various NDT techniques, one can distinguish the radiography technique with spatial resolution in the micron region, the ultrasonic mapping which is capable of mapping 3-dimensional defects relatively fast with a sub-mm resolution and the liquid penetrating technique utilizing UV light illumination of

fluorescence. Other acoustic techniques have also been developed utilizing electromagnetic acoustic transducers and laser techniques [185].

The magnetic non destructive techniques are also widely used. One of them is the magnetic particle inspection, according to which small magnetic particles, diluted in liquid of well defined viscosity and evenly spread on a magnetized magnetic surface are concentrated in the areas of surface defects and cracks, due to the magnetic field gradient. The resolution of such a method depends on the size of the magnetic particles, which is of the order of 0.1 mm.

The magnetic flux leakage technique can be considered as an evolution of the magnetic particle technique, since the magnetic field gradient in the areas of cracks and defects can be detected and monitored by electronic field sensors [186], after a surface magnetization process in 1-4 kA/m.

The eddy current technique is based on the contact-less transmission of alternating magnetic field on a metallic surface, causing an increase of density of the generated eddy currents in the vicinity of cracks and defects concerning a small depth of the material. The presence of cracks and defects results in a concentration of eddy currents around them detected as amplitude and phase modulation of the voltage output across the eddy current sensing coils, indicating the size of the defect. The measurable depth of cracks and defects is restricted by the depth of magnetic field penetration, which is dependent on the frequency of the alternating magnetic field. Resolution can be of the order of 10  $\mu\text{m}$ .

Our motivation was the development of NDT sensors based on magnetic materials and especially on the magnetostrictive delay line (MDL) technique.

---

### **8.1.2 Magnetostrictive Delay Lines in Magnetic Anomaly Based Defect Detection**

---

Our first trial to involve the MDL technique on magnetic non-destructive testing was the realization of the dc field dependence of the MDL output, having a range and sensitivity of the order of 50  $\mu\text{T}$  and 5 nT respectively. This was achieved due to the response of magnetoelastic materials after careful magnetic field annealing at 350°C and 250 A/m for ½ hour in inert atmosphere, as well as due to the negligible presence of Barkhausen noise caused by the MDL operation in high frequency pulsed fields, with amplitudes well above the anisotropy field barrier. Such dependence, as illustrated in Figure 8.3, offers

the possibility to test the existence of cracks on the surface of a ferromagnetic material. A single point field sensor was initially developed as shown in Figure 8.1. Despite the relatively good sensitivity of the sensor, its use requires an X-Y translator for point-to-point mapping reasons. Therefore, its practical application would be comparable to a Hall, or MI, or GMI element, while the last may exhibit better performance.

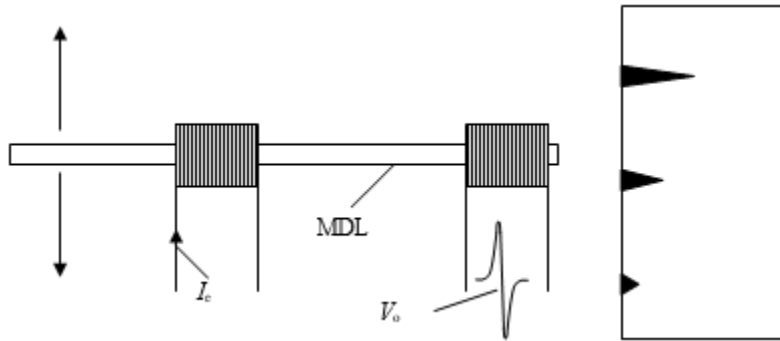


**Figure 8.1.** A single point field sensor for magnetic anomaly non-destructive testing.

Having as target the decrease of time of a ferromagnetic surface scanning, we have developed the sensor shown in Figure 8.2, which is an application-specific-device based on the field distribution sensor, shown in Figure 7.5. A long magnetostrictive element, preferably in the shape of wire, is used as the magnetostrictive delay line (MDL). A short coil, set around the MDL at the one end of it, is used to transmit the pulsed current  $I_e$ . An one-layer long search coil is wound around the MDL to detect any fluctuation of magnetic flux. Transmitting pulsed current through the short coil results in a microstrain generation and an elastic pulse propagating along the MDL.

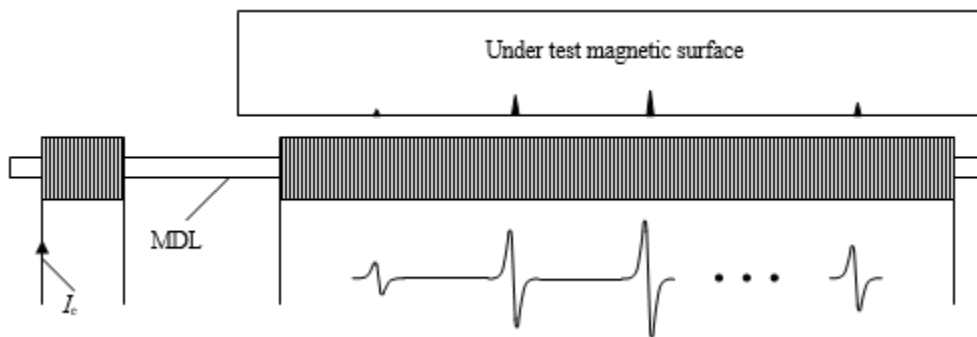


**Figure 8.2.** A magnetic anomaly distribution sensor.

Provided that the ambient field around the MDL is uniform and the MDL element is magneto-elastically uniform, the search coil can detect only two small voltage peaks, corresponding to the ends of the long

search coil. Approaching the sensing arrangement to a metallic surface without cracks, the MDL operation is not disturbed significantly, resulting again into two voltage peaks, typically larger than before, corresponding to the ends of the long search coil.

Approaching the sensor to a magnetic surface crack, the magnetic leakage of the crack breaks the magnetoelastic symmetry of the MDL, resulting in the generation of an elastic pulse at the vicinity of the MDL above the crack and correspondingly on a pulsed voltage output, with time delay and amplitude corresponding to the position and size of the crack respectively. This magnetic NDT sensor offers the possibility of shortening the inspection time due to the multiplexing or serialization of the crack measurements of an axis to a single voltage output response. Unfortunately, the sensitivity and the spatial resolution of such an arrangement are limited to 0.3 mm and 30 mm respectively.

In order to improve the above described sensor, we have developed the device depicted in Figure 8.3, which is based on the MDL arrangement illustrated in Figure 2.23. According to it, a conducting cylinder is used as the substrate for a thin magnetostrictive tube. Passing pulsed current through the conductor, the magnetostrictive thin tube is excited circumferentially, thus resulting in a circumferential microstrain along the whole length of the tube. Provided that the material has undergone proper tailoring to obtain magnetoelastic uniformity, the propagating microstrains are only those originated at the ends of the magnetostrictive tube in the absence of magnetic anomalies along its length. In the presence of magnetic anomalies like field spikes due to cracks on a magnetic surface, the magneto-elastic symmetry

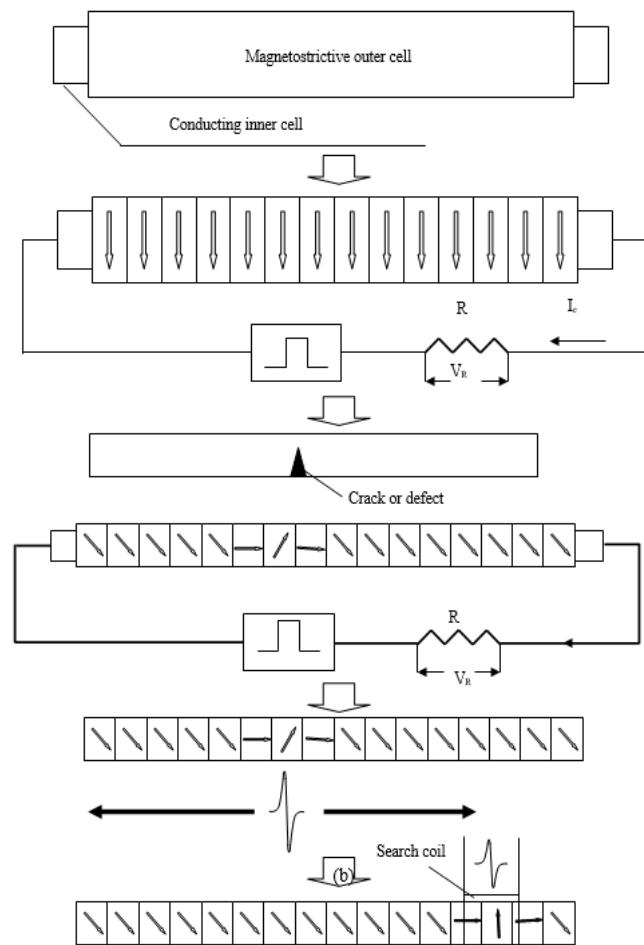


**Figure 8.3.** Magnetic anomaly NDT sensor based on the arrangement of Figure 2.20.

breaks down, resulting in discrete elastic pulses propagating along the material. We performed tests for this sensor on artificially developed line and hole cracks. Line cracks had either constant width of 1 mm and varying depth of 0.1 mm to 1 mm in steps of 0.1 mm, or constant depth of 1 mm and varying width of 0.1 mm to 1 mm in steps of 0.1 mm. Artificial holes had a given depth of 1 mm and diameter from 0.1 mm to 1 mm in steps of 0.1 mm. The response of the sensor is shown in Figure 8.4, illustrating acceptable behavior down to 0.1 mm region of measurements, with a spatial resolution of 1 mm.

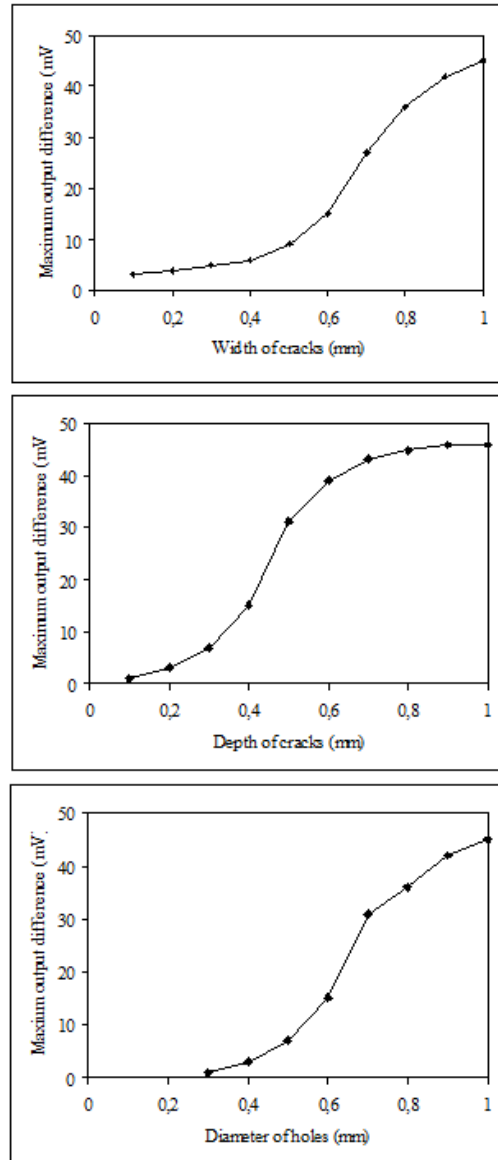


**Figure 8.4.** A typical response of the sensor of Figure 7.3 in measuring width and depth of cracks as well as diameter of holes in metallic surfaces.

---

### 8.1.3 Magnetostrictive Delay Lines in Eddy Current Based Defect Detection

---

Having as motivation the realization of a sensor able to perform fast scanning on non magnetic surfaces, the sensor demonstrated in Figure 8.5a has been developed, based on the MDL set-up, illustrated in Figure 1.15. A long MDL and a pair of pulsed current conductors are set parallel to the under test surface. The transmitted pulsed current induces pulsed magnetic field perpendicular to the MDL, resulting in no propagating elastic pulse. A search coil is wound around the one end of the MDL to detect any fluctuation of magnetic flux. Approaching the sensing arrangement to a metallic surface with no cracks or defects, the generated eddy currents are uniformly distributed on the metallic surface, as illustrated in Figure 8.5b. Thus, no elastic strain is generated into the MDL. Assuming that the under test specimen has a defect as illustrated in Figure 8.5c, the pulsed eddy current density around this defect is increased, inducing a pulsed field component along the length of the MDL at positions determined by the shape and size of the defect, as illustrated in Figure 8.5d. Hence, a travelling elastic wave is generated in the MDL, which can be detected as a pulsed voltage by the receiving coil. The size of the pulsed voltage output defines the magnitude of the eddy current, which is related to the size of the crack, while its time delay determines the position of the crack.

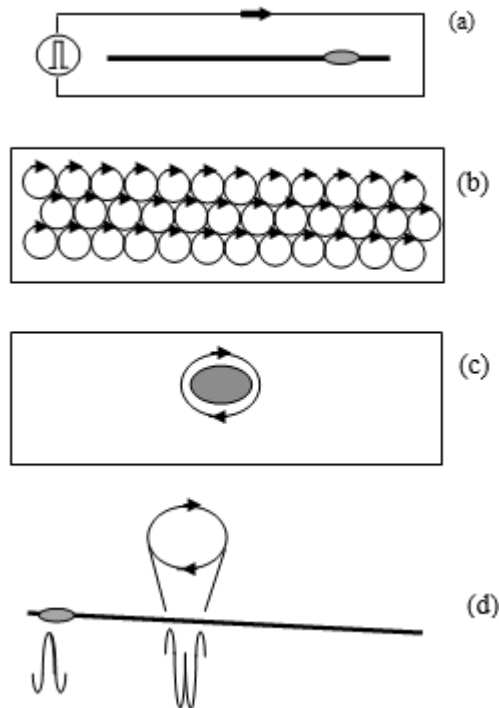


**Figure 8.5.** Detecting cracks on a metallic surface using a combination of MDLs and eddy currents.

The operation of the sensor is illustrated in Figure 8.6. Having a number of such defects along the MDL axis results in the generation of discrete elastic strains in the MDL, at the defect-MDL intersections correspondingly detected by means of a train of pulsed voltages at the receiving coil. Moving the MDL along the under test specimen, results in mapping those defects. If a defect is parallel to the MDL axis, only the defect boundaries contribute to the generation of elastic strains. Thus, mapping the MDL voltage output in two orthogonal axes and consequently superimposing the two sets of measurements result in the complete mapping the surface defects of the under test surface.

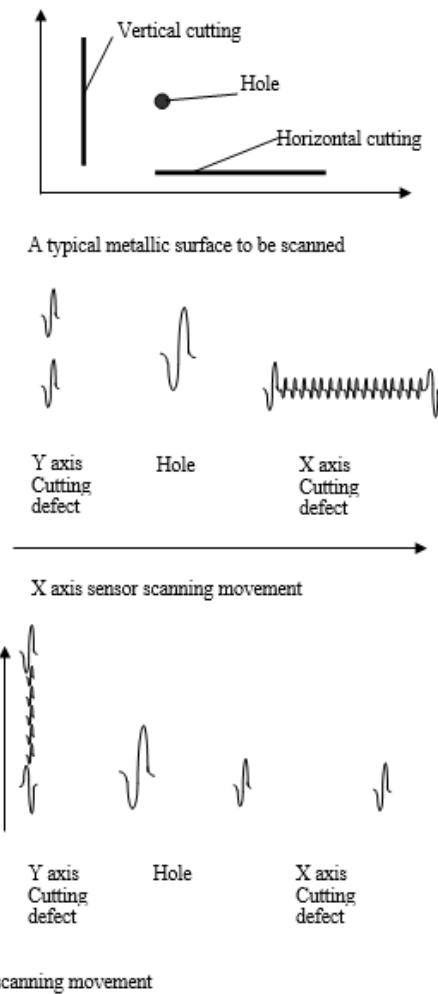
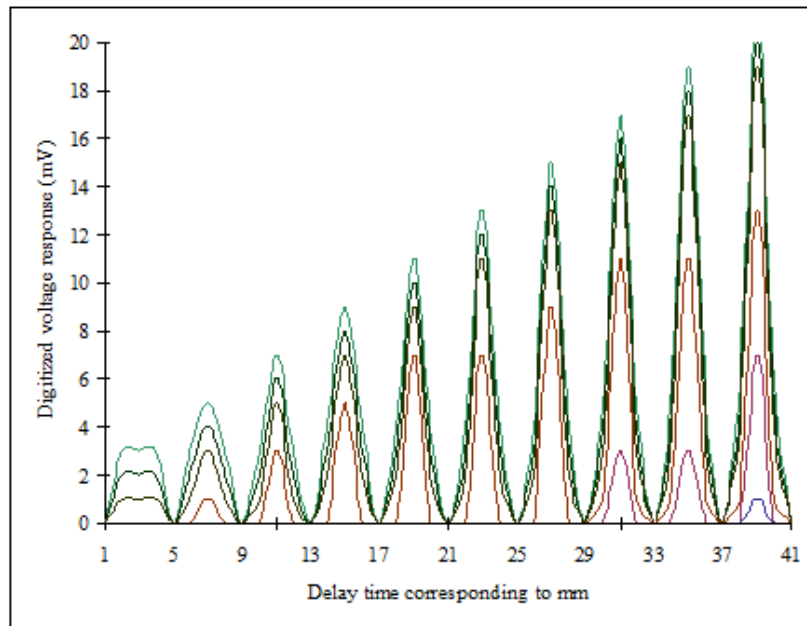


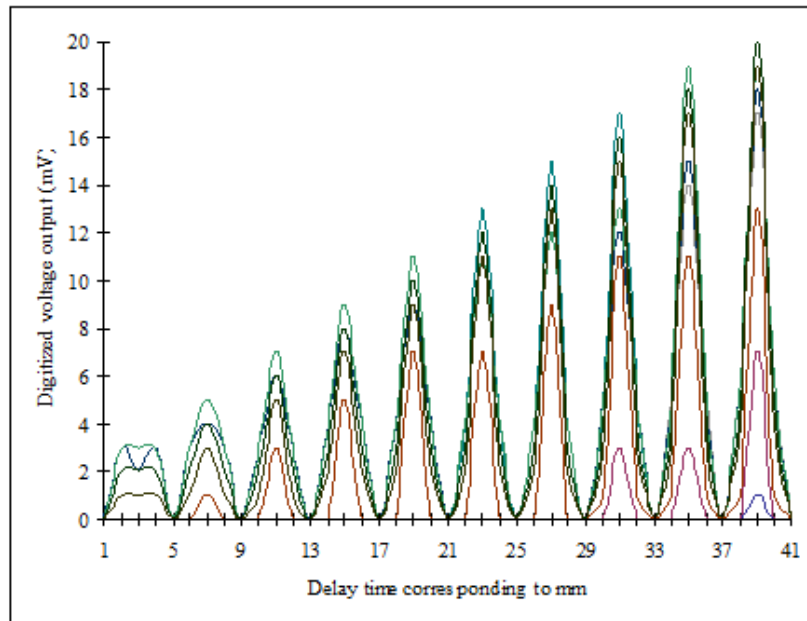
**Figure 8.6.** Operation of the sensor of Figure 8.5

Using a 20 mm by 15 mm aluminium metallic matrix, having ten sequential artificial cuttings of depth equal to 1 mm in all of them and width varying from 0.1 mm to 1 mm in steps of 0.1 mm, the obtained MDL response is illustrated in Figure 8.7a. Using a similar aluminium matrix having ten sequential artificial

cuttings of width equal to 1 mm in all of them and depth varying from 0.1 mm to 1 mm in steps of 0.1 mm resulted in the MDL response illustrated in Figure 8.7b. Higher levels of voltage outputs correspond to different excitation currents.



(a)



(b)

**Figure 8.7.** Response of the sensor based on Figure 8.4, concerning aluminum artificial defects. Different voltage outputs at the same delay time or artificial defects, correspond to different excitation current  $I_e$ .

---

### 8.1.4 Magnetostrictive Delay Lines in Permeability Measurements

---

Having the motivation to measure the surface magnetic permeability as well as its distribution uniformity along the under test surface, we have developed a new NDT method based on an old sensing principle and analyzed in section 5.1. A balanced structure of MDL excitation conductors is used to detect the amplitude and the change of magnetic permeability on a ferromagnetic surface. Such magnetic permeability uniformity function determines the quality of the surface under inspection. The method is based on the arrangement of Figure 8.8. The balanced structure of MDL using a pair of pulsed current excitation conductors is employed, allowing the MDL to be free of stresses under any circumstances.

When a pulsed current  $I_e$  is transmitted in the same direction in the two pulsed current conductors, in the absence of any other magnetic element in the neighborhood, there is no magnetic flux in the delay line and consequently zero pulsed voltage output is detected.

In the presence of the reference soft ferromagnetic element, the amount of flux inside the MDL is maximized and the pulsed voltage output amplitude  $V_o$  is maximized. When an under test ferromagnetic element is positioned close to the MDL, the magnetic flux unbalance in the MDL decreases. The amount of decrease depends on the magnetic permeability of the under test sample.

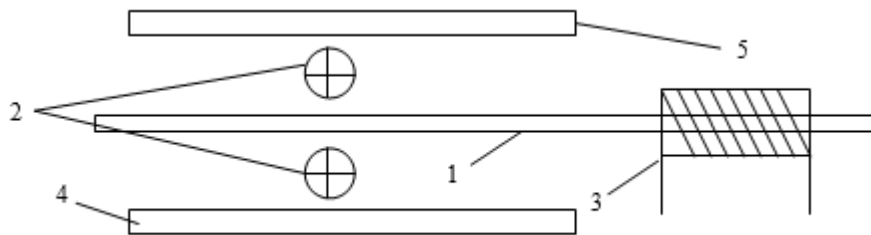


**Figure 8.8.** Arrangement based on the sensor of Figure 5.1c, used for permeability measurement. (1) MDL, (2) Pulsed current conductors, (3) Search coil, (4) Reference soft ferromagnetic material, (5) Under test ferromagnetic surface.

Consequently, the amplitude of the MDL pulsed voltage output decreases. The amount of the unbalanced flux inside the MDL depends on the magnetic permeability of the approaching under test magnetic sample as well as on the distance between the MDL balanced structure and the magnetic element. Maintaining the distance between the device and the under test surface unchanged and scanning the ferromagnetic surface results in the determination of the magnetic permeability of the magnetic surface. The uniformity

of the magnetic permeability determines the quality of the tested surface. In all measurements the amplitude of the pulsed voltage output  $V_o$  is the system output.

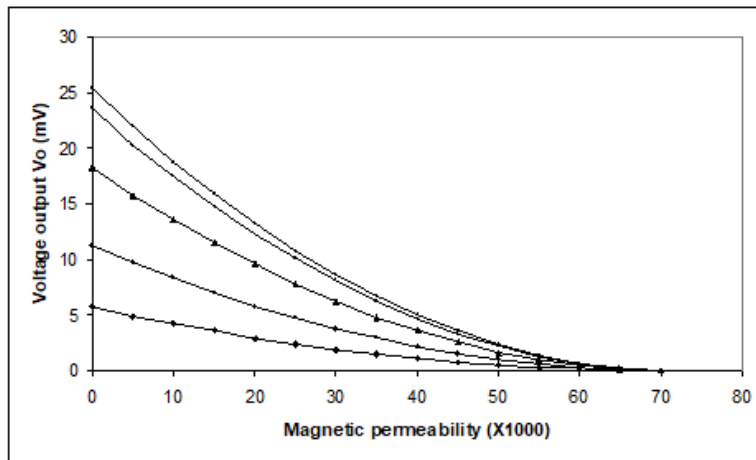


**Figure 8.9.** Typical MDL voltage dependence on the permeability of ferritic steel.

Various ferromagnetic samples of different permeability have been used to evaluate and calibrate the device. These samples were ferrite steels used after different heat treatment and cold drawing. Their permeability has been determined by using ac magnetometry. The dependence of the voltage output  $V_o$  on the permeability of ferritic steel under test is illustrated in Figure 8.9.

In all these measurements the reference standard was a Metglas ribbon of relative permeability equal to  $\sim 70000$ . The distance between the device and the under test specimen has been maintained equal to 0.2 mm. Taking into account that the distance between the device and the under test specimen is of critical importance, we performed measurements of voltage output dependence on the device – under test surface distance. From these results it became apparent that the device response does not change significantly for distances lower than 0.4 mm.

---

### 8.1.5 On the use of MDLs for Non-destructive Testing

---

The presented devices used for magnetic non-destructive testing have got some advantages and disadvantages. Among advantages, the ability of multiplexing or serializing the information of the position and size of a crack or defect below the MDL in one single reading may be important for industrial

applications. In particular, the device depicted in Figure 8.3 can be used for magnetic anomaly inspection of ferromagnetic surfaces, with a spatial resolution of 1 mm, while the device of Figure 8.5 can be used for non magnetic metallic surface crack testing. The major disadvantages of the presented devices are the relatively poor sensitivity in comparison to some other techniques, the restricted spatial resolution, as well as the ability to perform only surface measurements. Of course, the surface measurements can also be correlated with the subsurface structure of the material. This is especially valid for the device presented in Figure 8.8, able to perform surface permeability measurements. Applications of the above presented devices can be continuous monitoring of the stress distribution and corrosion on magnetic and non magnetic surfaces like bridges and tunnels.

Finally, it is worth mentioning that the MDL technique can also be used for non destructive testing of magnetostrictive materials in the shape of an acoustic waveguide, like ribbons and wires. In this case the under test material is the MDL itself. The magnetoelastic uniformity tests can be performed using the arrangement illustrated in Figure 8.2. Furthermore, measurements of the longitudinal sound velocity and its uniformity can also be obtained by measuring the delay time between two distinct positions of the excitation and search MDL coils, offering information about the Young's modulus and its uniformity.

---

## **8.2**      *MDLs for chemical and biomedical engineering applications*

---

Coagulation sensors based on the magnetostrictive delay line technique are presented in this section. They are based on magnetostrictive ribbons and are used for measuring the coagulation, curing or solidification time of different liquids. Experimental results indicate that the presented sensing elements can determine the blood coagulation with remarkable repeatability, thus allowing their use as blood coagulation sensors. Additionally, results indicate that they can also measure curing time of resins, solidification of fluids and coagulation of chemical substances, therefore allowing their implementation in chemical engineering applications.

---

## 8.2.1 The state of the art in blood coagulation and curing point measurements

---

Blood coagulation is a dynamic physiological process, which is deployed after a vessel injury causing bleeding, aiming to seal the bleeding vessel and eliminate haemorrhage. Blood coagulation results from the activation of a series of enzymatic reactions, known as the coagulation cascade. These reactions activate one after another inactive components that create as final result fibrin fibres which are formed as a net, entrap platelets and form the fibrin clot which seals the injured bleeding vessel. This final stage of the coagulation process is of utmost importance for the current application because it results in a viscosity change that can be measured with a magnetostrictive sensor. Thrombotic conditions affect more than 50 million Americans. This means that their blood has a tendency to coagulate itself without the normal precursor of injury. Due to this alteration in blood viscosity many adverse clinical conditions can occur and these patients have a need for coagulation monitoring. On the other hand, abnormalities in the platelets, coagulation factors and blood vessel defects can all attribute to excessive bleeding during an elective surgical procedure. In all the aforementioned conditions there is a need for rapid, precise measurement of blood clotting time.

The currently accepted methodologies for determining blood clotting times are optical and mechanical coagulometry [187,188]. Optical detection can be performed either with the naked eye or as a reduction in transmittance when light is passed through the sample. Mechanical transduction is typically carried out with a vibrating or rotating metal ball. Cessation of the ball's movement is considered the endpoint of coagulation. These methods require trained personnel, a well-organized hospital laboratory, a large, anticoagulated sample of blood and are time consuming (at least 30 minutes from sampling). These limitations are significant in clinical practise. There are instances that require immediate evaluation of blood's coagulation status (p.e intra-operative bleeding) or repeated assessment in patients receiving coagulopathy treatment at home, which must return repeatedly to the hospital solely for the blood-coagulation measurement. In an effort to overcome those limitations newer methods have been studied in the last few years. The first uses a piezoelectric quartz crystal (PQC), which is a surface acoustic wave (SAW) device that can respond to changes in viscosity [189]. Other methods employ surface plasmon resonance (SPR) to detect biological interactions and changes in the properties of blood [190] or blood rheological characterization using the thickness-shear mode resonator.

The cure analysis of thermosetting resins has been mostly studied by differential scanning calorimetry (DSC) and to a lesser extent by other methods such as rheometry, electron spin resonance, Fourier

transform, infrared spectroscopy, stress-temperature measurements, calorimetric studies, fluorescence and scanning electron microscopy [191-195]. Magnetostrictive coagulation sensors have been developed in the past [189], offering many benefits over these technologies by being simple and inexpensive, requiring a minimal volume of blood to operate. Taking into account these advantages, which promise a viable method for blood coagulation monitoring, we developed a magnetostrictive delay line (MDL), set-up able to operate as coagulation sensor. The coagulation sensor is presented next with some indicative results on measuring coagulation of blood as well as on curing time of resins, solidification of fluids and coagulation of chemical substances. These results may prove that MDL coagulation sensor is promising repeatable response, thus being usable in biomedical and chemical engineering applications.

---

## 8.2.2 The proposed sensing element

---

The coagulation-sensing element is illustrated in Figure 8.10. The MDL, having the shape of an acoustic waveguide with rectangular cross section area is the sensing core. It can be made of any magnetostrictive composition, although experimental results have indicated that positive magnetostrictive materials mainly in amorphous state, especially the family of FeSiB amorphous ribbons, offer high magneto-mechanical coupling factor and the smallest possible hysteresis [190]. An excitation coil, set around one end of the MDL, is used to transmit pulsed magnetic field along the length of the MDL, thus generating pulsed microstrains due to the magnetostriction effect, which are summed up to an elastic pulse, which splits up in two parts and propagates along the two directions of the MDL; after the microstrain generation, the MDL acts as an acoustic waveguide of the propagating elastic pulse. The excitation coil is practically made of a few turns to allow for easy electronic driving, which is accomplished by a MOS-FET circuit. The thickness and the frequency response of the MDL, which are of the order of several microns and of a few microseconds respectively, suggest that the propagating elastic pulse has a wavelength of the order of several mm. In fact it is between 15 mm and 50 mm. This suggests that the mode of acoustic propagation taking place in the MDL is a “Lamp” wave, exciting all of the cross section area of the acoustic waveguide.

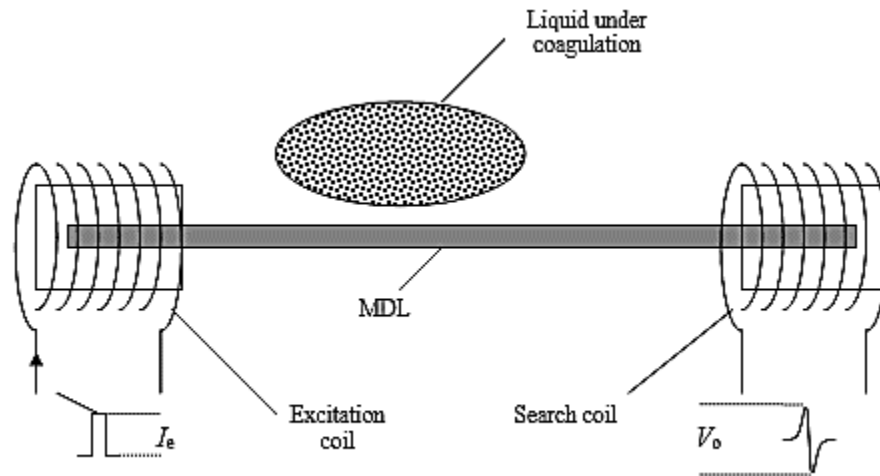


**Figure 8.10.** The coagulation-sensing element.

The end of the MDL is preferably inside the excitation coil, in order to take advantage of the elastic pulse being reflected at the end of it. By applying pressure at the end of the ribbon, the reflecting pulse maintains the waveform of the initial signal. If the excitation coil has a critical length significantly smaller than the wavelength of the propagating elastic pulse, the propagating elastic pulse will approximate the sum of the two propagating pulses.

Following the analysis of the MDL operation given in Chapter 2, as the elastic pulse propagates along the MDL, it causes the magnetization in its path to change due to the inverse magnetostriction effect. Therefore, the domain magnetization changes with respect to the propagating elastic pulse. Provided that the MDL has its magnetic dipoles well oriented along a given orientation due to an external field, the infinitesimal changes in the magnetization are superimposed, thus resulting in a total, macroscopic change of magnetization.

Considering that the above mentioned MDL elements are made of amorphous FeSiB alloys, the earth's field is enough to magnetize them. However, the presence of a permanent magnetic field surrounding the MDL can ensure the permanent magnetization of the MDL along a given direction, regardless of its position with respect to the geomagnetic poles. Setting a search coil around the MDL, this change of magnetization is detected as an induced voltage pulse.

This voltage pulse is proportional to the first derivative of the magnetization of the MDL part being inside the search coil. As mentioned before if the search coil is at the end of the MDL and has a length

considerably smaller than the propagating wavelength, the effect is maximized because the reflected signal is also superimposed to the main propagating one.

The search coil ought to be sensitive enough to detect as good as possible any magnetization changes, but it also should have such a Q factor not to affect the detected signal. Coils having more than 100 turns/mm and being 1-2 mm long yield acceptable levels of sensitivity while signal distortion occurs for more than 300 turns/mm and coils longer than 3 mm.

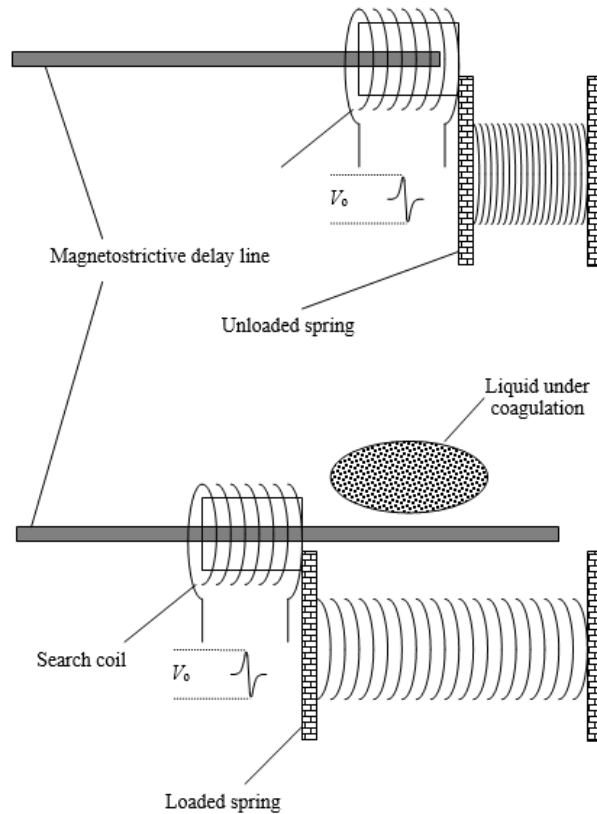


**Figure 8.11.** Overcoming the problem of mass quantity.

Applying a liquid on the surface of the MDL, which acts now as an acoustic waveguide, at a point between the excitation and the search coils, a part of the energy of the propagating elastic pulse is driven to the afore mentioned liquid. The closer the density of the liquid is to the density of the MDL material, the larger portion of elastic energy is driven to the liquid. As the liquid densifies its density tends towards the density of the MDL material and consequently a smaller amount of energy continues to propagate along the MDL. Hence, the voltage output of the MDL is expected to be inversely proportional to the coagulation procedure of the liquid, i.e. to decrease with time. Considering the peak-to-peak pulsed MDL

voltage output as the output of the system, the coagulation time of the liquid, set on the MDL waveguide surface, can be determined. Therefore the described process can be used as a coagulation sensor.

A drawback of the sensor is the amount of liquid set on the MDL. The volume of the liquid also determines the signal output of the MDL. Different quantities of the same liquid may result in different signal outputs, thus making the distinction between liquid quantity and coagulation time difficult. One first step towards maintaining the repeatability of the coagulation sensor is to use precise volume meters in order to control the quantity of the under test liquid. However, this still introduces uncertainties to the sensor response. The way to overcome this problem is depicted in Figure 8.11, illustrating how the liquid is set below the search coil: before setting the liquid on the MDL surface, the search coil, together with its rectangular support, is moved towards the excitation coil, using a mechanical means like a spring. The liquid is set in place and then the search coil is released back to its initial position. Thus, the amount of liquid remaining on the MDL surface covered by the search coil is well controlled in terms of volume.

This technique offers the following advantage: the densification process of the liquid results in additional tensile stresses applied on the surface of the MDL. Provided that the MDL is a positive magnetostrictive material, such tensile stresses result in a reduction of the above mentioned inverse magnetostriction effect, since they help the magnetization to orient easier along the axis of the applied stresses. Therefore the signal of the MDL in such a case decreases for two reasons: one is the elastic energy driven to the liquid as it densifies and the other is the tensile stresses during liquid densification which also reduce the amount of the measured voltage output.

The pulsed mode of MDL operation results in non continuous elastic vibration throughout the volume of the MDL. This assists the densification process in non-Newtonian liquids such as blood, thus offering an additional advantage of the proposed system. This operation theoretically suggests a more sensitive response with respect to the inductive measurements using magnetostrictive elements because of the combination of the two involved effects that are (in inductive measurements only the tensile stresses affect the response of the magnetostrictive element). It also offers a measurement not dependent on the quantity of the applied liquid, since the sensor itself utilizes only the quantity behind the sensing element.

---

## 8.2.2 Experiments

---

The above described coagulation sensor has been realized for testing blood coagulation, by using a  $\text{Fe}_{78}\text{Si}_7\text{B}_{15}$  amorphous ribbon as MDL sensing core. The decision for such a composition of the MDL core was based on the fact that it is commercially available in vast quantities and in relatively inexpensive price. The 10-turn excitation and 300-turn search coils were made of 0.1 mm enameled Cu wire, 1 mm and 2 mm long respectively. Two cylindrical permanent magnets, offering a biasing field of 20 kA/m along their axis were used for the biasing of the two coils.

The electronic circuit for the generation of the excitation pulsed current  $I_e$ , transmitting the pulsed field responsible for the microstrain generation, was based on a FET circuit, driven by an arbitrary wave generator, controlled by a PC. The amplitude of the pulsed current  $I_e$  was controlled by the biasing voltage of the FET circuit.

The voltage output was amplified using a low noise and high bandwidth amplification circuit. The output of the amplifier was connected to a digital oscilloscope, which was connected with the above mentioned PC. Therefore, the experiment was automatically controlled. The schematic of the experimental set-up is shown in Figure 8.12.

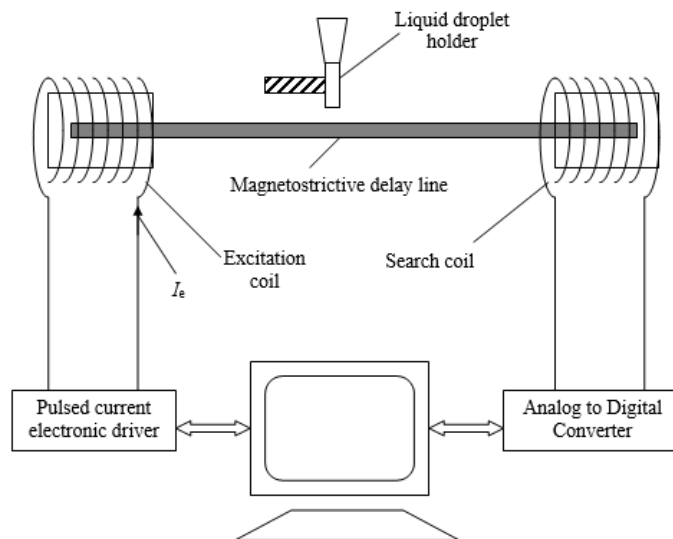


**Figure 8.12.** The schematic of the experimental set-up for the blood coagulation measurement.

Data collection was obtained by using two Visual Basic programs that were specifically written for this purpose. The first program operates in a time sweep mode. The computer controls the pulsed signal

generator that creates the applied magnetic field. The resulting signal is then recorded and converted into a voltage output. The second program records the peak to peak voltage output over time.

Blood setting was realized by moving the search coil, following the method illustrated in Figure 8.11. The mechanical spring allowed a repeatable mechanical response for the duration of all experiments. Placing 0.05 ml of blood onto the surface of the magnetostrictive sensor, covered afterwards by the search coil, resulted in a repeatable detection of the signal distortion.

A typical dependence of the MDL pulsed voltage output on time is illustrated in Figure 8.13. It can be seen that the delay time between excitation and output signal does not significantly change. As the blood was coagulating, additional changes could be observed in the voltage profile of the sensor. The amplitude of the voltage output decreased with time.

This was due to the blood viscosity change during clot formation. A typical dependence of the pulsed voltage output on time is illustrated in Figure 8.14, concerning normal blood, i.e. blood of a person without coagulopathy. This response is an exponential function of time:

$$V_o(t) = V_o e^{-at} \quad (8.1)$$

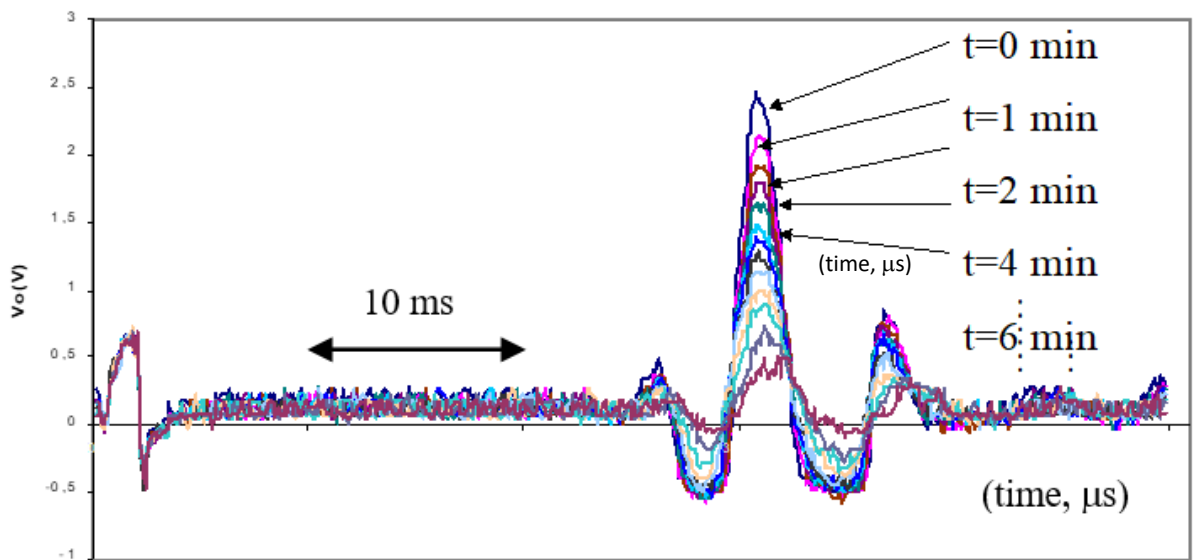


**Figure 8.13.** A typical dependence of the MDL pulsed voltage output on coagulation time.

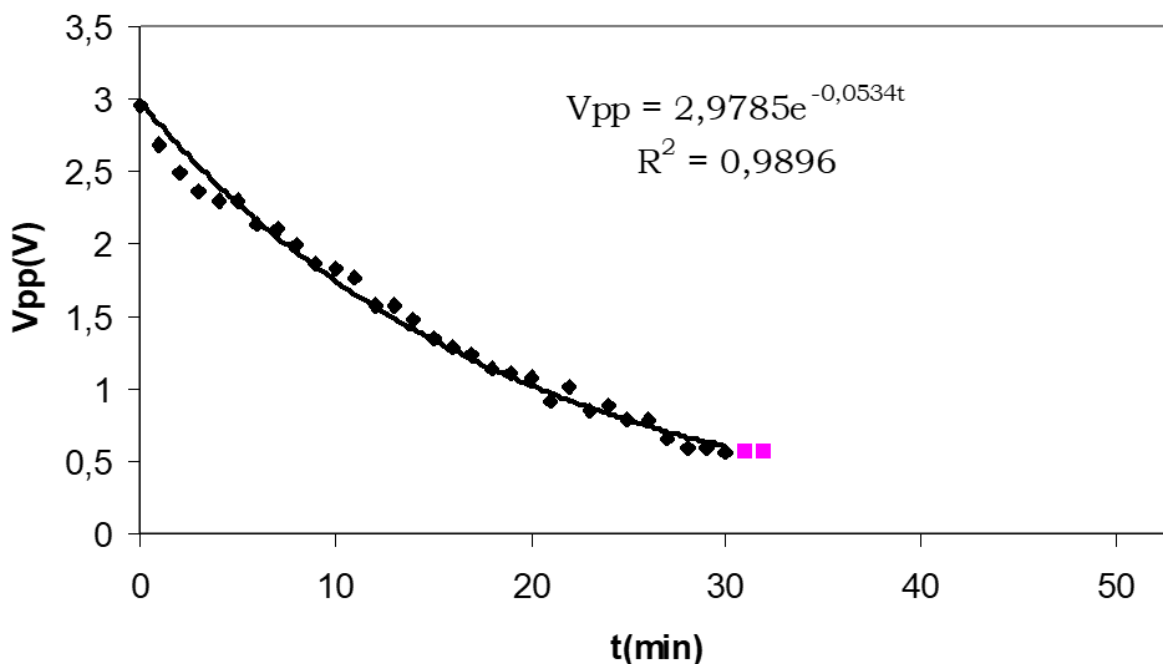


Figure 8.14. MDL pulsed voltage output dependence on coagulation time.

Table 8.1. Values of the coefficient a of Figure 8.14.

<b>Blood</b>	0.0533	0.0531	0.0530	0.0534	0.0538	0.0539	0.0536	0.0531	0.0537	0.0533
<b>Epoxy resin</b>	0.1642	0.1644	0.1648	0.1647	0.1649	0.1642	0.1643	0.1640	0.1641	0.1639
<b>Silicon glue</b>	0.0252	0.0253	0.0253	0.0254	0.0252	0.0253	0.0255	0.0252	0.0253	0.0253
<b>Thixotropic polyester</b>	0.0535	0.0533	0.0533	0.0534	0.0533	0.0530	0.0531	0.0531	0.0534	0.0534

The zero point of time refers to the time that blood is placed onto the surface of the sensor. Experiments performed using the same blood in different quantities resulted in a repeatable determination of  $V_0$  and the exponential coefficient  $a$ . Their values are indicated in Figure 8.14, thus ensuring that the method is independent on the quantity of the tested blood as well as repeatable in time.

This measurement was repeated for more than 10 times for the same blood. The determined values of  $a$  are given in Table 8.1, illustrating a mean value of  $0.0535 \pm 0.0005$ , offering an uncertainty of  $\sim 0.9\%$ . Such measurement has to take place within a small time window in order to keep experimental conditions as

constant as possible. Possible changes in the value of  $a$  are attributed not only to the sensor noise but also to the change of the blood quality itself.

Testing different samples of blood resulted in the very same amplitude of  $V_o$ , but in different values of the exponential coefficient  $a$ . Hence, it is claimed that the amplitude of the exponential coefficient  $a$  is indication of the blood coagulation. The same sensing principle has also been used in chemical engineering applications, for the solidification of fluids or curing of resins or coagulation. Results on solidification measurements of metal glue (a), coagulation of silicon glue (b), as well as curing of epoxy resin (c) and thixotropic polyester (d) were obtained.

Taking into account that the above mentioned processes could easily be destructive for the search coil, the experimental set-up shown in Figure 8.12 was used. This means that the voltage output was not related to the tensile stress applied on the surface of the MDL, but only on the elastic energy transferred into the under measurement sample. Apart from that, all other experimental details described in the previous chapter have been maintained.

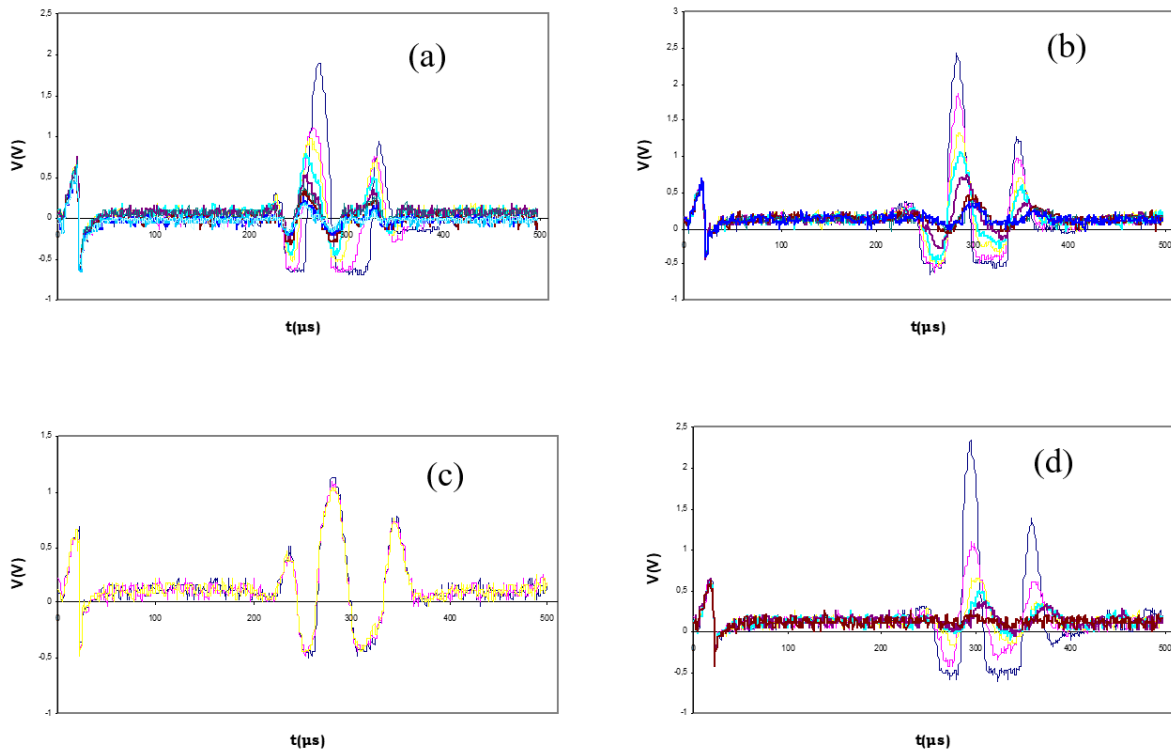


**Figure 8.15.** Typical distortion of the MDL output waveforms with curing time.

A typical distortion of the MDL output waveforms for the above mentioned materials is illustrated in Figure 8.15. From these figures it can be seen that the acoustic delay time in all liquids except the metal glue is increased. This may suggest a phase shift in group velocities rather than MDL longitudinal sound velocity and density modification, due to the different mode of interface tensile stresses between MDL and liquid.

A typical dependence of the MDL pulsed voltage output on the solidification, curing and coagulation of the above mentioned liquids is illustrated in Figure 8.16. The same exponential behavior is also observed in these liquids, as in the case of blood. The different amplitudes of  $V_0$  are attributed to the different amount and spread of the liquids on the MDL surface. Maintaining the same volume of the same liquid, almost identical response was obtained, thus ensuring the repeatability of the measuring system.

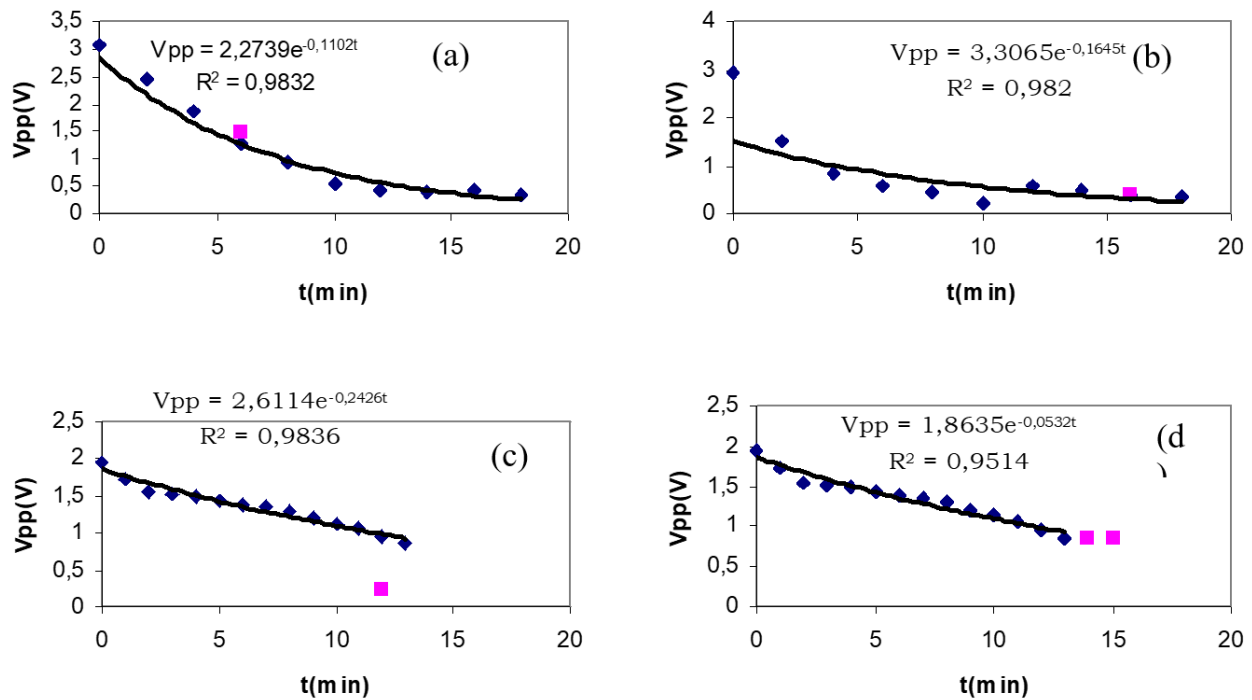


**Figure 8.16.** Typical dependence of the MDL pulsed voltage output on the curing of the above mentioned liquids.

The solidification of the metal glue is a physical phenomenon based mainly on the evaporation of the diluent component. The curing of the epoxy resin and the thixotropic polyester is a chemical effect based on their post-polymerization. The coagulation of silicon glue is a physico-chemical effect based on solidification without evaporation. Thus, solidification, curing and coagulation time can also be determined for the case of chemical engineering applications.

Repeatability measurements were also performed for the case of epoxy resin, silicon glue, and thixotropic polyester, repeated for more than 10 times each. The determined values of the coefficient  $a$  are also given in Table 8.1, illustrating mean values of  $0.1645 \pm 0.0005$ ,  $0.0253 \pm 0.0001$  and  $0.0532 \pm 0.0002$  for epoxy resin, silicon glue, and thixotropic polyester respectively, offering an uncertainty of  $\sim 0.3\%$ . These results are more repeatable than the blood measurements. Such behaviour is attributed to the more stable quality of these materials with respect to blood.

---

### 8.2.3 Discussion

---

From the above illustrated experimental results it is evident that the time required to measure the coagulation of a liquid with this technique is of the order of several minutes. This is due to the fact that the amplitude of the voltage output is indicative of the endpoint of the coagulation process. When the output signal becomes steady within the limits of a pre-set level threshold, it can be said that coagulation has been achieved. But, since the exponential coefficient  $a$ , is considered as the indicative parameter of blood coagulation, such a measurement may not require to be finalized at the above mentioned time threshold. Following measurements during coagulation, computational techniques can determine the coefficient  $a$ . Hence, measurements of several seconds may be sufficient enough in order to determine the coefficient  $a$ . Apart from this problem the repeatability when using the set-up of Figure 8.10 may be significant. To avoid destroying the search coil because of the solidification of some chemical liquids, one can use a disposable intermediate support layer head below the search coil surrounding the delay line–liquid system. In this way the sensitivity may be decreased due to the larger cross section of the search coil, but it can be faced-up using precise amplification techniques.

The determination of blood coagulation time is an essential part of monitoring therapeutic anticoagulants and treating life threatening acute coagulopathies. Standard methodologies for the measurement of blood coagulation time require specialized personnel a well organized laboratory facility involves blood-sampling procedures and is time consuming. It is the standard practise for a patient under anti-thrombotic treatment to visit a laboratory facility on a regular basis (every two weeks for at least six months) in order to evaluate the clotting status of his/her blood. The benefit in cost effectiveness for this measurement is self evident if a portable simple and accurate instrument would be available. Additionally, in many emergency cases, the coagulation cascade functions abnormally altering individuals clotting ability or

bleeding potential within a few minutes. It is obvious that in these cases the time of 30 minutes that is required today for measuring blood's clotting time is extremely prolonged. Currently, in those cases the therapeutic actions are based in clinical criterion, which is developed only by well trained and experienced clinicians. Misjudgement in this scenario could have a detrimental effect in patient's prognosis.

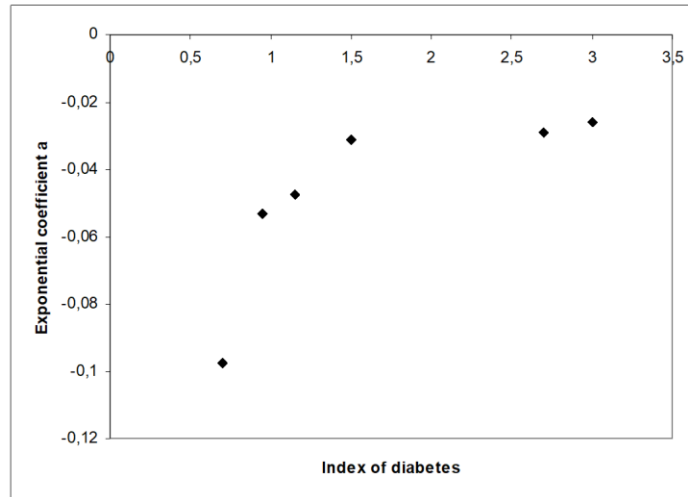


**Figure 8.17.** Correlation between exponential coefficient a and the index of diabetes measured in blood.

The development of a method that could evaluate blood coagulation time within a few minutes would offer an in-time objective result, thus improving the standard of care in the afore mentioned acute situations. The method that is evaluated in this experiment shows at this initial step that can overcome all the limitations of the currently deployed technique. This way, the blood coagulation sensor may be proven a significant aid in judicious clinical decisions, or a bedside domestic instrument that could save public and private resources. Additionally to that, taking into account the index of diabetes of the tested blood as an indication of the blood coagulation a correlation between exponential coefficient a and the index of diabetes measured in the under test blood is illustrated in Figure 8.17.

Apart from the afore-mentioned measurements, we performed measurements of the delay time between the main and the reflected signal, during blood coagulation. In this experiment, the ribbon MDL sensing core was longer, allowing a large part of the MDL to be out of the area between excitation and search coils, as shown in Figure 8.18. Blood was set at the visible end of the MDL. The output waveform illustrating the time shift of the reflected signal with respect to the main pulse is given in Figure 8.19, while the dependence of the delay time between the main and the reflected signal is shown in Figure 8.20.

Preliminary results indicate that such response is not dependent on the quantity of the tested blood, when blood is set in a length smaller than the wavelength of the propagating elastic pulse. This sensing technique can be applied for the in-situ and continuous measurement for various engineering processes, in order to estimate the curing time of commercial thermosetting resins. Such applications could be the curing of polyester resin alone or as matrix reinforced with glass or other fibers in various manufacturing sectors, e.g. ship-manufacturing, water-proving adhesives and molding articles.

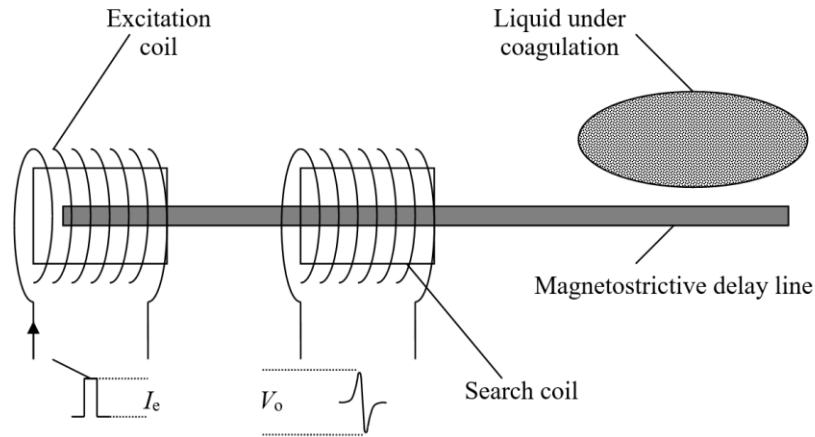


**Figure 8.18.** Measuring blood coagulation using reflections of the MDL set-up.

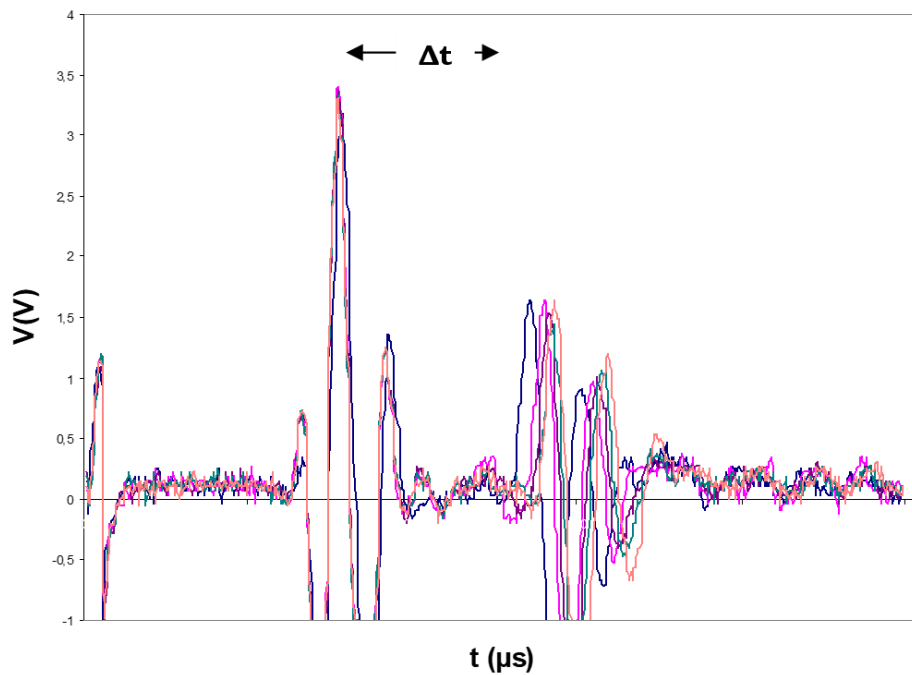


**Figure 8.19.** Reflection based blood coagulation time measurement.

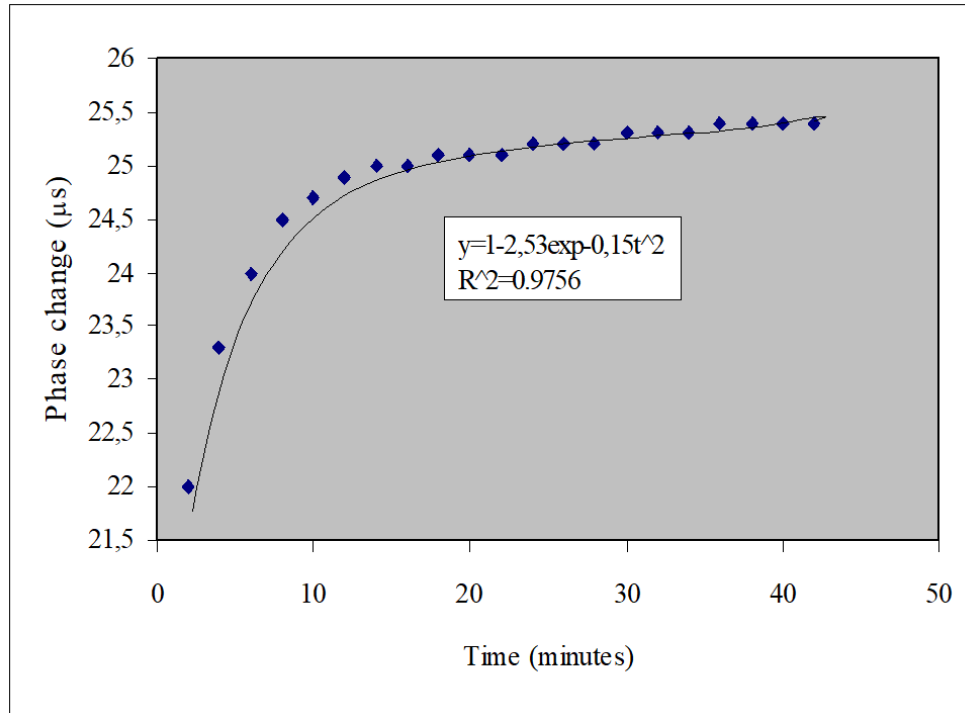


**Figure 8.20.** Dependence of the MDL reflection amplitude of time, during blood coagulation.

---

### 8.3 MDLs for civil and mining engineering applications

---

The MDL applications in civil and mining engineering are mainly special types of stress and displacement sensors. The most important application refers to a cordless and conduct-less tensile stress sensor. The principle of operation of such a sensing element based on the elastomagnetic properties of the magnetostrictive metallic glasses has been discussed. In these alloys, made by the rapid solidification process, their relative permeability is dependent on the tensile stress, which is applied on their surface.

The principle of the sensor is illustrated in Figure 8.21. In this sensor the MDL has to remain free of stresses, under any circumstances. According to the schematic, pulsed current is transmitted in the same direction in the two conductors. So, in the absence of the core S, there is no magnetic flux in the delay line and consequently zero pulsed voltage output is detected. When core S is positioned unstressed and close to the MDL, the pulsed voltage output is maximized. Applying stress on the stressable ribbon results in a

decrease of the relative permeability. Therefore, the output signal decays. Further increasing the stress on the stressable ribbon may result in making the core  $S$  magnetically transparent and the MDL voltage output zero.

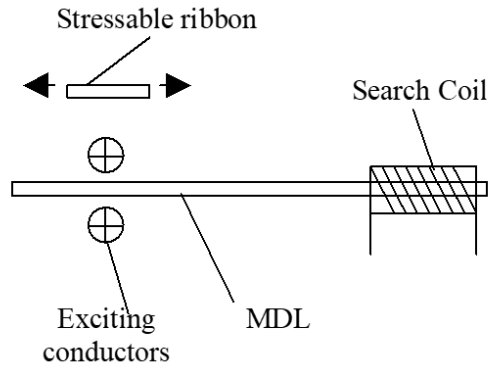


**Figure 8.21.** Schematic of the tensile stress sensor.

The above described principle can be used as a cordless tensile stress sensor as shown in Figure 8.22. The sensing element is connected on a beam structure. Tensile stress on the beam results in tensile stress on the sensing element. Approaching a balanced MDL arrangement close to the sensing core results in detecting the applied tensile stress. A typical response of the sensor is illustrated in Figure 8.23. For mining and civil engineering applications, this sensor does not require cabling out of the sensing element, provided that the balanced MDL arrangement is approached close to the sensing element, when stress measurements are required.

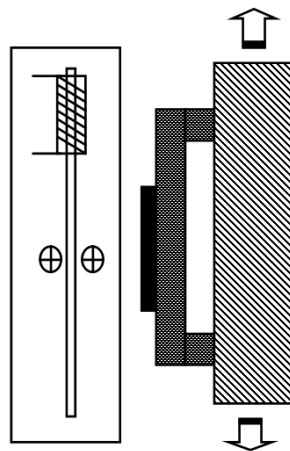


**Figure 8.22.** A cordless arrangement of the tensile stress sensor.

A critical problem arises concerning the importance of the gap between sensing element and balanced MDL set-up. If, for any reason, the gap between sensing element and balanced MDL set-up varies, the

sensor output does not correspond to the actual tensile stress. This effect is also known as the lift-off effect. For this reason, we performed measurements concerning the dependence of the distance between sensing element and the closest pulsed current conductor. Figure 8.24 illustrates the dependence of the MDL output on the mentioned distance, concerning width of sensing elements and MDL of 10 mm and 1 mm respectively.

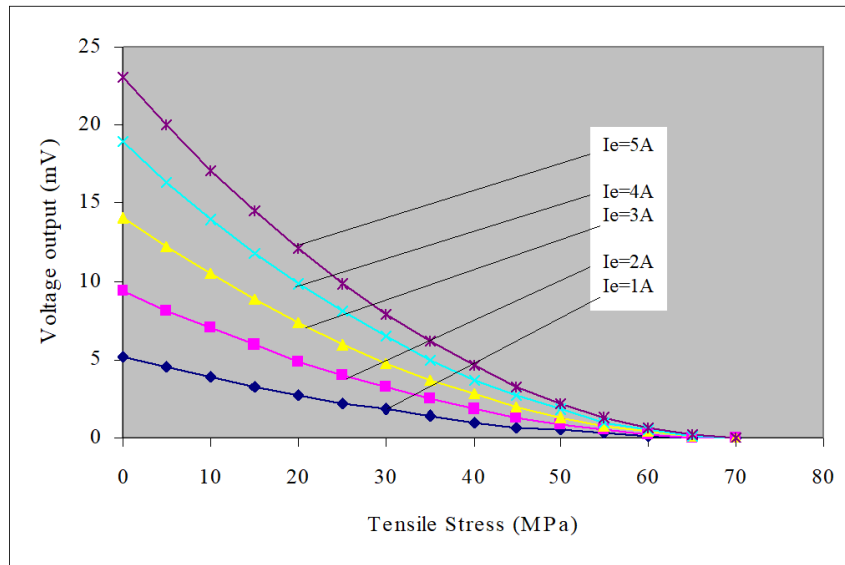


**Figure 8.23.** A typical response of the tensile stress sensor, for different pulsed excitation current amplitudes.

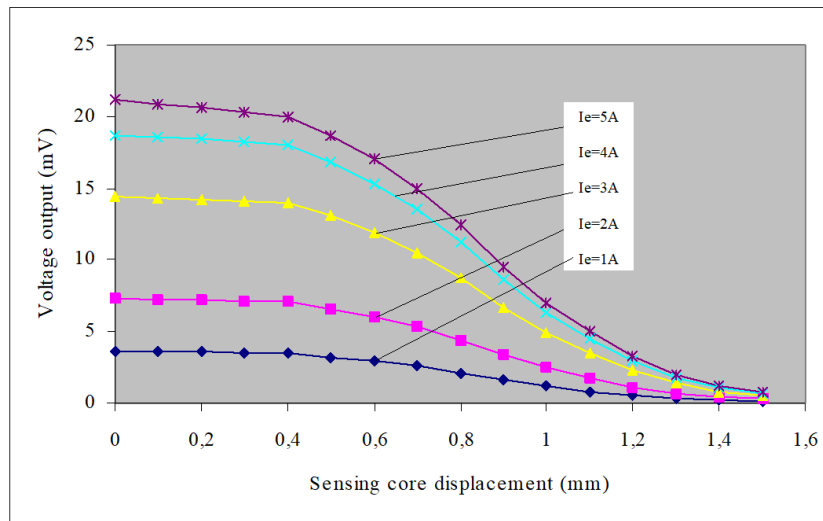


**Figure 8.24.** MDL output dependence on the distance between tensile stress sensing core and MDL set-up.

From this response, it was determined that the lift-off effect was not significant for distances up to 0.5 mm. We also observed that the ratio of the width of sensing core and MDL was important for such a response. An optimum maximum ratio equal to  $\sim 20$  was determined when using FeSiB amorphous ribbons. Accordingly, we performed stress measurements in various gaps between MDL set-up and sensing core.

The response of these measurements is illustrated in Figure 8.25, concerning width of sensing core and MDL of 20 mm and 1 mm respectively. It can be seen that for gaps up to 0.4 mm the response did not change significantly. This indicates that this type of sensor can be used in a cordless mode for gaps up to 0.4 mm.

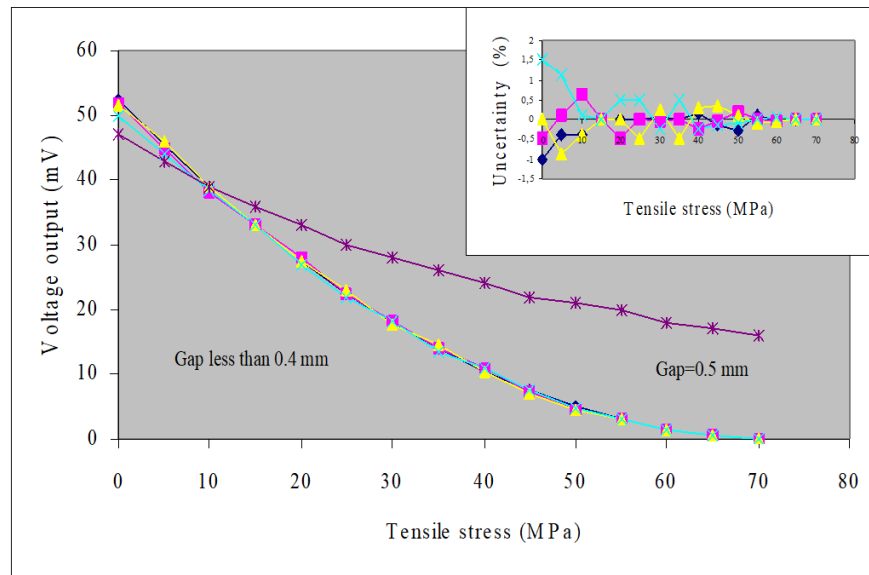


**Figure 8.25.** Response of the tensile stress sensor concerning various gaps of sensing core and MDL.

---

## 8.4 MDLs for sports field applications

---

An automated system able to measure performance in field sports is presented. The system can detect automatically the length of jumps and triple jumps as well as the position of throws in field sports. The method of detection is based on an application-specific magnetostrictive delay line set-up, using the delay time due to the acoustic signal propagation. The system is able to perform measurements with accuracy

better than 1 mm, thus overcoming the accuracy of the present semi-automatic or manual techniques of measurement. A lot of measurements in field sports activities are obtained using manual or semi-automatic techniques. Such a measuring technique may involve time delays or possible inaccuracies in the final result. Therefore, it could be desirable, at least for important games, like Olympic Games or International Championships in Athletics, to use automatic measurement techniques for detection of position of jump, triple jump length or throw of discus, hammer and javelin. Such automatic measurement could also be demonstrated to the stadium walls, so that viewers could observe in a better way the procedure.

This was our motivation. We decided to use delay time techniques to design and develop such sensing system, because of the relatively large range of measurement. It is mentioned that, large ranges of position measurement require easily integrated measuring techniques, such as optic or delay time methods. Therefore, we implemented the magnetostrictive delay line (MDL) technique, which has already been used for many sensing applications including position and displacement sensors [196-197]. In this specific arrangement the emphasis should be given in the proper design of long and robust delay lines in order to commute acoustic waves without significant dispersion and attenuation. Without any loss of the generality, we initiated our activity in designing a sensing system for measuring the long jump performance, bearing in mind that any modification for other field applications refers to sensor geometrical changes only. The specifications of measurement are that the uncertainty and range of measurement are 0.1 mm and 10 m respectively.

---

#### 8.1.4 The sensor

---

The sensor is illustrated in Figure 8.26. Below the sand, an array of parallel pairs of conductors (1) is set orthogonal to the jump axis, connected with a battery (2). Each individual pair of conductors is made so that under no load there is no closed electric loop, while in case of load the two parts of the sandwich are in touch, thus allowing a closed electric loop and consequent current transmission. A straight long magnetostrictive wire (3), MDL for short, covered by a protective cell to avoid random shocks, is placed along the jump direction, between the parallel pairs of conductors at one of their edges, as shown in Figure 8.26b. One short search coil (4) is set around the MDL at a known position, preferably close to the

long jump starting point. The two ground means (5) are common for all parallel current conductors, one of them passing by the search coil.

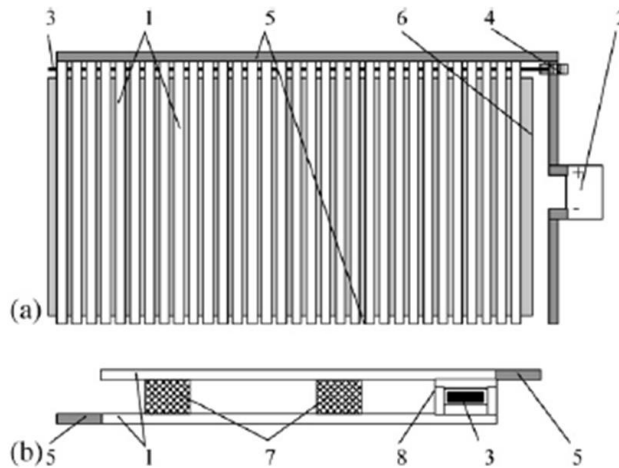


**Figure 8.26.** The sensor arrangement. (a) Schematic of the sensor, (b) Details of the pair of conductors: (1) array of parallel conductors sandwich, (2) rechargeable battery, (3) MDL, (4) search coil, (5) ground of current conductors, (6) long jump field, (7) insulating soft plastic springs, and (8) MDL support.

When load is applied on anyone of the parallel conductor sandwiches an electric loop is formed, allowing current to flow through the loop. This transient current induces an almost instant voltage spike at the search coil. It also induces a transient magnetic field at the corresponding intersection of the conductor sandwich and the MDL. The transient magnetic field generates an elastic microstrain at the above-mentioned intersection which is detected as pulsed voltage output at the search coil with a delay time  $T$  equal to the ratio of the length of the MDL between coil and pressed conductor sandwich over the longitudinal sound velocity of the MDL. Provided that only the shortest delay time is measured, this time delay is linearly proportional to the obtained jump and given by the formula:

$$L = \frac{T}{v} + L_o \quad (8.2)$$

where  $L$  is the jump performance,  $T$  the delay time,  $v$  the longitudinal sound velocity of the MDL and  $L_o$  the offset distance between search coil and long jump starting point. In order to measure the delay time  $T$  and display  $L$ ; the output of the coil is connected with a microprocessor controlled circuit, which counts the delay time  $T$  using an oscillator and digital gate technology. The same sensing system can be used to detect the position of the foot of the athlete at the long jump or triple jump starting point. Other sensing principles implementing 2-dimensional or 3-dimensional digitizers, like the ones illustrated in Figures 2.11, 2.14 and 2.16 may also serve as MDL sensors for this type of measurement.

---

## 8.4.2 Experiment and discussion

---

We have developed an experimental set-up to verify and evaluate the response of the sensing system described above. Without any loss of the generality, a 10m long, 125  $\mu\text{m}$  diameter FeSiB amorphous magnetostrictive wire has been used as the MDL. Copper conductor pairs of 9 cm width, 100 cm length and 0.1mm thickness were used as the conductor array. A 10mm pitch of the conductor pairs allowed the installation of 10 pairs in a length of 10 cm. For the needs of the experiment, the copper conductors were separated with 100 plastic spring insulators of 2mm<sup>2</sup> cross section. The 300 turns, 2 mm long search coil made of 0.1mm enamelled copper wire, was set around the MDL at a 5 m distance from the array of conductors. The microprocessor circuit used a 27 MHz clock for the delay time counting. The loading on the conductor pairs was initially applied manually. The detected sensitivity and uncertainty was 100 and 200  $\mu\text{m}$ , respectively. We also measured the durability of the sensor. In order to simulate the effect of the human loading on it, we used a large woofer speaker with a plastic rod at the end of it to repetitively apply shocks on the upper surface of the conductor pairs. Controlling the woofer motion by a pulse signal generator, we measured the sensor output with respect to the number of shocks. The sensor was broken after 10 h using a period pulse of 1 ms indicating that its response was repeatable for at least 106 load repetitions.

Although this pilot sensing arrangement promised that the sensor should work in real conditions, we had to face up the problem of the acoustic signal dispersion and its attenuation. When the delay line has a large length, the acoustic signal suffers from dispersion and consequently attenuation. The degree of dispersion and attenuation depends on the magneto-elastic uniformity of the delay lines. We determined the dispersion rate  $D(x)$  at a position  $x$  as the ratio between the width of the detected pulsed voltage output at the point  $x$  and a distance equal to 3 cm, which is the minimum detectable distance between the points of acoustic signal generation and detection. We also determined the attenuation rate  $A(x)$  at a position  $x$  as the ratio between the amplitudes of the detected pulsed voltage output at the point  $x$  and a distance equal to 3 cm too. We tested amorphous FeSiB wires and ribbons to determine and tailor these effects. The results of dispersion and attenuation in as-cast wires and ribbons are illustrated in Figures 8.27 and 8.28, respectively. It can be seen that the signal dispersion and attenuation prohibits readings in a delay line larger than 10 m.

There are two reasons responsible for the widening and damping of such an acoustic signal, one being the phonon scattering and local non-homogeneities and stresses and the other being the elastic modulus of

the material and the non-uniform anisotropy distribution in them. Both can be improved by using field and stress annealing techniques. We annealed the as-cast wire and ribbon in 350°C for 1/2 h under 200 mA DC current through the material, in Ar atmosphere. The heating rate up to the target temperature was 10°C/min, while cooling down process took place inside the oven for 24 h under Ar atmosphere. The results of dispersion and attenuation in the annealed wires and ribbons are illustrated in Figures 4.29 and 4.30, respectively. These results indicate that an acoustic signal could be detected in distances as large as 100m. We believe that the reasons for such improvement are the stress relief process, resulting in reduction of the scattering centres as well as the uniform orientation and arrangement of the magnetic domains in the material. We have also performed measurements in real conditions, using the athletic facilities of the stadium of the Campus of the National Technical University of Athens at Zografou, Athens. We installed the sensing system in the long jump facility and we compared it with respect to the classic metric measurement. The uncertainty of our sensing system with respect to the classical measurement is illustrated in Figure 8.21. Provided that the required uncertainty should be better than 5mm and the fact that our facility has a maximum uncertainty of 1mm indicates that our sensor is applicable in field sports measurements. Using the sensing system at the long jump starting point resulted in uncertainties of less than 1 mm.

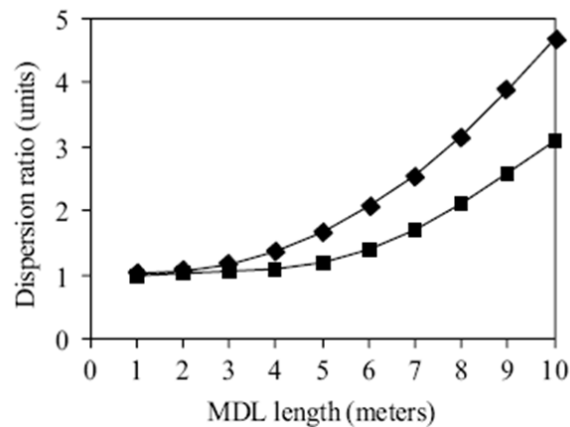


**Figure 8.27.** Acoustic dispersion in as-cast wires (rectangles) and ribbons (rhombs).

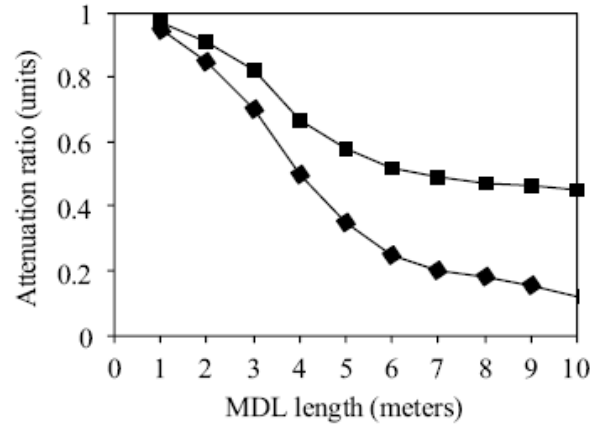


**Figure 8.28.** Acoustic attenuation in as-cast wires (rectangles) and ribbons (rhombs).

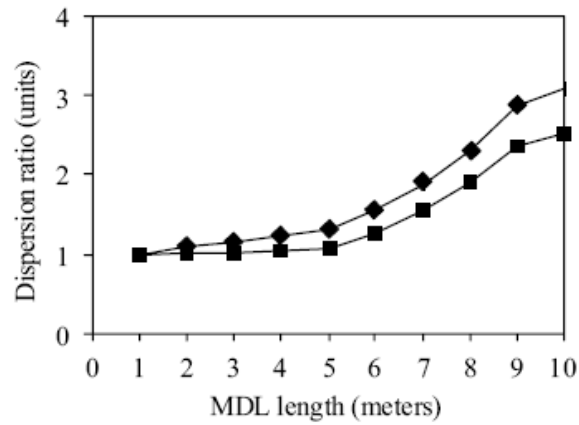


**Figure 8.29.** Acoustic dispersion in annealed wires (rectangles) and ribbons (rhombs).

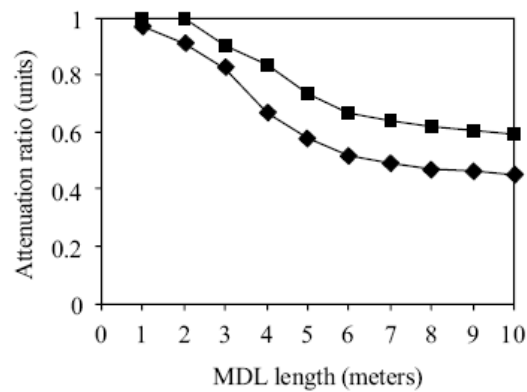


**Figure 8.30.** Acoustic attenuation in annealed wires (rectangles) and ribbons (rhombs).

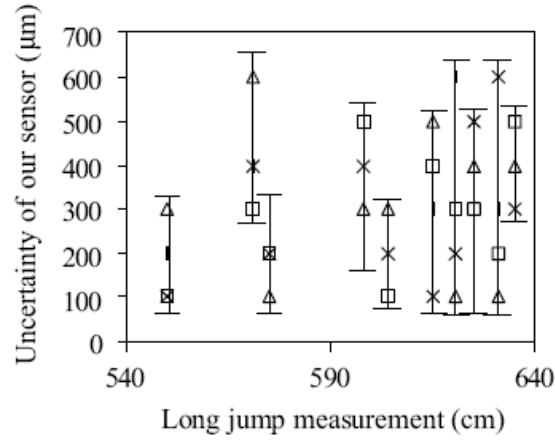


**Figure 8.31.** The uncertainty of our sensing system with respect to classical metric measurement.

---

## 8.5 MDLs in the determination of the properties of magnetostrictive materials

---

Following the theory developed in Chapter 2, the voltage output  $V_o(t)$  at the search coil is given by equation 2.9:

$$V_o(t) = -A \cdot a \cdot \mu(H_{or}) \cdot \frac{d\lambda(H_{oe}+H_e(t))}{dt} = -A \cdot a \cdot \mu(H_{or}) \cdot \frac{d\lambda}{dH} \frac{d(H_{oe}+H_e(t))}{dt} \quad (8.3)$$

It will be hereinafter shown how this procedure can result in the experimental determination of the M-H and  $\lambda$ -H loops of magnetostrictive ribbons and wires as well as their corresponding uniformity functions.

## 8.5.1 M-H loop

Keeping the excitation and biasing fields at the excitation region  $H_e$  and  $H_{oe}$  respectively constant, while the biasing field  $H_{or}$  at the receiving region changes, the peak amplitude of the MDL pulsed voltage output  $V_o$  is given by equation 2.11 corresponding to the first derivative of  $M(H_{or})$ . Normalizing  $V_o$  as well as its integral function and calibrating the MDL set-up using a standard Ni magnetostrictive wire of known M-H loop, the  $\mu$ -H and M-H loops at the region of the receiving coil of the MDL can be determined. Since the applied biasing field is dc, the method determines the dc  $\mu$ -H and M-H loops. As the sample is vibrated by the propagating elastic pulse, the method is an alternative vibrating sample magnetometer (VSM) technique, so it can be named MDL-VSM technique.

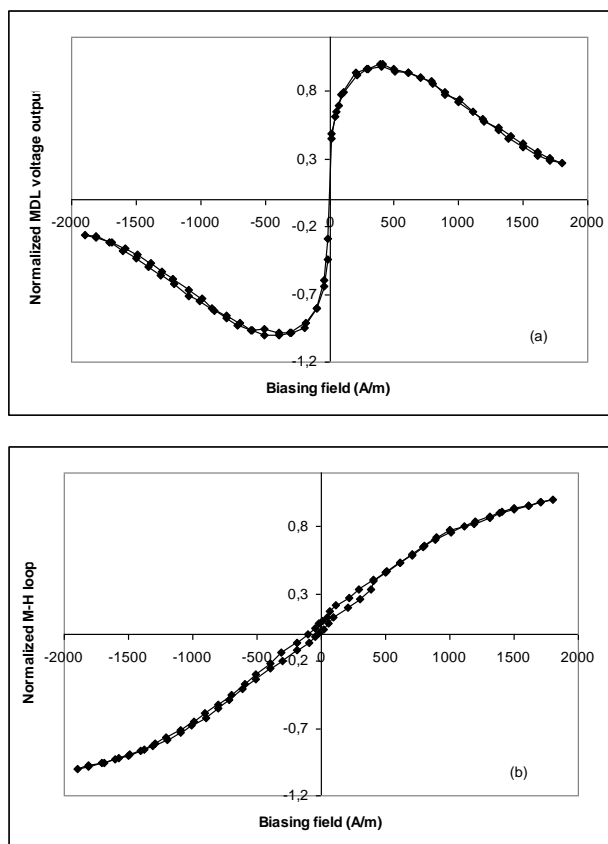


**Figure 8.32.** Permeability (a) and magnetization loops (b) concerning Fe<sub>78</sub>Si<sub>7</sub>B<sub>15</sub> amorphous wire after stress-current annealing.

A number of magnetostrictive ribbons and wires have been tested according to this method. In this report, indicative data of amorphous positive magnetostrictive ribbons and wires of the rather typical Fe<sub>78</sub>Si<sub>7</sub>B<sub>15</sub> composition are presented. Figure 8.32a and 8.32b illustrate the dependence of the normalized MDL voltage output, which is equal to the magnetic permeability  $\mu$  as well as the magnetization M loops on the biasing field H, concerning an amorphous Fe<sub>78</sub>Si<sub>7</sub>B<sub>15</sub> magnetostrictive ribbon, after stress-current annealing under 400 MPa and 0,5 A for 10 minutes. Figure 8.33a and 8.33b illustrate the same response for the case of amorphous Fe<sub>78</sub>Si<sub>7</sub>B<sub>15</sub> ribbon after thermal annealing in 450°C and Ar atmosphere for 1 hr and consequent slow rate cooling. The observed hysteresis may be attributed to the partial crystallization

of the ribbon. Such a technique can be used for studying various hysteretic properties of magnetostrictive materials.

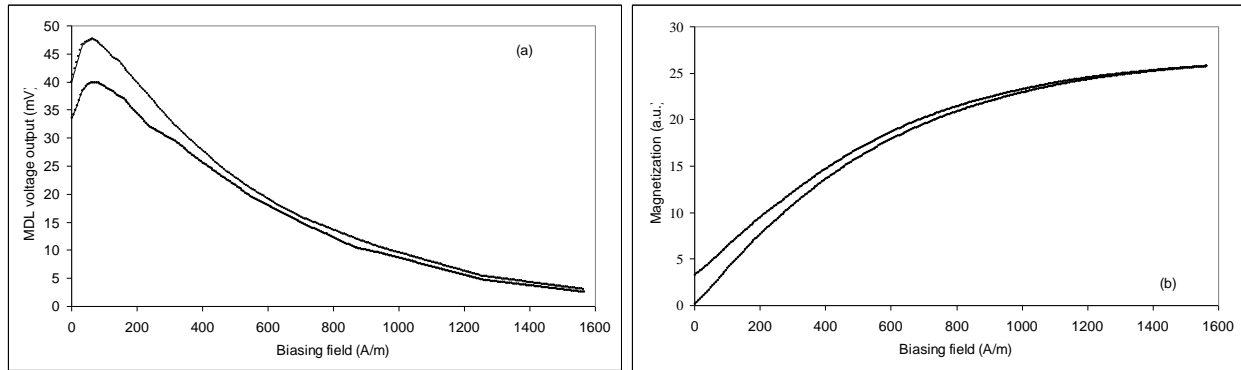


**Figure 8.33.** Permeability (a) and magnetization loops (b) concerning  $\text{Fe}_{78}\text{Si}_7\text{B}_{15}$  amorphous ribbon after thermal annealing.

As an example the sharp and bistable behaviour of as-cast amorphous magnetostrictive  $\text{Fe}_{78}\text{Si}_7\text{B}_{15}$  wires, corresponding to the Large Barkhausen jump, can be observed with this experiment, allowing the ability of observing the uniformity of the bistable behaviour along the length of the wire.

---

### 8.5.2 $\lambda$ -H loop

---

Keeping  $H_e$  and  $H_{or}$  constant, while the biasing field  $H_{oe}$  changes, the peak amplitude of the MDL pulsed voltage output  $V_o$  is given by equation 2.12, being proportional to  $d\lambda(H_{oe})/dH$ . Normalization process and calibration against a standard Ni magnetostrictive wire of known  $\lambda$ -H loop results in the dc  $\lambda$ -H function determination. Among various tested magnetostrictive materials, indicative results are presented concerning amorphous as-cast positive  $\text{Fe}_{78}\text{Si}_7\text{B}_{15}$  magnetostrictive wires. Figure 8.34a and 8.34b illustrate the normalized MDL response and the  $\lambda$  dependence on  $H_{oe}$  respectively.

Maintaining the basing fields  $H_{oe}$  and  $H_{or}$  steady and changing the excitation field  $H_e$ , the peak amplitude of  $V_o/H_e$  is given by equation 2.13. Thus, the integral of  $V_o/H_e$  on  $H_e$  is proportional to the magnetostriction  $\lambda$ . Normalization and calibration against a standard Ni magnetostrictive wire of known  $\lambda$ -H loop results in the  $\lambda$ -H loop determination. Figure 8.35a and 8.35b demonstrate indicatively the normalized MDL response and its integral corresponding to the  $\lambda$ -H function for the case of as-cast amorphous  $\text{Fe}_{78}\text{Si}_7\text{B}_{15}$  wires.

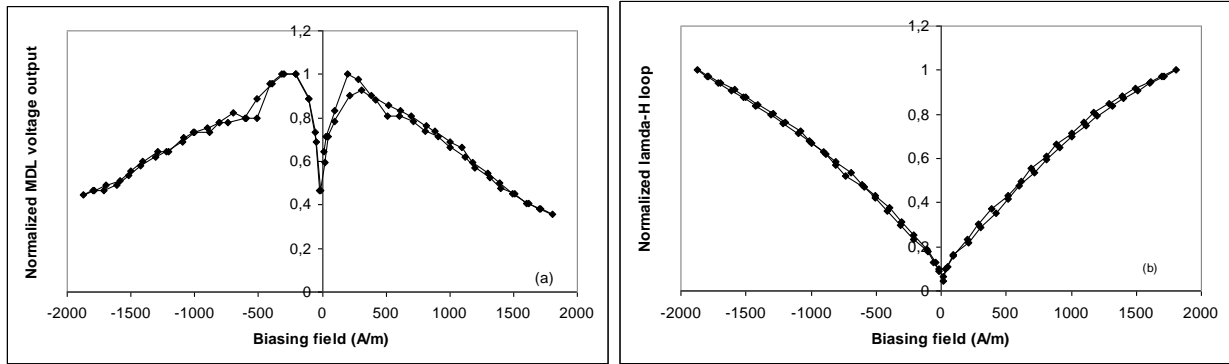


**Figure 8.34.** Normalized MDL response on biasing field at the excitation point (a) and integration of the MDL voltage output corresponding to the dc  $\lambda$ -H loop (b).

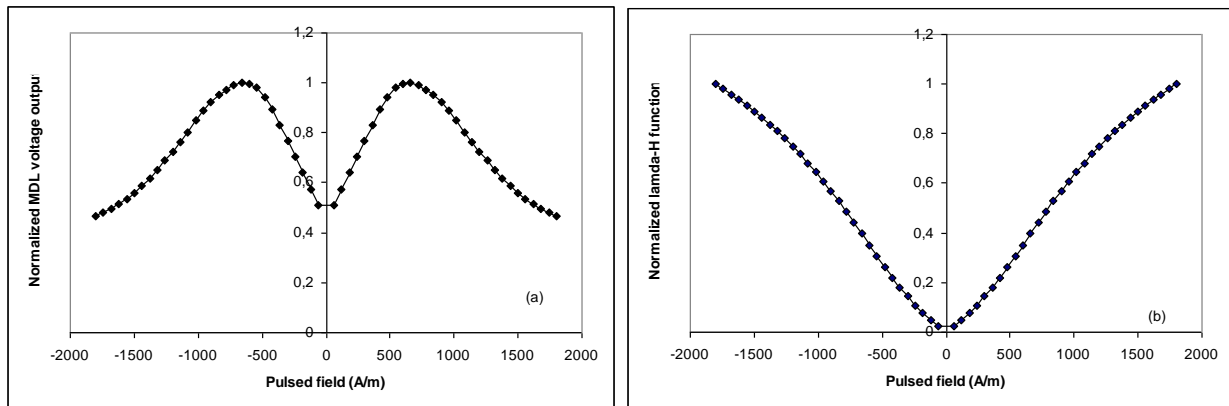


**Figure 8.35.** Normalized  $V_o/H_e$  MDL response on the pulsed field (a) and integration of  $V_o/H_e$  corresponding to the ac  $\lambda$ -H loop (b).

---

### 8.5.3 On the M(H) and $\lambda$ (H) results

---

The main advantage of the MDL-VSM technique with respect to the VSM technique is the by-design ability of non-destructive magnetic testing. Normally, in a classic VSM, the sample has to be cut in small pieces in order to be accommodated inside the VSM holder. Another significant advantage is the ability of measuring permeability, magnetization and flux density uniformity of the under test specimen, by moving the position of the receiving coil and the surrounding biasing coil.

Using this technique it is also possible to measure the M-H loop of magnetostrictive elements, not having the shape of acoustic waveguide by gluing them on a glass substrate. Thus, the elastic pulse generated either by magnetostrictive or piezoelectric means, is coupled to the under test magnetostrictive specimen

via the glass substrate and therefore, the dependence of  $\lambda$  and  $M$  may also be determined. This method can be also applied for the stress dependence determination of the  $M$ - $H$  and  $\lambda$ - $H$  loop.

Controlling the temperature of the set-up, one can determine the dependence of the  $\mu$ - $H$ ,  $M$ - $H$  and  $\lambda$ - $H$  loops on temperature. Accordingly, changing the biasing field with a given frequency, always less than the frequency corresponding to the pulsed current excitation period, which is of the order of 1 ms thus corresponding to 1 kHz maximum limit of biasing field frequency, the dependence of  $\mu$ - $H$ ,  $M$ - $H$  and  $\lambda$ - $H$  loops on frequency may also be determined. Temporal dependence tests of  $\mu$ - $H$ ,  $M$ - $H$  and  $\lambda$ - $H$  loops may also be performed.

---

## **8.6 MDLs for Residual Stress Monitoring in Magnetostrictive Cylinders and Tubes**

---

Magnetic non-destructive methods have been extensively used to correlate stresses and defects in steels with different magnetic properties, like magnetization, coercivity, permeability, Barkhausen noise, magnetoelastic waves, flux leakage etc. Some of these studies achieved to correlate directly residual stresses or microstrains with magnetic properties, namely Barkhausen noise (BHN) and differential permeability, with the advantage of achieving a Universality Law of the dependence of the localized magnetic property component on the localized stress component. The evaluation of stresses and stress fields needs the combined knowledge of the structural and magnetic configuration for testing and evaluating microstructure and mechanical properties of ferromagnetic steels grades.

Magnetostrictive steels of uniform cross sections, such as cylinders, tubes and parallelepipeds, can be considered as magnetostrictive delay lines (MDLs). This was the motivation of employing the MDL method, to precisely measure the localized stress fields in steel cylinders or tubes. The main idea to implement the MDL technique in steel cylinders and tubes is to surround them with excitation and search coils, allowing for the generation, propagation and detection of elastic waves, due to the magnetostriction and inverse magnetostriction effect. This way, all possible MDL configurations should be tested to provide the optimum monitoring conditions.

---

### 8.6.1 The under test cylinder and tube

---

The selected steel cylinder was a 25 mm diameter and 1000 mm length low-carbon-steel (LCS) with a magnetostriction constant  $\lambda_s$  in the order of 20-25 ppm at 800-900 A/m. The selected steel tube was a 25 mm external diameter, 2 mm thickness and 1000 mm length LCS with similar magnetostrictive characteristics. The magnetostrictive characteristics were determined along the length of the cylinder and the tube, by using strain gauges and an excitation solenoid in open circuit arrangement, controlled by a KEPCO amplifier.

A portable RF induction heating coil, operating at 30 kHz was used to locally heat the LCS cylinder and tube at two different local regions respectively. The local temperature was monitored by a thermal camera (FLUKE) and was not exceeding 500°C. Immediately after heating the cylinder and the tube, at temperatures between 450°C and 480°C were immersed in room temperature water, thus undergoing quenching. Since the purpose of the experiment was the proof of concept of the method, no residual stress profile was determined.

In case that the actual amount of surface residual stresses is to be measured, the X-Ray Diffraction in the Bragg-Brentano set-up could be used, to determine the localized microstrains and therefore the localized residual stresses.

---

### 8.6.2 Magnetoelastic uniformity set-up

---

The schematic of the first measuring instrument, concerning the classic magnetoelastic uniformity (classic MEU) measurement, is illustrated in Fig. 1. A 5-turn excitation coil made of 1 mm diameter enameled Cu wire of a length of ~5 mm, was wound on top of a plastic cylindrical substrate of 27 mm internal diameter, allowing for easy sliding of the excitation coil along the magnetostrictive cylinder or tube. Such a coil was able to provide pulsed current of 1 kA, 3  $\mu$ s duration and 1 ms repetition rate. The pulsed current generator has been home-made, using the principle of capacitive discharge. Thus, a pulsed field of maximum amplitude of 1 mT could be applied along the length of the excitation coil, able to generate a magnetoelastic pulse due to the magnetostriction effect in the used LCS cylinder and tube. The 300-turn 15-layer search coil was made of 0.1 mm diameter enameled Cu wire, with length of ~3 mm. The search coil was also wound on top of a plastic cylindrical substrate of 27 mm internal diameter, also allowing for easy sliding of the search coil along the under test cylinder or tube. In this arrangement, the search coil

was preferably moving along the cylinder or the tube to detect the changes of the magnetic flux at the volume inside the search coil, due to the inverse magnetostriction effect. The output of the search coil was directly driven to an 8-bit, 100 MHz digital oscilloscope, offering an output of tens of mV.

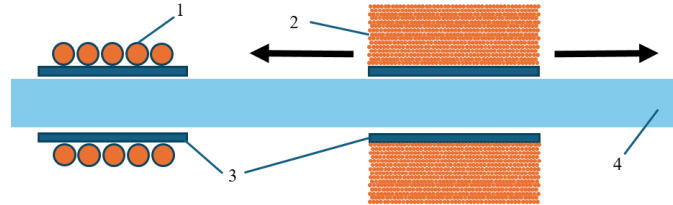


**Figure 8.36.** The schematic of the classic MEU instrument. The 5-turn excitation coil (1) was used to generate the elastic pulse, while the 300-turn search coil (2), developed on top of two substrates (3). The search coil was sliding on the under test cylinder (4), while its peak pulsed voltage output was monitored.

According to this instrument, the voltage output at the search coil should be attenuated after overpassing a volume with enhanced stress field. In a similar way, the excitation coil could also slide along the length of the cylinder or coil in order to monitor similar uniformity response. However, the repeatability of the magnetoelastic uniformity results was not sufficiently acceptable, thus allowing for the displacement of the search coil only, which were repeatable under different conditions of tested cylinders and tubes, as well as under different magnetic bias conditions.

---

### 8.6.3 Longitudinal sound velocity monitoring set-up

---

The second type of measuring instrument is illustrated in Figure 8.37. For this type of measurement, the same excitation and search coils, as well as the current generator and digital oscilloscope of the previous set-up (classic MEU) were used.

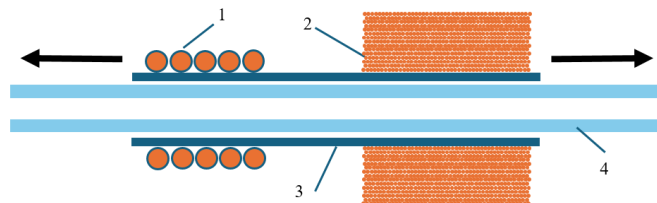


**Figure 8.37.** The schematic of the sound velocity instrument. The assembly of the excitation (1) and search (2) coils, fixed at a distance of 70 mm between them, developed on a single substrate, was sliding along the length of the magnetostrictive tube (4), measuring the delay time between the excitation and the voltage output pulse.

However, in this case, the excitation and search coils were fixed in a distance of 70 mm, in order to avoid overlapping of the detected propagating elastic wave and the inductive impulse response of the excitation coil. As illustrated in Figure 8.38, the duration of the voltage output of the search coil is 10-12  $\mu\text{s}$ . Since the longitudinal sound velocity of the LCS cylinder and tube is  $\sim 5 \text{ mm}/\mu\text{s}$ , the distance between the two coils set at 70 mm is safe enough to avoid such overlapping.



**Figure 8.38.** A typical pulsed voltage output of the search coils of Figures 8.36 and 8.37. The time scale (X-axis) is in seconds and the voltage scale is in Volts.

The assembly of the excitation and search coil was able to slide along the length of the cylinder or the tube and the time difference between the impulse inductive signal due to the coupling of the excitation coil on the search coil and the peak amplitude of the pulsed voltage output of the propagating elastic pulse offers the determination of the time delay between the excitation impulse and the peak amplitude of the elastic wave. Therefore, the local sound velocity within the volume included in the 70 mm long part of the cylinder or tube was determined.

---

### 8.6.4 Fast magnetoelastic uniformity set-up

---

Figure 8.29 illustrates the third experimental MDL arrangement. For this arrangement, allowing for a fast magnetoelastic uniformity measurements (fast MEU) the same excitation coil and generator, as for the case of the other two set-ups was used. However, in this set-up, the search coil of the MDL was a 2-layer long solenoid, made of 0.1 mm enameled copper wire on top of a 27 mm internal diameter and 900 mm long plastic substrate, covering a large volume of the under test LCS cylinder and tube.

In this case, in the absence of any residual stresses in the cylinder or tube, the only expected signals of the long search coil would be two pulses, corresponding to its boundaries, since all the rest pulsed voltage outputs at the infinitesimal volumes where the elastic pulses exist, are cancelled by the neighboring ones. Thus, a fast magnetoelastic uniformity measurement, should provide the areas of the localized stresses.

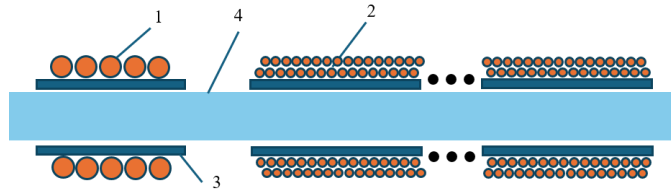


**Figure 8.39.** The schematic of the fast MEU instrument. The 5-turn excitation coil (1) was used to generate the elastic pulse, while the two-layer 900 mm long search coil (2), developed on top of a long substrate was steady in position, to test without moving the under test cylinder (4).

## 8.6.5 Experiment results and Discussion

Experiments were realized for the cylinder and the tube, using all three types of MDL sensors.

Figure 8.40 depicts the magnetoelastic uniformity response of the LCS cylinder, where the search coil moves along its length. It can be seen that the magnetoelastic response decreases significantly as soon as the search coil is on top and overpasses the first quenched volume and it decreases furthermore after the second quenched volume. This result is expected, since the generated stress field in these two volumes, causes large amount of reflections, thus permitting a portion of the elastic wave to continue propagating along the length of the cylinder.

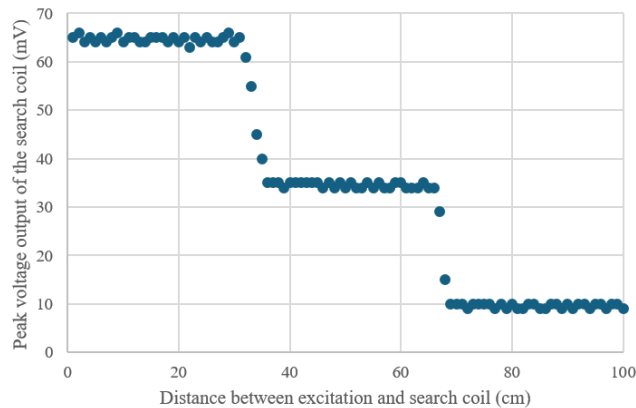


**Figure 8.40.** Response of the classic MEU instrument, illustrating the dependence of the pulsed voltage output of the search coil on the distance from the excitation coil. The effect of the two artificially made stress fields at a 40 cm distance between each other is clearly observable. After overpassing each stress field, the amplitude of the propagating elastic pulse decreases due to reflections at the stress field area.

However, this practically means that the magnetoelastic uniformity method will not be able to characterize a large amount of residual stresses along the length of the cylinder. The minimum time of scanning each infinitesimal volume of the LCS cylinder within the search coil was 2 ms. Thus, considering a sliding motion using a stepper motor to move the search coil, detecting the pulsed voltage output every 1 mm, which is a logical incremental step considering the length of the coil, the time for the test of the whole cylinder is 2 s, resulting in a maximum speed of detection equal to 0.5 m/s.

Figure 8.41 illustrates the change of the delay time between the excitation impulse and the peak amplitude of the detected sound velocity along the length of the LCS tube, as the assembly of the excitation and search coil separated by 70 mm, slides along the tube. It is clear that for this instrument the different stress field measurements are not accumulated with the rest of them, resulting in the ability to clearly detect the effect of each localized stress field separately. Besides, the measurement of the longitudinal sound velocity change is a non-linear acoustic method, offering the direct measurement of the stress field in the corresponding volumes. Apart from that, the time needed for such sound velocity measurement is the same as for the previous case, namely 2 s, resulting in a maximum detection speed of 0.5 m/s. The ability to distinguish different stress fields in different volumes of the LCS tube offers an advantage of the sound velocity measurement with respect to the classic MEU measurement.

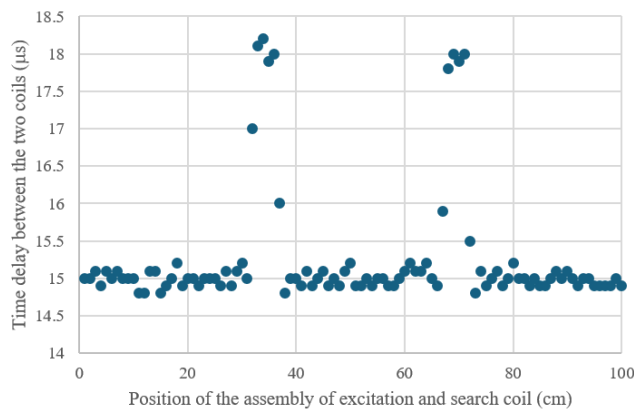


**Figure 8.41.** Response of the sound velocity instrument, illustrating the dependence of the delay time excitation and detected pulse, corresponding to the change of sound velocity of the material, since the two coils are fixed in position. No damping effect is observable, as expected.

Measurements using the fast MEU instrument have been also realized in both the LCS cylinder and tube. Figure 8.42 represents the fast MEU response of the long search solenoid, for the case of the LCS cylinder. It is clear that the response of the long coil suffers from the same accumulation of stress fields as for the

case of the classic MEU, since the response of the second pulsed voltage output of the long search coil is affected by the first stress field. However, the time needed for the whole measurement is only 2 ms, resulting in a maximum detection speed of 2 ms/m. Another handicap of the fast MEU instrument is the difficulty of preparing longer search coils. Thus the method should be limited to laboratory use.

These three types of non-linear magnetoacoustic measurements was also compared with more classical techniques. The first one was the alternating-field B-H hysteresis loop measurement, using quasi-stating sinusoidal excitation frequency, in the order of 0,1 Hz up to 0,5 Hz, to detect the stress field effect of the sample, avoiding the eddy current contribution, observable in higher frequencies. The instrument for the B-H loop hysteresis loop measurement operates in open magnetic circuit and employs a primary coil on top of a search coil, coupled together, thus offering a direct measurement of the change of the flux density along the length of the under test LCS cylinder and tube.

The same arrangement was used for high frequency excitation, in the order of 10 kHz, to observe the eddy current effect at the different volumes of the under test steel due to the change of the resistance caused by the stress field. In both frequencies, resulting in two different types of response, the peak amplitude of the secondary (search) coil at each position of measurement was determined.

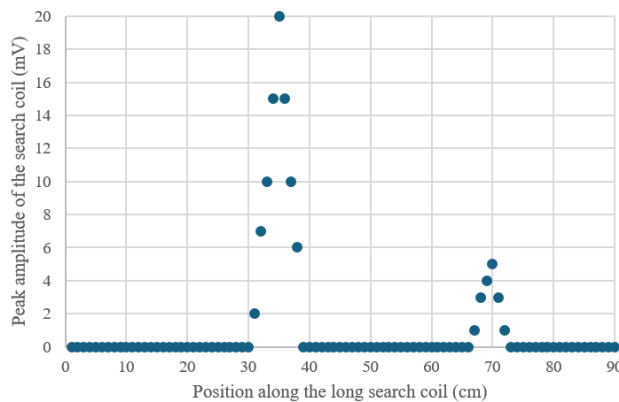


**Figure 8.42.** Response of the fast MEU instrument, illustrating the dependence of the pulsed voltage output of the search coil on the distance from the excitation coil. The response is similar to the response of the classic MEU, without sliding need of the search coil.

The schematic of the coupled coils is illustrated in Figure 8.43. A plastic substrate of 27 mm internal diameter, as for the case of the MDL instruments, was used to support the search and excitation coils. The 5 mm long, 300-turn search coil made of 0.1 mm enameled Cu wire, was directly wound on the plastic

substrate. The 15 mm long, 45-turn excitation coil was wound on top of the search coil, after a paper insulation between the two coils. The excitation for the case of the low frequency measurement was realized by a Series BOP KEPCO power amplifier, offering up to 5 A peak amplitude at frequencies between 0,2 Hz and 0,5 Hz, while the excitation of the  $\sim 10$  kHz high frequency was realized by a signal generator.

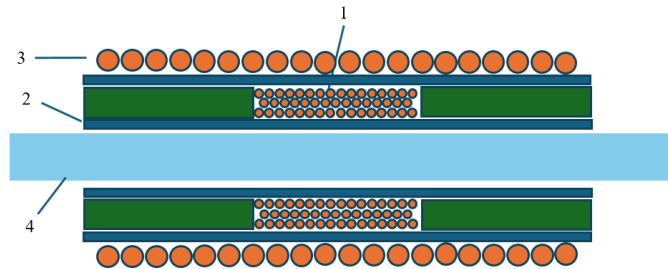


**Figure 8.43.** The schematic of the B-H loop and eddy current instrument. The 300-turn secondary coil (1) was developed directly on top of the plastic substrate (2), while the three-times longer excitation coil (3) was on top of the search coil. The assembly was sliding on the under test cylinder or tube (4), while the peak voltage output of the secondary coil was monitored.

Several measurements for low and high frequency response, corresponding to permeability and eddy current measurements have been realized on the same LCS cylinder and tube. Figures 8.44 and 8.45 illustrate the dependence of the peak amplitude of the secondary coil for 0,2 Hz and 10 kHz excitation frequency for the tube and the cylinder respectively.

An agreement between the two responses, as well as between the response of the three MDL arrangements can be observed. The advantage of the low frequency measurement is the direct correlation with residual stresses, since the peak amplitude of the secondary coil is related to the differential permeability of the under test steel, with the disadvantage of the long time need for the measurement, in the order of at least 2 s up to 10 s per point of measurement, for a single period of measurement.

The advantage of the high frequency instrument is the time needed for measurement. A common disadvantage of both measurements is the low voltage output response, resulting in low sensitivity of measurement, in comparison with the three MDL arrangements.

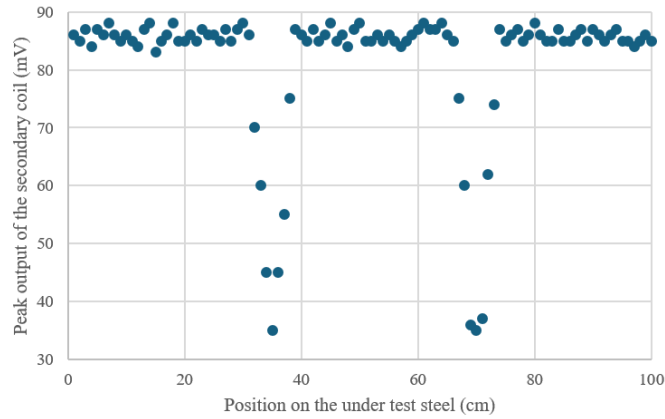


**Figure 8.44.** B-H loop response

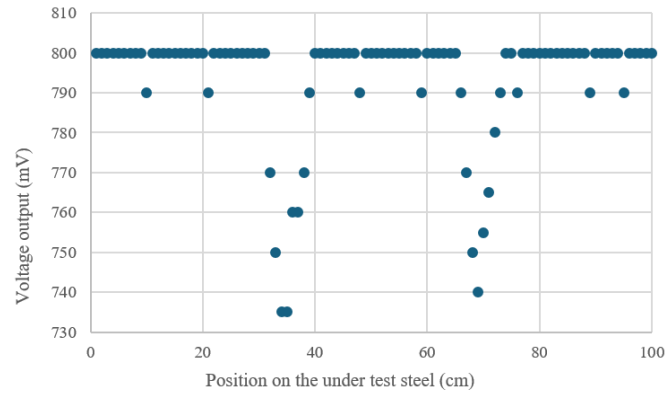


**Figure 8.45.** Eddy current response

The comparison of the response of the three MDL arrangements, the effective permeability and the eddy current response is provided in Table 8.2.

**Table 8.2.** Comparison between MDL, B-H Loop and Eddy Current setups

Instrument Property	Classic MEU	Sound velocity	Fast MEU	B-H loop	Eddy current
Point sensitivity	Order of mV	Order of 10 ns	Order of mV	Order of mV	Order of V
Stress accumulation	Yes	No	Yes	No	No
Speed of measurement	0,5 m/s	0,5 m/s	2 km/s	2 mm/s	2 m/s

Table 1 depicts the necessary information on the use of the five different detecting instruments. It is clear that all MDL instruments are sensitive enough even in comparison with B-H loop and eddy current measurements. The ability to monitor large scale stress distribution is actually available in the sound velocity MDL instrument and the classic B-H loop and eddy current measurement. Finally, the speed of measurement of the MDL measuring instruments is superior than the B-H loop instrument and comparable to the eddy current set-up. It is therefore concluded that the sound velocity instrument has all the required properties to be used for stress distribution monitoring, with sensitive response, ability to avoid stress accumulation and acceptable speed of measurement.

This MDL instrument can decrease the average volume of the under test steel, by means of reducing the distance between excitation and search coils. This can be achieved by reducing the duration of the detected voltage output, which can be achieved by using anisotropic magnetoresistance (AMR) heads instead search coils. All these instruments can be used in production lines, by including them in properly selected parts of the production-manufacturing line with temperatures close to room temperatures. They can also be used in field measurements by developing split excitation and search coils to accommodate them around the under tests cylinders or tubes.



# Conclusions and future work

In the presented work, the magnetostrictive delay lines and their engineering applications have been thoroughly studied. At the first place, the generation, propagation and detection of an elastic pulse in the simplest MDL arrangements have been investigated. Such a study has resulted in understanding the mechanisms and parameters of elastic pulse generation and detection, namely being the excitation and biasing fields as well as the mechanical action on the MDL. Understanding these mechanisms and parameters allowed for the conceiving and development of different MDL arrangements, which may serve either as signal multiplexers and demultiplexers or as sensing and distribution sensing elements. Consequently, the main properties of the MDLs have been determined and introduced. The basic properties, such as sensitivity, linearity and hysteresis, as well as methods of tailoring them have been discussed, followed by the determination of the MDL parametric dependence on the field, frequency, stress, temperature and time. The magnetoelastic uniformity, the sound velocity and the MDL resolution, three important properties of MDLs defining the performance of MDLs, have also been introduced and analyzed. Taking into account the main MDL arrangements and properties, various magnetoelastic materials have been tested, concluding that amorphous ribbons and wires are suitable for sensing applications, without excluding thin film set-ups. The properties of these materials may serve as a database for possible use in engineering, mainly sensing applications.

Having introduced the MDL arrangements, properties and materials, the main MDL sensors have been presented. For studying comprehension reasons, they have been split up into three main categories, namely position, stress and field sensors. Several position sensors have been developed based on amplitude or time delay modulation, able to measure static or dynamic displacement. Various field sensors have also been developed, such as tensile stress sensors, load cells, torque meters, pressure gauges and force digitizers, offering some advantages with respect to the state of the art. Field sensors based on the MDL technique have also been presented, offering distribution measurement ability but poor uncertainty of measurement. Furthermore, manufacturing technologies have been introduced allowing low cost and acceptable uncertainty of the sensing elements. Finally, some critical applications of MDL have been discussed, such as non-destructive testing applications based on eddy current or field

detection, blood and chemical composites coagulation studies, civil and mining engineering applications as well as sports field applications. As a last, but not least, application of the MDL technique, a method for  $M(H)$  and  $\lambda(H)$  measurement has been illustrated, according to which the loop and the uniformity of magnetization and magnetostriction along the length of a magnetostrictive material in the shape of an acoustic waveguide can be determined.

The summary of the MDL technology depicted in this work does not indicate the termination of the research and development activity on magnetostrictive delay lines. On the contrary, it may serve as the boost for further study in the following fields:

- Better understanding of the mechanisms of generation, modification during propagation and detection of elastic pulses, based on the structure and microstructure of the magnetostrictive element
- Development of the most attractive mechanical sensors based on the MDL technology, able to be used in industry, transportation, energy, biomedicine and other engineering applications
- Development of composite materials, such magnetostrictive – electrostrictive composites for engineering applications

# References

1. E.O. Doebelin, *Measurement Systems: applications and design*, fourth edition, McCraw-Hill, 1990
2. E.E. Herceg, *Handbook of measurement and control*, rev. ed., Schaevitz Engineering, Pennsauken, N.J. 1976
3. R. Boll, *Soft magnetic materials*, *Vacuumschmelze handbook*, Heyden & Son, 1977
4. *Magnetic Sensors and Magnetometers*, P. Ripka (ed), *Meas. Sci. Technol.*, 13, 2002
5. J.M. Daughton, *GMR applications*, *Journal of Magnetism and Magnetic Materials*, 192, p. 334-342, 1999
6. K. Mohri, K. Bushida, M. Noda, H. Yoshida and L.V. Panina, T. Uchiyama, *Magneto-impedance element*, *IEEE Transactions on Magnetics*, 31, p. 2455 –2460, 1995
7. E. du Tremolet de Lacheisserie, *Magnetostriction: Theory and Applications of Magnetoelasticity*, CRC Press, Boca Raton, FL, 1994
8. J.D. Jackson, *Electricity and Magnetism*, Wiley, NY, 1965
9. D. Jiles, *Introduction to the electronic properties of materials*, Chapman & Hall, 1993
10. D. Jiles, *Introduction to magnetism and magnetic materials*, Chapman & Hall, 1991
11. R.C. O’Handley, *Modern magnetic materials*, Wiley, 1999
12. A.P. Thomas, M.R.J. Gibbs, J.H. Vincent and S.J. Ritchie, *Technical magnetostriction parameters for application of metallic glasses*, *IEEE Transactions on Magnetics*, 27, p. 5247 –5249, 1991
13. J.P. Hayes, L.A. Stone, H.V. Snelling, A.G. Jenner and R.D. Greenough, *Magnetic and magnetoelastic properties of thin films by pulsed laser deposition*, *IEEE Transactions on Magnetics*, 33, p. 3613 – 3615, 1997
14. N.J. Grabham, S.P. Beeby and N.M. White, *The formulation and processing of a thick-film magnetostrictive material*, *Meas. Sci. Technol.*, 13, p. 59-64, 2002
15. A. Hernando, M. Vazquez and J.M. Barandiaran, *Metallic glasses and sensing applications*, *J. Phys. E: Sci. Instrum.*, 21, p. 1129-1139, 1988
16. A. Biekowski, *Magnetoelastic Villari effect in Mn-Zn ferrites*, *Journal of Magnetism and Magnetic Materials*, 215-216, p. 231-233, 2000
17. A. Aharoni, *Introduction to the theory of Ferromagnetism*, Clarendon Press, Oxford, 1996

18. M. Onoe, Theory of Ultrasonic Delay Lines for Direct Current Pulse Transmission, *J. Acoust. Soc. Am.*, 34, p. 1247, 1962
19. M. Vazquez, C. Gomez-Polo, D.X. Chen and A. Hernando, Magnetic bistability of amorphous wires and sensor applications, *IEEE Transactions on Magnetics*, 30, p. 907–912, 1994
20. M. Mizutani, H. Katoh, L.V. Panina, K. Mohri and F.B. Humphrey, Distance sensors utilizing large Barkhausen effect excited by wire current pulse train in twisted amorphous magnetostrictive wires, *IEEE Transactions on Magnetics*, 29, p. 3174–3176, 1993
21. K. Kawashima, T. Kohzawa, H. Yoshida and K. Mohri, Magneto-inductive effect in tension-annealed amorphous wires and MI sensors, *IEEE Transactions on Magnetics*, 29, p. 3168–3170, 1993
22. L.V. Panina and K. Mohri, Effect of magnetic structure on giant magneto-impedance in Co-rich amorphous alloys, *Journal of Magnetism and Magnetic Materials*, 157-158, p. 137-140, 1996
23. A. Mitra, M. Vazquez, A. Hernando and C. Gomez-Polo, Field Flash Annealing of Co-Rich Amorphous Alloy, *IEEE Transactions on Magnetics*, 26, p. 1415-1417, 1990
24. S. Chikazumi, *Physics of Magnetism*, John Wiley & Sons, 1964
25. Y.H. Chen and D.C. Jiles, The magnetomechanical effect under torsional stress in a cobalt ferrite composite, *IEEE Transactions on Magnetics*, 37, p. 3069–3072, 2001
26. T.B. Thompson and J.A.M. Lyon, Analysis and application of magnetostrictive delay lines, *Transactions IRE PGUE-4*, 8, 1956
27. K.G. Van den Berg, A multiple wire magnetostrictive delay line for improved signal and reduced reflections, *J. Phys. E: Sci. Instrum.*, 15, p. 325-327, 1982
28. M. Inoue, N. Fujita and T. Fujii, Propagation characteristics of magnetoelastic surface waves in magnetic layer on non-piezomagnetic substrate, *IEEE Transactions on Magnetics*, 20, p. 1406-1408, 1984
29. H. Epstein and O.B. Strum, A high performance magnetostriction-sonic delay line, *Transactions IRE PGUE-5*, 1, 1957
30. K. Kakuno, S. Masuda and T. Yamada, Scattered magnetoelastic waves in amorphous wires, *J. de Physique*, C8, p. 2037, 1988
31. M. Inoue, Y. Tsuboi, A. Makita, N. Fujita, T. Miyama and T. Fujii, Effect of eddy current loss on the propagation properties of magneto-surface-acoustic-waves in highly magnetostrictive alloy film deposited on glass substrate, *Japanese Journal of Applied Physics*, 25, p. 157-159, 1986

32. P.T. Squire and M.R.J. Gibbs, Ultrasonic shear-wave absorption in amorphous magnetic ribbons, *Journal of Applied Physics*, 64, p. 5408-5410, 1988
33. M.G. Scott and A. Kursomovic, Use of elastic waves to study relaxation in metallic glasses, *Metal. Sci.*, 15, p. 583-586, 1981
34. K. Kakuno, S. Masuda, T. Yamada and H. Mochida, Effects of wire drawing and annealing on propagation of magnetoelastic waves in amorphous wires, *IEEE Transactions on Magnetics*, 23, p. 2554-2556, 1987
35. L. Lanotte, Z. Kaczkowski and L. Maritato, Enhancement of magnetoelastic wave amplitude in amorphous Co-P alloy by multilayer structure, *Europhys. Lett.*, 8, p. 717-722, 1992
36. L. Lanotte, C. Luponio and A. Annunziata, Magnetic and structure phase transitions investigated by standing magnetoelastic waves, *Journal of Magnetism and Magnetic Materials*, 80, p. 153-158, 1989
37. N. Tsuya, K.I. Arai and T. Oksaka, Saturation magnetostriction of iron rich amorphous ribbons and electronically variable delay line, *IEEE Transactions on Magnetics*, 14, p. 946-948, 1978
38. M. Inoue, Study on propagation properties of magnetoelastic waves in Fe-based highly magnetostrictive amorphous materials and their applications, Doctoral Thesis, Toyohashi University of Technology, 1989
39. S. Masuda and K. Kakuno, Properties and structure of scattering centers for magnetoelastic waves in amorphous wires, *IEEE Transactions on Magnetics*, 26, p. 1801-1803, 1990
40. R.D. James, Recent research in ferromagnetic shape memory materials and films, *Proceedings of the 5th Conference on Magnetic Materials Measurements and Modeling*, Iowa State University, Ames, USA, 2002
41. E. Quandt, Giant magnetostrictive thin film materials and applications, *Journal of Alloys and Compounds*, 258, p. 126-132, 1997
42. E.T.M. Lacey, D.G. Lord and P.J. Grundy, Sputtered films of TbDyFe, *IEEE Transactions on Magnetics*, 24, p. 1713–1715, 1988
43. M. Pasquale, A. Infortuna, L. Martino, C. Sasso, C. Beatrice and S.H. Lim, Magnetic properties of TbFe thin films under applied stress, *Journal of Magnetism and Magnetic Materials*, 215-216, p. 769-771, 2000
44. H. Chiriac and T.A. Ovari, Amorphous glass covered magnetic wires: preparation, properties, applications, *Progress in Materials Science*, 40, p. 333-407, 1996

45. H. Chiriac, T.A. Óvári, Gh. Pop and F. Barariu, Amorphous glass-covered magnetic wires for sensing applications, *Sensors and Actuators A: Physical*, 59, p. 243-251, 1997
46. M. Vázquez, Soft magnetic wires, *Physica B: Condensed Matter*, 299, p. 302-313, 2001
47. G.E. Fish, Soft magnetic materials, *Proceedings of the IEEE*, 78, p. 947 –972, 1990
48. R. Hasegawa, Soft Magnetic Properties of Metallic Glasses, *Journal of Magnetism and Magnetic Materials*, 41, p. 79-85, 1984
49. A.F. Cobeño, A. P. Zhukov, E. Pina, J.M. Blanco, J. Gonzalez and J.M. Barandiaran, Sensitive magnetoelastic properties of amorphous ribbon for magnetoelastic sensors, *Journal of Magnetism and Magnetic Materials*, 215-216, p. 743-745, 2000
50. K. Imamura, S. Kwang-Ho, K. Ishiyama, M. Inoue and K.I. Arai, Anisotropy control of magnetostrictive film patterns, *IEEE Transactions on Magnetics*, 37, p. 2025 –2027, 2001
51. A.G. Jenner, J.P. Hayes, L. A. Stone, H.V. Snelling and R.D. Greenough, Pulsed laser deposition-an alternative route to the growth of magnetic thin films, *Applied Surface Science*, 138-139, p. 408-412, 1999
52. H. Chiriac, M. Pletea and E. Hristoforou, Magnetoelastic Characterization of Thin Films Dedicated to Magnetomechanical Microsensor Applications, *Sensors and Actuators A: Physical*, 68, p. 414-418, 1998
53. G. Herzer, Grain Size Dependence of Coercivity and Permeability in Nanocrystalline Ferromagnets, *IEEE Transactions on Magnetics*, 26, p. 1397-1402, 1990
54. P. Marín, M. López, P. Agudo, M. Vázquez and A. Hernando, Applications of amorphous samples presenting high magnetomechanical coupling during the first stages of nanocrystallisation process, *Sensors and Actuators A: Physical*, 91, p. 218-222, 2001
55. B. Ahamada, F. Alves and R. Barrué, Improvement of magnetoelastic properties of nanocrystalline materials for magnetostrictive sensors, *Journal of Magnetism and Magnetic Materials*, 242-245, p. 1443-1445, 2002
56. L. Lanotte, G. Ausanio, V. Iannotti and C. Luponio, The potentiality of composite elastic magnets as novel materials for sensors and actuators, *Proceedings of the 4th European Magnetic Sensor and Actuator Conference*, Athens, Greece, 2002
57. J.L. Prieto, P. Sánchez, C. Aroca, E. López, M.C. Sánchez, O. de Abril and L. Pérez, Improving the characteristics in magnetostrictive-piezoelectric sensors when the viscous interface is removed, *Sensors and Actuators A: Physical*, 84, p. 338-341, 2000

58. J. Füzér, P. Brauer and O.V. Nielsen, Magnetic behaviour of amorphous ribbons with creep-induced helical anisotropy and their fluxgate properties, *Journal of Magnetism and Magnetic Materials*, 188, p. 286-290, 1998
59. J.L. Costa, Y. Makino and K.V. Rao, Effects of longitudinal currents and torsion on the magnetization processes in amorphous wires, *IEEE Transactions on Magnetics*, 26, p. 1792 –1794, 1990
60. A.P. Thomas, M.R.J. Gibbs. and P.T. Squire, Dependence of Magnetostriction on Induced Anisotropy in Metallic Glasses, *IEEE Transactions on Magnetics*, 26, p. 1403-1405, 1990
61. C. Garcia, A. Chizhik, J.J. del Val, A. Zhukov, J.M. Blanco and J. Gonzalez, Structural, magnetic and electrical transport properties in cold-drawn thin Fe-rich wires, *Journal of Magnetism and Magnetic Materials*, 294, p. 193-201, 2005
62. I. Ogasawara and K. Mohri, Tension Annealing Cold-Drawn Amorphous CoFeSiB Wires, *IEEE Transactions on Magnetics*, 26, p. 1795-1797, 1990
63. J. Gonzalez, J.M. Blanco, J.M. Barandiaran, M. Vazquez, A. Hernando, G. Rivero and D. Niarchos, Helical Magnetic Anisotropy Induced By Current Annealing Under Torsion in Amorphous Wires, *IEEE Transactions on Magnetics*, 26, p. 1798-1800, 1990
64. L. Kraus, A novel method for measurement of the saturation magnetostriction of amorphous ribbons, *J. Phys. E: Sci. Instrum.*, 22, p. 943-947, 1989
65. M. Kaneko, S. Hashimoto, M. Hayakawa and K. Aso, Measuring the magnetostriction of thin films using an optical displacement meter, *J. Phys. E: Sci. Instrum.*, 21, p. 487-489, 1988
66. G. Vlasak, P. Duhaj, H. Patrasova and P. Svec, Apparatus for thermal dilatation and magnetostriction measurements of amorphous ribbons, *J. Phys. E: Sci. Instrum.*, 16, p. 1203-1207, 1983
67. J. Heremans, J.P. Michenaud, Y. Iye, N. Miura, G. Kido, K. Nakamura and S. Tanuma, A capacitive instrument for the measurement of magnetostriction in pulsed fields, *J. Phys. E: Sci. Instrum.*, 16, p. 382-386, 1983
68. R.D. Greenough and C. Underhill, Strain gauges for the measurement of magnetostriction in the range 4K to 300K, *J. Phys. E: Sci. Instrum.*, 9, p. 451-454, 1976
69. Y.D. Shin, Y.H. Lee, and J.R. Rhee, Observation of thin film magnetostriction using a piezoelectric sensor, *IEEE Transactions on Magnetics*, 29, p. 3025 –3027, 1993
70. C.S. Gudeman, Magnetostriction mapping of soft magnetic films on thick rigid substrates, *IEEE Transactions on Magnetics*, 26, p. 2580 –2582, 1990

71. L. Kvarnsjö and G. Engdahl, A set-up for dynamic measurements of magnetic and mechanical behavior of magnetostrictive materials, *IEEE Transactions on Magnetics*, 25, p. 4195–4197, 1989
72. P.T. Squire, Magnetomechanical measurements of magnetically soft amorphous materials, *Meas. Sci. Technol.*, 5, p. 67-81, 1994
73. D.J. García and B. Alascio, Low field magnetoresistance in double exchange compounds, *Physica B: Condensed Matter*, 320, p. 7-12, 2002
74. Y.K. Kim, S.C. Sanders and S.E. Russek, Low magnetostriction in annealed NiFe/Ag giant magnetoresistive multilayers, *IEEE Transactions on Magnetics*, 31, p. 3964–3966, 1995
75. G. Dumpich, T.P. Krome and B. Hausmanns, Magnetoresistance of single Co nanowires, *Journal of Magnetism and Magnetic Materials*, 248, p. 241-247, 2002
76. S. Li and M. Greenblatt, Large intragrain magnetoresistance in the double perovskite BaLaMnMoO<sub>6</sub>, *Journal of Alloys and Compounds*, 338, p. 121-125, 2002
77. M. Angelakeris, P. Pouloupoulos, O. Valassiades, N.K. Flevaris, D. Niarchos and A. Nassiopoulou, GMR study leading to sensor fabrication on the Ag<sup>-</sup>Co system, *Sensors and Actuators A: Physical*, 91, p. 180-183, 2001
78. K-M.H. Lenssen, H.W. Van Kesteren, J.C.S. Kools, M.C. De Nooijer, R. Coehoorn, W. Folkerts and Th.G.S.M. Rijks, Giant magnetoresistance and its application in recording heads, *Sensors and Actuators A: Physical*, 60, p. 90-97, 1997
79. L. Kraus, GMI modeling and material optimization, *Proceedings of the 4th European Magnetic Sensor and Actuator Conference*, Athens, Greece, 2002
80. K.R. Pirota, L. Kraus, H. Chiriac and M. Knobel, Magnetostriction and GMI in Joule-heated CoFeSiB glass-covered microwires, *Journal of Magnetism and Magnetic Materials*, 226-230, p. 730-732, 2001
81. M. Tejedor, B. Hernando, M.L. Sánchez, V.M. Prida and P. Gorria, Magnetic domains and magnetoimpedance effect during the nanocrystallization of Fe<sub>73.5</sub>Cu<sub>1</sub>Nb<sub>3</sub>Si<sub>16.5</sub>B<sub>6</sub> ribbons, *Journal of Non-Crystalline Solids*, 287, p. 396-400, 2001
82. T. Yoshinga, S. Furukawa and K. Mohri, Magneto-impedance effect in etched thin amorphous wires, *IEEE Transactions on Magnetics*, 35, p. 3613–3615, 1999
83. M. Vázquez, M. Knobel, M.L. Sánchez, R. Valenzuela and A.P. Zhukov, Giant magnetoimpedance effect in soft magnetic wires for sensor applications, *Sensors and Actuators A: Physical*, 59, p. 20-29, 1997

84. K. Kawashima, I. Ogasawara, S. Ueno and K. Mohri, Asymmetrical magneto-impedance effect in torsion-annealed Co-rich amorphous wire for MI micro magnetic sensor, *IEEE Transactions on Magnetics*, 35, p. 3610–3612, 1999
85. L.P. Shen, T. Uchiyama, K. Mohri, E. Kita and K. Bushida, Sensitive stress-impedance micro sensor using amorphous magnetostrictive wire, *IEEE Transactions on Magnetics*, 33, p. 3355–3357, 1997
86. P.P. Freitas, F. Silva, N.J. Oliveira, L.V. Melo, L. Costa and N. Almeida, Spin valve sensors, *Sensors and Actuators A: Physical*, 81, p. 2-8, 2000
87. S.D. Kim, O.M. J. van't Erve, R. Jansen, P.S. Anil Kumar, R. Vlutters and J.C. Lodder, Fabrication technology for miniaturization of the spin-valve transistor, *Sensors and Actuators A: Physical*, 91, p. 166-168, 2001
88. K. Attenborough, H. Boeve, J. de Boeck, G. Borghs and J-P. Celis, Ultra-sensitive spin-valve structures grown on n-GaAs by single bath electrodeposition, *Sensors and Actuators A: Physical*, 81, p. 9-12, 2000
89. F.E. Stanley, C.H. Marrows, I. Zoller, E.W. Hill and B.J. Hickey, Optimisation of spin-valves on rough substrates, *Sensors and Actuators A: Physical*, 81, p. 32-36, 2000
90. Y. Kitade, H. Kikuchi, H. Kishi, M. Otagiri and K. Kobayashi, Giant magnetoresistance effect in CoNiFe/Cu spin valves, *IEEE Transactions on Magnetics*, 31, p. 2600–2602, 1995
91. S. Yuasa, T. Nagahama and Y. Suzuki, Spin-polarized resonant tunneling in magnetic tunnel junctions, *Science*, 297, p. 234-237, 2002
92. D. Kechrakos and K.N. Trohidou, Spin correlations and electronic transport in magnetic nanoclusters, *Physica B: Condensed Matter*, 318, p. 360-364, 2002
93. K. Diaz de Lezana, A. García-Arribas, J.M. Barandiarán and J. Gutiérrez, Comparative study of alternative circuit configurations for inductive sensors, *Sensors and Actuators A: Physical*, 91, p. 226-229, 2001
94. O.V. Nielsen, P. Brauer, F. Primdahl, J.L. Jørgensen, C. Boe, T. Risbo, M. Deyerler and S. Bauereisen, A high-precision triaxial fluxgate sensor for space applications: Layout and choice of materials, *Sensors and Actuators A: Physical*, 59, p. 168-176, 1997
95. H. Chiriac, E. Hristoforou, M. Neagu, M. Pieptanariu and F.G. Castano, Linear Variable Differential Transformer Sensor using Fe-rich Amorphous Wires as Active Core, *J. Appl. Phys.*, 87, 9, p. 5344-5346, 2000

96. D. Robbes, Highly sensitive magnetometers-a review, *Sensors and Actuators A: Physical*, 129, p. 86-93, 2006
97. J.M. Barandiaran and J. Gutierrez, Magnetoelastic sensors based on soft amorphous magnetic alloys, *Sensors and Actuators A: Physical*, 59, p. 38-42, 1997
98. M. Vázquez and A. Hernando, A soft magnetic wire for sensor applications, *J. Phys. D: Appl. Phys.*, 29, p. 939-949, 1996
99. Y. Kano, S. Hasebe, C. Huang, T. Yamada and M. Inubuse, Linear Position Detector with Rod Shape Electromagnet, *IEEE Transactions on Magnetics*, 26, p. 2023-2025, 1990
100. G. Vertesy, J. Szollosy and A. Lovas, Magnetoinductive Position Sensor, *IEEE Transactions on Magnetics*, 26, p. 2026-2028, 1990
101. K. Mohri and T. Shirosugi, New Extensometers Using Amorphous Magnetostrictive Ribbon Wound Cores, *IEEE Transactions on Magnetics*, 17, p. 1317-1319, 1981
102. J.M. Barandiaran, J. Gutierrez and C. Gómez-Polo, New sensors based on the magnetoelastic resonance of metallic glasses, *Sensors and Actuators A: Physical*, 81, p. 154-157, 2000
103. T.K. Worthington and D.A. Thompson, A Magnetoacoustic Position Sensor, *IEEE Transactions on Magnetics*, 6, p. 693-695, 1980
104. D.A. Thompson and T.K. Worthington, Transducers for a magnetostrictive position sensor, *IBM Tech. Discl. Bull.* 22, p. 5561, 1980
105. P. Campbell, Magnetostrictive Sensors for Rotary Position Encoders, *IEEE Transactions on Magnetics*, 26, p. 2029-2031, 1990
106. G. Lemarquand, Annular Magnet Position Sensor, *IEEE Transactions on Magnetics*, 26, p. 2041-2043, 1990.
107. R. Lassow and T. Meydan, An angular accelerometer using amorphous wire, *IEEE Transactions on Magnetics*, 31, p. 3179 –3181, 1995
108. T. Meydan and P. Choudhary, A novel accelerometer design using the inverse magnetostrictive effect, *Sensors and Actuators A: Physical*, 59, p. 51-55, 1997
109. L.P. Shen, K. Mohri, T. Uchiyama and Y. Honkura, Sensitive acceleration sensor using amorphous wire SI element combined with CMOS IC multivibrator for environmental sensing, *IEEE Transactions on Magnetics*, 36, p. 3667 –3669, 2000
110. V. Lemarquand, A new bi-directional inductive force sensor, *IEEE Transactions on Magnetics*, 34, p. 1333 –1335, 1998

111. D. Son and J. Sievert, Force sensor making use of changes in the maximum induction of an amorphous alloy, *IEEE Transactions on Magnetics*, 26, p. 2017–2019, 1990
112. L. Kraus, P. Svec and J. Bydovský, Amorphous CoFeCrSiB ribbons for strain sensing applications, *Journal of Magnetism and Magnetic Materials*, 242-245, p. 241-243, 2002
113. M. Pasquale, C.P. Sasso, M. Velluto and S.H. Lim, Stress sensing with Co based ferrite composites, *Journal of Magnetism and Magnetic Materials*, 242-245, p. 1460-1463, 2002
114. J. Arcas, M. Vázquez, A. Hernando and C. Gómez-Polo, Sensor applications based on induced magnetic anisotropy in toroidal cores, *Sensors and Actuators A: Physical*, 59, p. 101-104, 1997
115. M.R.J. Gibbs, R. Watts, W. Karl, A.L. Powell and R.B. Yates, Microstructures containing piezomagnetic elements, *Sensors and Actuators A: Physical*, 59, p. 229-235, 1997
116. W. Affane, A.L. Powell and M.R.J. Gibbs, Performance modelling of micromachined sensor membranes coated with piezomagnetic material, *Sensors and Actuators A: Physical*, 51, p. 219-224, 1996
117. M.K. Jain and C.A. Grimes, A wireless magnetoelastic micro-sensor array for simultaneous measurement of temperature and pressure, *IEEE Transactions on Magnetics*, 37, p. 2022–2024, 2001
118. W.J. Karl, A.L. Powell, R. Watts, M.R.J. Gibbs and C.R. Whitehouse, A micromachined magnetostrictive pressure sensor using magneto-optical interrogation, *Sensors and Actuators A: Physical*, 81, p. 137-141, 2000
119. C. Fosalau, M. Cretu and O. Postolache, Circular displacement sensor using magnetostrictive amorphous wires, *IEEE Transactions on Magnetics*, 36, p. 557–560, 2000
120. Y. Chen, J.E. Snyder, C.R. Schwichtenberg, K.W. Dennis, R.W. McCallum and D.C. Jiles, Metal-bonded Co-ferrite composites for magnetostrictive torque sensor applications, *IEEE Transactions on Magnetics*, 35, p. 3652–3654, 1999
121. L.P. Shen, Y. Naruse, D. Kusumoto, E. Kita, K. Mohri, T. Uchiyama and T. Yoshinaga, Sensitive stress sensor using amorphous magnetostrictive wires on both ends fixed double beam and diaphragm, *IEEE Transactions on Magnetics*, 35, p. 3619–3621, 1999
122. I.J. Garshelis, A torque transducer utilizing a circularly polarized ring, *IEEE Transactions on Magnetics*, 28, p. 2202–2204, 1992
123. K. Miyashita, T. Takahashi, S. Kawamata, S. Morinaga and Y. Hoshi, Non contact magnetic torque sensor, *IEEE Transactions on Magnetics*, 26, p. 1560–1562, 1990

124. W.J. Fleming, Magnetostrictive torque sensor performance-nonlinear analysis, *IEEE Transactions on Vehicular Technology*, 38, p. 159 –167, 1989
125. I. Sasada, T. Tanaka, M. Baba and K. Harada, Detection of instantaneous torque using the magnetostrictive effect in a practical ferromagnetic shaft, *IEEE Transactions on Magnetics*, 24, p. 2886 –2888, 1988
126. D. Son, S.J. Lim and C.S. Kim, Noncontact torque sensor using the difference of maximum induction of amorphous cores, *IEEE Transactions on Magnetics*, 28, p. 2205 –2207, 1992
127. K. Ishikawa, K. Mohri, K. Akagi, Y. Kashiwagi and H. Fukasaku, Torque sensor using perpendicularly magnetizing coils, *IEEE Transactions on Magnetics*, 27, p. 4849 –4851, 1991
128. F.E. Pinkerton, J.F. Herbst, C.H. Olk, M.S. Meyer and J.J. Moleski, Tb<sub>1-x</sub>Dy<sub>x</sub>Fe<sub>2</sub>/Fe composites: compositional effects on torque response, *Journal of Magnetism and Magnetic Materials*, 241, p. 162-172, 2002
129. Y. Chen, B.K. Kriegermeier-Sutton, J.E. Snyder, K.W. Dennis, R.W. McCallum and D.C. Jiles, Magnetomechanical effects under torsional strain in iron, cobalt and nickel, *Journal of Magnetism and Magnetic Materials*, 236, p. 131-138, 2001
130. E. Hristoforou, J.N. Avaritsiotis and H. Chiriac, New Flowmeters Based on Amorphous Magnetic Wires, *Sensors and Actuators A: Physical*, 59, p. 94-96, 1997
131. Non destructive evaluation and Quality Control, *Metals Handbook*, Volume 17, Ninth Edition, American Society for Metals, 1989
132. D.O. Ki, J. Ranade, V. Arya, A. Wang and R.O. Claus, Optical fiber Fabry-Perot interferometric sensor for magnetic field measurement, *IEEE Photonics Technology Letters*, 9, p. 797 –799, 1997
133. A.R. Davis, S.S. Patrick, A. Dandridge and F. Bucholtz, Remote fibre-optic AC magnetometer, *Electronics Letters*, 28, p. 271 –273, 1992
134. F. Bucholtz, D.M. Dagenais and K.P. Koo, High-frequency fibre-optic magnetometer with 70 ft/square root (Hz) resolution, *Electronics Letters*, 25, p. 1719 –1721, 1989
135. K.P. Koo, F. Bucholtz, D.M. Dagenais and A. Dandridge, A compact fiber-optic magnetometer employing an amorphous metal wire transducer, *IEEE Photonics Technology Letters*, 1, p. 464 –466, 1989
136. D.M. Dagenais, F. Bucholtz, K.P. Koo and A. Dandridge, Demonstration of 3 pT/square root (Hz) at 10 Hz in a fibre-optic magnetometer, *Electronics Letters*, 24, p. 1422 –1423, 1988

137. P. Ripka and W.G. Hurley, Excitation efficiency of fluxgate sensors, *Sensors and Actuators A: Physical*, 129, p. 75-79, 2006
138. P. Ripka, New directions in fluxgate sensors, *Journal of Magnetism and Magnetic Materials*, 215-216, p. 735-739, 2000
139. J.F. Doherty, S. Arigapudi and R.J. Weber, Spectral estimation for a magnetostrictive magnetic field sensor, *IEEE Transactions on Magnetics*, 30, p. 1274 –1290, 1994
140. D.M. Dagenais, F. Bucholtz, K.P. Koo and A. Dandridge, Detection of low-frequency magnetic signals in a magnetostrictive fiber-optic sensor with suppressed residual signal, *Journal of Lightwave Technology*, 7, p. 881 –887, 1989
141. M.D. Mermelstein and A. Dandridge, Magnetostrictive metallic glass ribbon gradiometer, *Electronics Letters*, 24, p. 895 –896, 1988
142. M.C. Sánchez, C. Aroca, P. Sánchez, J.L. Prieto and E. López, Current effects in magnetostrictive piezoelectric sensors, *Journal of Magnetism and Magnetic Materials*, 174, p. 289-294, 1997
143. R. Chung, R. Weber and D.C. Jiles, A Terfenol based magnetostrictive diode laser magnetometer, *IEEE Transactions on Magnetics*, 27, p. 5358 –5360, 1991
144. T. Uchiyama, K. Mohri, L.V. Panina and K. Furuno, Magneto-impedance in sputtered amorphous films for micro magnetic sensor, *IEEE Transactions on Magnetics*, 31, p. 3182 –3184, 1995
145. K. Inada, K. Mohri and K. Inuzuka, Quick response large current sensor using amorphous MI element resonant multivibrator, *IEEE Transactions on Magnetics*, 30, p. 4623 –4625, 1994
146. H. Hauser, R. Steindl, C. Hausleitner, A. Pohl and J. Nicolics, Wirelessly interrogable magnetic field sensor utilizing giant magneto-impedance effect and surface acoustic wave devices, *IEEE Transactions on Instrumentation and Measurement*, 49, p. 648 –652, 2000
147. D. Attkinson, P.T. Squire, M.G. Maylin and J. Gore, An integrating magnetic sensor based on the giant magneto-impedance effect, *Sensors and Actuators A: Physical*, 81, p. 82-85, 2000
148. P. Dimitropoulos, Ph.D. Thesis, National Technical University of Athens, 2001
149. E. Pulido, R.P. del Real, F. Conde, G. Rivero, M. Vazquez, E. Ascasibar and A. Hernando, Amorphous wire magnetic field and DC current sensor based on the inverse Wiedemann effect, *IEEE Transactions on Magnetics*, 27, p. 5241 –5243, 1991
150. J. Gutierrez and J.M. Barandiaran, High magnetostriction metallic glasses used as magnetoelastic labels, *IEEE Transactions on Magnetics*, 31, p. 3146 –3148, 1995

151. K. Ishiyama, K. Imamura and K.I. Arai, Smart actuator with magneto-elastic strain sensor, *Journal of Magnetism and Magnetic Materials*, 242-245, p. 1163-1165, 2002
152. I. Altpeter, W.A. Theiner, E. Schneider, S.E. Pritchard and M.G. Silk, Non-destructive evaluation of stress states in steels, *NDT & E International*, 29, p. 342, 1996
153. I. Sasada and N. Watanabe, Eddy current probe for nondestructive testing using cross-coupled figure-eight coils, *IEEE Transactions on Magnetics*, 31, p. 3149–3151, 1995
154. L.G. Ullate, A. Ibanez, J.J. Anaya and M.T. Sanchez, Performances of remote digital processing in automated non-destructive evaluation, *Sensors and Actuators A: Physical*, 68, p. 447-453, 1998
155. A. Parakka and D.C. Jiles, Magneprobe: A portable system for non-destructive testing of ferromagnetic materials, *Journal of Magnetism and Magnetic Materials*, 140-144, p. 1841-1842, 1995
156. I. Sasada, N. Suzuki, T. Sasaoka and K. Toda, In-process detection of torque on a drill using magnetostrictive effect, *IEEE Transactions on Magnetics*, 30, p. 4632–4634, 1994
157. P. Adi, Z.A. Memon, D.J. Mapps and R.T. Rakowski, Serpentine MR Elements for Tactile Sensor Applications, *IEEE Transactions on Magnetics*, 26, p. 2047-2049, 1990
158. H. Okabe and H. Wakaumi, Grooved Bar-Code Pattern Recognition System with Magnetoresistive Sensor, *IEEE Transactions on Magnetics*, 26, p. 1575-1577, 1990
159. C. Hausleitner, R. Steindl, A. Pohl, H. Hauser, A.M.J. Goiser and F. Siefert, Cordless batteryless wheel mouse application utilizing radio requestable SAW devices in combination with the giant magneto-impedance effect, *IEEE Transactions on Microwave Theory and Techniques*, 49, p. 817–822, 2001
160. G.M. Glover, G. Hall, A.J. Matheson and J.L. Stretton, A magnetostrictive instrument for measuring the viscoelastic properties of liquids in the frequency range 20-100 kHz, *J. Phys. E: Sci. Instrum.*, 1, p. 383-388, 1968
161. M.J. Brennan, J. Garcia-Bonito, S.J. Elliott, A. David and R.J. Pinnington, Experimental investigation of different actuator technologies for active vibration control, *Smart Mater. Struct.*, 8, p. 145-153, 1999
162. M.J. Brennan, S.J. Elliott and R.J. Pinnington, A non-intrusive fluid-wave actuator and sensor pair for the active control of fluid-borne vibrations in a pipe, *Smart Mater. Struct.*, 5, p. 281-296, 1996
163. F.J. Castano, M. Vazquez, T.A. Ovari, D.X. Chen and A. Hernando, AC field-induced rotation of magnetostrictive wires: operating principle for field positioning microrotor sensors, *IEEE Transactions on Magnetics*, 36, p. 2791–2793, 2000
164. T. Meydan and H. Oduncu, Enhancement of magnetostrictive properties of amorphous ribbons for a biomedical application, *Sensors and Actuators A: Physical*, 59, p. 192-196, 1997

165. T. Klinger, H. Pfutzner, P. Schonhuber, K. Hoffmann and N. Bachl, Magnetostrictive amorphous sensor for biomedical monitoring, *IEEE Transactions on Magnetics*, 28, p. 2400–2402, 1992
166. T. Klinger, F. Schmollebeck, H. Pfutzner and P. Schonhuber, 3D-CAD of an amorphous magnetostrictive sensor for monitoring the movements of the human spine, *IEEE Transactions on Magnetics*, 28, p. 2397–2399, 1992
167. H. Oduncu and T. Meydan, A novel method of monitoring biomechanical movements using the magnetoelastic effect, *Journal of Magnetism and Magnetic Materials*, 160, p. 233-236, 1996
168. L.P. Shen, K. Mohri, AL.X. Abudukelimu and H. Aoyama, Mechano-encephalogram based on amorphous wire micro SI acceleration sensor, *IEEE Transactions on Magnetics*, 37, p. 2007–2009, 2001
169. A. Aston, Biological warfare canaries, *IEEE Spectrum*, p. 35-40, 2001
170. IEC standards on electromagnetic compatibility
171. C.P.O. Treutler, Magnetic sensors for automotive applications, *Sensors and Actuators A: Physical*, 91, p. 2-6, 2001
172. T. Uchiyama, K. Mohri, H. Itho, K. Nakashima, J. Ohuchi and Y. Sudo, Car traffic monitoring system using MI sensor built-in disk set on the road, *IEEE Transactions on Magnetics*, 36, p. 3670–3672, 2000
173. Y. Honkura, Development of amorphous wire type MI sensors for automobile use, *International Workshop on Magnetic Wires*, San Sebastian, Spain 2001
174. Y. Nishibe, Y. Nonomura, K. Tsukada, M. Takeuchi, M. Miyashita and K. Ito, Determination of engine misfiring using magnetoelastic torque sensor, *IEEE Transactions on Instrumentation and Measurement*, 47, p. 760–765, 1998
175. W. Wulfhekel, H.F. Ding, R. Hertel and J. Kirschner, Amorphous wires as tips in spin-polarized scanning tunneling microscopy, *International Workshop on Magnetic Wires*, San Sebastian, Spain 2001
176. P.T. Olsen, W.L. Tew, E.R. Williams, R.E. Elmquist and H. Sasaki, Monitoring the mass standard via the comparison of mechanical to electrical power, *IEEE Transactions on Instrumentation and Measurement*, 2, p. 115-120, 1991
177. D.W. Forester, C. Vittoria, D.C. Webbs and K.L. Davis, Variable delay lines using magnetostrictive metallic glass film overlays, *Journal of Applied Physics*, 49, p. 1794-1796, 1978
178. M. Yamaguchi, K.Y. Hashimoto, H. Kogo and M. Naoe, Variable SAW delay line using TbFe<sub>2</sub> film, *IEEE Transactions on Magnetics*, 16, p. 916-918, 1980

179. M. Inoue and N. Fujita, Optimum geometrical structure of highly magnetostrictive multilayer films for horizontally polarized high frequency magneto-surface-acoustic-wave propagation, *Journal of Applied Physics*, 73, p. 6159-6161, 1993
180. L. Lanotte and V. Iannotti, Effects of local magnetization changes on resonant standing magnetoelastic waves, *Intern. J. Appl. Electromagn. Mech.*, 16, p. 155-163, 1995
181. L. Lanotte, Z. Kaczkowski, R. Pasquino, L. Palezzo and V. Tagliaferri, Magnetoelastic wave application to investigate laser annealing effects in ferromagnetic glass, *Journal of Magnetism and Magnetic Materials*, 135, p. 265-270, 1994
182. G. Ausanio, C. Hison, V. Iannotti, C. Luponio and L. Lanotte, Elastomagnetic effect in novel elastic magnets, *Journal of Magnetism and Magnetic Materials*, 272-276, p. 2069-2071, 2004
183. An integrated EMAT/laser NDT device, UK patent n° 8922891, 1989
184. Defect detection by flux leakage, Patent n° 9401512, 2001
185. Magnetisation without contact by rotating magnetic field, Patent n° 944700301, 2001
186. H-C. Chang, T-J. Cheng, T-H. Wu and T-M. Lin, Determination of coagulation time in whole blood containing anticoagulant by piezoelectric quartz crystal sensor, *Sensors and Actuators B: Chemical*, 66, p. 296-298, 2000
187. T.P. Vikinge, K.M. Hansson, J. Benesch, K. Johansen, M. Ranby, T.L. Lindahl, B. Liedberg, I. Lundstrom and P. Tengvall, Blood plasma coagulation studied by surface plasmon resonance, *J. Biomed. Opt.*, 5, p. 51-55, 2000
188. J. Simitzis, A. Stamboulis, D. Tsoros and N. Martakis, Kinetics of curing of unsaturated polyesters in the presence of organic and inorganic fillers, *Polymer International* 43, p. 380-384, 1997
189. L.G. Puckett, G. Barrett, D. Kouzoudis, C. Grimes and L.G. Bachas, Monitoring blood coagulation with magnetoelastic sensors, *Biosensors and Bioelectronics*, 18, p. 675-681, 2003
190. L.G. Puckett, J.K. Lewis, A. Urbas, X. Cui, D. Gao and L.G. Bachas, Magnetoelastic transducers for monitoring coagulation, clot inhibition, and fibrinolysis, *Biosensors and Bioelectronics*, 20, p. 1737-1743, 2005
191. H.L. Bandey, R.W. Cernosek, W.E. Lee, III and L.E. Ondrovic, Blood rheological characterization using the thickness-shear mode resonator, *Biosensors and Bioelectronics*, 19, p. 1657-1665, 2004
192. A.K. Gopal, S. Adali and V.E. Verijenko, Optimal temperature profiles for minimum residual stress in the cure process of polymer composites, *Composite Structures*, 48, p. 99-106, 2000

193. W. Jenninger, J.E.K. Schawe and I. Alig, Calorimetric studies of isothermal curing of phase separating epoxy networks, *Polymer*, Volume 41, Issue 4, February 2000, Pages 1577-1588
194. J. Pozuelo and J. Baselga, Curing of polymer matrix composites: Fluorescence study of dansyl fluorophore labeled to glass fibers and DGEBA–ethylenediamine epoxy resin, *Journal of Materials Processing Technology*, Volumes 143-144, 20 December 2003, Pages 332-336
195. M. Muthukumar and D. Mohan, Studies on polymer concretes based on optimized aggregate mix proportion, *European Polymer Journal*, Volume 40, Issue 9, September 2004, Pages 2167-2177
196. H. Chiriac and C.S. Marinescu, New position sensor based on ultraacoustic standing waves in FeSiB amorphous wires, *Sensors and Actuators A: Physical*, 81, p. 174-175, 2000
197. R. Germano and L. Lanotte, Application of magnetoelastic waves for sensors of displacement, *Sensors and Actuators A: Physical*, 59, p. 337-341, 1997



# Publications

- **E. Mangiorou**, T Damatopoulou, S. Angelopoulos, A. Ktena, E. Hristoforou, "Residual Stress Monitoring in Magnetostrictive Cylinders and Tubes" , IEEE Transactions on Magnetics, 2024
- **Mangiorou, E.**, Petrou, J., Damatopoulou, T., (...), Ktena, A., Hristoforou, E. "Hall sensors for magnetization loop determination in thin films", Journal of Magnetism and Magnetic Materials, 596, 171775, 2024
- **Mangiorou, E.**, Damatopoulou, T.V., Angelopoulos, S., (...), Ktena, A., Hristoforou, E., "Revisiting the universality law in magnetically detected residual stresses in steels", AIP Advances, 14(2), 025126, 2024
- S. Angelopoulos, P. Vourna, A. Ktena, **Mangiorou, E.**, P. Tsarabaris and E. Hristoforou, "Design and development of a new magnetic sensor for stress monitoring and annihilation/control in steel", IEEE Transactions on Magnetics, vol. 55(1), 2018.
- P. Vourna, E. Hristoforou, A. Ktena, P. Svec, **E. Mangiorou**, "Dependence of Magnetic Permeability on Residual Stresses in Welded Steels", IEEE Transactions on Magnetics, Vol. 53, No. 4,, PP. 1-1, 10.1109/TMAG.2016.2628025, 2017
- M. Hasicic, S. Angelopoulos, **E. Mangiorou**, A. Ktena, E. Hristoforou, "The Effect of Strain on the Magnetization Process as Hard/Soft Phase Interplay", 2023, (pre-print) 10.2139/ssrn.4528328.
- G.Antipas, **E.Mangiorou**, "Atomic topology and electronic structure of a melt-spun Al92U8 metallic glass", Computational and Theoretical Chemistry, 1036, 2014
- G. Antipas, **E.Mangiorou**, E. Hristoforou, "Solute–solvent interactions and atomic cohesion in GeSe4 and GeSe4In5 metallic glasses", Materials Research Express,1(1):015202, 1036, 2014
- G.Antipas, **E.Mangiorou**, E. Hristoforou, "The Effect of Indium Content on the Atomic Environment and Cluster Stability of GeSe4Inx=10,15 Glasses", Metals, 5, 1,2014

- D.N. Kosyvakis S. Vassiliadis, C. Vossou, **E. Mangiorou**, “Computational Analysis of a Thermoelectric Generator for Waste-Heat Harvesting in Wearable Systems”, *Journal of Electronic Materials*, 45(6), 2016
- Evangelos V Hristoforou, Aphrodite Ktena, Polyxeni Vourna, **Eleni Mangiorou**, Stelios Mores, “A New Magnetic Method for Stress Monitoring in Steels”, *International Conference on Systems, Control and Information Technologies*, Warsaw (2016)
- Evangelos Hristoforou, Aphrodite Ktena, Polyxeni Vourna, **Eleni Mangiorou**, “New advances on stress monitoring in ferromagnetic steels”, *14th International Conference “Application of Contemporary Non-destructive testing in Engineering”*, Portoroz, Slovenia (2017)
- **E. Mangiorou**, “Correlation of grain growth phenomena with magnetic properties in non - oriented electrical steels”, *IOP Conf. Series: Materials Science and Engineering*, vol. 108, 2016.
- **E.Mangiorou**, “Design and development of a new magnetic sensor for stress monitoring and annihilation/control in steels”, *IOP Conf. Series: Journal of Physics*, vol. 939, 2017.
- **E. Mangiorou**, X. Vourna, A. Ktena, E. Hristoforou, Correlation of the magnetocrystalline energy with the magnetic parameters in electrical steels, *International Scientific Conference eRA-10 Piraeus University of Applied Sciences* (2015)
- S. Vassiliadis, D.N. Kosyvakis, K. Prekas, C. Vossou, **E. Mangiorou**, S. Potirakis, “A Magnetostrictive Textile - Integrated Magnetic Sensing Device for the detection of static magnetic fields”, *15th AUTEX World Textile*, 2015
- **E. Mangiorou**, X. Vourna, A. Ktena, E. Hristoforou, Correlation of the magnetocrystalline energy with the magnetic parameters in electrical steels, *International Scientific Conference eRA-10 Piraeus University of Applied Sciences* (2015)
- E. Hristoforou, A. Ktena, P. Vourna, **E. Mangiorou**, S. Aggelopoulos, P. Svec, C. Hervoche, *19th World Conference on Non-Destructive Testing 2016*, “Monitoring Magnetic Property Tensor Across the Weld at the Same Points where Stress Tensor was Monitored”, Munich, Germany, June 13-17, 2016.
- S. Vassiliadis, S. Potirakis, **E. Mangiorou**, C. ahnedin, “Calculation of Key Structural Parameters of Woven Fabrics Pores through Image Analysis”, *VI International Technical Textile Congress*, 2015

- S. Vassiliadis, S. Potirakis, **E. Mangiorou**, C. ahnedin, "Estimating Woven Porosity in Terms of Fractal Theory", VI International Technical Textile Congress, 2015
- **E. Mangiorou**, "Magnetometry in Space Exploration", Key Engineering Materials, 2016, vol 644, 266-269
- **E. Mangiorou**, " A Critical Assessment of the Four Basic Methods of Tomographic Imaging", Key Engineering Materials, 2014, vol 605, 657-660